Ghent University
Faculty of Sciences
Department of Solid State Sciences
Krijgslaan 281/S1, 9000 Ghent, Belgium

Phase formation and texture of thin film nickel germanides

Bob De Schutter

Promotor: Prof. Dr. Christophe Detavernier (UGent)

Members of the Jury:

Prof. Dr. Natalie Jachowicz (UGent, chair)
Prof. Dr. Christophe Detavernier (UGent)
Prof. Dr. Christian Lavoie (IBM)
Prof. Dr. André Vantomme (KULeuven)
Prof. Dr. Dirk Poelman (UGent)
Dr. Fabrice Nemouchi (CEA-LETI)
Dr. Davy Deduytsche (UGent)

This research was supported by the 'Fonds voor wetenschappelijk onderzoek Vlaanderen' (FWO).

Thesis submitted for the degree of
Doctor in Sciences: Physics
2016

Preface

This PhD thesis treats the texture of thin films of silicide or germanide materials, which are used as contacting materials in microelectronics. More specifically, this work focusses on how this texture can help us understand the details of the phase formation sequence during the formation of a specific silicide or germanide phase. In this context, a new interface visualisation technique was developed that helps us understand the crystallographic constraints of different observed texture components. Experimentally, this thesis focusses on the phase formation sequence and texture evolution during the solid state reaction between a thin Ni film and a (001) or (111) oriented Ge substrate. The experimental work started in October 2011 and results obtained up to June 2015 are included. It was mainly carried out at the Department of Solid State Sciences of Ghent University and at the X20A and X20C beamlines of the National Synchrotron Lightsource at Brookhaven National Lab in collaboration with IBM. The RBS and TEM results presented in this thesis were only possible thanks to close collaboration with the IKS institute at KU Leuven and the EMAT group at Antwerp University respectively.

This thesis is article based and almost all the results are presented by means of papers that have been published, accepted or submitted to peer-reviewed journals. The context of this research and an extensive overview of the related literature are presented in a separate review chapter, which was also submitted as a review paper to *Applied Physics Reviews*. In chapter three, some supplemental information that could not be included in the papers is provided in two extra sections. In this way, I hope to have provided a nice flow throughout this thesis, linking together the different papers in an attractive way.

Bob
Ghent, June 2016

Table of Contents

English Summary

1 Introduction

Silicides and germanides are compounds consisting of a metal and silicon or germanium. In the microelectronics industry, silicides are the material of choice for contacting silicon based devices, while germanides are considered as a top candidate for contacting future germanium based electronics. Since strain engineering through the use of $Si_{1-x}Ge_x$ in the source/drain/-gate regions of MOSFET devices is an important technique for improving device characteristics in state-of-the-art microelectronics industry, a profound understanding of the formation of silicide/germanide contacts to silicon and germanium is of utmost importance.

The texture of these films, which is defined as the statistical distribution of the orientation of the grains in the film, has been the subject of scientific studies since the 1970's. In recent years, it has become increasingly clear that film texture can have a profound influence on the formation and stability of silicide/germanide contacts, as it controls the type and orientation of grain boundaries (affecting diffusion and agglomeration) and the interface energy (affecting nucleation during the solid-state reaction). Importantly, the texture also affects the electrical characteristics of the contact, as the orientation and size of individual grains will affect functional properties such as contact resistance and sheet resistance and will induce local variations in strain and Schottky barrier height.

2 Review of texture studies in silicide and germanide thin films

The first chapter in this thesis provides an overview of the research that has been performed over the past decades targeting the texture in thin silicide and germanide films.

First, the two most important techniques that are used in modern texture studies are discussed. These are synchrotron based X-ray pole figures

and electron backscattered diffraction (EBSD). The first technique provides a straightforward way for a qualitative identification of the different phases and texture components that are present in the film, while the latter technique can provide a more quantitative picture of the different texture components and of the microstructure (grain size, grain morphology, etc.) of the film.

Next, the chapter provides a historical overview of how texture in these films was addressed during the early years of silicide research, when focus was mainly directed towards the growth of epitaxial silicides. At this point in the chapter, the driving forces for the development of texture in these films are discussed. It is argued that a minimization of interface energy drives the film grains to grow with a preferential orientation that results in a periodic interface structure in either one (axiotaxy) or two (epitaxy) directions.

The remainder of the chapter is aimed at providing a structured overview of texture research on thin silicide and germanide films that has been published since the early 2000's, when the technique of high-resolution synchrotron base X-ray pole figure measurements was introduced. It is discussed that texture measurements are often crucial to unambiguously identify the correct phase formation sequence during silicide/germanide formation, as highly textured phases are easily overlooked using standard measurement techniques. Furthermore, the influence of texture on different important thin film properties such as phase stability, morphological stability and electrical properties are discussed. As texture has an important influence on these properties, it is important to understand the factors that can affect film texture. One can then exploit these in an attempt to control the texture of these films. The final part of the chapter discusses some examples of how this can be achieved, e.g. by alloying the binary film with a third element that is either soluble or insoluble in the targeted silicide/germanide.

3 Interface visualisation

The texture observed in thin silicide or germanide films on single crystal silicon or germanium substrates is often a complex combination of different texture components (axiotaxy, epitaxy and fiber). So far, attempts to explain the observation of certain epitaxial and axiotaxial components have been made by looking at cross-sections of real-space ball-and-stick models of the film and substrate lattice near the interface region. However, such visualizations have proven to be cluttered and often hard to interpret.

In the second chapter, a novel technique is introduced to visualize the

periodicity within the interface plane between two different crystal structures (e.g. a silicide or germanide and the silicon or germanium substrate) in a simple 2D plot. Furthermore, we show how this visualization enables a classification for epitaxial orientations that is based on how the periodicity in the interface plane is achieved and relies on a possible alignment between low-index lattice planes from film and substrate across the interface. Finally, the usefulness of this technique is demonstrated by applying it to the known texture components found in thin α-$FeSi_2$ and NiSi films grown on single crystal Si(001) and Si(111) substrates.

4 Phase formation and texture in nickel germanides on Ge(001) and Ge(111) substrates

In the third chapter, the thesis focusses on nickel germanides. Since contacting materials (both silicides and germanides) are usually formed through a thermally induced solid state reaction between a thin metal film and the Si/Ge substrate, a profound understanding of this reaction is very important. Because NiGe is the top candidate to be used as contacting material in future, Ge-based MOSFET devices, this chapter provides a detailed study on the phase formation sequence and texture evolution during the solid state reaction between a thin Ni film and a Ge substrate toward the NiGe end phase.

First, a paper is presented concerning phase formation in Ni films that are pre-mixed with different amounts of Ge (between 0 and 50%). The thermally induced reaction between such films and an inert SiO_2 or a single crystalline Ge(001) substrate are studied. The formation of a hexagonal, metastable nickel germanide (called either the 'HEX-phase' or 'ϵ-phase') on both substrate types is described. This phase is found to form below its bulk stability temperature within a range of Ge concentrations between 24 and 48% and is even observed to form in the as-deposited film for Ge concentrations between 36 and 42%.

A second paper covers the formation of NiGe through a solid state reaction between a pure Ni film and a Ge(001) or Ge(111) oriented substrate. Using pole figure measurements, it is shown that the Ni-rich germanide that forms before NiGe is the same metastable, hexagonal germanide (ϵ-phase) that was observed in the mixed Ni(x%Ge) films. However, on these single crystalline substrates, this phase is found to exhibit a strong epitaxial texture, which is why this Ni-rich phase was wrongly identified in previous studies. A detailed study of the ϵ-phase texture is provided. Next, pole figures collected on samples quenched at different temperatures during the solid state reaction are used to discuss the complete phase formation se-

quence towards NiGe. Complementary information on the kinetics during the reaction is provided through the use of *in situ* Rutherford backscattering spectroscopy (RBS). These results reveal a simultaneous growth of the Ni-rich ϵ-phase and NiGe on both substrate types. However, this effect is much more pronounced on the Ge(001) substrate.

At the end of the chapter, an overview is given on how the interface visualization technique discussed in the second chapter is practically used with the aid of software developed during the course of this PhD. One of the observed epitaxial texture components of the ϵ-phase is used as an example.

Nederlandstalige Samenvatting –Summary in Dutch–

1 Introductie

Silicides en germanides zijn verbindingen die bestaan uit een metaal en silicium (voor silicides) of germanium (voor germanides). In de microelectronica zijn silicides het materiaal bij uitstek voor het contacteren van silicium gebaseerde micro-elektronische componenten zoals veldeffect transistoren. Germanides worden momenteel aangeprezen als kandidaat materiaal voor het contacteren van toekomstige germanium gebaseerde componenten. Bovendien wordt $Si_{1-x}Ge_x$ momenteel gebruikt in de source en drain gebieden van MOSFET transistoren omdat de elastische vervorming die veroorzaakt wordt door het toevoegen van germanium een positieve invloed heeft op de prestaties van de transistoren. Het is dus duidelijk dat een degelijke kennis van de vorming van silicide en germanide gebaseerde contacten op silicium en germanium zeer belangrijk is.

De textuur van dunne films van deze materialen, die gedefinieerd is als de statistische distributie van de oriëntatie van de verschillende korrels in de film, wordt reeds bestudeerd sinds de jaren 1970. Over de jaren is het duidelijk geworden dat de textuur van deze films een belangrijke invloed heeft op de vorming en stabiliteit van de contacten omdat het type en de oriëntatie van de korrelgrenzen (die diffusie en agglomeratie beïnvloeden) en de interface energie (die nucleatie tijdens een vaste-stofreactie beïnvloedt) erdoor bepaald worden. De textuur heeft ook een belangrijke invloed op de elektrische eigenschappen van het silicide of germanide contact. De oriëntatie en de grootte van de individuele korrels beïnvloeden immers functionele eigenschappen zoals contactweerstand en vierkantsweerstand (sheet resistance) en induceren lokale variaties in spanning en Schottky barrière hoogte.

2 Overzicht van textuurstudies in silicide en germanide films

Het eerste hoofdstuk in deze thesis geeft een overzicht van het onderzoek over textuur in dunne silicide en germanide films dat werd uitgevoerd gedurende de voorbije decennia.

Eerst worden de twee belangrijkste meettechnieken besproken die worden gebruikt in moderne textuurstudies, namelijk synchrotron gebaseerde X-stralen poolfiguurmetingen en diffractie van terugverstrooide electronen (EBSD). De eerste techniek maakt een kwalitatieve identificatie van de verschillende fases en textuurcomponenten die aanwezig zijn in een dunne film mogelijk. De laatste techniek geeft een meer kwantitatief beeld van de verschillende textuurcomponenten en van de microstructuur (korrelgrootte, morfologie van de korrels, enz.) van de film.

Vervolgens wordt d.m.v. een historisch literatuuroverzicht getoond hoe textuur in dergelijke dunne films werd onderzocht gedurende de beginjaren van het onderzoek naar silicide films, toen de focus nog vooral lag op het groeien van epitaxiale dunne lagen. Op dit punt worden ook de drijvende krachten voor de ontwikkeling van textuur in dergelijke films besproken. Er wordt beargumenteerd dat een minimalisatie van interface energie ervoor zorgt dat de korrels in de film groeien met een voorkeursoriëntatie die resulteert in een periodieke interface structuur in één (axiotaxie) of twee (epitaxie) richtingen.

De rest van dit hoofdstuk tracht een gestructureerd overzicht te geven van textuuronderzoek op dunne silicide en germanide films dat gepubliceerd is vanaf het begin van de jaren 2000, wanneer de techniek van hogeresolutie, synchrotron gebaseerde poolfiguurmetingen geïntroduceerd werd. Er wordt aangetoond dat textuurmetingen dikwijls cruciaal zijn om op onweerlegbare wijze de correcte opeenvolging van fases te identificeren gedurende de vorming van een bepaalde silicide- of germanidefase, omdat sterk getextureerde fases gemakkelijk ongedetecteerd blijven wanneer standaard meettechnieken gebruikt worden (zoals bv. $\theta/2\theta$ X-stralen metingen). Vervolgens wordt de invloed van textuur onderzocht op verschillende belangrijke eigenschappen van de dunne films, zoals fasestabiliteit, morfologische stabiliteit en elektrische eigenschappen. Omdat textuur een duidelijke invloed heeft op dergelijke eigenschappen is het ook belangrijk dat we begrijpen welke factoren de textuur beïnvloeden. Deze kennis kunnen we dan gebruiken om de textuur van dergelijke films te proberen manipuleren. Het laatste deel van het hoofdstuk geeft enkele voorbeelden van hoe dit kan worden bereikt, bijvoorbeeld door het mengen van de binaire film met een derde element dat ofwel oplosbaar ofwel niet oplosbaar is in de gewenste silicide- of germanidefase.

3 Visualisatie van de interface

De textuur in dunne silicide of germanide films op Si en Ge éénkristalsubstraten is meestal een combinatie van verschillende textuurcomponenten (epitaxy, axiataxy en fiber). Pogingen om de aanwezigheid van bepaalde epitaxiale en axiotaxiale componenten te verklaren gebeurden tot nog toe door het bestuderen van doorseneden van een atomistisch 'ball-and-stick' model van het film- en substraatrooster in de nabijheid van de interface. Deze visualisaties blijken echter meestal moeilijk te interpreteren.

In het tweede hoofdstuk wordt een nieuwe techniek geïntroduceerd om de periodiciteit in het vlak van de interface tussen twee verschillende kristalstructuren (bv. een silicide of germanide en het silicium of germanium substraat) te visualiseren in een eenvoudige 2-dimensionale figuur. Verder wordt getoond hoe een dergelijke visualisatie helpt in het opstellen van een classificatie voor epitaxiale textuurcomponenten. Deze classificatie is gebaseerd op de manier waarop de periodiciteit in het interfacevlak tot stand komt en kijkt naar een eventuele alignering doorheen het interface vlak tussen netvlakken met lage indices van de film en het substraat. De bruikbaarheid van deze techniek wordt tenslotte gedemonstreerd door ze toe te passen op de gekende textuurcomponenten die voorkomen in een dunne α-$FeSi_2$ of NiSi film op een Si(001) of Si(111) georiënteerd substraat.

4 Fasevorming en textuur in nikkel germanides op Ge(001) en Ge(111) substraten

Het derde hoofdstuk spitst zich toe op nikkel germanides. Contacteringsmaterialen (zowel silicides als germanides) worden typisch gevormd via een thermisch geïnduceerde vastestofreactie tussen een dunne metaalfilm en een silicium of germanium substraat. Daarom is het belangrijk om de details van deze reacties goed te bestuderen. Omdat NiGe wordt beschouwd als een veelbelovend materiaal om te worden gebruikt als contact in toekomstige Ge-gebaseerde MOSFET transistoren, worden in dit hoofdstuk twee papers gepresenteerd die een gedetailleerde studie beschrijven over de fasevorming en textuurevolutie gedurende de vastestofreactie tussen een dunne Ni film en een Ge substraat, die resulteert in de vorming van NiGe.

De eerste paper behandelt fasevorming in Ni films die opgemengd werden met verschillende hoeveelheden Ge (tussen 0 en 50%) vóór de reactie werd gestart. De thermisch geïnduceerde reactie tussen dergelijke films en een inert SiO_2 of een éénkristal Ge(001) substraat worden bestudeerd en de vorming van een metastabiel, hexagonaal nikkel germanide (de 'HEX-

fase' of 'ϵ-fase' genoemd) op beide substraattypes wordt beschreven. Deze fase vormt bij temperaturen lager dan deze waarbij ze stabiel hoort te zijn (volgens het bulk fasediagram) en vormt voor een reeks van Ge concentraties tussen 24 en 48%. Voor concentraties tussen 36 en 42% wordt ze zelfs gezien in de gedeponeerde Ni(x%Ge) lagen, vóór de start van de reactie.

In de tweede paper wordt de vorming van NiGe via een vastestofreactie tussen een dunne Ni film en een Ge(001) of Ge(111) substraat besproken. Door middel van poolfiguurmetingen wordt getoond dat het nikkel rijke germanide dat vormt vóór de uiteindelijke NiGe fase dezelfde metastabiele ϵ-fase is dan deze die werd geobserveerd in de gemengde Ni(x%Ge) lagen. Op deze éénkristal substraten heeft deze fase echter een sterke epitaxiale textuur, waardoor deze niet correct kon worden geïdentificeerd in voorgaande publicaties. Een gedetailleerde studie van de textuur van deze fase wordt hier dan ook gepresenteerd. Vervolgens worden poolfiguren die opgemeten werden op samples die opgewarmd werden tot verschillende temperaturen tijdens de vastestofreactie gebruikt om de volledige fasesequentie en textuurevolutie tot de vorming van NiGe te bestuderen. Complementaire informatie omtrent de kinetiek gedurende de reactie werd verkregen via *in situ* Rutherford terugverstrooiing spectroscopie (RBS). Deze resultaten tonen een temperatuursinterval waar gelijktijdige groei van de ϵ-fase en NiGe plaatsvindt op beide types substraat. Dit effect is evenwel meer uitgesproken op het Ge(001) substraat.

Aan het einde van het hoofdstuk wordt een overzicht gegeven over hoe de techniek van interface visualisatie (zoals geïntroduceerd in het tweede hoofdstuk) in de praktijk kan worden toegepast gebruik makende van twee software paketten die in de loop van dit doctoraatsonderzoek werden ontwikkeld of uitgebreid. Eén van de epitaxiale textuurcomponenten die werden waargenomen in de ϵ-fase wordt hierbij als voorbeeld gebruikt.

List of Abbreviations

SALICIDE	Self-Aligned Silicide
MOSFET	Metal-Oxide-Semiconductor Field Effect Transistor
CMOS	Complementary Metal-Oxide-Semiconductor
XRD	X-Ray Diffraction
EBSD	Electron Backscattered Diffraction
EBSP	Electron Backscattered Diffraction Pattern
SEM	Scanning Electron Microscopy
TEM	Transmission Electron Microscopy
STEM	Scanning Transmission Electron Microscopy
HAADF-STEM	High-Angle Annular Dark Field Scanning Transmission Electron Microscopy
BF-TEM	Bright-Field Transmission Electron Microscopy
HR-TEM	High Resolution Transmission Electron Microscopy
RBS	Rutherford Backscattering Spectroscopy
CCD	Charge-Coupled Device
SPE	Solid Phase Epitaxy
MBE	Molecular Beam Epitaxy
OME	Oxide Mediated Epitaxy
TIME	Titanium Mediated Epitaxy
APT	Atom Probe Tomography
SBH	Schottky Barrier Height
MS	Metal-Semiconductor
BEEM	Ballistic Electron Emission Spectroscopy
SOI	Silicon On Insulator
DRAM	Dynamic Random-Access Memory
MOCVD	MetalOrganic Chemical Vapor Deposition
MIP	Map of Interfacial Periodicity

Introduction

Ever since the advent of the modern computer in the 1950s, people have become increasingly used to the fact that these computers and other electronic devices continuously become smaller and more importantly, faster. From a technology point of view, this is achieved by making the transistors, which are the fundamental electronic building blocks of any modern electronic device, smaller and smaller. This transistor downscaling results in the ability to manufacture an increasing amount of transistors on a single chip, providing smaller devices with higher performance. However, over the past decade, the engineering challenges that were faced in order to keep the downscaling of silicon based transistor technology on track became harder as physical limits concerning the size of individual Si-based transistors were reached. To keep the performance increase of our devices going, research is now focussing on the use of alternative materials to silicon, like Ge or III-V semiconductors, having superior intrinsic properties (like electron and hole mobilities), which results in better performing transistors at similar sizes. At the time of writing, a functional 7nm transistor technology using a $Si_{1-x}Ge_x$ gate instead of a Si gate has already been demonstrated and research is now looking into increasing the Ge content in these channels and adopting pure Ge channels in the near future.

The research presented in this thesis covers a detailed study of the solid state reaction between a thin Ni film and a (001) or (111) oriented, single crystal Ge substrate. This reaction results in the formation of NiGe, a germanide material which is considered as the top candidate to function as electrical contacting material between a state of the art Ge-based transistor and the interconnect lines on an integrated circuit (IC). A good understanding of this reaction is important as it can help us to understand and eventually engineer the properties of the NiGe contact, similar to what has been done in the past to improve the properties of silicide contacts to Si-based transistors. As preceding studies in our group have revealed an important influence of the texture of silicide films on some of their key

properties, a large part of the research performed in this PhD was devoted to identifying and understanding the texture of the different germanide phases that occur during the reaction.

Outline

The first chapter of this thesis is devoted to providing a comprehensive overview of texture research on thin silicide and germanide films on single crystal Si and Ge substrates. As different people of our research group have been actively engaged in this research since the early 2000s, this PhD thesis seemed like the right place to bundle all this research, together with studies from other groups that have been performed since the advent of texture research on thin silicide films, into a review (which was then submitted to *Applied Physics Reviews*). First, the different measurement techniques that are used to study texture in thin films are discussed. Next, a historical overview of texture studies in thin silicide films is provided, along with a summary of the texture components that are observed in the three technologically most important silicide materials (i.e. C54-$TiSi_2$, $CoSi_2$ and NiSi). The rest of the chapter focusses on modern texture research on polycrystalline thin silicide and germanide films that has been performed since the early 2000s, when the introduction of high-resolution pole figures made the detailed study of such films possible. The influence of texture on different properties of the resulting silicide/germanide is discussed, followed by an overview of different studies that investigated which factors can influence the final texture of a silicide/germanide film in an attempt to engineer this texture.

The research that was performed during the course of this PhD is provided in an article-based manner in the remaining chapters. In chapter 2, a new visualization technique is introduced that helps at understanding the interface structure for an epitaxial alignment between two dissimilar crystal structures. This can then be used to identify and classify the multitude of epitaxial texture components that are encountered in thin silicide and germanide films. Chapter 3 bundles two articles that investigate the phase formation sequence during the reaction of a thin Ni film on a single crystal (001) or (111) oriented Ge substrate. After a general introduction summarizing previous literature on this subject, the first article investigates the reaction between an intermixed Ni(x %Ge) film and a Ge substrate. In the second article, the solid state reaction between a pure Ni film and a

Ge(001) or Ge(111) substrate, which results in the formation of NiGe, is studied. At the end of the chapter, a final section is devoted to applying the interface visualization technique discussed in chapter 2 to the epitaxial texture components that are observed during the reaction between a pure Ni film and Ge.

1

Texture in silicides and germanides

Paper I

Texture in thin film silicides and germanides: a review
B. De Schutter, K. De Keyser, C. Lavoie and C. Detavernier
Applied Physics Reviews, submitted, November 2015

1.1 Introduction

Silicides and germanides are compounds consisting of a metal and the semiconductor silicon or germanium respectively. Since a large fraction of the known metals react with silicon or germanium to form one or more silicides or germanides, a huge collection of these materials is known to exist and their properties have been the subject of many scientific studies over the past decades. As a result, a sound collection of books, book chapters and review articles covering different aspects of silicide/germanide properties and applications are available to the reader[1–13].

A very well-known use of silicides is as a contacting material in microelectronic devices. Ever since the development of the *Metal-Oxide-Semi-*

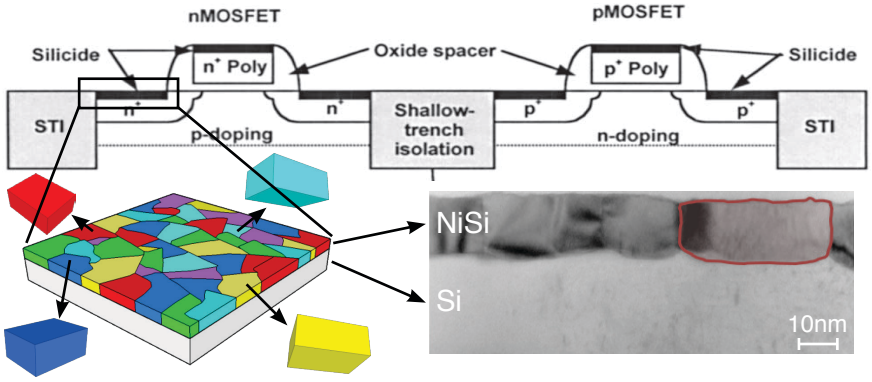

Figure 1.1. *top* schematic cross-section of the typical planar CMOS n- and p-type transistors. Silicides are used to contact the source and drain regions. Pre-45nm node transistors also featured silicides to contact the gate. *bottom* Schematic detail and TEM picture for a typical polycrystalline thin silicide/germanide. Different grains in the film can exhibit different orientations with respect to the substrate.

conductor Field Effect Transistor (MOSFET) and the advent of the Si based CMOS technology, downscaling of these silicon based micro-electronic devices resulted in a massive increase of their speed and complexity. The purpose of a contacting material in such a device is to ensure a good electrical connection (low contact resistance, good adhesion to Si, high thermal stability, ...) between the source, drain or gate of a transistor and the interconnect lines that link it to the billions of other transistors present in a typical processor. In this context, silicides were introduced as a contacting material in the 1980s as a replacement for pure metals like Al which started to show severe issues as feature sizes decreased[14, 15]. Initially, a wide variety of silicide materials such as PtSi, Pd_2Si, $MoSi_2$, WSi_2 or $TaSi_2$ were considered. Eventually, the industry settled on the use of $TiSi_2$ in the early 90s but issues with nucleation of the low-resistive C54-$TiSi_2$ within the initially formed high-resistive C49-$TiSi_2$ phase in lines narrower than 250nm forced a change to $CoSi_2$ [16]. When feature sizes eventually reached sub 50nm dimensions, $CoSi_2$ started showing severe voiding issues in these narrow lines which led to the introduction of NiSi [17]. In modern planar CMOS technology, NiSi modified by the addition of a small amount of Pt still is the contacting material of choice[18]. For new device architectures such as finFETs, which allow for a further size-reduction, the criteria for contacting materials have changed drastically. These new criteria together with the availability of fast anneals have allowed the contacts to evolve

back towards silicides that can withstand higher thermal budgets[19, 20]. For a more comprehensive historical overview on the use of silicides in micro-electronics, the reader is referred to refs. [5–7].

Silicide contacts are typically formed through a solid state reaction between a thin film of the metal of choice and the single-crystal silicon substrate by heating the metal/silicon stack to an elevated temperature. In CMOS fabrication, this is achieved through the so-called *self-aligned silicide* (SALICIDE) process, where the metal is deposited over the whole planar device structure but will only react in the regions where it is exposed to the silicon during a typical formation anneal, resulting in contact formation only on the desired locations. After this formation anneal, the unreacted metal which is positioned over the dielectric regions can be selectively etched away (For the interested reader, a detailed explanation of the SALICIDE process is provided in ref. [7]). A schematic cross-section of a traditional CMOS device structure is provided in Fig. 1.1, showing the resulting silicide contacts on the source, drain and gate regions.

In modern devices, the limitations of classical dimensional downscaling force scientists and engineers to come up with innovative techniques in order to maintain the continuous improvement of device performance. This has resulted in many material innovations such as the use of strained silicon in the channel region of the MOSFET (achieved through replacing Si by $Si_{1-x}Ge_x$ in the source and drain regions or through the use of nitride stressors) and the replacement of the SiO_2/polycrystalline silicon gate by a high-k/metal gate, restricting the use of silicides as contacting material to the source and drain regions. More recently, alternative channel materials like $Si_{1-x}Ge_x$ are being adopted in industry and research is now focussing on increasing the Ge content in these channels or even adopting pure Ge as a channel material, as both $Si_{1-x}Ge_x$ and pure Ge have much higher carrier mobilities compared to Si [21]. In this context, germanides appear as a natural candidate to act as contacting material for the germanium-rich source and drain regions, since they can be formed in a similar self-aligned manner as mentioned above for silicides [22].

As is depicted in Fig. 1.1, the solid state reaction between the metal and the silicon or germanium substrate leads to the formation of a polycrystalline silicide/germanide film on top of a single crystalline substrate. In available CMOS technology, these films usually have a thickness of less than 30nm and consist of a single layer of grains, as can be seen in the TEM micrograph of a NiSi film formed on Si (Fig. 1.1). If we want to understand and/or predict the properties of these poly-crystalline films, it is essential

to have a good understanding of their microstructure. One important aspect of this microstructure is the *texture*, which describes the orientations of the different grains and the frequency of occurrence of these different orientations within the film. This concept of texture originated from the field of bulk metallurgy, where it is known that specific preferential grain orientations can greatly influence certain properties of the materials (e.g. the strength of a rolled sheet of aluminum depends greatly on the texture of the sheet). As a detailed description on the concept and mathematics of texture in materials research is beyond the scope of this review, the interested reader is referred to refs. [23–25].

In this review, we will focus on the texture observed in thin silicide and germanide films formed on single crystal silicon or germanium substrates. In such films, the orientation of the grains is determined with respect to the reference frame of the single crystal substrate. Grains can either be randomly oriented or they can exhibit a preferential orientation with respect to the substrate. Grains that exhibit a similar preferential orientation are said to belong to a specific *texture component* and they can exhibit one of three types of texture: (1) *epitaxy* or in-plane texture, where the orientation of the grains is uniquely defined with respect to the substrate and only one single orientation (and the symmetrically equivalent orientations) occurs; (2) *fiber*, where one of the (hkl) planes is oriented (nearly) parallel to the film/substrate interface and different grains exhibit a different rotation around the axis perpendicular to the interface, i.e. the fiber axis; (3) *axiotaxy*, where a specific plane in the film is aligned to a specific plane in the substrate which is not parallel to the interface, resulting in an off-normal fiber texture. More detail on these texture types, especially the axiotaxy texture, will be provided in section 1.3.

Because these silicides and germanides are important materials in microelectronics, a thorough understanding of their properties has direct impact on device fabrication and performance. As will be discussed in this review, texture can have a profound influence on the formation and stability of these silicide/germanide contacts as it controls the type and orientation of grain boundaries (affecting diffusion and agglomeration) and the interface energy (affecting nucleation during the solid-state reaction). Furthermore, texture also has an impact on the electrical characteristics of the contact as the orientation and size of individual grains will influence functional properties such as contact resistance and sheet resistance and will induce local variations in strain and Schottky barrier height. Of course, the ultimate goal is to be able to predict the texture that will de-

velop for a certain set of experimental parameters (e.g. thin film material, annealing conditions, substrate properties like doping and cleaning methods, etc.). However, results obtained so far in this area simply do not allow yet to construct such predictive theories. Therefore, studies concerning attempts to influence texture formation in specific cases will be discussed at length in this review, but no general theories for texture prediction will be put forward.

The plan for this review is as follows. In section 1.2, we will briefly discuss the most important experimental techniques for measuring texture that have been used in literature over the past decades, along with their advantages and disadvantages. With sections 1.3 to 1.5, we aim to provide a comprehensive overview of literature reports in the field over the past few decades. We start off with a general overview of the types of texture observed in different silicide and germanide materials in section 1.3, with a focus on the concept of axiotaxy. Section 1.4 covers studies probing the influence of texture on the silicide/germanide thin film properties such as formation characteristics, phase stability, agglomeration behavior and electrical properties. Finally, in section 1.5, we discuss different factors that can influence the texture of the final silicide phase during its formation and that hence can be exploited in efforts to control the texture of the contacting material.

1.2 Measuring texture in thin silicide/germanide films

In this section, we provide a brief introduction of the two best suited techniques to study texture in thin film silicides/germanides, i.e. X-ray pole figures and Electron Backscatter Diffraction (EBSD). It must be noted though that these techniques are not the ones that were adopted in the early days of texture research on thin silicide films. As will be discussed in section 1.3.A, during the 70s and 80s, research efforts were mainly focussed on the growth of epitaxial silicide films. In order to probe the epitaxial quality of the grown films, two techniques were mainly used: ion channeling and transmission electron microscopy.

Ion channeling is usually performed using Rutherford Backscattering Spectroscopy, which is why this technique is often referred to as *RBS-channeling*. In such an experiment, the sample is aligned with a major crystallographic direction directed along the incoming ion beam. The re-

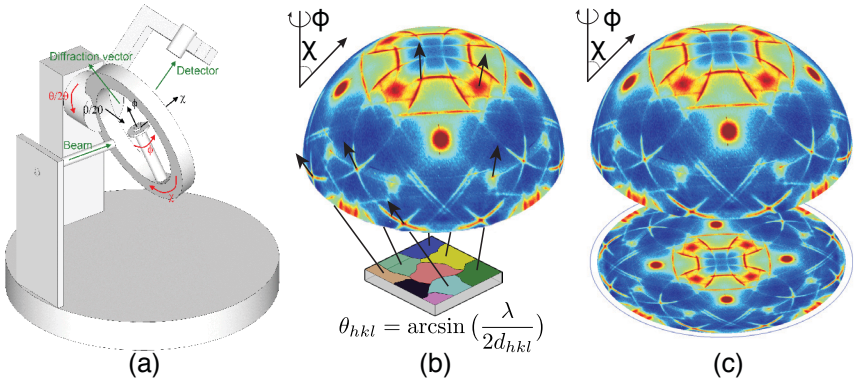

Figure 1.2. (a) Illustration of a four-circle diffractometer used in the Schulz method. The different rotation axes (ϕ, χ and θ) are depicted along with the corresponding rotation directions. (b) Theoretical construction of a pole figure. The intensity distribution on the imaginary hemisphere is created by marking the intersection of the normals of the diffracting planes (those that fulfill the Bragg condition for the chosen d-spacing) with the hemisphere for each grain in the film. (c) Projection of the intensity distribution on the hemisphere onto a planar surface results in a pole figure for a specific family $\{hkl\}$ of lattice planes. The data used in this illustration are for a (112) pole figure of a NiSi film on Si(001).

duced yield of backscattered ions is then used as a measure for the epitaxial quality of the film. For a more detailed explanation of the technique, the interested reader is referred to Ref. [26].

Transmission Electron Microscopy or TEM is a technique in which electrons are transmitted through very thin samples that are either prepared in plan view (electrons are incident perpendicular to the silicide film surface) or in cross section (electrons are incident parallel to the interface). The transmitted electrons can be used for standard high resolution imaging or for diffraction to determine the structure and orientation of crystallites in the film. The high spatial resolution of TEM based techniques is also their major drawback when applied to texture studies: because only a limited number of grains can be measured within a reasonable time, a material with a complex texture will only be partially characterized. While this technique is still heavily used today for microstructure characterization, the statistical reliability of claims regarding texture based solely on TEM measurements is low and complementary techniques like EBSD and X-ray pole figure measurements are required.

1.2.1 X-ray Diffraction - Pole figures

X-ray diffraction is a widely adopted technique for studying the internal (crystalline) structure of materials. The most used geometry for X-ray diffraction characterization is the so called $\theta/2\theta$-measurement in which an X-ray beam impinges on a sample at an incoming angle θ with respect to the sample surface and a detector is positioned at an exit angle of 2θ with respect to the direction of the incoming beam. In this configuration, diffraction can be observed from a set of planes with interplanar spacing d_{hkl} oriented parallel to the sample surface if the Bragg condition $n\lambda = 2d_{hkl}\sin(\theta)$ is fulfilled (with λ the wavelength of the X-ray beam). The resulting diffraction pattern is a characteristic fingerprint of interplanar distances present in a specific crystalline material. As such, it provides an ideal basis for material identification. In thin film silicide/germanide research, this $\theta/2\theta$-scan has become a *run-of-the-mill* technique for identifying the specific silicide/germanide phase(s) present in a film.

The main disadvantage of such a standard $\theta/2\theta$ scan is the aforementioned fact that it is only sensitive to sets of lattice planes oriented parallel to the sample surface (thus parallel to the substrate). For a film consisting of randomly oriented grains this characterization is sufficient, since different lattice planes will be parallel to the substrate in at least some of the grains. However, for a textured film where the grains have a strong preferential alignment with respect to the substrate, one can imagine that certain lattice plane sets will never be aligned parallel to the surface and thus will never meet the diffraction criterion. As a result, in a $\theta/2\theta$-scan of a textured film, certain diffraction peaks will be absent, making phase identification considerably harder. In this case, pole figure measurements are necessary to uniquely identify the observed phase and its texture.

A geometry commonly used to measure pole figures using X-ray diffraction is based on the Schulz method [27], introduced in 1949 and embraced for texture studies in the field of metallurgy. Here, the sample is placed on a four-circle diffractometer which allows to tilt (χ angle) and rotate (ϕ angle) it and to choose its inclination with respect to the incoming X-ray beam (θ angle). The detector is then positioned at an angle 2θ with respect to the incoming X-ray beam in order to fulfill the bragg diffraction condition. A schematic of this setup can be found in Fig. 1.2a. By using a point detector and fixing the θ angle, one measures the diffracted intensity of a specific family of crystal planes. Measuring this diffracted intensity while tilting the sample around χ and rotating it around ϕ allows one to measure

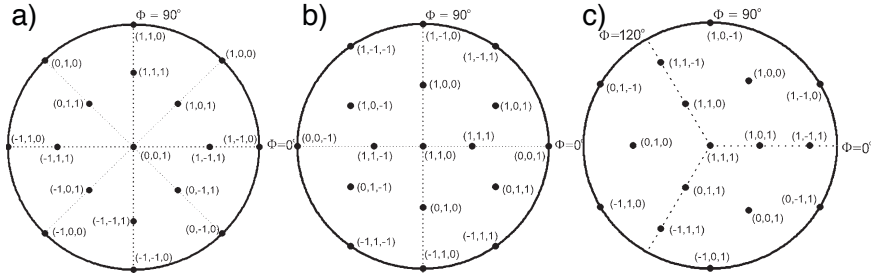

Figure 1.3. Reference frames for the three types of Si or Ge substrates: a) (001), b) (110) and c) (111). The figures show the (χ, ϕ) locations of the low-index poles of the substrate.

diffraction for the chosen family of lattice planes for every possible grain orientation, not just the one where the planes happen to be parallel to the sample surface. The result of such a measurement can be understood by imagining the sample placed at the centre of a hemisphere on which one marks for each grain the intersection between the normal to the chosen family $\{hkl\}$ of lattice planes (also called the pole of the plane family) and the sphere (see Fig. 1.2b as an illustration). The final (hkl) pole figure is then obtained by projecting the density of marks on the sphere onto a planar surface (see Fig. 1.2c) and thus depicts the statistical angular distribution of the direction of the normal to this plane family. The spherical coordinates (χ, ϕ) of the poles now become polar coordinates, with χ the radial distance and ϕ the polar angle. For a more detailed description on pole figures, the interested reader is referred to refs. [23–25].

In order to relate the directions of the film poles observed in a pole figure to directions of substrate poles and thus determine the orientation of a grain with respect to the substrate, a frame of reference is needed. This frame of reference is established by aligning the sample in order to locate poles for low-index substrate planes at specific (simple) (χ, ϕ) coordinates. The most frequently used reference frames in literature for (001), (110) and (111) Si or Ge substrates are depicted in Fig. 1.3. Unless stated otherwise, the pole figures shown in this review are measured using these reference frames.

An early use of this technique in texture research on thin film silicides dates back to 1992, when Bulle-Lieuwma *et al.* used lab-based X-ray diffraction to measure pole figures for texture studies of $CoSi_2$ films [28] (see Fig. 1.4a). In 2002, Özcan *et al.* [29] used synchrotron radiation to measure pole figures on $TiSi_2$ films, greatly reducing the measurement time for a

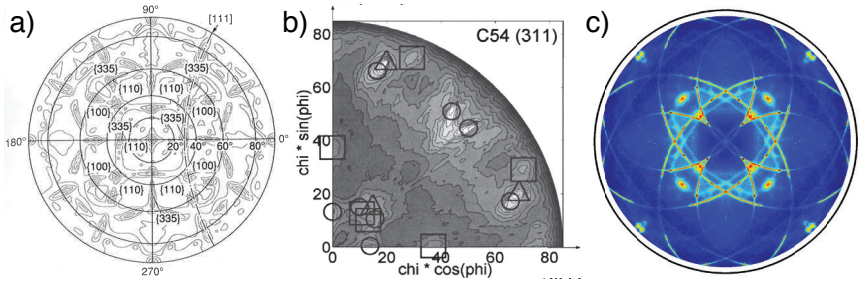

Figure 1.4. (a) $CoSi_2(110)$ pole figure recorded using a lab-based X-ray diffraction setup (reprinted with permission from Bulle-Lieuwma et al., J Appl Phys 71, 2211 (1992). Copyright 1992, American Institute of Physics). (b) C54-$TiSi_2(311)$ pole figure (reprinted with permission from Özcan et al., J Appl Phys 92, 5011 (2002). Copyright 2002, American Institute of Physics) and (c) NiSi(002)/(011) pole figure measured using a synchrotron based diffraction setup.

single measurement compared to a lab-based X-ray setup (see Fig. 1.4b). Further improvements to the technique eventually led to the discovery of axiotaxy in NiSi films [30] (see Fig. 1.4c), which will be discussed in section 1.3.3. Over the past decade, the texture of several thin film silicides and germanides has been investigated using these high-resolution synchrotron based pole figure measurements (see section 1.3.2). It must be noted that with the term *high-resolution* we want to emphasize the much improved resolution compared to pole figures measured on thin silicide/germanide films using a lab-based X-ray source. The typical resolution in such a synchrotron based pole figure measurement is 1° in χ, while the stepsize in ϕ is usually dynamically adapted during the measurement in order to obtain a uniform measurement grid.

A pole figure measured using the Schulz method described above only provides information for one specific d-spacing, i.e. usually a single lattice plane. Because the orientation of one plane does not fix the orientation of a grain, multiple pole figures for multiple families of crystal planes have to be measured in order to obtain complete texture information. As the measurement time for a single pole figure measurement on a thin silicide film typically requires a few hours, this process becomes very time-consuming. A solution is to use a linear or area detector covering a range of 2θ angles (or d-spacings) instead of a point detector, which only records diffraction at a single 2θ angle. In this way, several pole figures for different d-spacings can be measured simultaneously in a single measurement. Furthermore, the use of linear/area detectors also allows for the study of films contain-

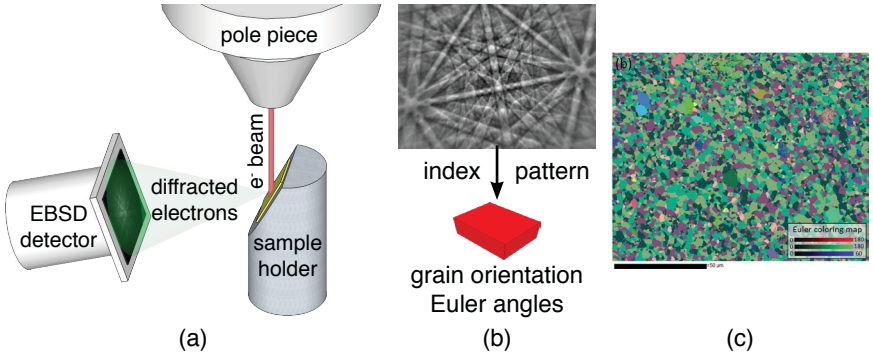

Figure 1.5. a) Schematic of a typical EBSD setup inside a SEM (Scanning Electron Microscope). b) Example of a recorded electron backscattered pattern (EBSP) showing the Kikuchi bands. Indexing such a pattern provides information on the local crystal phase and orientation. c) EBSD map carried out on θ-nickel-silicide over a rectangular measurement grid[38]. Different crystal orientations are given a unique color. In this way, individual grains and grain boundaries become visible.

ing unknown phases for which the 2θ positions of diffraction peaks are not known prior to the measurment. This idea of simultaneously measuring pole figures for different 2θ angles was introduced in the field of metallurgy in the 80's [31], but was only recently adopted in the field of thin silicide/germanide films [32–35]. Technical and mathematical details on using linear or area detectors for pole figure measurements can be found in Refs. [36] and [37].

1.2.2 Electron Backscattered Diffraction (EBSD)

Over the past decades, research fields such as metallurgy, ceramics and geology have exploited Electron Backscattered Diffraction (EBSD) which has become a standard technique to study different structural material properties such as grain size, grain boundary types and crystallographic texture. In this paragraph, the applicability of this technique for texture studies in thin film silicides/germanides will be discussed.

A typical EBSD setup (see Fig. 1.5a) is integrated in a Scanning Electron Microscope (SEM) and consists of a dedicated sample holder with a high tilt angle and an EBSD detector (usually a combination of a phosphor screen located in front of a CCD camera). The interaction between the incoming electron beam and the nuclei in the sample results in the generation of backscattered electrons. Part of these backscattered elec-

trons will eventually leave the sample after being diffracted by the local crystal structure on their way out. These electrons will generate an Electron Backscattered Diffraction Pattern (EBSP) which displays a collection of bands called *Kikuchi* lines (see top part of Fig. 1.5b). Analysis of the generated EBSP from a single grain is done by a procedure called indexing and provides information on the crystal structure and its orientation with respect to the substrate and the neighboring grains. For a detailed description of the generation and indexing of these EBSP's, the reader is referred to ref. [39].

While local determination of crystal structure and orientation can definitely prove very useful, the power of the EBSD technique resides mostly in its ability to perform measurements on a large grid. By measuring and indexing an EBSP on every grid point (which can be done automatically with dedicated indexing software), one can identify areas with the same crystal orientation. This large dataset provides a way to visualize the individual grains in the film along with their orientation and hence allows to study micro-structural features such as grain sizes, grain boundaries and texture. Furthermore, the local orientation information of a single grain and its neighbors provided by EBSD can be very useful in understanding macroscopically observed film properties (stress, contact resistance,...), as some silicides/germanides are known to be highly anisotropic (e.g. NiSi). An example of such an EBSD map on θ-nickel-silicide performed on a 50μm $\times$ 50μm rectangular grid can be seen in Fig. 1.5c, where each color corresponds to a specific crystal orientation.

The application of EBSD in the field of texture studies on thin silicide/germanide films was first reported in 2007 by De Keyser *et al.* [40], who used the technique to study the texture of NiSi films on Si(001). Doing so, they were able to confirm the texture components that were previously reported in NiSi films using X-ray pole figure measurements, but EBSD also allowed them to directly calculate volume fractions for the different texture components, which is indirect and much more involved to extract from X-ray pole figure measurements.

Although EBSD appears ideal to study texture in thin film silicides/germanides, some important limitations must be recognized [38, 40]. First of all, as grain sizes in very thin films can be quite small, the spatial resolution of a typical EBSD setup (usually a few tens of nanometers) may be inadequate to resolve individual grains. This leads to poorer quality and more difficult indexing of the recorded EBSD patterns as different grains (and thus different crystal orientations) will contribute to a single mea-

sured pattern. Secondly, interaction between the electron beam and the sample surface will lead to decomposition of residual hydrocarbons in the SEM chamber, resulting in a trail of carbon deposited on the sample. As an EBSD pattern is a diffraction pattern, any surface contamination will negatively influence the pattern's quality. One can circumvent this second issue by working with a (very expensive) UHV system. Ultimately, a trade-off has to be made between increasing the measurement time to increase the number of collected electrons in an effort to improve the pattern quality and decreasing it to lower surface contamination. In addition, lower quality EBSP's were also observed for alloyed silicides like $Ni_{1-x}Pt_xSi$, possibly due to the lower crystallinity of these materials[40]. Nonetheless, EBSD has been successfully applied to a couple of thin film silicide and germanide materials over the past years[35, 40–45].

1.3 Overview of texture in thin silicide/germanide films

In this section we survey the earlier research on texture in thin silicide and germanide films. Firstly, a short historical overview will be given covering the focus on epitaxial silicides during the 70's, 80's and 90's up until the advent of more detailed studies on polycrystalline silicide and germanide films using high-resolution synchrotron based pole figure measurements. Secondly, we will focus on the driving forces for texture development and the phenomenon of axiotaxy, a new type of texture in thin silicide/germanide films that was first reported in 2003 [30]. Finally, we will briefly discuss the texture observed in the three silicides that have been technologically most relevant over the past two decades: C54-$TiSi_2$, $CoSi_2$ and NiSi. As a summary, table 1.1 gives an overview of texture studies performed on a selection of silicide and germanide thin film materials. For each material, the observed texture components are provided along with key references, categorized by the measurement technique(s) used in the studies.

1.3.1 History of texture studies in thin silicide/germanide films

Interest in the texture of thin film silicides increased through the 1970s when it was discovered that certain silicides -which were investigated at

Material	observed texture	References per measurement technique RBS-C[a]	ED[b]	XRD[c]	EBSD[d]
NiSi	*epi, axio, fiber, transrot*		[46–48]	[30, 48–50]	[40]
$NiSi_2$	*epi*	[51–53]	[46, 51–53]	[51]	
δ-Ni_2Si/θ-Ni_2Si	*epi, fiber, transrot*			[32, 34, 45]	[45]
$TiSi_2$ (C49/C54)	*epi, axio*		[54–60]	[29, 58–62]	
$CoSi_2$	*epi, axio*	[53], [63]	[28, 53, 63, 64]	[28, 64–66]	
α-$FeSi_2$	*epi, axio*			[67], [68]	
Pd_2Si	*epi*	[69], [53]	[53, 69–71]		
PtSi/Pt_2Si	*epi*		[72–75]		
$CrSi_2$	*epi, axio*		[76]	[76]	
Rare-earth silicides/germanides	*epi*	[77]	[78], [77]	[77], [79], [80]	
NiGe	*epi, axio*			[81], [82]	
Co_5Ge_7	*epi, axio*	[83]	[83], [84]	[41]	[41]
$CoGe_2$	*epi, axio*	[83]	[83]	[41]	[41]
Pd_2Ge/PdGe	*epi, axio, fiber*		[85]	[85], [86]	
Pt-germanides	*epi*		[87], [88]	[88]	

Table 1.1. Overview of published studies concerning texture in thin silicid/germanide films on single crystal Si or Ge substrates. For each material, the types of texture that have been observed in different studies are given, along with references to the studies grouped by the experimental technique that was adopted.

[a] RBS-Channeling
[b] Electron Diffraction techniques
[c] X-Ray Diffraction
[d] Electron Backscatter Diffraction

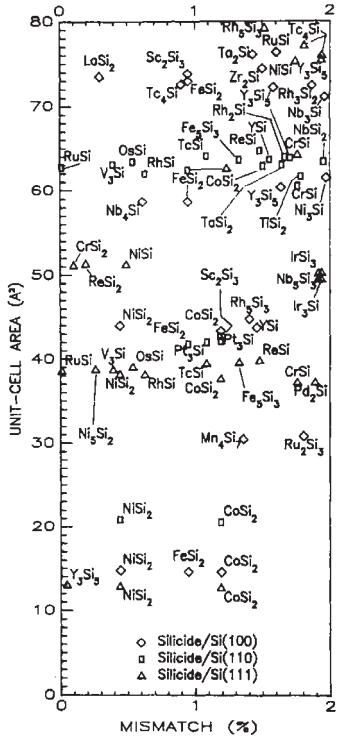

Figure 1.6. Overview of transition-metal silicides as a function of the lattice mismatch between film and substrate and the unit-cell-area of the matching area between film and substrate for Si(100), Si(110) and Si(111) substrates. Figure reprinted with permission from Zur et al., J Appl Phys 57, 600 (1985). Copyright 1985, American Institute of Physics

that time for use as ohmic contacts, Schottky barriers, gate electrodes and interconnects in microelectronic devices- grew epitaxially on single crystal silicon substrates. By the end of the 70s, there were four generally known epitaxial silicides, i.e. $NiSi_2$ [51], $CoSi_2$ [53], PtSi [72] and Pd_2Si [69, 70], for which the research on their epitaxial growth was reviewed by Tung *et al.* in 1982 [89]. In the following years, the focus in texture research on silicide films remained on the epitaxial growth as it was believed that using epitaxial silicides in microelectronics would lead to enhanced electrical contacts due to the excellent quality of the epi-silicide/silicon interface [90].

In general, epitaxy can be expected when the silicide and the silicon substrate have matching periodicity in the plane of the interface. For an

epitaxial alignment to be observed, it is generally assumed that the mismatch between the lattices must be below 2% in the plane of the interface. Fig. 1.6 shows an overview of different silicide phases along with their lattice mismatch to Si(001), Si(110) and Si(111) and their unit cell area. From the substantial amount of silicide phases visible in this figure, only the bottom left part (with $NiSi_2$ and $CoSi_2$ as the most important ones) will actually form epitaxial silicides through a simple solid-state reaction between a thin metal film and a silicon substrate. By the early 90s, a lot of effort had gone into improving existing and developing novel deposition techniques in order to grow silicides -at least partially- epitaxial on silicon [90]. The most important techniques are listed below:

- *Solid Phase Reaction (SPR)* - A thin metal film is deposited on the silicon substrate, usually through evaporation techniques, followed by a thermal anneal to form the desired epitaxial silicide phase.
- *Co-depostion and Reactive Deposition Epitaxy (RDE)* - Co-deposition of metal and Si vapor onto a heated substrate (often in an MBE system) results in the deposition of silicide layers. By controlling the metal/Si flux and the temperature, several authors have reported the formation of nucleation-controlled disilicides at temperatures significantly below their standard nucleation temperature[91, 92].
- *Templated MBE* - A thin epitaxial silicide film is grown using SPE which then serves as a template for continued growth through MBE[93].
- *Oxide/Titanium Mediated Epitaxy (OME/TIME)* - Dedicated technique for growing epitaxial $CoSi_2$ films, introduced by Dass[94] (TIME, 1991) and Tung[95] (OME, 1996). Epitaxial $CoSi_2$ layers are grown by introducing a very thin interlayer of Titanium (TIME) or silicon oxide (OME) between the silicon substrate and the Co film. Annealing this stack between 500-700°C leads to the growth of epitaxial $CoSi_2$ films. It is believed that the interlayer acts as a diffusion barrier, limiting the flux of Co towards the Si substrate and in this way promoting epitaxy. The OME technique turned out to deliver the best quality of epitaxial $CoSi_2$ films[96]. Later, it was also observed that interlayers of other metals like Cr, Mo, Ta and W can lead to epitaxial $CoSi_2$ if the thickness of the interlayer is carefully chosen[97, 98]
- *Ion beam synthesis (sometimes referred to as mesotaxy)* - A technique to form epitaxial silicides buried in the silicon substrate. First, the

buried silicide is formed through ion implantation of the transition metal (e.g. Co) into the substrate at an elevated temperature (300-400°C). Next, an anneal at higher temperature results in an epitaxial buried silicide. The technique was introduced by White *et al.* in 1986[99]. The interested reader is referred to ref. [100] for a detailed review on the technique.

- *Allotaxy* - An alternative technique for the growth of epitaxial buried silicides by using standard Molecular Beam Epitaxy instead of ion implantation, introduced by Mantl *et al.* in 1992[101]. The technique uses a sequence of MBE steps to grow epitaxial silicide precipitates in a single crystalline Si matrix on top of the Si substrate. High temperature annealing then forms the buried epitaxial layer out of the precipitates. A more detailed description can be found in ref. [102].

As texture research on thin film silicides at that time was mainly focussed on the growth of epitaxial films, little attention was given to the texture of silicides that were not suited for epitaxial growth, i.e. the majority of silicides. Because a solid-state reaction driven growth of these non-epitaxial films mostly leads to small-grained polycrystalline films, they were assumed to be randomly textured. During the 90s, it became increasingly clear that the use of epitaxial silicides in commercial microelectronic devices would be very difficult. As the SALICIDE process became the industry's technique of choice for the formation of silicide contacts on CMOS devices, studies started to emerge focussing on the texture of these polycrystalline, technologically relevant silicide thin films ($CoSi_2$, $TiSi_2$) [28, 58]. It was readily observed that these polycrystalline films display complex texture. This is illustrated by the Bragg-Brentano XRD spectra of NiSi on different Si substrates shown in Fig. 1.7, where it can be observed that the films are not randomly textured, as the relative peak intensities differ greatly from what is expected for a random powder of NiSi (indicated by the vertical lines at the bottom of the figure). The use of high-resolution synchrotron based pole figure measurements in the early 2000s really accelerated the study of texture in these thin silicide films.

And what about germanides? Because silicon had been the dominant material in the semiconductor industry for more than three decades, applications for germanide films were far less common than for silicide films. As a result, most early studies focus on silicide materials. However, since the early 2000s, germanium has been reintroduced in the semiconductor industry through the use of $Si_{1-x}Ge_x$ either to stress the channel of the

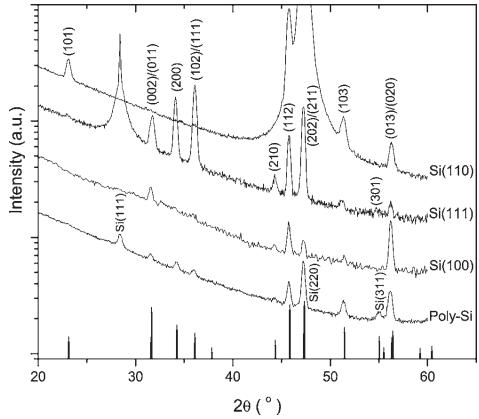

Figure 1.7. $\theta/2\theta$ XRD measurements for a thin NiSi film on Si(001), Si(110), Si(111) and poly-crystalline Si (poly-Si). The indexing of the peaks is done based on orthorhombic NiSi (JCPDS 73-1843). The theoretically expected relative peak intensities for a randomly oriented NiSi powder are visualized by the series of vertical lines at the bottom of the figure. The different relative intensities of the peaks for the single crystalline substrates are indicative of a non-random texture on these substrates. Figure reprinted with permission from Detavernier et al., J Appl Phys 103, 113526 (2008), Copyright 2008, American Institute of Physics.

transistor or more recently even as a replacement material for the channel altogether. For the future, researchers have been investigating the use of pure Ge as an alternative channel material because of its superior carrier mobilities compared to Si [21]. In this context, germanides are now being investigated as possible contacting materials for these Ge based devices, resulting in a considerable increase in germanide research during the past decade [22]. Nonetheless, literature on texture in these germanide materials is still scarce. There are a few early studies on the texture of Co_5Ge_7 on Ge(001) and (111) [83, 84], $CoGe_2$ on Ge(111) [83], Pd_2Ge on Ge(111) [85], Pt_2Ge, PtGe and $PtGe_2$ on Ge(111) [87] and NiGe on Ge(111) [103]. As for silicides, the introduction of high resolution pole figure measurements has allowed for a more detailed assessment of the texture in a few thin film germanides over the past decade [41, 82, 86].

1.3.2 Pole figure based texture studies

Figure 1.8 shows a collection of high-resolution synchrotron based X-ray pole figures measured over the past decade on a variety of silicide and germanide thin films grown on different substrate types. Complex patterns consisting of a combination of lines and spots can be observed, indicat-

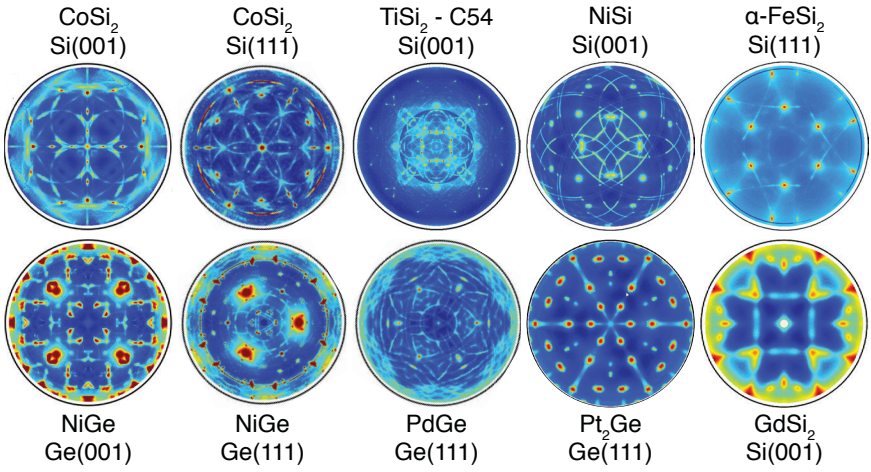

Figure 1.8. Collection of pole figures measured on different silicide and germanide materials grown on different substrate orientations. The pole figures were measured during the past decade using the high-resolution synchrotron based approach. Complex patterns of lines and spots can be observed, indicating complex non-random texturing in these films.

ing complex texturing of these films. The different texture components listed in the introduction that can occur in thin silicide/germanide films all produce specific features in a pole figure. This makes pole figure measurements an ideal technique to identify which texture components are present in a thin silicide/germanide film. The patterns that are generated by the different texture components are briefly discussed below:

- *Random texture* - Random (or absence of) texture corresponds to a uniform distribution of grain orientations, i.e. no preferential orientation is present in the film. This means that the pole figure for a specific {hkl} family of crystal planes will look featureless since every orientation of the {hkl} pole will be equally probable. This is illustrated in Fig. 1.9a.

- *Fiber* - A fiber texture is characterized by the constraint that one plane normal in all of the grains is perpendicular to the interface (this direction is called the fiber-axis). This will translate into a single spot in the center of the pole figure for that specific (hkl) plane. Due to the rotational degree of freedom around the fiber axis for the grains in a fiber texture, the plane normal of any other crystal plane will describe a circle around the fiber axis. This translates into a cen-

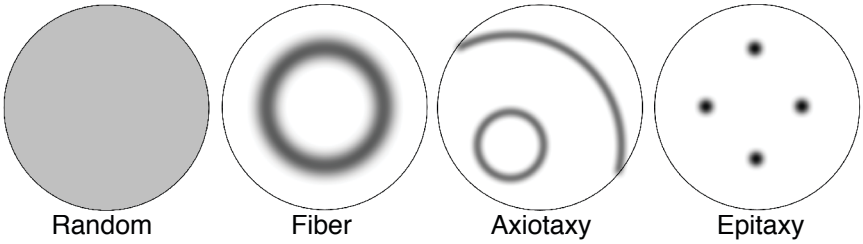

Figure 1.9. Sketches of pole figure features generated by the four possible texture components: random, fiber, axiotaxy and epitaxy.

tered ring on the pole figure (see Fig. 1.9b). Since a pole figure measurement for a specific (hkl) plane (thus for a specific d-spacing) also records diffracted intensity for all the symmetrically equivalent planes, as well as for other planes that happen to share the same d-spacing, multiple centered rings can appear on a single pole figure.

- *Axiotaxy* - Axiotaxy can be understood as an off-normal fiber texture (i.e. the fiber axis is not perpendicular to the interface). As such, this results in pole figures displaying circles around off-center positions on the pole figure (see Fig. 1.9c). A detailed description of this texture component, first measured in 2003 using high-resolution X-ray pole figures [30], will be given in the following section.

- *Epitaxy* - All grains belonging to a specific epitaxial texture component have the same orientation. This means that for any crystallographic plane, the plane normal will have a unique orientation. This will lead to a set of well-defined spots on the pole figures (due to symmetrically equivalent planes being recorded too). This is illustrated in Fig. 1.9d.

As can be seen from table 1.1, a combination of different texture components has been observed in many silicide/germanide thin films grown by solid-state reactions. These observations have only been possible thanks to the development of the synchrotron based X-ray pole figure technique introduced by Özcan *et al.* in 2002 to study the texture of C54-$TiSi_2$ [29]. Only a year later, the use of *high-resolution* synchrotron based pole figures resulted in the discovery of axiotaxy [30]. In the following years, detailed texture studies of different silicide and germanide materials were carried out using this technique, revealing axiotaxy in a considerable number of

silicide/germanide materials (see table 1.1). More recently, the use of a linear or area detector instead of a point detector [36, 37] and the introduction of EBSD as a complementary technique [40] have enabled the ability to perform unambiguous phase identification of highly textured transient phases that form during the formation of NiSi[32, 34] or NiGe [104] (see section 1.4.1). In the near future, area detectors will be routinely used to record texture information in situ, enabling the study of texture evolution during silicide/germanide formation. This is possible as using an area detector effectively shortens the time needed for a pole figure measurement from hours to minutes, allowing one to measure a pole figure every few minutes while heating the sample at a steady heating rate [37].

1.3.3 Driving forces for texture selection

In general, the preferential orientation of grains in a thin film with respect to a single crystal substrate is driven by a minimization of the interface energy. Grains with different orientations will exhibit different interface energies as the bonding across the interface will be different. Thus, the lowest interface energies are achieved by optimizing this bonding across the interface between the film grain and the single crystal substrate.

1.3.3.1 Importance of periodicity

First, we consider the case of a perfectly flat interface between the film grain and the substrate. As both the film grain and the substrate have a periodic crystal structure, bonding can only be systematically optimized along a certain direction within the plane of the interface if the interface structure is periodic. This periodic interface structure then amounts to a 'matching' of the grain lattice and the substrate lattice along that direction within the plane of the interface. Optimization of the bonding may then occur through interface reconstruction, whereby the atoms in the first few atomic layers near the interface are re-arranged, analogous to surface reconstruction at the crystal/vacuum interface.

For a grain with an epitaxial orientation, this means that a periodic interface structure and thus a match within the plane of the interface must be achieved in two independent directions. When the film lattice and the substrate lattice have a similar crystal structure and the mismatch between the lattice constants of film and substrate is small, this can be easily achieved (e.g. $NiSi_2$ on Si). In the situation where the film and substrate mate-

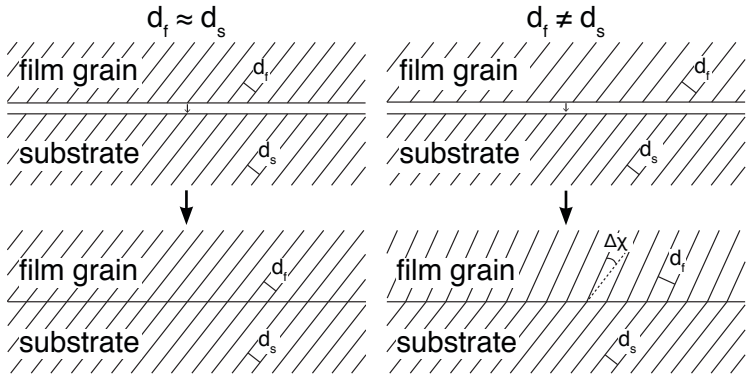

Figure 1.10. Illustration of how a low-index film plane and a low-index substrate plane can be matched at the interface to create a 1-dimensional periodic interface structure. Such a preferential grain orientation is called axiotaxy. If the matching planes have identical d-spacings, then they will be aligned across the interface (situation on the left). For planes with different lattice spacings, a relative tilt can still induce matching at the interface, but the planes will not be aligned (situation on the right). In practice, axiotaxy only seems to occur for aligned or nearly aligned planes (tilt angle $\Delta\chi < 5°$).

rial have a different crystal structure, such a 2D interface match is much less likely. In this case, a reduced interface energy can still be achieved by a match between a low-index plane from the grain and a low-index plane from the substrate that arrive at the interface, effectively creating a 1-dimensional periodicity within the plane of the interface. The simplest way in which this can be accomplished is when the film and substrate lattice plane have a (nearly) identical d-spacing. In this case, the film and substrate planes will be parallel and aligned across the interface (see Fig. 1.10, left column). This kind of preferential grain orientation is called 'axiotaxy' and was first observed in thin NiSi films on Si(001) by Detavernier *et al.* in 2003 [30]. Because of the 1-dimensional periodic interface structure achieved by plane alignment, the grains are left with one rotational degree of freedom around the normal to the matched plane in the film. As mentioned earlier, this causes circles on a pole figure which are centered around the location of the normal to the matched plane, called the 'off-normal fiber axis' or 'axiotaxy axis' (see Fig. 1.9).

In principle, such a 1-dimensional interface structure by plane matching can also be achieved for film and substrate planes with a different d-spacing by tilting the grain (over an angle $\Delta\chi$) in such a way that the d-spacing projected onto the interface plane becomes equal for the film and lattice

plane (see Fig. 1.10, right column). As such, axiotaxy could be expected to form very easily. However, texture studies on different silicides and germanides (see table 1.1) have shown that when axiotaxy is observed, the circles on the pole figures are always centered around a point that coincides or nearly coincides with the location of the pole of the low-index substrate plane that is matched with a low-index film plane, meaning that the tilt angle $\Delta\chi$ must be small for axiotaxy to occur. This suggests that axiotaxy only occurs if the grain can be oriented in such a way that a low-index film plane and a low-index substrate plane are (nearly) aligned across the interface.

To illustrate this, we consider the four axiotaxy components that are observed for NiSi on Si(001). The two most intense components are caused by plane alignment across the interface between NiSi(211) or NiSi(202) and Si(220), characterized by a difference in d-spacing between film and substrate planes of merely 0.05% for both NiSi planes. The two other components are only weakly visible in pole figures and are caused by a matching at the interface between NiSi(103) or NiSi(112) and Si(220) planes. The difference in d-spacing (at room temperature) between these NiSi planes and Si(220) is -7.6 and +3% for NiSi(103) and NiSi(112) respectively. For these orientations, the center of the axiotaxy circles has been observed at $\chi = 40.8°$ and $\chi = 46.5°$. As the Si(220) pole is located at $\chi = 45°$, this means that the NiSi(103) and NiSi(112) planes have a tilt $\Delta\chi$ of -4.2 and $+1.5°$ respectively, reducing the difference in the projected d-spacing with Si(220) to less then 0.01% in both cases [30, 50], which creates the 1-dimensional interface match as sketched in the left column of Fig. 1.10. The fact that these two last components are only weakly observed illustrates the general observation that axiotaxy preferably occurs when the interface match can be achieved through plane alignment ($d_f \approx d_s$, $\Delta\chi \approx 0$) and is less likely to be observed when larger tilt angles are needed to obtain the match at the interface. In practice, axiotaxy components where tilt angles larger than 5° are needed to ensure interface matching have not been observed.

To understand why axiotaxy is only observed when the matching between lattice planes of film and substrate is achieved through plane alignment or through very small tilt angles, Detavernier *et al.* considered the robustness of the formed 1-dimensional periodic interface structure with respect to interfacial roughness [30]. The insets of Fig. 1.11 clearly show that for perfect plane alignment across the interface, the 1D periodic match is ensured irrespective of the interface curvature, while for a 1-dimensional

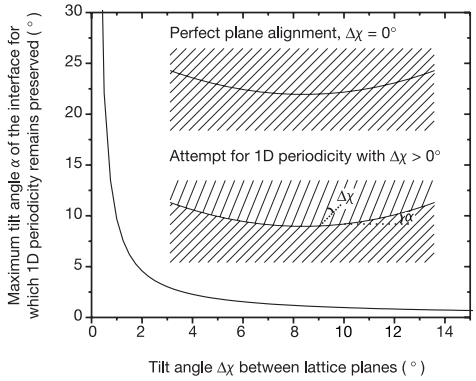

Figure 1.11. Maximum tilt angle α through which the interface can curve while maintaining good periodicity (defined as a maximum mismatch of 0.5% between the projected d-spacing of film and substrate planes) as a function of the tilt angle $\Delta\chi$ of the film planes. The larger the allowed value of α, the more stable the 1-dimensional periodic interface structure is with respect to interfacial curvature. Reprinted with permission from Detavernier et al., Nature 426, 641 (2003). Copyright 2003, Nature Publishing Group.

match obtained through a tilt angle $\Delta\chi \neq 0$ the match at the interface deteriorates as the interface tilt angle α increases. The graph in Fig. 1.11 shows the maximum interface tilt that still preserves a good periodic interface match (defined as a maximum difference of 0.5% in projected d-spacing) as a function of the tilt angle $\Delta\chi$ between the film and substrate planes. This clearly shows that for increasing $\Delta\chi$, the range of curvature over which the interface maintains good periodicity shrinks dramatically. The fact that axiotaxy is only observed for small tilt angles $\Delta\chi$ is probably related to the irregularly shaped interface that is present during the nucleation of a new phase during a solid-state reaction between the film and the Si/Ge substrate. This will be discussed in more detail in the next section.

Due to the 1-dimensional match within the interface plane for an axiotaxy texture, the different grains belonging to an axiotaxy texture component are distributed with varying rotations around the axiotaxy axis, which results in the observed circular patterns when measuring pole figures. However, when glancing over the different axiotaxy containing pole figures included in this review or in the references included in table 1.1, one can observe that the intensity along such an axiotaxy circle is rarely uniform. This can be understood by considering that for grains belonging to the same axiotaxy component, a different film plane will be parallel to the interface depending on the rotation around the axiotaxy axis. For any

such rotation, the interface will at least be periodic in one direction (due to the axiotaxy-related plane alignment), but some rotations around the axiotaxy axis might result in periodicity along a second, independent direction within the plane of the interface, resulting in an even lower interface energy. As a result, a larger fraction of the axiotaxy grains will orient in this way, resulting in a higher intensity on the axiotaxy rings for those rotations around the axiotaxy axis. If the periodicity in the second direction is well-defined, a 2-dimensional periodic interface structure is obtained and the subset of grains having this orientation will cause well-defined epitaxy spots on the pole figures at certain positions along the axiotaxy lines. As such, these grains constitute an epitaxial texture component that is a subset of the underlying axiotaxy texture. In some cases, such epitaxial spots are observed at the crosspoint between axiotaxy circles from two different axiotaxy components. In this case, the two determining constraints for the epitaxial alignment are defined by the two axiotaxy relations and the epitaxy is referred to as *double axiotaxy* (see e.g. section 1.3.4.2 on $CoSi_2$ texture). From the arguments above, one can expect an epitaxial texture component that is a double axiotaxy to be unaffected by interface roughening (e.g. in the case of agglomeration), whereas an epitaxy that results from mere interface matching will disappear in case of interface roughening.

1.3.3.2 Texture selection during solid state reactions

So far, axiotaxy has mainly been observed in materials that are formed through solid-state reactions between a thin film and an underlying substrate. For silicides, observations are reported for NiSi on Si(001), Si(110) and Si(111) [50], $CoSi_2$ on Si(001), Si(110) and Si(111) [66], α-$FeSi_2$ on Si(001) and $CrSi_2$ on Si(001) [76]. In the case of germanides, axiotaxy has been reported for NiGe on Ge(001) and Ge(111) [82], Co_5Ge_7 and $CoGe_2$ on Ge(001) and Ge(111) [41] and PdGe on Ge(001) and Ge(111) [86]. Beside the typical observations in silicide/germanide materials, axiotaxy has also been observed more recently in Ti_2AlC films formed on (0001), $(10\bar{1}0)$ and $(1\bar{1}02)$ oriented saphire substrates [105] and for MnP nanoclusters formed in GaP epilayers on GaP(001) substrates [106]. All these results have in common that the materials under consideration are *formed* through solid-state reactions that are governed by (long range) solid-state diffusion and nucleation. Regarding texture selection during these types of reactions, there are two important points to consider.

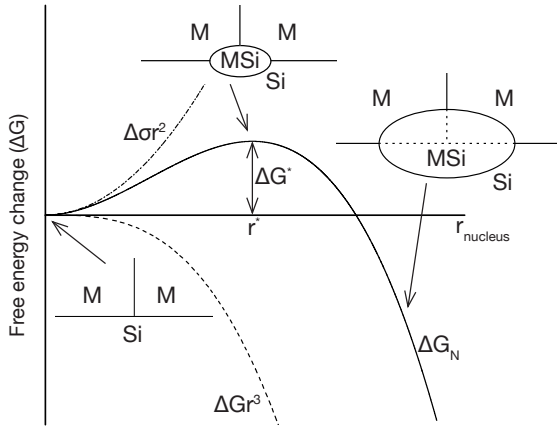

Figure 1.12. Evolution of the free energy change associated with the creation of a nucleus with radius r. The contributions of the surface energy 'cost' $\Delta\sigma_A$ and the volume energy gain ΔG_V are drawn separately. The competition between these opposing effects gives rise to an energy barrier ΔG^* (and an associated critical radius r^*) that a growing nucleus must overcome before it can continue to grow.

First, the formation of a new phase in the phase sequence during a solid-state reaction starts with the nucleation of very small nuclei of the new phase at the interface between the preceding phase and the substrate [107]. Even if the barrier for nucleation is low and diffusion becomes the rate-limiting factor, the nucleation must still occur. This means that the orientation of the new grains and thus the texture of the film will be determined at the interface between the nuclei of the new phase and the substrate. According to the classical theory of nucleation, the change in free energy associated with the creation of a shperical nucleus of a new phase (e.g. a metal silicide MSi) with radius r at the interface between the metal film M and the Si substrate is determined by a competition between two energy contributions. On the one hand, there is a 'gain' in volume free energy $\Delta G_V \sim r^3 \Delta G$ as the formation of the phase MSi is enabled by it's lower volume free energy ΔG compared to the separate phases M+Si. On the other hand, there is a surface energy 'cost' $\Delta\sigma_A \sim r^2 \Delta\sigma$ associated with the change in interface energy $\Delta\sigma$ due to the creation of the MSi nucleus. The total free energy change for a nucleus with radius r is thus given by:

$$\Delta G_N(r) = ar^2 \Delta\sigma - br^3 \Delta G \tag{1.1}$$

Here, a and b are constants that account for the reality of a nucleus being not perfectly spherical. This evolution of the free energy ΔG_N with the nucleus radius r is illustrated in Fig. 1.12, where the surface energy 'cost' and the volume energy 'gain' are shown together with the combined free energy change ΔG_N. From equation 1.1 and Fig. 1.12, it is clear that there is an energy barrier ΔG^* for nucleation to proceed with a corresponding critical nucleus radius r^* given by:

$$r^* \sim \frac{\Delta\sigma}{\Delta G} \tag{1.2}$$

$$\Delta G^* \sim \frac{\Delta\sigma^3}{\Delta G^2} \sim \frac{\Delta\sigma^3}{(\Delta H - T\Delta S)^3} \tag{1.3}$$

From the arguments above, one can see that the nucleation of a new phase can be facilitated by reducing the energy 'cost' $\Delta\sigma_A$, which can be achieved in a couple of ways. Firstly, nucleation of grains of a new phase typically takes place at the grain boundaries (see sketches in Fig. 1.12) as this results in the removal of the grain boundary interface energy. Secondly, the orientation of the newly formed nucleus with respect to the substrate directly impacts the interface energy. This is where texture comes into play as e.g. an epitaxial grain orientation will result in a very low interface energy due to the 2-dimensional periodic interface structure. Lastly, if the low interface energy of an epitaxial orientation is not accessible, a forming nucleus can still reduce the energy cost $\Delta\sigma_A$ by obtaining a curved interface as this minimizes the interface area between the new phase and the surrounding phase(s) and substrate. In this case, an axiotaxial grain orientation can form at this curved interface as was discussed above, resulting in an extra reduction in interface energy.

Second, equation 1.3 shows that the activation energy for the nucleation of a new silicide/germanide phase at the interface of the preceding phase with the Si/Ge substrate varies as $\Delta\sigma^3$ and $1/\Delta G^2$, with $\Delta G = \Delta H - T\Delta S$ the free energy change for the reaction between the substrate and the preceding phase into the new phase. In a typical binary solid-state reaction, the entropy change ΔS is small compared to ΔG and thus the enthalpy change ΔH can be taken as a good measure for ΔG. From this $\Delta\sigma^3/\Delta H^2$ dependence of the activation energy for nucleation it follows that for phases having a low enthalpy change, the contribution of the interface energy becomes much more important [107]. As a result, for these phases, the preferential grain orientation has a high impact on the

nucleation barrier. This explains the observation that, when considering literature reports on texture in thin silicide/germanide films over the past decade, texture is typically much more pronounced for phases that appear at a later stage in a phase formation sequence, as they are usually characterized by a smaller enthalpy change (ΔH) compared to the phase(s) that appear(s) first [107].

Up until this point, the focus of this discussion has been on nucleation. However, one might argue that diffusion processes are equally important in the kind of solid-state reactions under discussion when the activation energies for both kinds of processes are comparable. For example, the identity of the dominant diffusing species is considered an important parameter in silicidation and germanidation reactions. When focussing on the texture evolution during such a reaction, one might intuitively argue that axiotaxy is more likely when the metal is the diffusing species. While this is true e.g. for the formation of NiSi or $CoSi_2$ where the metal is the dominant diffusing species and an axiotaxial grain orientation is indeed observed, the opposite is observed in the Ti-Si system where Si is the dominant diffusion species during the formation of $TiSi_2$ and an axiotaxial alignment is also obtained (see par. 1.3.4.1). In general, the influence of diffusion processes on the texture evolution during these solid-state reactions is currently far from understood and further investigation is needed. For nucleation however, the connection with texture evolution is much clearer (as was discussed above): it is at nucleation that a grain will fix its orientation. Even when the barrier to nucleation is low, it must still occur! So far, there has only been one, very recent observation reported in literature of a silicidation reaction where the orientation of the grains of a single phase changes after nucleation. For 50nm Pd films deposited on Si(001), Richard *et al.* [108] observed the formation of a peculiar texture when the Pd_2Si phase forms. The initially formed Pd_2Si layer showed four orientation variants and a large tilt ($19.5°$) of the c-axis with respect to the surface normal. After the formation of a continuous Pd_2Si film, the grains were found to collectively rotate during a further heat treatment. This rotation was argued to result from the drive to lower the grain-boundary (GB) energy of the high-energy GBs that result from the initial grain orientation variants. This lowering of GB energy is believed to occur through GB diffusion. As such, this study and more specifically the introduction of *in situ* pole figure acquisition during heat treatments might be the starting point for future investigations concerning the link between texture evolution and diffusion processes during silicidation and germanidation reactions.

1.3.4 Texture of $TiSi_2$, $CoSi_2$ and NiSi

In order for a silicide or germanide to be useful as a contacting material in MOSFET devices, the material has to fulfill a number of requirements such as low electrical resistivity, low contact resistance, good thermal stability, etc. (see ref. [109] for a full list of requirements). Even if the silicide's bulk properties are acceptable, often it was proved to be challenging to form the required phase in the small contact areas where they are needed. Over the years, three silicides have found extensive use as contacting material in MOSFET devices, i.e. C54-$TiSi_2$, $CoSi_2$ and NiSi. Below, we will briefly describe the texture of thin films of these materials when formed through a solid state reaction between a thin metal layer (Ti, Co or Ni) and a single crystalline silicon substrate.

1.3.4.1 $TiSi_2$

The first silicide to be used on a large scale with the SALICIDE process was $TiSi_2$. There are two polymorphs of this phase, i.e. base-centered orthorhombic C49-$TiSi_2$ (JCPDS 23-964, a=0.3562 nm, b=1.353 nm and c=0.355 nm) and face-centered orthorhombic C54-$TiSi_2$ (JCPDS 35-0758, a=0.8268 nm, b=0.8553 nm and c=0.4798 nm). Of these two, the C54 phase has by far the lowest resistivity and thus is the polymorph needed in the contact regions. For devices with feature sizes larger than 250 nm, different techniques were developed to form this low-resistive C54 phase [110]. For smaller devices, the nucleation controlled transformation from C49 (which forms before C54 in the solid state reaction) to C54 is inhibited, making it very difficult to form the desired C54-$TiSi_2$. Thus, for devices with feature sizes below 250nm, a process using an alternative silicide such as $CoSi_2$ or NiSi had to be developed.

Early studies on texture of C54-$TiSi_2$ thin films on silicon date back to the late 1980s [54–57]. These studies focussed mainly on the texture of C54 on Si(111) as it was observed that the growth of this phase on Si(111) was mainly epitaxial and the interest in epitaxial silicides was high at that time. These studies mainly used XRD ($\theta/2\theta$ and grazing incidence) and electron diffraction techniques to identify two main epitaxial texture components for C54 on Si(111): (1) C54(110)//Si(111) & C54($\bar{3}31$)//Si($2\bar{2}0$) and (2) C54(100)//Si(111) & C54(040)//Si($02\bar{2}$).

Epitaxial growth of C54 on Si(001) was also studied by several groups during the 1990s [58–61]. It was found that C54 epitaxy on Si(001) is more difficult than on Si(111), especially for C54 films grown by a solid-

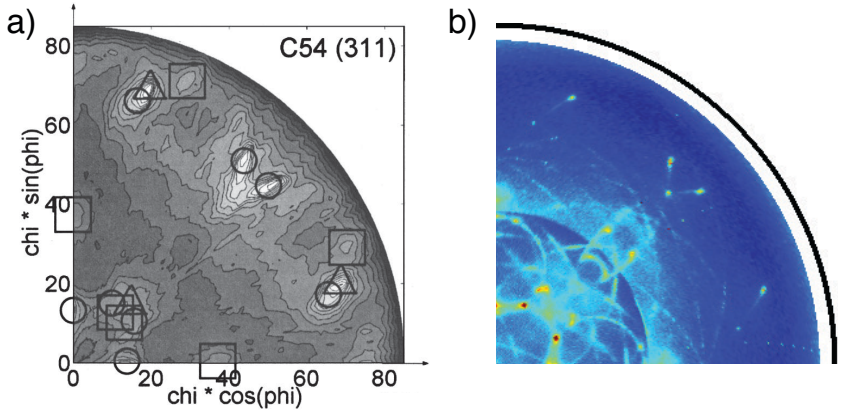

Figure 1.13. Selection of $TiSi_2$ pole figures with a) $TiSi_2$(311) on Si(100) (reprinted with permission from Özcan et al., J Appl Phys 92, 5011 (2002). Copyright 2002, American Institute of Physics) and b) $TiSi_2$(311) on Si(100) measured with high resolution pole figure setup.

state reaction from Ti films deposited at low temperatures. In 2002, Özcan *et al.* performed a detailed study on the texture of the C54 (and C49) phase formed on Si(001) by using synchrotron based pole figure measurements [29]. For C54 films grown on Si(001) from both sputter- and CVD-deposited Ti films they observed epitaxial components in which a low-index C54 plane is parallel to a Si{111} plane (similar to the observed epitaxies of C54 on Si(111)) instead of parallel to the Si(100) interface plane. They explained these observed orientations by ledging of the substrate on {111} planes during silicide formation. Next to these epitaxial texture components, more recent, yet unpublished high-resolution pole figure data also show the presence of axiotaxy in C54-$TiSi_2$ films on Si(100) [111].

1.3.4.2 $CoSi_2$

When feature sizes in MOSFET devices dropped below 250nm, $CoSi_2$ became the contacting silicide of choice as it does not suffer from the nucleation problems observed with $TiSi_2$ contacts in these smaller lines [16]. This silicide was used until linewidths in devices reached 50nm and several issues with $CoSi_2$ formation in these narrow lines arose [17]: void formation, the inability to form $CoSi_{2-x}Ge_x$ phases and the higher formation temperature of $CoSi_2$ when Ge is introduced in the source and drain

regions and the high silicon consumption for $CoSi_2$ formation, which can be problematic when using SOI (Silicon On Insulator) substrates.

Because of the small lattice mismatch ($\approx$ 1.2%) and similar crystal structure between $CoSi_2$ (cubic CaF_2 structure, a=0.536nm) and Si (cubic diamond structure, a=0.543nm), $CoSi_2$ is expected to easily form epitaxially on Si substrates. As a result, a lot of effort was put in developing and optimizing methods to grow epitaxial $CoSi_2$ layers during the 80s and 90s (MBE, OME/TIME, mesotaxy, see section 1.3.1). However, it has proven surprisingly difficult to grow epitaxial layers of $CoSi_2$ through a simple solid-state reaction between a thin Co film and a Si substrate, especially on Si(001). Such a reaction results in a polycrystalline $CoSi_2$ film, the texture of which was first studied in detail by Bulle-Lieuwma *et al.* [28] in 1992 using pole figures and TEM. They observed that forming $CoSi_2$ on Si(001) through such a solid-state reaction resulted in different epitaxial components occurring simultaneously, which explained the polycrystalline nature of the films.

In 2004, Özcan *et al.* used high-resolution synchrotron based X-ray pole figure measurements to re-assess the texture of $CoSi_2$ on Si(001) [65]. In addition to the epitaxial components, their detailed measurements allowed them to identify three axiotaxy components that result from the alignment of a $CoSi_2\{110\}$-type of plane with a $Si\{110\}$-type of plane. A few years later, De Keyser *et al.* used the same type of pole figure measurements to perform a detailed study of the texture of $CoSi_2$ films on three substrate orientations, i.e. Si(001), Si(110) and Si(111) [66]. Their results revealed a complex texture on all three substrate orientations, as evidenced by the complex patterns of epitaxial spots and axiotaxy lines visible on the $CoSi_2$(111) and (110) pole figures on different substrate orientations shown in Fig. 1.14. The axiotaxial alignment that was previously observed by Özcan *et al.* on Si(001) substrates [65] was observed here on all three substrates. Furthermore, De Keyser *et al.* found that almost all observed epitaxial components were strongly related to the observed axiotaxy, with either one or both constraints of each epitaxial component arising from the axiotaxial alignment of the $CoSi_2\{110\}$ and $Si\{110\}$ planes across the interface. The case where both epitaxial constraints are linked to axiotaxy or plane alignment was termed 'double axiotaxy' (see also section 1.3.3). For a full discussion of all texture components observed in $CoSi_2$ films, the reader is referred to ref. [66].

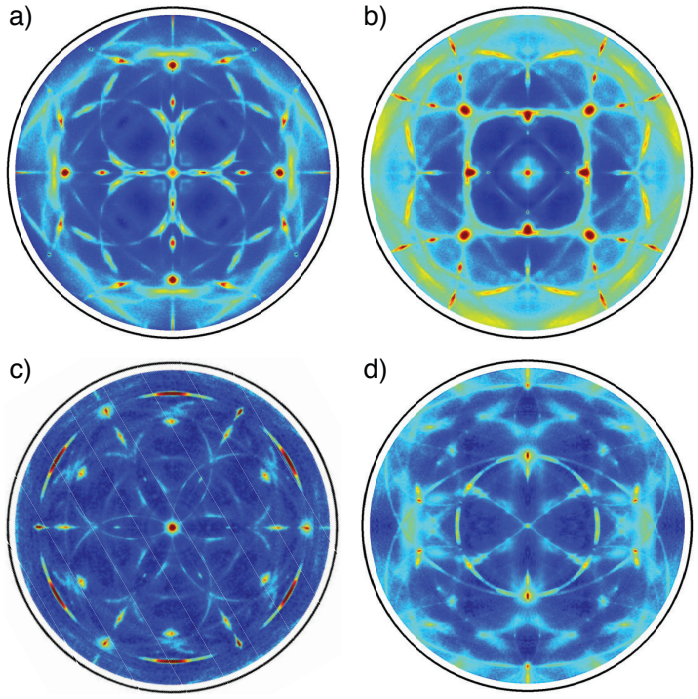

Figure 1.14. Selection of $CoSi_2$ pole figures with a) $CoSi_2(111)$ on Si(100), b) $CoSi_2(110)$ on Si(100), c) $CoSi_2(111)$ on Si(111) and d) $CoSi_2(111)$ on Si(110)

1.3.4.3 NiSi

For technology nodes starting from 65nm, NiSi became the industry standard contacting material due to its low formation temperature, low resistivity, compatibility with SiGe, low Si consumption (compared to $CoSi_2$ and $TiSi_2$) and absence of fine-line effects. However, there are two important issues with NiSi thin films, i.e. thermal stability (NiSi transforms into $NiSi_2$ at higher temperatures) and morphological stability (NiSi films agglomerate at higher temperatures), the latter degradation mechanism being the most important for thin films (<30nm) [112]. In 1999, Mangelinck *et al.* [18] discovered that alloying a NiSi film with Pt (10-15 at.%) can improve its thermal stability substantially. In section 1.4.3 we will discuss how the texture of a NiSi film partly explains this stabilization through Pt alloying.

As NiSi was not one of the silicides considered for epitaxial thin film

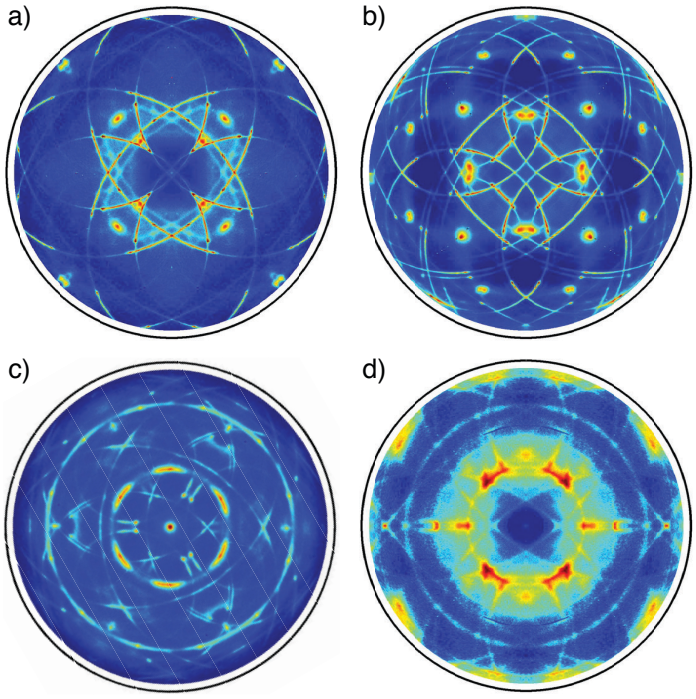

[t]

Figure 1.15. Selection of NiSi pole figures with a) NiSi(002)/(110) on Si(100), b) NiSi(112) on Si(100), c) NiSi(002)/(110) on Si(111) and d) NiSi(002)/(110) on Si(110)

growth (unlike $NiSi_2$, which has a very close match to Si), little attention was given to its texture until it was considered as a possible replacement for $CoSi_2$ at the 65nm technology node. Because early studies showed that polycrystalline silicide films could display unusual and complex texture [28, 29], interest in the texture of NiSi films increased dramatically. High resolution X-ray pole figure measurements performed at the IBM X20A beamline (Brookhaven National Lab, NY, USA) on thin NiSi films grown on Si(001) substrates were carried out and eventually led to the discovery of axiotaxy in 2003 [30]. In 2008, Detavernier *et al.* published a detailed follow-up study on the texture of thin NiSi films on Si(001), Si(110) and Si(111) substrates. Pole figures of NiSi films on these three substrates reveal a complex texture (see Fig. 1.15) that is a combination of axiotaxy and epitaxy components. On all three substrates, the bright patterns of lines are caused by two axiotaxy components for which either the NiSi{202} or {211} planes are aligned with Si{110} planes across the interface. Two

weaker axiotaxy components were also identified on Si(001) and Si(111). These components result from a match at the interface between either the NiSi{103} or {112} plane and the Si{220} plane which is made possible by a slight tilt of the off-normal fiber axis[30, 50] (resulting in a difference in projected d-spacing of less then 0.5%). Next to the axiotaxy, several epitaxial components were also identified on all three substrate types. Similar to the case of $CoSi_2$ discussed above, some of these epitaxial components could be linked to the axiotaxy, i.e. one of the two epitaxial constraints is defined by the alignment of NiSi(211) or (202) and Si(220). However, for NiSi, no epitaxial components that result from 'double axiotaxy' were observed. For a complete overview and discussion of the texture components observed in NiSi thin films, the reader is referred to ref. [50].

In addition to the axiotaxy and epitaxy, a different microstructure has been reported to occur in thin NiSi films on Si(001). Alberti *et al.* observed the formation of so-called 'transrotational' domains, both in Ni_2Si and NiSi films [48, 113]. These domains result from a bending (either spherical or cylindrical) of specific crystallographic planes of the film in order to adapt to the crystal structure of the substrate [48]. This tranrotational NiSi has been observed to form under different experimental conditions (annealing ambient, substrate doping, etc.) as long as specific care is taken during the deposition of the initial Ni film: the Ni must be deposited at slightly elevated temperatures in order to obtain a Ni-rich intermixed Ni:Si layer and when the thickness of the deposited Ni surpasses $\sim$7nm, a low temperature isothermal anneal is necessary to form transrotational NiSi. Recently, Alberti *et al.* extensively reviewed the formation and properties of these transrotational Ni-silicides [114].

1.4 Influence of texture on silicide/germanide formation and properties

As was mentioned in the preceding sections, contact formation in CMOS fabrication happens through a solid-state reaction between a thin metal film and the Si or Ge substrate. The formation of a thin silicide/germanide film through such a solid-state reaction proceeds through a complex interplay of silicon and/or metal diffusion and nucleation of new silicide phases. Texture can greatly influence this process as the orientation of the individual grains determines the type and orientation of grain boundaries (affecting diffusion) and the interface energy (affecting nucleation). For similar

reasons, texture will also influence the stability of these films against either agglomeration (breaking-up of the film into islands, destroying the low resistance) or transformation into a thermodynamically more stable silicide (e.g. transformation of NiSi to $NiSi_2$ at high temperatures).

A high quality silicide/germanide contact is characterized by functional properties such as low sheet resistance, low contact resistance, low stress, appropriate Schottky barrier height, etc. [7]. With the continued reduction in feature sizes, the contact formation scheme has evolved from a self aligned silicide contact to what is referred to as a *trench contact*. Here, the silicide is formed at the bottom of a very narrow trench (< 20nm in width) and then filled with a conductive metal. As a result, the resistivity of the silicide itself is much less critical since the current can be carried laterally in the metal. However, because of the size reduction, the intrinsic contact resistance of the silicide/Si interface becomes the dominant factor in the external resistance of devices. Thus, understanding and controlling interface properties becomes crucial. As such, properties like Schottky barrier height, doping concentrations, interfacial bonding and effects of impurities must be controlled in dimensions that become smaller than a typical grain.

Over the years, film texture has been shown to affect all of these interfacial properties. As the bonding with the Si/Ge substrate varies with film orientation, interfacial properties will vary with film texture. Furthermore, many of these properties will be affected by the anisotropy of the film lattice. The manifestation of this anisotropy on the macroscopic level will depend on how the individual grains in the film are oriented, i.e. on the texture. One can imagine that for films consisting mainly of epitaxially aligned grains the anisotropy can be maintained macroscopically. For a randomly textured film or a film with many different texture components, the anisotropy will be averaged out and the film will display isotropic behavior on the macroscopic scale with possible local variations due to the different components. As an example, the NiSi lattice is extremely anisotropic and shows very large thermal expansion coefficients with even larger variations depending on the crystal axis (from about 40 ppm/°C to about -40 ppm/°C) [115]. This will cause local variations in strain at the interface.

Clearly, the influence of texture on the formation, the stability and general properties of these thin silicide/germanide films can be significant. Texture studies using pole figures or EBSD can provide conclusive information when identifying silicide/germanide phases formed during a solid-

state reaction. This is especially the case when the formed phase exhibits strong epitaxial or fiber components, as standard $\theta/2\theta$ XRD techniques provide limited information for such films [36] (see also section 1.2.1). In this section, we will give a comprehensive overview of studies that have investigated the influence of texture on silicide/germanide phase formation and properties.

1.4.1 Influence on phase formation

In literature on thin film silicides and germanides, the concept of 'phase formation' refers to the sequence of silicide/germanide phases that form during the solid-state reaction between the metal film and the silicon/germanium substrate. An efficient technique to identify the different silicide/germanide phases that form during the reaction is *in situ* X-ray diffraction, where a linear detector is used to repeatedly capture an X-ray diffraction spectrum with a set time-interval while the sample is heated to a specific temperature at a fixed heating rate. However, as was mentioned earlier, the fixed $\theta/2\theta$ geometry used in this measurement only represents a very small subset of possible diffraction positions and limits our ability to detect phases that are highly textured. In a case where ambiguous diffraction peaks or no diffraction peaks are detected at a given temperature, pole figure or EBSD measurements performed on samples quenched at that specific temperature help to unequivocally identify the crystal structure present at that stage of the reaction.

We will illustrate this point by using the phase formation sequence during the reaction of a thin Ni film on Si. Because of the importance of NiSi as a contacting material in modern CMOS devices, this Ni-Si system has received a lot of attention in literature. Phase formation in this system has been extensively studied over the past three decades using TEM based techniques in the older studies (80s and 90s) and *in situ* XRD in the more recent studies (late 90s and 2000s), often complemented with additional techniques like RBS (for elemental depth distributions), laserlight scattering (for monitoring film roughness) and resistivity measurements [17, 46, 47, 116–119]. Most of these studies focussed on phase formation on a Si(001) substrate, as this is technologically the most relevant orientation. Fig. 1.16 shows an *in situ* XRD measurement for a 10nm Ni film on Si(001) which clearly shows a complex phase formation sequence before the formation of the wanted NiSi phase. The relatively low amount of observed peaks and the overlap of different peaks made the identification

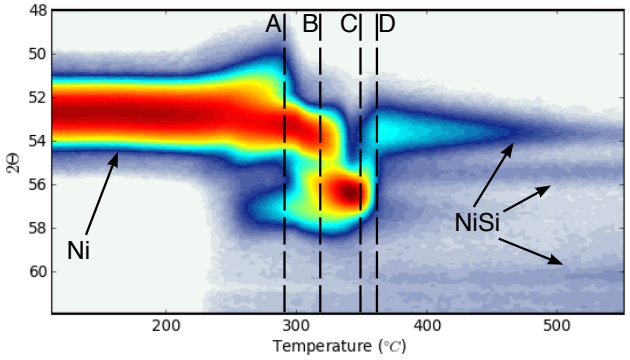

Figure 1.16. *in situ* XRD ($\lambda = 0,18$nm) on a 10nm Ni film on Si(001) measured at a heating rate of $1°$C/s, showing the XRD peaks as a function of temperature. A complex phase formation sequence can be observed between the as-deposited Ni and the wanted NiSi phase. The dashed lines mark the temperatures where pole figures were measured by Gaudet *et al.*[34] (see Fig. 1.17)

of the phases not straightforward. By the mid 2000s, consensus was more or less reached on the co-existence of multiple metal-rich phases (observations of δ-Ni_2Si, $Ni_{31}Si_{12}$ and Ni_3Si_2 were reported) that are possibly highly textured[119, 120].

However, the growing interest in the texture of these thin silicide films during the past decade and the corresponding development of high resolution XRD pole figure measurements on such films drove researchers to reassess the complex metal-rich phase formation sequence in the Ni-Si system. In 2010, Gaudet *et al.* published a detailed study on this subject using *in situ* XRD combined with high-resolution pole figures measured on samples quenched at different temperatures during the solid state reaction (see figures 1.16 and 1.17). According to the observations of Gaudet *et al.*, the as-deposited Ni displays a strong fiber texture with the Ni(111) plane being parallel to the substrate, which is evidenced by the spot in the center and the ring at $\chi = 70.5°$ (= angle between Ni{111} planes) in the Ni(111) pole figure (top left in Fig. 1.17). Upon annealing, the reaction commences with the formation of orthorhombic δ-Ni_2Si (*Pnma*, $a = 0.499$nm, $b = 0.372$nm, $c = 0.706$nm), exhibiting two strong fiber components (see Fig. 1.17, quench at 290°C) having either a {013} ($d = 0.199$nm) or a {020} ($d = 0.186$nm) plane parallel to the substrate. Diffraction peaks of these planes are visible in the *in situ* XRD measurement in Fig. 1.16 at 53.6° and 57.6°. In addition to the δ-Ni_2Si phase, the pole figure measurements performed by Gaudet *et al.* revealed a second phase with a strong epitaxial

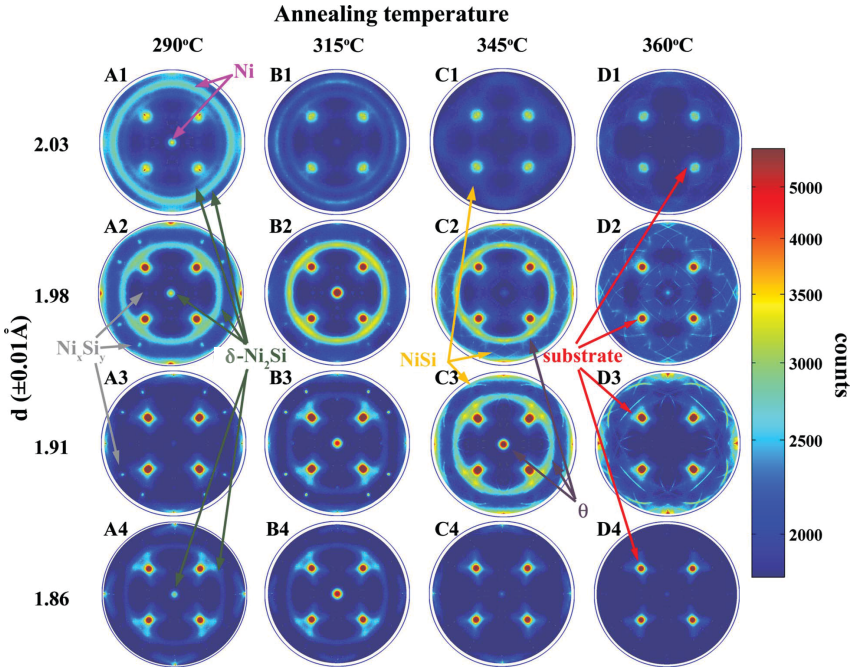

Figure 1.17. XRD pole figures for four different d-spacings ($\lambda = 0.15406$nm) measured on samples quenched at different temperatures during the reaction of a 10nm Ni film on Si(001). Figure reprinted with permission from Gaudet et al., J Appl Phys 107, 093515 (2010). Copyright 2010, American Institute of Physics.

texture (marked as Ni_xSi_y in Fig. 1.17) which is therefore bound to form at the interface with the single-crystal substrate. The precise nature of this phase is still an open question as no known phase from the Ni-Si phase diagram is able to explain the observed epitaxial spots in the pole figures [32, 34]. Due to the specific epitaxial orientation of this unknown phase, it was never observed in earlier studies using standard *in situ* XRD.

After the formation of δ-Ni_2Si and the unknown epitaxial phase, the reaction continues with the formation of another phase, characterized by the strong diffraction peak around 56-57° in the *in situ* XRD measurement of Fig. 1.16. In earlier studies, this peak was attributed to a strongly textured Ni_3Si_2 phase, the (350) plane of which could cause the diffraction peak observed in standard *in situ* XRD measurements. However, the pole figure measurements performed by Gaudet *et al.* revealed that this peak is caused by another phase with a strong fiber texture (see Figs. 1.17, B3 and

C3). Detailed analysis of the observed features in the pole figures allowed to identify the θ-nickel-silicide phase formed with a strong {110} fiber texture. This θ phase is a non-stoichiometric compound with a hexagonal crystal structure (spacegroup $P6_3/mmc$) in which a variable amount of Ni atoms can be present depending on the locations they occupy in the lattice, resulting theoretically in a possible Si content ranging between 33 and 55%. However, according to the Ni-Si binary phase diagram, this θ phase is only thermodynamically stable above 825°C in a bulk material when it contains between 33 and 41% Si [121], making the formation of this metastable phase at low temperatures rather unexpected.

Although the formation of this θ phase is thermodynamically unexpected at these low temperatures, its observation by Gaudet *et al.* during the solid-state reaction of a thin Ni film on Si(001) was actually consistent with the earlier results of De Keyser *et al.* in 2008, who observed the formation of this metastable phase when studying the solid-state reaction between co-sputtered Ni-Si films with varying Si concentrations (Si content between 37 and 42 at.%, Ni content equivalent to a 50nm Ni film) and a Si(001) or (111) substrate [45]. Because their *in situ* XRD patterns on both substrate orientations showed temperature windows with little or no diffraction peaks, they turned to pole figure and EBSD measurements and identified the presence of an epitaxially oriented θ phase which forms from the mixed Ni-Si film and reacts into NiSi at higher temperatures on both Si(001) and (111) substrates. These epitaxial orientations on both substrate types seemed to be closely related as they both have a θ{0001} basal plane parallel (or nearly parallel in the case of Si(001)) to a Si{111} plane [45]. The alignment of these planes can be understood by considering the small mismatch ($\approx 0.9\%$) in the distance between neighboring Si atoms in the θ{0001} basal plane and the Si{111} plane [45]. According to De Keyser *et al.*, the nucleation of this metastable θ phase can be attributed to a combination of interface stabilization thanks to the epitaxial orientation (low interface energy) and the fact that the θ phase can crystallize congruently with limited diffusion from the amorphous co-deposited Ni-Si mixture, as the θ phase can grow in exactly the same composition as this mixture. Furthermore, Gibson *et al.* and Gaudet *et al.* both reported the existence of very thin layers (< 2nm) of this θ phase at the interface with the same epitaxial orientation as reported by De Keyser *et al.* when depositing pure Ni on Si(111), which can probably be attributed to the thin amorphous Ni-Si mixed layer that forms at the interface during Ni deposition [32, 45, 122].

The influence of texture on phase formation is also clear when comparing the phase formation sequence for a thin Ni film on Si(001) and Si(111) substrates. A detailed comparison between the formation sequences on both substrates was published by Gaudet *et al.* in 2011 [32] and revealed a significant difference in the formation sequence prior to the formation of the technologically relevant axiotaxial NiSi. In contrast to the mainly fiber-textured phases formed on Si(001) (see discussion above), the phase formation on Si(111) is dominated mainly by epitaxially textured phases. The as-deposited state is characterized by a mixture of epitaxial, fiber and random Ni grains together with a very thin layer of epitaxial θ (see previous paragraph). Upon annealing, the reaction proceeds with the formation of epitaxial δ-Ni_2Si and a so far unknown epitaxial silicide, followed by epitaxial Ni_3Si_2 which then transforms into NiSi with the axiotaxy texture described in section 1.3.4.3 [32]. The different δ-Ni_2Si texture (epitaxy vs fiber) on Si(111) clearly influences the rest of the phase formation sequence as Ni_3Si_2 is formed on Si(111) instead of the θ phase on Si(001). Gaudet *et al.* suggested different thermodynamic and kinetic explanations as to why the θ phase forms on Si(001) while Ni_3Si_2 forms on Si(111). For more details, the reader is referred to ref. [32].

Very recently, we have obtained similar results in the phase formation sequence of a thin Ni film on Ge. Pole figure measurements at different stages during the reaction towards NiGe have revealed the presence of a similar transient hexagonal, metastable germanide, i.e. ϵ-Ni_5Ge_3, forming epitaxially before the formation of NiGe on both Ge(001) and Ge(111) substrates [123].

From the discussion above, it is clear that texture measurements at different stages during a solid-state reaction can provide valuable information in order to identify the phase(s) present at different temperatures during the formation sequence, especially when the forming phases are heavily textured. Furthermore, the orientation of the single crystalline substrate has a strong effect on the texture of the different phases in the formation sequence, leading to different interfaces and interface energies for different substrate orientations. This can affect the phase formation sequence by changing the formation temperature of a phase or by having extra phases forming or some not appearing depending on the substrate orientation.

1.4.2 Influence on phase stability

While the discussion in the previous subsection was focussed on how texture can influence the phase formation sequence during a solid-state reaction between a thin metal film and silicon or germanium, this subsection will handle the influence of texture on the phase stability of one specific phase. With the term 'phase stability', we refer to the maximum temperature up until which an intermediate phase is stable before it reacts with the substrate to form a phase that is more thermodynamically stable in contact with the pure Si or Ge substrate. To illustrate this point we will discuss the influence of texture on the stability of Co_5Ge_7, a germanide that forms during the solid-state reaction between a thin Co film and a Ge substrate. The complete phase formation sequence for a 30 nm Co film on a Ge(001) substrate was established by Gaudet *et al.* [22] in 2006 as being $Co \rightarrow CoGe \rightarrow Co_5Ge_7 \rightarrow CoGe_2$.

In 2010, De Keyser *et al.* published a detailed comparison between phase formation of a 30nm Co film on Ge(001) and (111) oriented substrates [41]. Using *in situ* XRD, they studied the phase formation sequence on both substrates (see Fig. 1.18). On Ge(001), the same phase formation sequence observed by Gaudet *et al.* [22] was measured, which is clearly visible in the *in situ* XRD measurement in Fig. 1.18a. However, on Ge(111), only the final $CoGe_2$ phase could be observed in the *in situ* XRD measurement, albeit characterized by different relative intensities for the diffraction peaks as on Ge(001), and no diffraction peaks could be observed at lower temperatures. More importantly, the formation temperature of $CoGe_2$, when formed using a ramp anneal at 3°C/s, is about 30°C higher on Ge(111).

As the difference in relative intensities of the $CoGe_2$ diffraction peaks on both substrate types and the absence of diffraction peaks at lower temperatures on the Ge(111) substrate are strong indications of a high amount of texturing in the films, De Keyser *et al.* used pole figure and EBSD measurements to study the texture of the formed films at two different temperatures. A first quench was taken at 725°C where $CoGe_2$ is visible on both substrates and a second quench was done before the formation of $CoGe_2$ at 600°C, where Co_5Ge_7 is visible on Ge(001). These texture measurements revealed that also on Ge(111) at 600°C, the film consists of Co_5Ge_7. However, this Co_5Ge_7 exhibits a strong epitaxial alignment for which the $Co_5Ge_7(0\bar{2}1)$ plane is parallel to the substrate and the $Co_5Ge_7(100)$ plane is parallel to $Ge(01\bar{1})$. When further annealing this film to 725°C, De

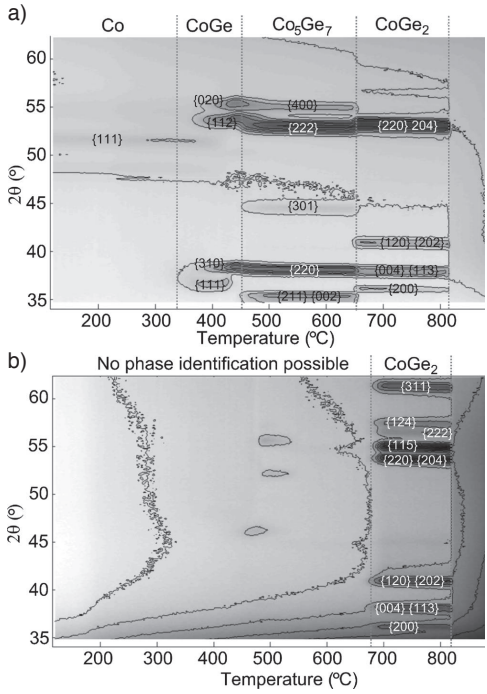

Figure 1.18. *in situ* XRD measurement for a 30nm Co film on a) Ge(001) and b) Ge(111). Darker areas indicate higher diffracted intensity. The heating rate during the measurements was 3°C/s. Reproduced with permission from De Keyser et al., J. Electrochem. Soc., **157**, H395 (2010). Copyright 2010, The Electrochemical Society.

Keyser *et al.* observed the presence of $CoGe_2$ which is mostly randomly oriented, along with some remaining epitaxial Co_5Ge_7. This formation of strongly epitaxial Co_5Ge_7 and the simultaneous presence of Co_5Ge_7 and $CoGe_2$ on Ge(111) is in sharp contrast to the phase formation sequence observed on Ge(001), where Co_5Ge_7 was observed to exhibit a complex texture with three epitaxy and two axiotaxy components [41]. Further annealing to 725°C on Ge(001) led to the formation of textured $CoGe_2$ exhibiting five different epitaxy and three axiotaxy components. No simultaneous presence of Co_5Ge_7 and $CoGe_2$ was observed for the reaction on Ge(001).

According to De Keyser *et al.*, the improved phase stability of Co_5Ge_7 and thus the increased formation temperature of $CoGe_2$ on Ge(111) can be attributed to the strong epitaxial orientation of Co_5Ge_7 on this substrate

as the lower interface energy of the epitaxial grains (compared to randomly oriented grains) leads to a lower driving force for the conversion to $CoGe_2$, shifting the $CoGe_2$ formation to higher temperatures. This explanation is corroborated by the microstructure of the films, which was measured using EBSD. In Fig. 1.19, EBSD maps performed on both substrates are shown for the same quenching temperatures as for the pole figure measurements. For Co_5Ge_7 on Ge(111) (top left EBSD map in Fig. 1.19), the microstructure seems to consist of a few larger grains embedded in a background of seemingly small grains. However, detailed analysis has shown that these seemingly small grains all belong to the same epitaxial Co_5Ge_7 orientation discussed above (rotationally equivalent orientations were indexed differently by the EBSD software) and that the average Co_5Ge_7 grain size is as large as 5μm. In contrast, the microstructure of Co_5Ge_7 on Ge(001) (top right EBSD map in Fig. 1.19) shows a typical polycrystalline film with an average grain size of 250nm, about 20 times smaller compared to Ge(111). The large Co_5Ge_7 grain size on Ge(111) leads to a much lower density of nucleation sites (triple and quadruple grain boundary points) for the nucleation controlled transformation of Co_5Ge_7 to $CoGe_2$ compared to the Ge(100) substrate. As a result, the nucleation rate for $CoGe_2$ is much lower on Ge(111), spreading the conversion from Co_5Ge_7 to $CoGe_2$ over a much longer time which results in Co_5Ge_7 being present at higher temperatures on Ge(111) compared to Ge(001) and consequently in the simultaneous observation of both phases on Ge(111) [41]. Furthermore, the low density of $CoGe_2$ nucleation centers available on Ge(111) also leads to large $CoGe_2$ grains on Ge(111) (see bottom left EBSD map in Fig. 1.19) as the nuclei can grow larger before encountering a competing $CoGe_2$ grain [41].

Clearly, texture can have a profound influence on phase stability during silicide/germanide formation. The low interface energy which is typical for a phase exhibiting a strong epitaxial orientation will result in a larger change in interface energy for the transformation to the next phase compared to the case where the phase has a less pronounced preferential orientation. As the activation energy for the transformation greatly depends on the change in interface energy [107] ($\Delta G^* \sim (\Delta\sigma)^3/(\Delta H)^2$), the activation energy for the transformation of the epitaxially textured phase will be higher, resulting in an increase of the formation temperature during a ramp anneal. Recently, we have observed similar results as discussed above for Co-Ge during the solid-state reaction between 30nm Pt films with Ge(001) and Ge(111) [88]. Pole figure measurements performed on

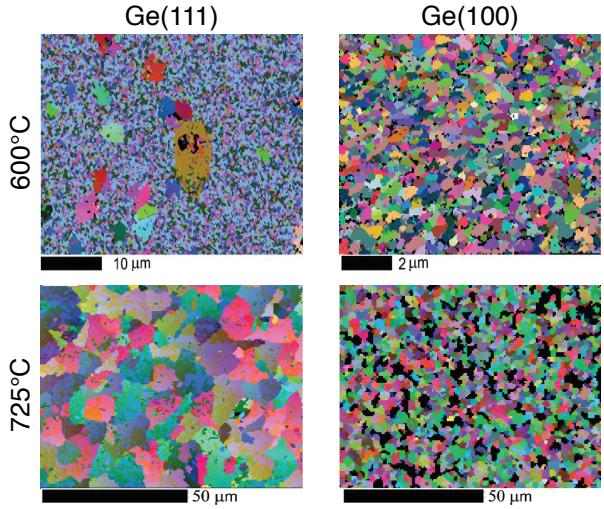

Figure 1.19. EBSD maps of 30nm Co films deposited on Ge(001) and Ge(111), quenched at 600°C and 725°C. Reproduced with permission from De Keyser et al., J. Electrochem. Soc., **157**, H395 (2010). Copyright 2010, The Electrochemical Society.

different quenches during the reaction revealed strong epitaxial alignments of Pt_2Ge, PtGe and $PtGe_2$ on Ge(111), while these phases are observed to be mostly randomly textured on Ge(001). The phase stability of the epitaxial phases on Ge(111) was found to be enhanced, leading to generally higher formation temperatures of the different platinum germanides on a Ge(111) substrate compared to a Ge(001) substrate.

1.4.3 Influence on morphological stability

Once a specific silicide/germanide phase has been formed to serve as an electrical contact to the source, drain and possibly the gate of a MOSFET device, it has to remain stable and not degrade during the subsequent CMOS fabrication processing steps. For NiSi, there are two important degradation mechanisms during temperature treatments. Firstly, since $NiSi_2$, not NiSi, is the end phase in the solid-state reaction between a thin Ni film and a Si substrate, further heating of the NiSi contact could lead to the formation of the undesired, high resistive $NiSi_2$ phase. This relates to the 'phase stability' that was discussed in the previous section for the case of Co_5Ge_7. Secondly, heating a NiSi film can lead to agglomeration, i.e. the breaking up of the film into small islands. The agglomerated film then

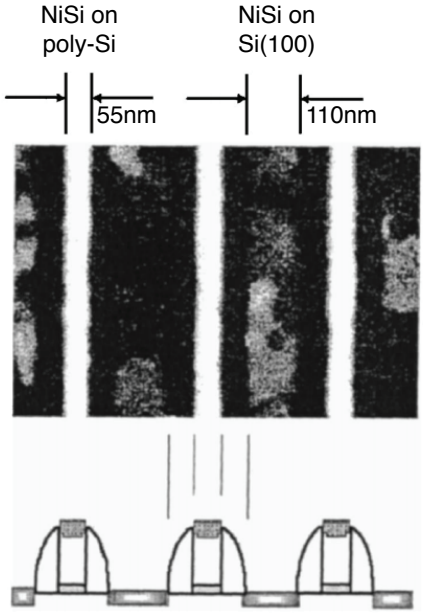

Figure 1.20. Top-view SEM picture of NiSi lines formed on the poly-Si gate and SOI source/drain regions of traditional MOSFET device structures. While subjected to the same thermal budget, the NiSi lines on the single-crystalline SOI regions are already agglomerated, while the lines on the poly-Si gate regions are still continuous. Figure reprinted with permission from Deduytsche et al., J Appl Phys 98, 033526 (2005). Copyright 2005, American Institute of Physics.

consists of small islands of low-resistive NiSi embedded in a background of high-resistive silicon, destroying the low resistivity of the contact.

A detailed study of these two degradation mechanisms of NiSi films was published in 2005 by Deduytsche *et al.* [112]. Their observations led to two important conclusions. First, for Ni films with thicknesses relevant for contact formation in CMOS devices (< 15nm), agglomeration of the film occurs at much lower temperatures than the conversion to $NiSi_2$, making agglomeration the main degradation mechanism for such films. Second, it was found that agglomeration occurs more quickly on a single crystalline (001) oriented SOI (Silicon On Insulator) substrate compared to a poly-crystalline Si substrate. This second observation is illustrated in Fig. 1.20, where the morphological stability of different NiSi lines, formed on poly-Si gate and SOI source/drain regions and subjected to the same thermal budget, is visible. It can be seen that the NiSi films on top of the single-

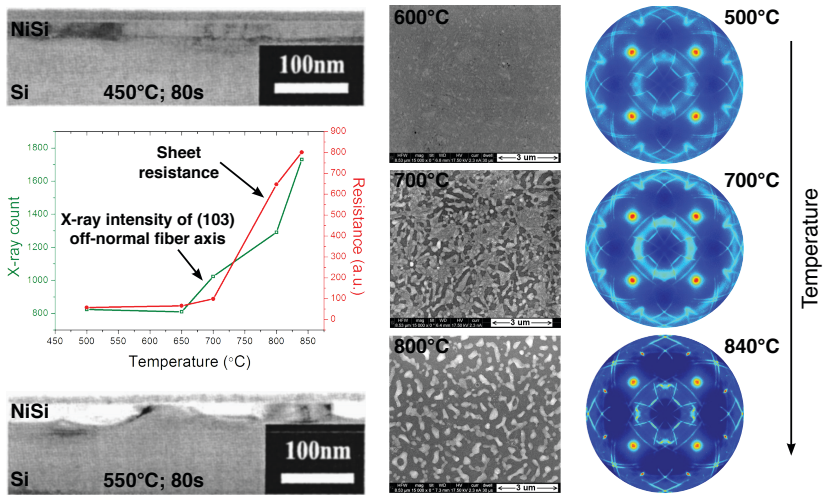

Figure 1.21. TEM (left column), SEM (middle column) and pole figure (right column) measurements for a thin Ni film on Si(001) at different temperatures representing different agglomeration stages. The samples for the SEM and pole figure measurements were quenched at the indicated temperatures using an anneal at a rate of 3°C/s. The samples for the TEM measurements were annealed during 80s at the indicated temperatures. The line graph in the left column shows the X-ray intensity of the (103) off-normal fiber axis -as obtained from the NiSi(103) pole figures taken on samples quenched at the different temperatures- along with the sheet resistance of the corresponding NiSi films. Agglomeration is characterized by the rise in the sheet resistance values.

crystalline source/drain regions are severely agglomerated while the films on top of the poly-Si gate regions are still nicely continuous. This result was very surprising, as previous studies of the morphological stability of thin silicide films systematically showed a better stability on single-crystal substrates [124]. Indeed, a typical process to stabilize a film on a polycrystalline Si substrate is to anneal the substrate prior to metal deposition. This anneal results in an increase of the grain size in the polycrystalline substrate, improving the morphological stability of the film. Hence, a film formed on a single crystalline substrate (which is basically one big grain) would be expected to exhibit the largest morphological stability. Although not backed by experimental evidence, Deduytsche *et al.* suggested the axiotaxial texture of NiSi on single-crystalline Si substrates as a possible explanation for the enhanced agglomeration on a single crystalline substrate [112].

In 2008, De Keyser *et al.* published a study focussing on the texture evolution of a thin NiSi film during agglomeration in an attempt to understand

the link between the NiSi axiotaxy texture and the agglomeration behavior on a single crystal Si(001) substrate [125]. To this end, XRD pole figures were recorded on 20nm NiSi films formed on Si(001) that were quenched at different temperatures. These NiSi(112) pole figures are visible in the rightmost column of Fig. 1.21 along with SEM and TEM pictures showing the morphology of the films at the quenched temperatures. It is clear that for higher temperatures and thus more severe stages of agglomeration (as evidenced by the SEM/TEM pictures), the axiotaxy lines increase in intensity and the background coming from randomly oriented grains decreases significantly. De Keyser *et al.* quantified the increase of axiotaxy in the film by recording the intensity of the (103) off-normal fiber axis pole in the (103) pole figure at the different temperatures. The result is visible in the line graph in Fig. 1.21 along with the corresponding sheet resistance of the film. From this graph, a clear correlation between the film agglomeration (characterized by the increase in sheet resistance) and the increase of the axiotaxy intensity is observed, suggesting that during agglomeration, randomly oriented grains disappear in favor of axiotaxial grains.

This raises the question of how the presence of axiotaxy renders a NiSi film more prone to agglomeration. Why does the intensity of the axiotaxy lines increase during the agglomeration process? The driving force for the agglomeration of a silicide/germanide film is considered to be a reduction of the surface and interface energy [124, 126]. However, from the TEM cross-section visible in the bottom left of Fig. 1.21 it seems that for an agglomerated NiSi film only the silicide/silicon interface is severely roughened while the surface remains flat, suggesting that minimizing the interface energy is the main driving force for the agglomeration. This interface energy can roughly be calculated as

$$E \sim \sum_i \gamma_i A_i \tag{1.4}$$

where the sum runs over all grains in the film, with γ_i the interface (and grain boundary) energy per unit area and A_i the interface (and grain boundary) area for grain i. Taking Eq. 1.4 into account, one can imagine that the drive for interface energy minimization will result in an abnormal grain growth promoting those grains with a low interface energy that are able to obtain a curved (spherical) interface with the substrate (as this amounts to the smallest interface area). This process is illustrated in Fig. 1.22, showing a simplified evolution of NiSi grains on Si(001) belonging to different texture components. High energy interfaces are colored in red, while the

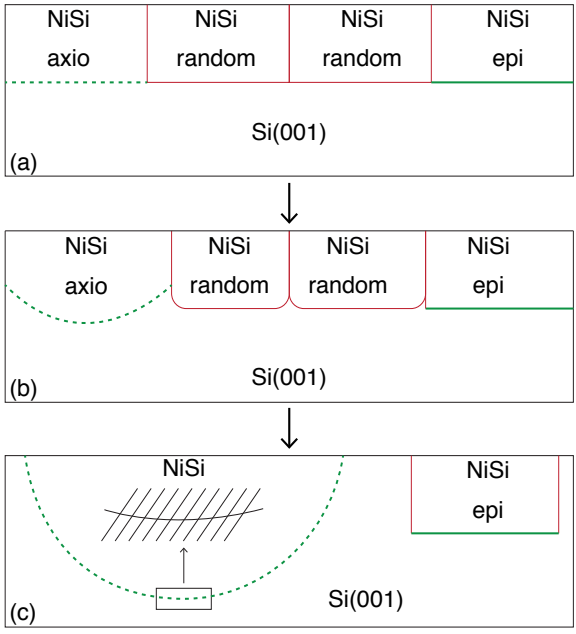

Figure 1.22. Illustration of the abnormal grain growth occurring in thin NiSi films on Si(001) for an increasing thermal budget. High energy interfaces are colored in red, medium (for axiotaxy) and low (for epitaxy) energy interfaces are represented by a dashed green or a full green line respectively.

medium (axiotaxy) and low (epitaxy) energy interfaces are indicated by dashed or full green lines respectively. Typically, grain growth in a single phase is assumed to happen through a process called *grain boundary grooving* [38, 126], where mass transport occurs from the high energy grain boundaries towards the grain/substrate interface of the grain with the lowest interface energy, resulting in a grooving of the grain boundary. This would imply that randomly oriented grains will be consumed by epitaxial and axiotaxial grains which have a significantly lower interface energy (Fig. 1.22b). However, the 2-dimensional matching at the interface between an epitaxial grain and the substrate would be destroyed by curving the interface, rendering a high energy interface. Thus, grain boundary grooving for an epitaxial grain will be difficult, which suppresses the growth of these grains. This explains why highly epitaxial films are typically observed to be very stable with respect to agglomeration. For axiotaxy grains on the other hand, the plane alignment and thus the 1-dimensional periodicity in the

interface plane is preserved irrespective of the curvature of the interface (see section 1.3.3). This means that the axiotaxy grains can easily grow and form a curved interface, thus minimizing the interface area, and maintain their low interface energy at the same time (see Fig. 1.22c). According to the model described above, the presence of axiotaxy should thus render a thin silicide/germanide film more prone to agglomeration.

Clearly, texture has a defining influence on the morphological stability of a thin NiSi film. As agglomeration was found to be the primary degradation mechanism for NiSi contacts, the development of methods that improve the morphological stability of NiSi are crucial for the fabrication of reliable microelectronic devices. In view of the discussion in this section, these methods should first aim at reducing the axiotaxy in these thin NiSi films. A widespread approach to improve the stability of NiSi contacts is to alloy the nickel film with additional elements. In particular, the addition of a few at.% of Pt to the nickel layer results in an improved morphological stability [120]. Furthermore, the addition of Pt has the added advantage that the phase stability of NiSi is also improved (by shifting the nucleation of $NiSi_2$ to higher temperatures) [18], thus tackling the second degradation mechanism. Details on how the addition of alloying elements can influence the texture and hence the morphological stability of NiSi (and other silicide) films will be discussed in section 1.5.3.

1.4.4 Influence on electrical properties

As silicides and germanides are commonly used in the microelectronics industry as electrical contacts to the source and drain regions of MOSFET devices, a clear understanding of the interface properties of a silicide/Si or germanide/Ge contact is very important. The intrinsic resistance of an interface between a metal and a semiconductor depends primarily on the dopant concentration within the semiconductor and the Schottky barrier height (SBH) between the metal and the semiconductor. This SBH represents the potential energy barrier for majority charge carriers that flow between the silicide and the semiconductor substrate. Due to its importance, a lot of research, both covering SBH determination of different metal-semiconductor (MS) contacts and theoretical modeling of SBH formation, has been published since the 1950s. The interested reader is referred to the excellent reviews by R.T. Tung on this subject [127, 128].

In its simplest form (the Schottky-Mott rule [129, 130]), the SBH for a metal-semiconductor contact is defined as the difference between the

metal work function (Φ_M) and the semiconductor electron affinity (χ_{SC}), i.e. $\Phi^0_{B,n} = \Phi_M - \chi_{SC}$ for an n-type semiconductor. This simple description only holds in the absence of any interaction between the metal and the semiconductor (like charge rearrangement and atomic relaxation) at the MS interface, which is not sufficient to describe 'real' MS interfaces. Over the past decades, research performed on SBH formation showed a clear dependence of the SBH on the local interface structure of the MS contact. Therefore, a so-called *interface dipole* term is added to the model which must account for the deviation of the observed SBH from the simple Schottky-Mott SBH, thus modeling the interface chemistry at the MS interface. However, the calculation of this interface dipole term is not straightforward [128].

As the SBH seems to depend greatly on the local structure of the MS interface, an influence of the texture of a silicide/germanide contact to Si or Ge on the SBH can be expected since the structure of the interface is naturally dependent on the local orientation of the silicide grains. This was experimentally observed in different studies during the 80s and 90s when SBH formation was studied for epitaxial $NiSi_2$ contacts on Si(111) and (001) [131–135]. Such studies were very important in the field of SBH research at first because it was believed that the SBH was the result of a difference between bulk properties of the metal and the semiconductor and as such should not depend on the crystal orientation. Therefore, the single-crystal epitaxial $NiSi_2$ films were ideal model systems for SBH formation studies because of the sharpness and the homogeneous atomic structure of such an epitaxial interface. For an epitaxial $NiSi_2$ film on Si(111), there are two possible grain orientations, called type A and type B respectively. Type A has the same orientation as the Si substrate while the type B orientation shares the Si(111) surface normal but is rotated over 180° around this axis. Different studies have shown that type B oriented $NiSi_2$ films show a distinctively higher SBH than type A oriented films on n-type Si(111) (difference of about 0.14eV) [131–134]. Furthermore, epitaxial $NiSi_2$ films on n-type Si(001) were observed to have a SBH that was about 0.40eV lower than the type B $NiSi_2$ films on n-type Si(111) [135].

A straightforward consequence of the dependence of the SBH on the local interface structure would be that a polycrystalline MS-contact exhibits a spatially inhomogeneous SBH. This would mean that the macroscopically measured value of the SBH for an entire MS-contact is just an average among a significant range of local SBH's spatially distributed over the contact. This idea of SBH inhomogeneity was introduced during the 80s when

it was found that assuming a distribution of SBH's in a contact instead of a single SBH could explain observed differences in the SBH value obtained from I-V measurements versus C-V measurements [136]. From then on, developments in SBH formation models consequently included the idea of SBH inhomogeneity [127, 128, 137–139]. With the development of Ballistic Electron Emission Microscopy (BEEM) in the late 80s [140], an experimental technique became available that was able to locally measure Schottky Barriers and thus spatially map SBH variations on the nanometer scale. Consequently, a range of studies were performed during the 90s where direct proof of SBH inhomogeneity was observed on different kinds of MS interfaces, e.g. for epitaxial $CoSi_2$ films[141–144] and Au/n-Si contacts [145]. A detailed overview of these studies can be found in the excellent reviews by Tung [127, 128]. In the case of silicides, a BEEM study on polycrystalline $CoSi_2$ contacts formed on n-type Si(001) was performed by Zhu *et al.* [146], who found an agreement between the SBH distribution obtained by either spatially mapping SBH variations using BEEM or using standard I-V/C-V measurements.

1.5 Factors affecting texture during solid state reactions

The discussions in the previous section clearly show that texture can have an important influence on some technologically very relevant properties of thin film silicides/germanides. As a result, film texture in a small contact will affect the electrical properties of a device. Therefore, the ability to control or influence the texture of silicides and germanides during contact formation could enable us to tune and optimize important contact properties. In this section, we aim to give an overview of different studies that investigated the influence of selected experimental parameters/techniques on the texture evolution of the desired silicide/germanide phase. As these studies typically focus on a single parameter, it must be noted that in reality, the final texture is determined by the interplay of different factors. This is what makes the development of a predictive theory for texture formation not straightforward. As was mentioned in the introductory chapter, the results obtained so far (which are discussed below) are not yet sufficient for such a theory to be developed.

1.5.1 Dopants

As silicide contact formation in CMOS technology takes place on the doped source and drain regions of the Si substrate, it is important to study the effects of dopant type and concentration as well as dopant redistribution during the solid-state reaction on the properties of the final silicide contact [147–149]. In this view, studying the influence of this dopant redistribution on the texture of the formed silicide phases is directly relevant. Nonetheless, literature reports that are concerned with the effect of substrate doping on silicide texture are scarce. This is probably a consequence of the complexity of the phenomenon, since a number of factors are at play such as dopant diffusivity, dopant solubility in both the silicon and the silicide, interface and surface segregation coefficients and evaporative or reactive dopant losses during the heat-treatment [148]. Moreover, because of the nature of diffusion and its dependence on available paths such as grain boundaries and interfaces, detailed studies of these redistribution processes require specialized experimental techniques like e.g. Atom Probe Tomography (APT) [150–152] which allow for full 3-dimensional elemental mapping.

Such dopant redistribution studies have been performed by a number of groups. It has been observed that for some dopant-silicide combinations the dopant species accumulate at the silicide/silicon interface [148, 149], an observation that is referred to as the 'snowplow' effect in literature and that has been observed e.g. in the case of Boron redistribution during NiSi formation [152] or As redistribution during δ-Ni_2Si formation [150]. In other cases, researchers observed redistribution of the dopants throughout the formed silicide [147, 148, 150], e.g. in the case of As redistribution during the formation of the transient θ-Ni-silicide phase, where the As was observed to form clusters within this θ-phase [150]. Especially in the case were the dopants are accumulated at the interface and thus where the initial low concentration of dopants piles up at the interface as the silicide is growing, an influence on the texture should not come as a surprise.

During the many years of high-resolution, synchrotron based pole figure studies on thin film silicides and germanides at the X20A beamline of the national synchrotron lightsource (NSLS) at Brookhaven National Lab (BNL) by the research groups of IBM and Ghent University, multiple measurements have been performed to probe the influence of dopants on silicide texture. Fig. 1.23 shows a small subset of these measurements. NiSi(112) pole figures ar shown for NiSi formed on single-crystalline sili-

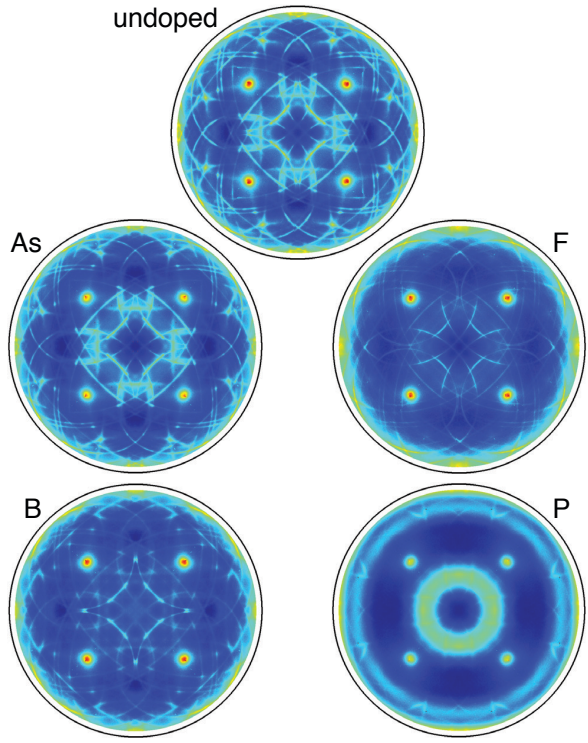

Figure 1.23. NiSi(112) pole figures for NiSi formed by annealing 10nm Ni deposited on doped SOI (silicon on insulator) substrates at 500°C. The dopant concentrations were $8 \times 10^{15}\text{cm}^{-2}$ for As, B and P and $3 \times 10^{15}\text{cm}^{-2}$ for F. The NiSi(112) pole figure for NiSi formed on an undoped SOI substrate is added at the top as a reference. The SOI substrates have a Si(001) orientation.

con-on-insulator (SOI) substrates doped with different elements at comparable doses. The NiSi(112) pole figure for NiSi formed on an undoped substrate is provided as a reference at the top of this figure. Different influences on the texture by different dopant species can clearly be observed. From this figure, it is clear that small concentrations of additional elements can have a drastic impact on the texture of the silicide film. Arsenic shows the mildest influence compared to the undoped Si. For Fluorine and Boron, a clear reduction in the intensity of the axiotaxy lines can be observed. Phosphorus has the most profound influence on the texture, as the axiotaxy has almost disappeared while a broad fiber texture develops and can only be detected on this P doped sample. In contrast, Kimura *et al.* ob-

served the formation of transrotational NiSi (see also section 1.3.4.3) on B-doped Si(001) substrates with a similar doping dose as was used in our measurements [153], suggesting that other experimental conditions are important as well. While variations in substrate and implantation conditions could be a factor here, it is likely that the annealing conditions play the critical role in the observed differences in final texture. As the tooling capabilities evolve, anneals in the industry are now typically done at much faster ramp rates leading to films exhibiting smaller microstructure (because of higher nucleation density). Slower anneals typically lead to larger grain sizes and significant variations in texture.

1.5.2 Lattice spacing of the substrate

For a textured thin silicide/germanide film on a single-crystal Si or Ge substrate, the driving force for the preferred orientation of the grains is a reduction in either surface energy (fiber texture) or interface energy (epitaxy, axiotaxy). In the latter case, the energy reduction results from an optimized bonding across the interface resulting from a 1- or 2-dimensional match between the film and substrate lattice in the plane of the interface. Therefore, texture development in such a thin silicide/germanide film should be sensitive to variations in lattice constants (and d-spacings) of either the substrate or the film. In this section, we will discuss an example of how a slight change in the lattice constants of the silicon substrate impacts the texture of NiSi.

In 2011, De Keyser *et al.* published a study where they investigated the phase formation and texture of NiSi films formed on Si(001) substrates for which the top 40nm consisted of an epitaxial $Si_{1-x}C_x$ layer containing either 1, 1.7, 2.2 or 2.5 at.% of substitutional carbon in the Si lattice [154]. The much improved morphological stability of NiSi on top of these $Si_{1-x}C_x$ layers [155] (from here on, these films will be referred to as NiSi(C)) can be explained because the C atom is known to prevent the diffusion of Si within the film and both elements must be mobile to allow for a modification of the morphology. Here, De Keyser *et al.* wanted to investigate whether changes in film texture could provide a second explanation for the enhanced morphological stability of these films.

The phase formation sequence towards NiSi(C) on these $Si_{1-x}C_x$ substrates was studied by De Keyser *et al.* using *in situ* X-ray diffraction. It was observed that, compared to the phase formation sequence on pure Si, the onset of the formation of both the transient Ni-rich phases and the NiSi

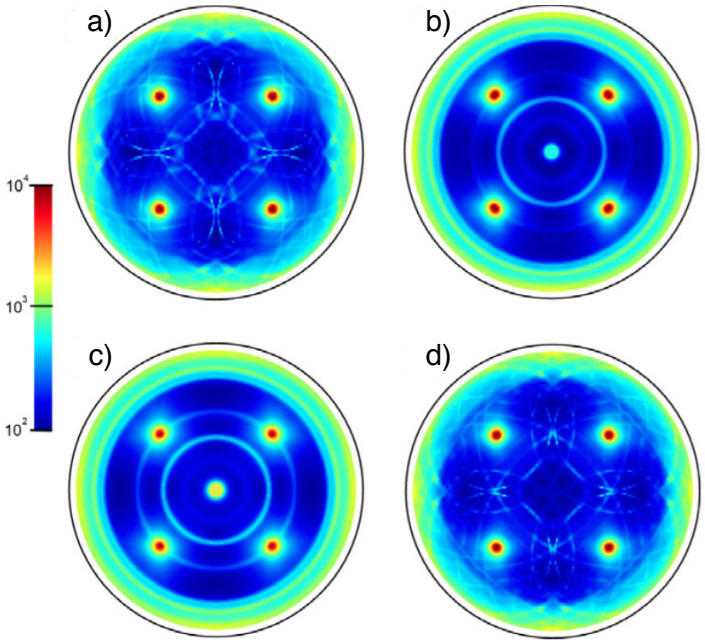

Figure 1.24. a)-d) NiSi(C){112} pole figures for NiSi(C) formed on $Si_{1-x}C_x$ substrates with different concentrations of C, i.e. a) with 1% C, b) with 1.7% C, c) with 2.2% C and d) with 2.2% C but where the substrate was subjected to a pre-anneal, reducing the actual substitutional C concentration to 0.9%. Figure reprinted with permission from De Keyser et al., Microelectron Eng 88, 536 (2011). Copyright 2011, Elsevier.

phase is significantly delayed and that the transient phases are present over a much wider temperature window. Furthermore, for NiSi(C) formed on $Si_{1-x}C_x$ samples with a C content of 2.5%, the intensities of the NiSi(C) diffraction peaks in the *in situ* XRD measurements were observed to be significantly different compared to NiSi(C) formed on $Si_{1-x}C_x$ samples with 1% of C and compared to NiSi formed on pure Si [33], suggesting a change in NiSi texture.

After NiSi(C) formation and a subsequent high-temperature anneal of 30 minutes at 750°C, De Keyser *et al.* investigated the texture of the resulting NiSi(C) films using high-resolution pole figures. In Fig. 1.24a-c we reproduced the NiSi(C){112} pole figures for NiSi(C) films formed on $Si_{1-x}C_x$ substrates with 1, 1.7 and 2.2 at.% of substitutional carbon. For NiSi(C) formed on the substrates containing more than 1% of carbon, the typical NiSi axiotaxy lines (see Fig. 1.15b) have disappeared and instead

a combination of NiSi(C){202}, {211} and {112} fiber textures is visible, evidenced by the concentric circles on the pole figures of Fig. 1.24b-c. Furthermore, De Keyser *et al.* investigated whether only the presence of carbon induces the change in the NiSi(C) texture or whether the location of the C atoms is also important. To this end, the texture was investigated for NiSi(C) formed on a $Si_{1-x}C_x$ substrate with 2.2% of C that was subjected to a spike anneal (He, 1050°C, 1.5s) prior to the deposition of Ni. This anneal effectively reduced the concentration of substitutional carbon atoms (C atoms that replace Si atoms in the Si lattice) from 2.2% to 0.9% by moving part of the substitutional C into interstitial sites. The pole figure in Fig. 1.24d shows that in this case the axiotaxy texture is present again, resembling the texture observed for the sample with 1% C in the original $Si_{1-x}C_x$ layer.

The substitution of Si atoms with C in the $Si_{1-x}C_x$ epi-layers of the substrate slightly changes the lattice constants with respect to a pristine Si lattice. As a result, the d-spacing of the Si{220} family of crystal planes will also change when more substitutional C is present in the substrate. Because the typical NiSi axiotaxy texture results from a matching between NiSi{202}, {211}, {103} and {112} planes and Si{220} planes at the interface, the change in Si{220} d-spacing due to the presence of substitutional C inhibits the plane matching and thus the axiotaxy texture when the d-spacing change is large enough (i.e. when more than 1% of substitutional C is present). The fact that the axiotaxy texture is present for a substrate where the 2.2% of substitutional C is reduced to 0.9% by spike annealing, strengthens the argument that the change in NiSi(C) texture is due to the change in substrate lattice spacing resulting from the substitutional carbon atoms. Finally, De Keyser *et al.* argued that the much improved thermal stability of these NiSi(C) films [155] can at least be partly explained by the suppression of the axiotaxy texture, because silicide/germanide films that exhibit strong axiotaxy texture are expected to be more prone to agglomeration (see the discussion in section 1.4.3).

1.5.3 Silicide/germanide alloying with soluble elements

In the previous section, we showed that a change in the lattice constants of the silicon/germanium substrate influences the resulting texture of the film by breaking the condition for axiotaxy. In principle, this condition can also be modified by a change in the silicide/germanide lattice which can be achieved by alloying the targeted silicide/germanide with a small

concentration of a soluble element. Here, soluble means that the alloying element can form a silicide that is miscible in the targeted silicide. Practically, the alloying can be accomplished by adding the alloying element to the silicide-forming metal layer during deposition. Besides the expected change in lattice constants caused by incorporating the alloying element into the silicide/germanide lattice, the presence of the alloying element can also influence the kinetics during the formation of the silicide/germanide, which in turn impacts the texture development during the solid-state reaction.

For NiSi contacts that are used in modern sub 100nm planar technology nodes, alloying with small concentrations of Pt is a standard procedure as this significantly improves the thermal and morphological stability of the thin NiSi film [18]. As the miscibility of PtSi in NiSi is high due to the similar orthorhombic MnP-type structure of the NiSi lattice and the PtSi lattice, the alloyed Pt gets easily incorporated into the NiSi and a $Ni_{1-x}Pt_xSi$ layer is formed. The influence of these small concentrations of Pt on the texture of the resulting $Ni_{1-x}Pt_xSi$ film compared to a pristine NiSi layer was investigated in 2004 by Detavernier *et al.* using synchrotron based pole figure measurements [49]. In Fig. 1.25, we reprinted a selection of NiSi(112) pole figures for $Ni_{1-x}Pt_xSi$ films that were formed by reacting 30nm layers of a Ni(Pt) alloy with different Pt concentrations on Si(001) at 500°C for 30s. For the lowest Pt concentration of 0.2%, it can be seen that the texture is the same as for a pristine NiSi film formed on Si(001) (see the NiSi(112) pole figure in Fig. 1.15b and the description of the NiSi texture in the corresponding section). The overlaid axiotaxy patterns in the top right pole figure for the lowest Pt concentration represent the calculated axiotaxy lines for the two most intense axiotaxy components (i.e. those for which either NiSi{202} or {211} planes are aligned to Si{220}). As the initial concentration of Pt in the Ni(Pt) is increased, a significant change in the texture of the final $Ni_{1-x}Pt_xSi$ phase can be observed. The axiotaxy lines for the two most intense NiSi axiotaxy components become weaker and less sharp for increasing Pt concentrations, while the weak NiSi{103} axiotaxy component (see section 1.3.4.3) becomes more prominent, as evidenced by the overlaid pattern in the bottom right pole figure of Fig. 1.25 which represents the calculated axiotaxy lines for this texture component. The overall reduction of axiotaxy through the alloying with Pt explains, at least partially, the improved morphological stability of the resulting $Ni_{1-x}Pt_xSi$ film compared to pure NiSi [18] (see section 1.4.3).

In their paper, Detavernier *et al.* argued that the change in texture ob-

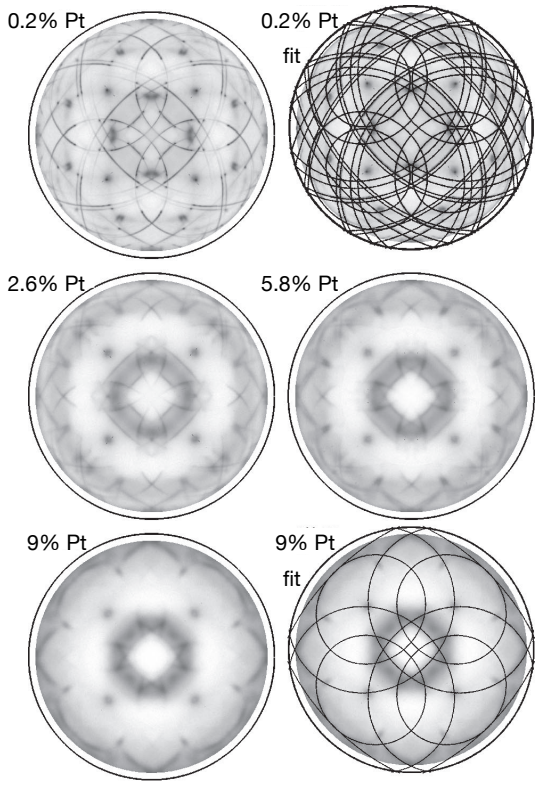

Figure 1.25. NiSi(112) pole figure for $Ni_{1-x}Pt_xSi$ films formed by the reaction of a 30nm Ni(Pt) alloy with Si(001) at 500°C for 30s. The concentration of Pt in the as-deposited alloys is 0.2%, 2.6%, 5.8% or 9%. The calculated axiotaxy lines overlaid on the 0.2% pole figure are for the NiSi(202) and (211) axiotaxy components, while the overlay on the 9%Pt pole figure is for the (103) axiotaxy component. Figure reprinted with permission from Detavernier et al., Appl Phys Lett 84, 3549 (2004). Copyright 2004, American Institute of Physics.

served for increasing Pt concentrations can be related to the expansion of the $Ni_{1-x}Pt_xSi$ unit cell when an increasing amount of Ni atoms are replaced with Pt. First, this unit cell expansion results in an increase of the d-spacing for the $Ni_{1-x}Pt_xSi${202} and {211} planes, causing the excellent match with the d-spacing of Si{220} planes to degrade as more Pt is added, which explains the decrease in intensity and eventually the disappearance of these axiotaxy components. A similar argument holds for the already weak NiSi{112} axiotaxy component. Second, the increased d-spacing of the $Ni_{1-x}Pt_xSi${103} planes due to the unit cell expansion leads to an im-

proved matching with Si{220} planes, allowing the match of the interplanar spacing at the interface between the $Ni_{1-x}Pt_xSi${103} and the Si{220} planes to be achieved through a smaller tilt angle (2.5° instead of 4.2°) than for a pure NiSi film. Therefore, the (103)-based axiotaxy is achieved more easily and thus becomes more prominent with increasing Pt content, as observed in the pole figures of Fig. 1.25.

As the nucleation stage of a new phase fixes the orientation of the grains, the argumentation of Detavernier *et al.* discussed above requires that Pt be present at the boundary between the metal-rich silicide and the Si substrate during the early stages of NiSi formation from a Ni(Pt) alloy. If Pt is not present at the interface, it can not be incorporated in the growing NiSi seeds and influence the texture directly. Hence, to understand the influence of the alloyed Pt on the texture development during the solid-state reaction, detailed information on the Pt redistribution during the reaction is crucial.

This Pt redistribution during $Ni_{1-x}Pt_xSi$ formation was extensively investigated by Demeulemeester *et al.* using *real-time Rutherford Backscattering Spectroscopy* (RT-RBS) [156–158]. With this technique, a 75nm thick Ni(Pt) alloy is deposited on a Si(001) substrate and annealed at a rate of 2°C/min. During the anneal, an RBS spectrum is collected every two minutes using a 2MeV He^+ beam which results in an RBS spectrum being collected every 4°C. Hence, this technique allows to probe elemental depth distribution during the silicidation with a relatively high temperature resolution, which allowed Demeulemeester *et al.* to perform a thorough study of the Pt redistribution during Ni(Pt)Si formation. The experiments revealed that at low temperatures, when δ-Ni_2Si forms prior to NiSi formation, only a small amount of the Pt available in the Ni(Pt) alloy gets incorporated in the growing Ni_2Si phase. The majority of the Pt piles up at the Ni/Ni_2Si interface and thus gets 'snowplowed' towards the surface as more Ni_2Si grows underneath. This situation is illustrated in the second step of Fig. 1.26. In this figure, important stages of the Pt redistribution process during the silicidation reaction are schematically depicted, along with two RBS spectra extracted from the RT-RBS data at temperatures in the second and third stage. The RBS spectrum extracted from the second stage (black spectrum) clearly shows the enhanced Pt concentration at the $Ni_2Si/Ni(Pt)$ interface[156, 157] (peak marked with '+' in Fig. 1.26). Around the same time, similar results were obtained by Hoummada *et al.* [159], who used standard RBS on 50nm Ni(5%Pt) samples on Si(001) that were subjected to isothermal anneals between 200-300°C for different durations.

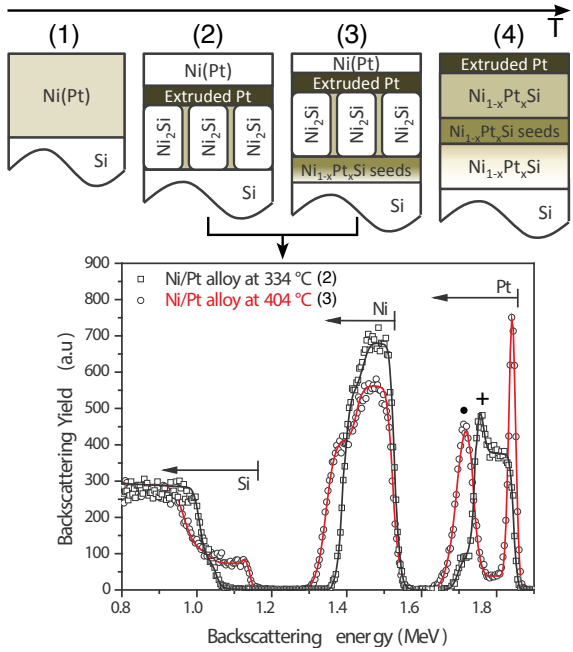

Figure 1.26. Top: schematic summary of several important stages during the formation of $Ni_{1-x}Pt_xSi$ from a Ni(Pt) alloy on Si(001) as observed by real-time RBS. Bottom: RBS spectra extracted from a real-time RBS measurement performed on a 75nm thin Ni(7%Pt) alloy deposited on Si(001) using a ramp anneal at 2°C/s. The spectrum at 334°C (open squares) is characteristic of stage 2, i.e. during Ni_2Si formation, while the spectrum at 404°C (open circles) characterizes stage 3, i.e. during $Ni_{1-x}Pt_xSi$ formation. The solid lines represent the RBS simulations. Figures reprinted with permission from Demeulemeester et al., J Appl Phys 108, 043505 (2010). Copyright 2010, American Institute of Physics.

At the onset of the monosilicide formation, the RT-RBS data of Demeulemeester *et al.* revealed the presence of a very thin NiSi layer at the Ni_2Si/Si interface together with a high concentration of Pt at the same depth. This high concentration can be observed in the red RBS spectrum of Fig. 1.26 through the peak in the platinum signal at the lowest energy (marked with '•'). This Pt concentration is high compared to the Pt concentration in the Ni_2Si layer above (valley to the right of the Pt peak marked with '•') and even slightly exceeds the Pt concentration in the initial Ni(Pt) alloy. As a consequence, the initial $Ni_{1-x}Pt_xSi$ seeds from which the rest of the phase grows and hence that establish the $Ni_{1-x}Pt_xSi$ texture nucleate in the presence of a high Pt concentration. This observation corroborates the explanation for the texture change put forward by Detavernier *et al.*

that was discussed above.

Next to the real-time RBS studies of Demeulemeester *et al.*, the redistribution of Pt during the reaction of a Ni(Pt) alloy with Si(001) has also been investigated by groups at the university of Aix-Marseille (France) and at the Northwestern University of Illinois (USA) using Atom Probe Tomography (APT). This APT technique allows for a 3-dimensional reconstruction of the elemental distribution in a small volume, providing both depth and lateral resolution, while RBS only provides depth resolution. However, the APT technique can not be used in real time during the annealing process. The French group observed that for 50nm Ni(5%Pt) films on Si(001) that were subjected to an isothermal anneal at 300°C and quenched during the early growth of the $Ni_{1-x}Pt_xSi$ seeds (i.e. before the total consumption of the Ni(Pt) layer), the Pt shows a very non-uniform lateral distribution [160]. It was found that only a limited amount of Pt is incorporated in the $Ni_{1-x}Pt_xSi$ grains, as the majority is located at the $Ni_{1-x}Pt_xSi$ grain boundaries and at the $Ni_{1-x}Pt_xSi/Ni_2Si$ interface, while very little Pt is measured at the $Ni_{1-x}Pt_xSi/Si$ interface. For films with $\geq$ 10% of Pt annealed using isothermals or very slow ramp anneals, the non-stoichiometric θ-phase was found to form epitaxially on Si(001) (instead of δ-Ni_2Si) [161, 162]. In contrast to what was observed for the δ-Ni_2Si phase that forms for lower Pt concentrations, the Pt does get incorporated into the θ-phase in a very non-uniform manner with an enhanced concentration ($\sim$ 20%) close to the interface with the unreacted Ni(10%Pt).

The group at Northwestern University studied Pt redistribution in similar Ni(5%Pt) films on Si(001), but with a thickness of only 10nm [163, 164]. After a rapid-thermal anneal at 420°C for 5s, they observed a 5nm stoichiometric NiSi film in contact with the Si(001) substrate growing outward toward the unreacted Ni(5%)Pt layer. In these samples, Pt was observed to have segregated uniformly at the NiSi/Si(001) interface. Furthermore, Pt was also observed to be concentrated at the Ni(5%)Pt/silicide interface and at the NiSi grain boundaries, indicating a very fast diffusion path along those GBs[163, 164]. They argued that these fast diffusion paths allow the Pt atoms to diffuse rapidly towards the NiSi/Si interface during the early stages of NiSi nucleation.

Although both the RT-RBS and the APT results discussed above show the complexity of the Pt redistribution process and its dependency on the initial Pt concentration and the annealing conditions, they do not show the location of the Pt atoms at the onset of nucleation of the $Ni_{1-x}Pt_xSi$ grains, either because lateral resolution is absent in the RT-RBS measurements or

because the films investigated by APT have already surpassed the initial $Ni_{1-x}Pt_xSi$ nucleation stage. As the orientation of these grains and thus the texture of the resulting $Ni_{1-x}Pt_xSi$ film is determined at the time of nucleation, Pt distribution experiments focussing on the $Ni_{1-x}Pt_xSi$ nucleation stage will be necessary to understand the exact influence of the Pt atoms on the texture of the resulting $Ni_{1-x}Pt_xSi$ film.

The fact that both a change in lattice constants and altered kinetics induced by alloying impact the texture development during the formation of a silicide/germanide has also been observed in the Co-Si system. In 2008, Smeets *et al.* investigated the influence of alloying increasing amounts of Ni in a Co film deposited on Si(001) on the texture of the resulting $Co_{1-x}Ni_xSi_2$ [43]. As it was discussed in section 1.3.1, both $NiSi_2$ and $CoSi_2$ can be grown epitaxially on Si(001) using a variety of techniques because of their CaF_2 structure which is very similar to that of Si. However, when these silicides are formed through a standard solid-state reaction between a thin Ni or Co film and Si(001), only $NiSi_2$ forms epitaxially while $CoSi_2$ (which has a slightly larger lattice mismatch of 1.23% with Si compared to 0.46% for $NiSi_2$) forms a polycrystalline film with different epitaxial components [66]. By studying the texture of $Co_{1-x}Ni_xSi_2$ films formed through a solid state reaction between a Co(Ni) alloy and Si(001), Smeets *et al.* investigated the quality of the resulting epitaxial film as a function of its lattice constant by introducing increasing amounts of Ni in the starting Co(Ni) alloy. As continuous addition of Ni is expected to generate a monotonic change in the lattice constant of the final $Co_{1-x}Ni_xSi_2$ film from that of $CoSi_2$ to that of $NiSi_2$, Smeets *et al.* expected to see a gradual increase in epitaxial quality by adding more Ni to the deposited Co(Ni) alloy.

In order to quantify the epitaxial quality of the film with increasing Ni content, the RBS channeling yield was measured as a function of the Ni content in the Co(Ni) alloy along with some high-resolution pole figures measured on selected samples (see Fig. 1.27). Based on these measurements, Smeets *et al.* were able to divide the texture evolution of the $Co_{1-x}Ni_xSi_2$ films with increasing Ni content into three regions. First, for Ni concentrations ranging between 0 and 15%, the addition of Ni gradually changes the typical polycrystalline axiotaxy $CoSi_2$ texture [66] to an epitaxially textured $Co_{1-x}Ni_xSi_2$ film where the {110} planes are aligned with the substrate (evidenced by the epitaxial spots visible in the 15% pole figure of Fig. 1.27 which can be explained with this orientation). This epitaxial alignment however differs from the expected $NiSi_2$-type epitaxy

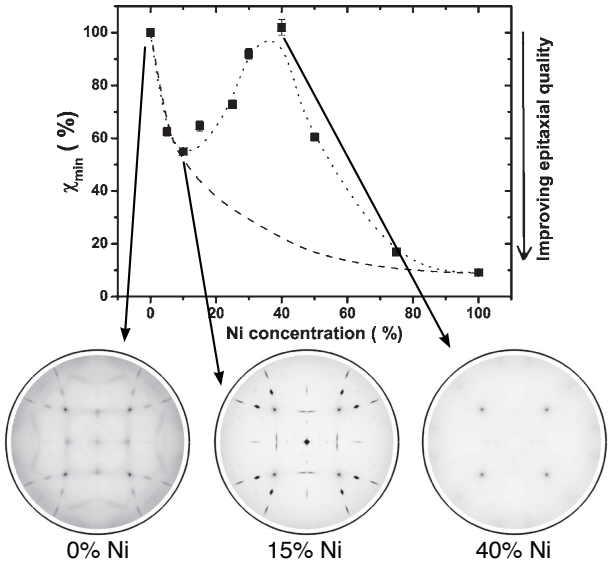

Figure 1.27. RBS channeling yield for $Co_{1-x}Ni_xSi_2$ films on Si(001) as a function of the Ni concentration in the deposited Co(Ni) alloy along with high-resolution pole figures measured on samples with Ni concentrations of 0, 15 and 40%. The dotted line in the RBS channeling yield plot is a guide to the eye while the dashed line depicts the expected improvement in epitaxial quality with increasing Ni concentration when only changes in lattice matching are taken into account. Figures reprinted with permission from Smeets et al., J Appl Phys 103, (2008). Copyright 2008, American Institute of Physics.

where a {001} plane is parallel to the interface. Second, increasing the Ni concentration from 15 to 40% destroys the {110} epitaxial orientation and a randomly oriented film is obtained for a Ni concentration of 40% (evidenced by the featureless 40% pole figure in Fig. 1.27). Third, increasing the Ni concentration beyond 50% and thus forming a Ni-rich $Co_{1-x}Ni_xSi_2$ film results in a gradually improving epitaxial {001} orientation as is expected for a $NiSi_2$ film.

Based solely on geometrical considerations and the improving lattice match between $Co_{1-x}Ni_xSi_2$ and Si with increasing Ni content, a steady improvement of the $Co_{1-x}Ni_xSi_2$ {001} oriented epitaxial quality of the film should be observed [43]. Thus, to explain the dominance of the {110} epitaxial orientation for low Ni concentrations (between 0 and 15%) and the deterioration of the epitaxial quality between 15 and 40%, Smeets *et al.* looked into the growth kinetics during $Co_{1-x}Ni_xSi_2$ formation. These kinetics were already investigated in detail by D'Heurle *et al.* [165] in the

mid 80s and showed that the preferred nucleation sites of $Co_{1-x}Ni_xSi_2$ were located at different locations in the film for different Ni concentrations in the deposited Co(Ni) alloy. A summary of these positions is provided in Fig. 1.28. For a low Ni concentration ($\leq$ 15%), the film consists of CoSi prior to the formation of the $Co_{1-x}Ni_xSi_2$ disilicide phase. Due to the immiscibility of CoSi and NiSi, the Ni is in solution and is found near the interface with the Si substrate. As the disilicide phase nucleates at that interface [43], a preferential orientation with respect to the substrate is enabled for the growing grains (see Fig. 1.28a). Smeets *et al.* proposed that the dominance of {110} oriented grains arises from a lower nucleation temperature and a larger lateral growth rate compared to grains belonging to the other texture components. For Ni concentrations between 15 and 40%, NiSi and CoSi are both present prior to $Co_{1-x}Ni_xSi_2$ formation due to their immiscibility. D'Heurle *et al.* observed that NiSi and CoSi are present in a bilayer structure with NiSi near the interface with the Si substrate and CoSi at the surface of the film. Surprisingly, they found that the formation of $Co_{1-x}Ni_xSi_2$ primarily happens in the interface region between the two monosilicide phases away from the Si substrate (see Fig. 1.28b). The nucleation at this interface can be attributed to the fact that the nucleation barrier is the smallest where the inhomogeneity in the metal distribution is the largest [43, 165, 166]. As this interface region is not in direct contact with the Si substrate, the nucleating grains can only develop a preferential orientation related to that of the CoSi and NiSi films, not directly to that of the Si(001) substrate. Increasing the Ni content in this concentration range gradually widens and moves the CoSi/NiSi interface region away from the substrate, resulting in an increasingly random texture as more and more $Co_{1-x}Ni_xSi_2$ grains will nucleate in that region. For Ni-rich concentrations (i.e. $>$ 50% Ni), the NiSi/CoSi interface region keeps moving further towards the surface and becomes smaller. This allows an increasing amount of Ni-rich $Co_{1-x}Ni_xSi_2$ grains to form in the NiSi region at the interface (see Fig. 1.28c) with the typical $NiSi_2$ {001} epitaxial orientation, which amounts to the improving epitaxial quality of the $Co_{1-x}Ni_xSi_2$ film when approaching the pure 100% Ni case.

From the discussion of the two examples above, it is clear that the use of soluble alloying elements during silicide formation greatly influences the texture of the resulting silicide phase. When trying to explain the observed influence on texture, it is clear that both the change in unit cell dimensions of the silicide due to the incorporation of the alloying element as well as the kinetics and redistribution of the alloying element during the solid-state

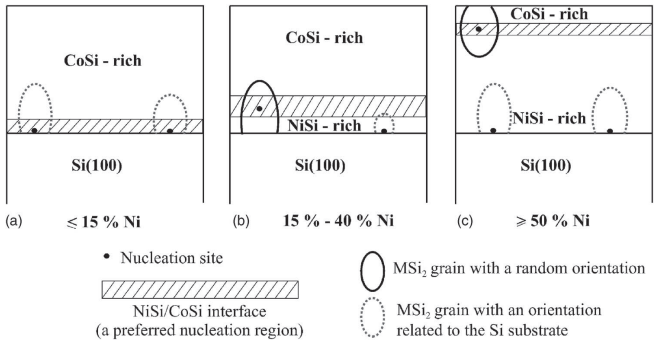

Figure 1.28. Schematic of the position of the preferred $Co_{1-x}Ni_xSi_2$ nucleation sites for three different Ni concentration ranges: (a) $\leq$ 15%; (b) 15-40%; (c) >50%. Figure reprinted with permission from Smeets et al., J Appl Phys 103, (2008). Copyright 2008, American Institute of Physics.

reaction have to be taken into account. Intuitively, a similar influence of alloying on the texture of germanides can be expected, although literature reports on this subject are hard to find at the time of writing.

1.5.4 Altered kinetics by adding insoluble elements: alloys and interlayers

Elements added to the metal-silicon/germanium system that are not significantly soluble in the targeted silicide/germanide are not expected to have an influence on the unit cell dimensions of that phase. As such, the texture of the targeted phase will mainly be influenced by altered formation kinetics due to the presence of the insoluble third element, as it can e.g. influence grain boundary or interface energies and grain boundary diffusion by residing at the grain boundaries of the silicide/germanide or at the interface between the silicide/germanide and the substrate.

In 2004, Özcan *et al.* published a detailed study on the texture of $CoSi_2$ that was formed through the solid-state reaction between a Si(001) substrate and a thin Co film alloyed with 5% Ti [65], a concentration that is well above the solubility limit of Ti in CoSi and $CoSi_2$. The upper part of Fig. 1.29 shows the *in situ* XRD measurements performed on both a pure Co film and a Co(5%Ti) alloy, which reveal a significant influence of the presence of Ti on the phase formation. From these measurements, it can be observed that the formation temperature of the three cobalt silicides, i.e. Co_2Si, CoSi and $CoSi_2$, is shifted to higher temperatures when formed

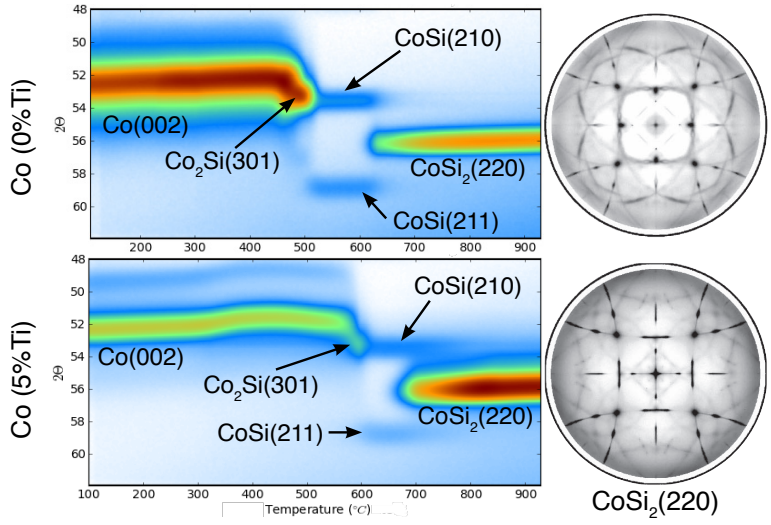

Figure 1.29. Top: *in situ* XRD measurements for the formation of $CoSi_2$ from a pure Co film (top row) and a Co film alloyed with 5% Ti (bottom row). The initial Co and Co(Ti) layers had a thickness of 20nm and were annealed at a rate of 3°C/s to 950°C to form $CoSi_2$ [65]. Next to the *in situ* XRD measurements, $CoSi_2$ (220) pole figures recorded on the final $Cosi_2$ film are presented. Pole figures reprinted with permission from Özcan et al., J Appl Phys 95, 8376 (2004). Copyright 2004, American Institute of Physics.

from the Co(5%Ti) alloy. Furthermore, the intensity of the $CoSi_2$(220) peak is significantly higher in the case of the Co(5%Ti) alloy (the maximum intensity in the lower *in situ* XRD pattern is about 3.5 times higher than in the upper one), indicating that the two films exhibit a different microstructure and overal texture.

The texture of the $CoSi_2$ formed from a pure Co film and a Co(5%Ti) alloy were measured using high-resolution pole figures (lower part of Fig. 1.29). A complete overview of the different texture components present in a pure $CoSi_2$ on Si(001) has been published by De Keyser *et al.* [66] and was summarized in section 1.3.4.2. From their observations, Özcan *et al.* observed that the addition of 5% Ti resulted in an increased intensity of the axiotaxy component that is related to the alignment of the $CoSi_2\{110\}$ planes that are perpendicular to the substrate surface (i.e. those having poles with $\chi = 90°$) with Si{110} planes. Furthermore, the increased number of $CoSi_2$ grains having their (110) plane parallel to the substrate, as suggested by the *in situ* XRD results, was confirmed by the pole figure measurements which showed an increased intensity for the spots belong-

ing to an epitaxial component with $CoSi_2$(110)//Si(001) [65]. Özcan *et al.* proposed different growth kinetics for the different texture components as an explanation for the observed change in relative volume fractions of the texture components between pure $CoSi_2$ and $CoSi_2$ formed from a Co(5%Ti) alloy. Because the presence of Ti pushes the nucleation temperature of $CoSi_2$ to a higher temperature (due to the influence on grain boundary and/or interface energy), the growth of the competing texture components at this elevated temperature can be expected to result in a change of relative volume fractions if their growth kinetics differ. The fact that growth kinetics can be different between texture components of a single silicide/germanide phase has also been observed in the case of C54-$TiSi_2$ [29].

In the early 90s, an even more pronounced influence of Ti on the texture of $CoSi_2$ was observed when a thin layer of Ti was introduced as an interlayer between the Co film and the Si substrate. Annealing such a Co/Ti/Si stack resulted in the formation of a thin, single crystal, epitaxial $CoSi_2$ layer. As epitaxial silicides were an important study subject at that time, this process was investigated further and was named *titanium mediated epitaxy* [96, 167] (TIME) (see also section 1.3.1). In the mid 90s, Tung *et al.* discovered that an interlayer of SiO_2 (the native oxide forming on Si) has a similar effect and even leads to better quality epitaxial $CoSi_2$ films than in the case of a Ti interlayer. This technique was termed *oxide mediated epitaxy* (OME) [95, 96]. The epitaxial disilicide formation achieved using TIME and OME can be linked to the altered phase formation sequence. Indeed, epitaxial $CoSi_2$ formation was also observed either using low-rate reactive deposition of Co onto a Si substrate, thereby skipping the metal-rich phases in the formation sequence, or by depositing Co atoms sufficiently slowly onto a heated Si(001) substrate (on which epitaxial $CoSi_2$ formation is impossible using a simple solid-phase reaction), which also resulted in the direct formation of epitaxial CoSi2 [91, 168]. The standard OME technique allowed for the growth of only a very thin layer of epitaxial $CoSi_2$ ($\sim$ 1-3nm), which was then used as a template layer for MBE growth of a thicker film of epitaxial $CoSi_2$. It was observed later that the use of a Ti capping layer on top of the Co/SiO_x/Si stack allowed for the formation of thicker layers of epitaxial $CoSi_2$ ($\sim$ 10-30nm) [96, 169–171].

Subsequently, Detavernier *et al.* observed that the use of interlayers of Mo or Cr [97], as well as alloys or interlayers of Ta or W [98] induces similar effects on the texture of the resulting $CoSi_2$ which grows with a strong preferential (110) and (100) orientation (i.e. the $CoSi_2$ grains pref-

erentially grow with their (110) or (100) plane parallel to the substrate). Based on their results, they proposed a mechanism explaining the influence of these interlayers on the $CoSi_2$ texture. For very thin interlayers, the insoluble element will be present on the grain boundaries of the preceding CoSi phase, influencing the grain boundary energy and thus the $CoSi_2$ nucleation which can result in a growth with a preferential orientation. Thicker interlayers will act as a diffusion barrier, limiting the flux of Co atoms diffusing towards the substrate. In this way, the formation of CoSi is inhibited and $CoSi_2$ can form as the first phase at the interface in contact with the single crystal Si substrate [98]. The presence of these two regimes was observed for all the elements studied. Not surprisingly, as diffusion properties depend on materials, the interlayer thickness for which the system moves from one regime to the other was found to depend on the element studied.

In the Ni-Si system, Deduytsche *et al.* reported in 2007 that the use of W, which is insoluble in NiSi, as an alloying element influences the texture of NiSi formed from a thin Ni(W) alloy. They observed that using small amounts of W ($\sim$ 2%) already significantly decreases the intensity of the axiotaxial NiSi texture components, while alloying with 7% W or more changes the overall texture of the resulting NiSi film from axiotaxy to epitaxy. However, an explanation as to why the observed epitaxial texture component forms was lacking and is still an open question today [38].

1.5.5 Texture inheritance from a precursor phase

In this last section, we discuss texture inheritance, a phenomenon in which the texture of a targeted silicide/germanide is influenced by a strong, distinct texture of the phase from which it forms. An example of this can be found in the case of silicide formation from a thin amorphous mixture of Ni with 40at.% of Si. In 2008, De Keyser *et al.* observed that annealing such a layer on a Si(001) or (111) substrate leads to the formation of an epitaxially aligned hexagonal θ phase as the first forming phase instead of the combination of different Ni-rich silicides that form for a pure Ni film [45] (see also section 1.4.1 for details on the phase formation for a pure Ni film on Si). This can be seen in the *in situ* XRD measurements for both a pure Ni film and a Ni(40%Si) mixture on Si(001) displayed in Fig. 1.30. The fact that hardly any diffraction peaks are visible in the measurement for the Ni(40%Si) mixture before the formation of NiSi suggests the presence of a highly epitaxial phase. Pole figure measurements along with EBSD

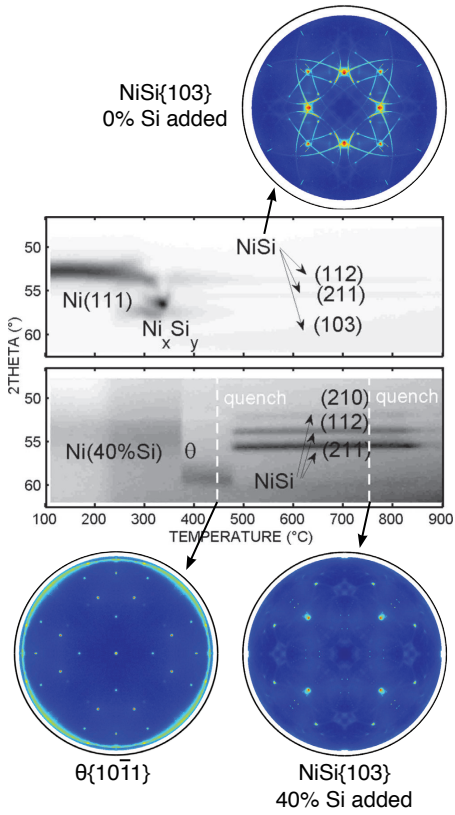

Figure 1.30. *in situ* XRD measurement of the formation of NiSi from a 10nm Ni (top) or 10nm Ni(40%Si) (bottom) film, through a ramp anneal at 3°C/s on a (001) oriented Silicon-On-Insulator (SOI) substrate. Pole figures for the NiSi phase in both cases and for the θ phase forming from the Ni(40%Si) film are included. *in situ* XRD measurements reprinted with permission from Van Bockstael et al., Appl Phys Lett 94, 033504 (2009). Copyright 2009, American Institute of Physics.

allowed De Keyser *et al.* to identify this phase as the θ phase [45], growing with a strong epitaxial texture as evidenced by the clear diffraction spots visible in the $\theta\{101\}$ pole figure in Fig. 1.30.

In 2009, Van Bockstael *et al.* [42] found that the texture of the NiSi phase that forms from the epitaxial θ phase in the case of a Ni(40%Si) film on Si(001) or (111) is very different to the texture of NiSi when formed from a pure Ni layer. On both substrates, the final NiSi displays an epitaxial alignment with large grains instead of the typical axiotaxy texture

that is expected for NiSi growing from a pure Ni film (see section 1.4.1), which is illustrated through the NiSi{103} pole figures shown in Fig. 1.30 for NiSi formed on a Si(001) substrate. Van Bockstael *et al.* argued that the peculiar epitaxial texture of NiSi formed from a Ni(40%Si) mixture must be a consequence of the presence of the epitaxial θ phase from which it forms. Otherwise, one would expect to observe this epitaxial NiSi component also in NiSi forming from a pure Ni layer, which is not the case (see section 1.3.4.3). Furthermore, it was pointed out that similarities between the crystal structures of the θ phase and NiSi suggest that the formation of NiSi out of θ only requires a relatively minor rearrangement of the Si atoms, implying that the Si sublattice can remain more or less stationary during the transformation of θ into NiSi. This could provide a mechanism through which the epitaxial alignment of the θ phase can be inherited by NiSi, explaining the observed epitaxial NiSi texture. On Si(111), Van Bockstael *et al.* observed that the epitaxial orientation of the θ phase and NiSi are indeed closely related, supporting the proposed mechanism of texture inheritance. However, on Si(001) no such simple relation between the two epitaxial alignments could be identified, showing that in this case the inheritance mechanism is more complex (and is still an open question). In addition, the inherited epitaxial texture of the NiSi phase was found to have an important impact on the morphological stability of the film. Van Bockstael *et al.* observed that the agglomeration temperature for an epitaxial NiSi film formed from a Ni(40%Si) mixture is significantly higher than for a NiSi film with the typical axiotaxy texture formed from a pure Ni layer (about 100°C higher for a 3°C/s anneal). This observation enhances our argument put forward in section 1.4.3 that the presence of axiotaxy promotes agglomeration.

More recently, a similar mechanism of texture inheritance has been put forward by Gaudet *et al.* to explain the observed fiber texture of the θ phase during the reaction of a pure Ni film with Si(001) [34]. According to Gaudet *et al.*, the θ phase inherits this fiber texture from the preceding δ-Ni_2Si phase, which also exhibits a fiber texture. Furthermore, it was observed in this study that the well-known axiotaxy texture of the NiSi phase is convoluted with a broad fiber texture. Gaudet *et al.* argued that the NiSi inherits this broad fiber from either the θ or the δ-Ni_2Si phase, as this latter phase was observed to re-appear right before NiSi growth starts.

1.6 Summary and conclusions

Thin films of silicides and germanides formed through a solid-state reaction between a thin metal film and a single crystal silicon or germanium substrate are widely studied in the microelectronics research community as they have an important application as electrical contacts in both present and future microelectronic devices. An important consequence of forming such thin films on a single crystal substrate is that the film grains can develop a preferential orientation with respect to the substrate during growth. This preferential grain orientation is referred to as the texture of the film. In this review, we provided an overview of the research that has been performed over the past decades targeting this texture in thin silicide/germanide films.

As the study of texture in such films initially relies on the ability to perform a measurement, we first discussed the two most important techniques that are used in modern texture studies, i.e. synchrotron based X-ray pole figures and electron backscattered diffraction. The first technique provides a straightforward way for a qualitative identification of the different phases and texture components that are present in the film, while the latter technique can provide a more quantitative picture of the different texture components and of the microstructure (grain size, grain morphology, etc.) of the film.

In the following section, we provided a historical overview of how texture in these films was addressed during the early years of silicide research, when focus was mainly directed towards the growth of epitaxial silicides. At this point, we discussed the driving forces for texture development in such films. It was argued that a minimization of interface energy drives the grains in the film to grow with a preferential orientation that results in a periodic interface structure in either one (axiotaxy) or two (epitaxy) dimension(s). It was pointed out that in the case of axiotaxy, plane alignment across the interface results in a periodic interface structure in one dimension, the periodic nature of which is preserved irrespective of interfacial curvature. For an epitaxial alignment, the periodic interface structure in one or both of the two dimensions can also be the result of plane alignment, in which case the epitaxy is more stable than when the periodicity within the interface plane is not caused by plane alignment.

The remainder of the review was aimed at providing a structured overview of texture research that has been published since the early 2000s, when the technique of high-resolution synchrotron based X-ray pole figure

measurements was introduced. It was pointed out that texture measurements are often crucial to unambiguously identify the correct phase formation sequence during silicide/germanide formation, as highly textured phases are easily overlooked using standard measurement techniques. The influence of texture on different important thin film properties such as phase stability, morphological stability and electrical properties were discussed. Importantly, it was argued that the agglomeration of a thin silicide/germanide film is promoted if axiotaxy is the dominant texture type.

As many properties of thin silicide/germanide films are influenced by their microstructure, it is important to understand the factors that can affect film texture. One can then exploit these and attempt to control the texture of these films. As an example, alloying of the binary films with a third element that is either soluble or insoluble in the targeted silicide/germanide has proven to effectively alter the final texture. Although a few detailed studies probing the influence of alloying elements on silicide texture have been performed and discussed in this review, open questions on how different alloying elements impact texture development (and hence the phase formation sequence) during silicide formation still remain. Furthermore, the impact of alloying on the texture of germanide films is a research area still to be explored.

References

[1] Maex, K. & Van Rossum, M. *Properties of Metal Silicides* (Inspec, 1995).

[2] Nicolet, M. A. & Lau, S. S. Formation and Characterization of Transition-Metal Silicides. In *VLSI Electronics: Microstructure Science* (1986).

[3] Osburn, C. M. Silicides. In *Rapid Thermal Processing Science and Technology* (ed. Fair, R. B.) (1993).

[4] Miglio, L. & d'Heurle, F. *Silicides: Fundamentals and Applications* (World Scientific, 1999).

[5] Lavoie, C., d'Heurle, F. M. & Zhang, S.-L. Silicides. In *Handbook of Semiconductor Manufacturing Technology* (eds. Nishi, Y. & Doering, R.) (2007).

[6] Chen, L.-J. *Silicide Technology for Integrated Circuits* (The Institution of Electrical Engineers, 2004).

[7] Zhang, S.-L. & Östling, M. Metal Silicides in CMOS Technology: Past, Present, and Future Trends. *Critical Reviews in Solid State and Materials Sciences* **28**, 1–129 (2003).

[8] Gambino, J. P. & Colgan, E. G. Silicides and ohmic contacts. *Materials Chemistry and Physics* **52**, 99–146 (1998).

[9] Murarka, S. P. Silicide thin films and their applications in microelectronics. *Intermetallics* **3**, 173–186 (1995).

[10] Murarka, S. P. Refractory silicides for integrated circuits. *J. Vac. Sci. Technol.* **17**, 775 (1980).

[11] Naik, G. V., Shalaev, V. M. & Boltasseva, A. Alternative Plasmonic Materials: Beyond Gold and Silver. *Adv. Mater.* **25**, 3264–3294 (2013).

[12] Schmitt, A. L., Higgins, J. M., Szczech, J. R. & Jin, S. Synthesis and applications of metal silicide nanowires. *J Mater Chem* **20**, 223–235 (2009).

[13] Kleinke, H. New bulk Materials for Thermoelectric Power Generation: Clathrates and Complex Antimonides. *Chem Mater* **22**, 604–611 (2009).

[14] Murarka, S. P. *Silicides for VLSI applications* (Academic Press, 1983).

[15] d'Heurle, F. M. Silicide interfaces in silicon technology. *Journal of Elec Materi* **27**, 1138–1147 (1998).

[16] Maex, K. Silicides for integrated circuits: $TiSi_2$ and $CoSi_2$. *Mat Sci Eng R* **11**, vii–153 (1993).

[17] Lavoie, C., d'Heurle, F. M., Detavernier, C. & Cabral, C. Towards implementation of a nickel silicide process for CMOS technologies. *Microelectron Eng* **70**, 144–157 (2003).

[18] Mangelinck, D., Dai, J. Y., Pan, J. S. & Lahiri, S. K. Enhancement of thermal stability of NiSi films on (100)Si and (111)Si by Pt addition. *Appl Phys Lett* **75**, 1736–1738 (1999).

[19] Yu, H. *et al.* 1.5×10^9 Ωcm^2 Contact Resistivity on Highly Doped Si:P Using Ge Pre-amorphization and Ti Silicidation. In *2015 International ELectron Devices Meeting* (2015).

[20] Lin, C. H. *et al.* High performance 14nm SOI FinFET CMOS technology with 0.0174μm^2 embedded DRAM and 15 levels of Cu metallization. In *2014 IEEE International Electron Devices Meeting (IEDM)*, 3.8.1–3.8.3 (IEEE, 2014).

[21] Pillarisetty, R. Academic and industry research progress in germanium nanodevices. *Nature* **479**, 324–328 (2011).

[22] Gaudet, S., Detavernier, C., Kellock, A. J., Desjardins, P. & Lavoie, C. Thin film reaction of transition metals with germanium. *J Vac Sci Technol A* **24**, 474 (2006).

[23] Bunge, H.-J. *Texture Analysis in Materials Science*. Mathematical Methods (Butterworths London, 1982).

[24] Kocks, U. F., Tomé, C. N. & Wenk, H. R. *Texture and Anisotropy*. Preferred Orientations in Polycrystals and their Effect on Materials Properties (Cambridge University Press, 2000).

[25] Randle, V. & Engler, O. *Introduction to Texture Analysis: Macrotexture, Microtexture, and Orientation Mapping, Second Edition* (CRC Press, 2009).

[26] Feldman, L. C. & Mayer, J. W. *Fundamentals of surface and thin film analysis* (Prentice Hall, 1986), 1st edn.

[27] Schulz, L. G. A Direct Method of Determining Preferred Orientation of a Flat Reflection Sample Using a Geiger Counter X-Ray Spectrometer. *J Appl Phys* **20**, 1030–1033 (1949).

[28] Bulle-Lieuwma, C. W. T., van Ommen, A. H., Hornstra, J. & Aussems, C. N. A. M. Observation and analysis of epitaxial growth of $CoSi_2$ on (100) Si. *J Appl Phys* **71**, 2211 (1992).

[29] Özcan, A. S. *et al.* Texture of $TiSi_2$ thin films on Si (001). *J Appl Phys* **92**, 5011 (2002).

[30] Detavernier, C. *et al.* An off-normal fibre-like texture in thin films on single-crystal substrates. *Nature* **426**, 641–645 (2003).

[31] Heizmann, J. J. & Laruelle, C. Simultaneous measurement of several

X-ray pole figures. *J Appl Crystallogr* **19**, 467–472 (1986).

[32] Gaudet, S., Desjardins, P. & Lavoie, C. The thermally-induced reaction of thin Ni films with Si: Effect of the substrate orientation. *J Appl Phys* **110**, 113524 (2011).

[33] De Keyser, K. *et al.* Phase formation and texture of nickel silicides on $Si_{1-x}C_x$ epilayers. *Microelectron Eng* **88**, 536–540 (2011).

[34] Gaudet, S., Coia, C., Desjardins, P. & Lavoie, C. Metastable phase formation during the reaction of Ni films with Si(001): The role of texture inheritance. *J Appl Phys* **107**, 093515 (2010).

[35] De Keyser, K. *et al.* Phase formation and thermal stability of ultrathin nickel-silicides on Si(100). *Appl Phys Lett* **96**, 173503 (2010).

[36] Gaudet, S. *et al.* Three dimensional reciprocal space measurement by x-ray diffraction using linear and area detectors: Applications to texture and defects determination in oriented thin films and nano-precipitates. *J. Vac. Sci. Technol. A* **31**, 021505 (2013).

[37] Mocuta, C. *et al.* Fast pole figure acquisition using area detectors at the DiffAbs beamline - Synchrotron SOLEIL. *J Appl Crystallogr* **46**, 1842–1853 (2013).

[38] De Keyser, K. *Texture of thin silicide and germanide films*. PhD thesis (Ghent University, 2011).

[39] Schwartz, A. J., Kumar, M., Adams, B. L. & Field, D. P. (eds.). *Electron Backscatter Diffraction in Materials Science* (Springer US, Boston, MA, 2009).

[40] De Keyser, K., Detavernier, C. & Van Meirhaeghe, R. L. Characterization of the texture of silicide films using electron backscattered diffraction. *Appl Phys Lett* **90**, 121920 (2007).

[41] De Keyser, K., Van Meirhaeghe, R. L., Detavernier, C., Jordan-Sweet, J. & Lavoie, C. Texture of Cobalt Germanides on Ge(100) and Ge(111) and Its Influence on the Formation Temperature. *J Electrochem Soc* **157**, H395–H404 (2010).

[42] Van Bockstael, C. *et al.* Influence of a transient hexagonal phase on the microstructure and morphological stability of NiSi films. *Appl Phys Lett* **94**, 033504 (2009).

[43] Smeets, D., Vantomme, A., De Keyser, K., Detavernier, C. & Lavoie, C. The role of lattice mismatch and kinetics in texture development: $Co_{1-x}Ni_xSi_2$ thin films on Si(100). *J Appl Phys* **103** (2008).

[44] Van Bockstael, C. *et al.* Effect of Pt addition on growth stress and thermal stress of NiSi films. *J Appl Phys* **104**, 053510 (2008).

[45] De Keyser, K. *et al.* Epitaxial Formation of a Metastable Hexagonal

Nickel-Silicide. *Electrochem Solid St* **11**, H266 (2008).

[46] Föll, H., Ho, P. S. & Tu, K. N. Transmission electron microscopy of the formation of nickel silicides. *Philosophical Magazine A* **45**, 31–47 (1981).

[47] Teodorescu, V. *et al.* In situ transmission electron microscopy study of Ni silicide phases formed on (001) Si active lines. *J Appl Phys* **90**, 167–174 (2001).

[48] Alberti, A. *et al.* Pseudoepitaxial transrotational structures in 14 nm-thick NiSi layers on [001] silicon. *Acta Crystallogr B Struct Sci* **61**, 486–491 (2005).

[49] Detavernier, C. & Lavoie, C. Influence of Pt addition on the texture of NiSi on Si(001). *Appl Phys Lett* **84**, 3549–3551 (2004).

[50] Detavernier, C., Jordan-Sweet, J. & Lavoie, C. Texture of NiSi films on Si(001), (111), and (110) substrates. *J Appl Phys* **103**, 113526 (2008).

[51] Tu, K.-N., Alessandrini, E. I., Chu, W.-K., Krautle, H. & Mayer, J. W. Epitaxial Growth of Nickel Silicide $NiSi_2$ on Silicon. *Jpn. J. Appl. Phys.* **13**, 669 (1974).

[52] Ishiwara, H., Hikosaka, K., Nagatomo, M. & Furukawa, S. Characterization of epitaxial metal silicide films grown on silicon. *Surface Science* **86**, 711–717 (1979).

[53] Saitoh, S., Ishiwara, H., Asano, T. & Furukawa, S. Single Crystalline Silicide Formation. *Jpn. J. Appl. Phys.* **20**, 1649–1656 (1981).

[54] Fung, M. S. & Cheng, H. C. Localized epitaxial growth of C54 and C49 $TiSi_2$ on (111)Si. *Appl Phys Lett* **47**, 1312–1314 (1985).

[55] Wu, I. C. & Chu, J. J. Local epitaxy of $TiSi_2$ on (111)Si: Effects due to rapid thermal annealing and to the annealing atmosphere. *J Appl Phys* **60**, 3172–3175 (1986).

[56] Chu, J. J. & Wu, I. C. Transmission electron microscope study of the growth kinetics of $TiSi_2$ epitaxy on (111)Si. *J Appl Phys* **61**, 549–551 (1987).

[57] Catana, A. *et al.* Atomic scale study of local $TiSi_2$/Si epitaxies. *J Appl Phys* **67**, 1820–1825 (1990).

[58] Wan, W.-K. & Wu, S.-T. Texture of titanium self-aligned silicide (salicide). *Scripta Materialia* **35**, 53–58 (1996).

[59] Wan, W.-K. & Wu, S.-T. Epitaxial $TiSi_2$ on silicon by rapid thermal annealing. *Materials Letters* **30**, 105–108 (1997).

[60] Wang, L.-M. & Wu, S.-T. Epitaxial Growth of $TiSi_2$ (C49) on (001)Si by Rapid Thermal Annealing. *Jpn. J. Appl. Phys.* **36**, 6475–6480

(1997).

[61] Svilan, V. *et al.* Crystallographic texture of C54 titanium disilicide as a function of deep submicron structure geometry. *Journal of Elec Materi* **26**, 1090–1095 (1997).

[62] La Via, F. *et al.* Role of the substrate in the C49-C54 transformation of $TiSi_2$. *J Vac Sci Technol B* **18**, 721–728 (2000).

[63] Yalisove, S. M., Tung, R. T. & Loretto, D. Epitaxial orientation and morphology of thin $CoSi_2$ films grown on Si(100): Effects of growth parameters. *J Vac Sci Technol A* **7**, 1472–1474 (1989).

[64] Zegenhagen, J., Patel, J. R., Freeland, P. E. & Tung, R. T. Co on Si(111) - Silicide Formation. *Phys. Rev. B* **44**, 13626–13630 (1991).

[65] Özcan, A. S., Ludwig Jr, K. F., Detavernier, C., Lavoie, C. & Jordan-Sweet, J. Axiotaxy of $CoSi_2$ thin films on Si(100) substrates and the effects of Ti alloying. *J Appl Phys* **95**, 8376 (2004).

[66] De Keyser, K., Detavernier, C., Jordan-Sweet, J. & Lavoie, C. Texture of $CoSi_2$ films on Si(111), (110) and (001) substrates. *Thin Solid Films* **519**, 1277–1284 (2010).

[67] Jedrecy, N., Zheng, Y., Waldhauer, A., Sauvage-Simkin, M. & Pinchaux, R. Epitaxy of β-$FeSi_2$ on Si(111). *Phys. Rev. B* **48**, 8801–8808 (1993).

[68] Detavernier, C., Lavoie, C., Jordan-Sweet, J. & Özcan, A. S. Texture of tetragonal α-$FeSi_2$ films on Si(001). *Phys. Rev. B* **69**, 174106 (2004).

[69] Bower, R. W., Sigurd, D. & Scott, R. E. Formation kinetics and structure of Pd_2Si films on Si. *Solid-State Electronics* **16**, 1461–1471 (1973).

[70] Buckley, W. D. & Moss, S. C. Structure and electrical characteristics of epitaxial palladium silicide contacts on single crystal silicon and diffused P-N diodes. *Solid-State Electronics* **15**, 1331–1337 (1972).

[71] Hutchins, G. A. & Shepela, A. Growth and Transformation of Pd_2si on (111), (110) and (100) Si. *Thin Solid Films* **18**, 343–363 (1973).

[72] Kawamura, T., Shinoda, D. & Muta, H. Oriented Growth Of The Interfacial PtSi Layer Or Between Pt And Si. *Appl Phys Lett* **11**, 101–103 (1967).

[73] Sinha, A. K., Marcus, R. B., Sheng, T. T. & Haszko, S. E. Thermal stability of thin PtSi films on silicon substrates. *J Appl Phys* **43**, 3637–3643 (1972).

[74] Ben Ghozlene, H., Beaufrère, P. & Authier, A. Crystallography of PtSi films on (001) silicon. *J Appl Phys* **49**, 3998–4004 (1978).

[75] Kumpf, C., Nicula, R. & Burkel, E. Growth and Structure of Thin Pt_2Si and PtSi Layers on Si(111) and (001) Characterized with In Situ Grazing Incidence Diffraction. *J Appl Crystallogr* **30**, 1016–1021 (1997).

[76] Falke, M. *et al.* Axiotaxy of $CrSi_2$ on Si(001); from the Micrometer- to the Angstrom-Scale. *Microscopy and Microanalysis* **13**, 396–397 (2007).

[77] Vantomme, A. *et al.* Stabilisation and phase transformation of hexagonal rare-earth silicides on Si(111). *Nucl Instrum Methods Phys Res B* **147**, 261–266 (1999).

[78] Knapp, J. A. & Picraux, S. T. Epitaxial growth of rare-earth silicides on (111)Si. *Appl Phys Lett* **48**, 466–468 (1986).

[79] Liew, S. L., Balakrisnan, B., Ho, C. S., Thomas, O. & Chi, D. Z. Phase and Texture of Er-Germanide Formed on Ge(001) Through a Solid-State Reaction. *J Electrochem Soc* **154**, H9–H12 (2007).

[80] Geenen, F. *et al.* On the formation and structural properties of hexagonal rare earth (Y, Gd, Dy, Er and Yb) disilicide thin films. *J Alloys Compd* **611**, 149–156 (2014).

[81] Balakrisnan, B. *et al.* Texture of NiGe on Ge(001) and its evolution with formation temperature. *Appl Phys Lett* **87**, 241922 (2005).

[82] Gaudet, S., Detavernier, C., Lavoie, C. & Desjardins, P. Reaction of thin Ni films with Ge: Phase formation and texture. *J Appl Phys* **100**, 034306 (2006).

[83] Hsieh, Y. F., Marshall, E. D. & Lau, S. S. Partial epitaxial growth of cobalt germanides on (111)Ge. *Appl Phys Lett* **51**, 1588 (1987).

[84] Sun, H. P. *et al.* Formation and evolution of epitaxial Co_5Ge_7 film on Ge (001) surface by solid-state reaction in an in situ ultrahigh-vacuum transmission electron microscope. *Appl Phys Lett* **87**, 211909 (2005).

[85] Hsieh, Y. F. Interfacial reactions of palladium thin films on Ge(111) and Ge(001). *Thin Solid Films* **162**, 295–303 (1988).

[86] Geenen, F. *et al.* Formation and texture of palladium germanides studied by in situ X-ray diffraction and pole figure measurements. *Thin Solid Films* **551**, 86–91 (2014).

[87] Hsieh, Y. F. Interfacial reactions of platinum thin films on (111) and (001) germanium. *J Appl Phys* **63**, 1177 (1988).

[88] De Schutter, B. *et al.* Phase Formation and Texture of Platinum Germanides on Ge(001) and Ge(111) (to be submitted).

[89] Tung, R. T., Poate, J. M., Bean, J. C., Gibson, J. M. & Jacobson, D. C.

Epitaxial silicides. *Thin Solid Films* **93**, 77–90 (1982).

[90] Tu, K. N. Epitaxial growth of transition-metal silicides on silicon. *Materials Science Reports* **6**, 53–140 (1991).

[91] Vantomme, A., Degroote, S., Dekoster, J., Langouche, G. & Pretorius, R. Concentration-controlled phase selection of silicide formation during reactive deposition. *Appl Phys Lett* **74**, 3137–3139 (1999).

[92] Pretorius, R., Theron, C. C., Vantomme, A. & Mayer, J. W. Compound Phase Formation in Thin Film Structures. *Critical Reviews in Solid State and Materials Sciences* **24**, 1–62 (1999).

[93] Tung, R. T., Gibson, J. M. & Poate, J. M. Growth of Single-Crystal Epitaxial Silicides on Silicon by the Use of Template Layers. *Appl Phys Lett* **42**, 888–890 (1983).

[94] Dass, M. L. A., Fraser, D. B. & Wei, C. S. Growth of epitaxial $CoSi_2$ on (100)Si. *Appl Phys Lett* **58**, 1308–1310 (1991).

[95] Tung, R. T. Oxide mediated epitaxy of $CoSi_2$ on silicon. *Appl Phys Lett* **68**, 3461 (1996).

[96] Tung, R. T. & Ohmi, S. Epitaxial silicide interfaces in microelectronics. *Thin Solid Films* **369**, 233–239 (2000).

[97] Detavernier, C. *et al.* Formation of epitaxial $CoSi_2$ by a Cr or Mo interlayer: Comparison with a Ti interlayer. *J Appl Phys* **89**, 2146–2150 (2001).

[98] Detavernier, C., Lavoie, C. & Van Meirhaeghe, R. L. CoSi2 formation in the presence of Ti, Ta or W. *Thin Solid Films* **468**, 174–182 (2004).

[99] White, A. E., Short, K. T., Dynes, R. C., Garno, J. P. & Gibson, J. M. Mesotaxy: Formation of Buried Single-Crystal $CoSi_2$ Layers by Implantation. *MRS Proceedings* **74**, 481 (1986).

[100] Mantl, S. Ion beam synthesis of epitaxial silicides: fabrication, characterization and applications. *Materials Science Reports* **8**, 1–95 (1992).

[101] Mantl, S. & Bay, H. L. New method for epitaxial heterostructure layer growth. *Appl Phys Lett* **61**, 267–269 (1992).

[102] Mantl, S. Molecular beam allotaxy: a new approach to epitaxial heterostructures. *J. Phys. D: Appl. Phys.* **31**, 1–17 (1998).

[103] Hsieh, Y. F., Marshall, E. D. & Lau, S. S. Partial Epitaxial Growth of Ni_2Ge and NiGe on Ge(111). *Thin Solid Films* **162**, 287–294 (1988).

[104] De Schutter, B. *et al.* Phase formation and texture of thin Ni films on Ge: formation of a transient hexagonal germanide and influence

of substrate orientation (to be submitted).
[105] Tucker, M. D. *et al.* Substrate orientation effects on the nucleation and growth of the $M_{n+1}AX_n$ phase Ti_2AlC. *J Appl Phys* **109**, 014903 (2011).
[106] Lambert-Milot, S. *et al.* MnP nanoclusters embedded in GaP epitaxial films grown by organometallic vapor-phase epitaxy: A reciprocal space mapping and transmission electron microscopy study. *J Vac Sci Technol A* **30**, 061510 (2012).
[107] d'Heurle, F. M. Nucleation of a New Phase from the Interaction of Two Adjacent Phases. *Journal of Materials Research* 100 (1987).
[108] Richard, M. I. *et al.* Continuous and Collective Grain Rotation in Nanoscale Thin Films during Silicidation. *Phys Rev Lett* **115**, 266101–5 (2015).
[109] Chen, L.-J. (ed.). *Silicide Technology for Integrated Circuits* (2009).
[110] Harper, J. M. E., C, C. J. & Lavoie, C. Mechanisms for Enhanced Formation of the C54 Phase of Titanium Silicide Ultra-Large-Scale Integration Contacts. *Annu Revs Mat Sci* **30**, 523–543 (2000).
[111] Geenen, F., Jordan-Sweet, J., Lavoie, C. & Detavernier, C. Texture of C49- and C54-$TiSi_2$ on Si(001) and Si(111) (to be submitted).
[112] Deduytsche, D., Detavernier, C., Van Meirhaeghe, R. L. & Lavoie, C. High-temperature degradation of NiSi films: Agglomeration versus $NiSi_2$ nucleation. *J Appl Phys* **98**, 033526 (2005).
[113] Alberti, A., Spinella, C., La Magna, A. & Rimini, E. Nucleation and growth of NiSi from Ni_2Si transrotational domains. *Appl Phys Lett* **90**, 053507–4 (2007).
[114] Alberti, A. & La Magna, A. Role of the early stages of Ni-Si interaction on the structural properties of the reaction products. *J Appl Phys* **114**, 121301 (2013).
[115] Detavernier, C., Lavoie, C. & d'Heurle, F. M. Thermal expansion of the isostructural PtSi and NiSi: Negative expansion coefficient in NiSi and stress effects in thin films. *J Appl Phys* **93**, 2510 (2003).
[116] d'Heurle, F. M., Petersson, C. S., Baglin, J. E. E., La Placa, S. J. & Wong, C. Y. Formation of thin films of NiSi: Metastable structure, diffusion mechanisms in intermetallic compounds. *J Appl Phys* **55**, 4208–4218 (1984).
[117] von Känel, H. Growth and characterization of epitaxial Ni and Co silicides. *Materials Science Reports* **8**, 193–269 (1992).
[118] Tinani, M. *et al.* In situ real-time studies of nickel silicide phase formation. *J Vac Sci Technol B* **19**, 376–383 (2001).

[119] Lavoie, C. *et al.* Reactive Diffusion in the Ni-Si System: Phase Sequence and Formation of Metal-Rich Phases. *Defect and Diffusion Forum* **237-240**, 825–836 (2005).

[120] Lavoie, C. *et al.* Effects of additive elements on the phase formation and morphological stability of nickel monosilicide films. *Microelectron Eng* **83**, 2042–2054 (2006).

[121] Nash, P. & Nash, A. The Ni-Si (Nickel-Silicon) system. *Bulletin of Alloy Phase Diagrams* **8**, 6–14 (1987).

[122] Gibson, J. M. & Batstone, J. L. In-situ transmission electron microscopy of $NiSi_2$ formation by molecular beam epitaxy. *Surface Science* **208**, 317–350 (1989).

[123] De Schutter, B. *et al.* Phase formation and texture of thin nickel germanides on Ge(001) and Ge(111). *J Appl Phys* **119**, 135305 (2016).

[124] Colgan, E. G., Gambino, J. P. & Hong, Q. Z. Formation and stability of silicides on polycrystalline silicon. *Mat Sci Eng R* **16**, 43–96 (1996).

[125] De Keyser, K., Detavernier, C., Van Meirhaeghe, R. L., Jordan-Sweet, J. & Lavoie, C. The Texture of Thin NiSi Films and Its Effect on Agglomeration. In *Applications of Texture Analysis* (ed. Rollett, A. D.), 1–9 (John Wiley & Sons, Inc., Hoboken, NJ, USA, 2008).

[126] Nolan, T. P., Sinclair, R. & Beyers, R. Modeling of agglomeration in polycrystalline thin films: Application to $TiSi_2$ on a silicon substrate. *J Appl Phys* **71**, 720–6 (1992).

[127] Tung, R. T. Recent advances in Schottky barrier concepts. *Mat Sci Eng R* **35**, 1–138 (2001).

[128] Tung, R. T. The physics and chemistry of the Schottky barrier height. *Applied Physics Reviews* **1**, 011304 (2014).

[129] Mott, N. F. The Theory of Crystal Rectifiers. *Proceedings of the Royal Society of London. Series A* **171**, 27–38 (1939).

[130] Schottky, W. Zur Halbleitertheorie der Sperrschicht- und Spitzengleichrichter. *Z. Physik* **113**, 367–414 (1939).

[131] Tung, R. T. Schottky-Barrier Formation at Single-Crystal Metal-Semiconductor Interfaces. *Phys Rev Lett* **52**, 461–464 (1984).

[132] Hauenstein, R. J., Schlesinger, T. E., McGill, T. C., Hunt, B. D. & Schowalter, L. J. Schottky barrier height measurements of epitaxial $NiSi_2$ on Si. *Appl Phys Lett* **47**, 853 (1985).

[133] Ospelt, M., Henz, J., Flepp, L. & von Känel, H. Schottky barriers of epitaxial $NiSi_2$ on Si(111). *Appl Phys Lett* **52**, 227 (1988).

[134] Vrijmoeth, J., van der Veen, J. F., Heslinga, D. R. & Klapwijk, T. M.

Medium-energy ion-scattering study of a possible relation between the Schottky-barrier height and the defect density at $NiSi_2$/Si(111) interfaces. *Phys. Rev. B* **42**, 9598–9608 (1990).

[135] Tung, R. T., Levi, A., Sullivan, J. P. & Schrey, F. Schottky-Barrier Inhomogeneity at Epitaxial $NiSi_2$ Interfaces on Si(100). *Phys Rev Lett* **66**, 72–75 (1991).

[136] Song, Y. P., Van Meirhaeghe, R. L., Laflère, W. H. & Cardon, F. On the difference in apparent barrier height as obtained from capacitance-voltage and current-voltage-temperature measurements on Al/p-InP Schottky barriers. *Solid-State Electronics* **29**, 633–638 (1986).

[137] Tung, R. T. Electron transport at metal-semiconductor interfaces: General theory. *Phys. Rev. B* **45**, 13509–13523 (1992).

[138] Tung, R. T. Electron-Transport of Inhomogeneous Schottky Barriers. *Appl Phys Lett* **58**, 2821–2823 (1991).

[139] Werner, J. H. & Güttler, H. H. Temperature dependence of Schottky barrier heights on silicon. *J Appl Phys* **73**, 1315 (1993).

[140] Bell, L. D. & Kaiser, W. J. Observation of Interface Band Structure by Ballistic-Electron-Emission Microscopy. *Phys Rev Lett* **61**, 2368–2371 (1988).

[141] Meyer, T., Sirringhaus, H. & von Känel, H. Studying interfaces on a nm scale by BEEM. *Thin Solid Films* **318**, 195–200 (1998).

[142] Lee, E. Y., Sirringhaus, H. & von Känel, H. Direct mapping of the $CoSi_2$/Si(111) interface by ballistic-electron-emission microscopy and modulation spectroscopy. *Phys. Rev. B* **50**, 14714–14717 (1994).

[143] Lee, E. Y., Sirringhaus, H., Kafader, U. & von Känel, H. Ballistic-electron-emission-microscopy investigation of hot-carrier transport in epitaxial $CoSi_2$films on Si(100) and Si(111). *Phys. Rev. B* **52**, 1816–1829 (1995).

[144] von Känel, H., Meyer, T. & Klemenc, M. Ballistic-Electron-Emission Microscopy on Epitaxial Silicides. *Jpn. J. Appl. Phys.* **37**, 3800–3804 (1998).

[145] Detavernier, C., Van Meirhaeghe, R. L., Donaton, R., Maex, K. & Cardon, F. Ballistic electron emission microscopy study of barrier height inhomogeneities introduced in Au/n-Si Schottky contacts by a HF pretreatment. *J Appl Phys* **84**, 3226 (1998).

[146] Zhu, S. *et al.* Ballistic electron emission microscopy studies of the temperature dependence of Schottky barrier height distribution in $CoSi_2$/n-Si(100) diodes formed by solid phase reaction **44**, 2217–

2223 (2000).
[147] Zaring, C., Jiang, H., Svensson, B. G. & Östling, M. Boron redistribution during formation of nickel silicides. *Applied Surface Science* **53**, 147–152 (1991).
[148] Murarka, S. P. & Williams, D. S. Dopant redistribution in silicide-silicon and silicide-polycrystalline silicon bilayered structures. *J Vac Sci Technol B* **5**, 1674–1688 (1987).
[149] Wittmer, M. Silicide contacts for shallow junction devices. *Thin Solid Films* **107**, 99–110 (1983).
[150] Hoummada, K., Tellouche, G., Blum, I. D., Portavoce, A. & Mangelinck, D. Arsenic clustering during formation of the transient Ni silicide. *Scripta Materialia* **67**, 169–172 (2012).
[151] Panciera, F. *et al.* Three dimensional distributions of arsenic and platinum within NiSi contact and gate of an n-type transistor. *Appl Phys Lett* **99**, 051911 (2011).
[152] Cojocaru-Mirédin, O., Perrin-Pellegrino, C., Mangelinck, D. & Blavette, D. Boron redistribution during reactive diffusion in Ni-Si contacts. *Microelectron Eng* **87**, 271–273 (2010).
[153] Kimura, H. & Tomita, R. Texture change of NiSi film with dopant implantation. In *Interconnect Technology Conference and Materials for Advanced Metallization (IITC/MAM), 2011*, 1–3 (2011).
[154] Bauer, M., Weeks, D., Zhang, Y. & Machkaoutsan, V. Tensile Strained Selective Silicon Carbon Alloys for Recessed Source Drain Areas of Devices. *ECS Transactions* **3**, 187–196 (2006).
[155] Machkaoutsan, V. *et al.* Improved thermal stability of Ni-silicides on Si:C epitaxial layers. *Microelectron Eng* **84**, 2542–2546 (2007).
[156] Demeulemeester, J. *et al.* Pt redistribution during Ni(Pt) silicide formation. *Appl Phys Lett* **93**, 261912 (2008).
[157] Demeulemeester, J. *et al.* The influence of Pt redistribution on $Ni_{1-x}Pt_xSi$ growth properties. *J Appl Phys* **108**, 043505 (2010).
[158] Demeulemeester, J. *et al.* On the growth kinetics of Ni(Pt) silicide thin films. *J Appl Phys* **113**, 163504 (2013).
[159] Hoummada, K., Perrin-Pellegrino, C. & Mangelinck, D. Effect of Pt addition on Ni silicide formation at low temperature: Growth, redistribution, and solubility. *J Appl Phys* **106**, 063511 (2009).
[160] Mangelinck, D. *et al.* Three-dimensional composition mapping of NiSi phase distribution and Pt diffusion via grain boundaries in Ni2Si. *Scripta Materialia* **62**, 568–571 (2010).
[161] Putero, M., Ehouarne, L., Ziegler, E. & Mangelinck, D. First silicide

formed by reaction of Ni(13%Pt) films with Si(100): Nature and kinetics by in-situ X-ray reflectivity and diffraction. *Scripta Materialia* **63**, 24–27 (2010).

[162] Panciera, F. *et al.* Direct epitaxial growth of θ-Ni_2Si by reaction of a thin Ni(10at.% Pt) film with Si(100) substrate. *Scripta Materialia* **78-79**, 9–12 (2014).

[163] Adusumilli, P. *et al.* Tomographic study of atomic-scale redistribution of platinum during the silicidation of $Ni_{0.95}Pt_{0.05}$/Si(100) thin films. *Appl Phys Lett* **94**, 113103–4 (2009).

[164] Adusumilli, P., Seidman, D. N. & Murray, C. E. Silicide-phase evolution and platinum redistribution during silicidation of Ni0.95Pt0.05/Si(100) specimens. *J Appl Phys* **112**, 064307–12 (2012).

[165] d'Heurle, F. M., Anfiteatro, D. D., Deline, V. R. & Finstad, T. G. Reaction of silicon with films of Co-Ni alloys: Phase separation of the monosilicides and nucleation of the disilicides. *Thin Solid Films* **128**, 107–124 (1985).

[166] Detavernier, C., Qu, X. P., Van Meirhaeghe, R. L., Li, B. Z. & Maex, K. Mixing entropy and the nucleation of silicides: Ni-Pd-Si and Co-Mn-Si ternary systems. *Journal of Materials Research* **18**, 1668–1678 (2003).

[167] Tung, R. T. & Schrey, F. Ti-Interlayer Mediated Epitaxy of $CoSi_2$ with Ti Capping. *MRS Proceedings* **402**, 173 (1995).

[168] Vantomme, A., Nicolet, M. A. & Theodore, N. D. Epitaxial Cosi2 Films on Si(100) by Solid-Phase Reaction. *J Appl Phys* **75**, 3882–3891 (1994).

[169] Kim, G. B., Kwak, J. S., Baik, H. K. & Lee, S.-M. Ex situ formation of oxide-interlayer-mediated-epitaxial $CoSi_2$ film using Ti capping. *J Vac Sci Technol B* **17**, 162–165 (1999).

[170] Detavernier, C., Van Meirhaeghe, R. L., Cardon, F., Donaton, R. A. & Maex, K. $CoSi_2$ formation in the presence of interfacial silicon oxide. *Appl Phys Lett* **74**, 2930 (1999).

[171] Detavernier, C., Van Meirhaeghe, R. L., Cardon, F. & Maex, K. $CoSi_2$ formation through SiO_2. *Thin Solid Films* **386**, 19–26 (2001).

2

Interface Visualisation

Paper II

Visualisation and classification of epitaxial alignment at hetero-phase boundaries
B. De Schutter, K. De Keyser and C. Detavernier
Thin Solid Films, 599, p. 104-112, 2016
doi:10.1016/j.tsf.2015.12.051

2.1 Introduction

Traditionally, epitaxy is considered within the context of (thin) film growth. Over the past decades, the majority of epitaxial growth experiments have been performed on inorganic films with a similar crystal structure and lattice spacing as the single crystal substrate, using techniques such as *Molecular Beam Epitaxy (MBE)* or *Metalorganic Chemical Vapour Deposition (MOCVD)* [1–3]. For example, there has been a lot of interest in the epitaxial growth of Ge and III-V films for (opto)electronic applications such as Ge or III-V based CMOS (Complementary Metal-Oxide-Semiconductor) devices [4–

6] and III-V/Si photonics (on-chip lasers, optical interconnects,...) [7, 8]. In view of this link with film growth, epitaxy is usually analysed as a two-dimensional problem and epitaxial alignment is explained by a tendency for 'matching' within the plane of the interface.

However, the concept of matching interfaces is not restricted to film deposition. In the field of metallurgy, it is well-known that certain types of grain boundaries (homo-interfaces) or precipitate/matrix boundaries (hetero-interfaces) are preferred [9, 10]. In thin film metallurgy, it is known that poly-crystalline thin films that are formed by a solid-state reaction are often strongly textured. Over the past decade, efforts in this field have been directed mostly towards the investigation of texture in silicides (or germanides) formed on single crystalline Si (or Ge) substrates due to their application as contacting material in CMOS devices [11–21]. A first major difference between these thin silicide films and most MBE-type epitaxially grown films is the different crystal structure between the silicide film (e.g. orthorhombic NiSi, tetragonal $FeSi_2$, cubic $CoSi_2$,...) and the Si substrate (cubic). This results in poly-crystalline films in which the grains can exhibit different types of texture: epitaxy (fixed orientation of the grain with respect to the substrate), random (no preferred grain orientation) and axiotaxy, a type of texture that was discovered by investigating the texture of NiSi on Si(001) [22], in which the grains exhibit a rotational degree of freedom around a specific crystal direction. A second difference is that in the case of these thin films formed through a solid-state reaction, the interface under consideration is usually not perfectly flat, as opposed to the case of film growth on single crystalline substrates. Therefore, it is important to evaluate the robustness of texture components found in these poly-crystalline films with respect to interfacial roughness.

Different crystallographic theories have been put forward that try to understand or predict texture components, such as the *coincidence site lattice* [23] and *O-lattice* [24] theories. While these theories have been successful at describing texture in systems for which the adjoining phases have a similar crystal structure, they have a harder time describing the aforementioned thin film hetero-phase silicide/germanide systems [25, 26]. In the latter field, some material-specific theories have been put forward [27] that try to explain the observed texture through the 'matching' of atom lines or crystal planes *at* the interface, but none of them provides a truly general technique for texture prediction.

So far, attempts to explain the observation of certain epitaxial and axiotaxial texture components in silicide films have been made by looking at

cross-sections of real-space ball-and-stick models of the film and substrate lattice near the interface region [28, 29]. However, such visualizations have proven to be cluttered and often hard to interpret (especially for complex interfaces in the case of dissimilar crystal structures). In this paper, we propose an alternative method to visualize the degree of matching within the plane of the interface. We argue that a matching periodicity between the film lattice and the substrate lattice within the plane of the interface is a necessary condition in order to achieve preferential grain growth in the film. Visualizing this match in periodicity allows one to interpret the quality and the geometrical nature of the matching periodicity for a certain grain orientation. Secondly, we argue that extending the traditional 2D approach of matching *at* the interface with the concept of plane alignment *across* the interface allows for an improved classification of low-energy interfaces. This is experimentally verified by comparing epitaxial texture components for α-$FeSi_2$ films and NiSi films on a Si(001) substrate.

2.2 Visualization of Interfacial Matching

The driving force for an epitaxial alignment of a silicide/germanide thin film on a single crystal silicon or germanium substrate consists of a minimization in interface energy which is achieved by optimizing the bonding across the interface, in the sense that all bonds are satisfied (which translates into dense packing for metallic bonding) and/or that the bonds are formed at 'natural' bond angles, resulting in a fully coherent interface. This reduction in interface energy usually occurs at the expense of a certain amount of strain energy. Optimization of the bonding may occur through interface reconstruction, whereby the atoms in the couple of atomic layers near the interface are re-arranged, analogous to surface reconstruction at the crystal/vacuum interface.

It is intuitively clear that in order for this interface optimization to occur, there must be some sort of 'match' between the crystal structures of the film and the substrate at the interface. This matching is easy to imagine if the crystal structure of the film is identical or very similar to that of the substrate (e.g. $NiSi_2$ on Si), but in the case of dissimilar crystal structures (which is the case for most silicide/germanide thin films on Si/Ge), determining which grain orientations give rise to a good match at the interface is a non-trivial problem. In order to assess this matching at the interface for a certain orientation of a film grain with respect to the substrate lattice,

some sort of visualization of the interface is indispensable.

2.2.1 Disadvantages of atomistic interface models

The most straightforward way for visualizing the film-substrate interface is by constructing a 'ball-and-stick' model of both crystal lattices and placing these on top of each other, taking into account a specific orientation of the film grain with respect to the surface. This has for example been used in the past to analyze the observed epitaxial alignments for a thin α-$FeSi_2$ film formed on Si(001) [29]. Figure 2.1 shows some examples of 2D projections of such a 3D interface model along three different directions, covering a couple of unit cells along the horizontal and vertical directions, for an α-$FeSi_2$ grain on (001) oriented Si, belonging to an epitaxial texture component whereby a $FeSi_2${110} is parallel to a Si{110} plane and the $FeSi_2$(214) plane is parallel to the interface. Although the projection along Si(010) seems to nicely reveal a match between the two crystal structures, there are some important issues with this approach.

Firstly, texture studies are mostly performed using X-ray diffraction pole figures or electron backscattered diffraction. While these diffraction based techniques provide detailed information on the relative orientation between the film grain and substrate, they give no information on the relative translation between the two lattices. As such, creating such an atomistic model of the interface forces one to choose this relative translation based on intuition without direct experimental evidence. Secondly, complex local reconstruction will occur at the interface during nucleation and subsequent growth of a film grain [30], which is hard to measure and requires the use of additional techniques such as transmission electron microscopy.

Furthermore, even if a veracious model can be constructed that correctly accounts for the relative translation and the local reconstruction, it actually provides only limited information concerning the 'matching' of the two lattices at the interface. A relatively small mismatch between the unit cells of film and substrate projected onto the interface plane might look good over the small distance displayed in the real-space atomistic model (usually only a few unit cells), while in reality this seemingly small mismatch might mean that a defect must be present e.g. every 20 cells for a 5% mismatch in order to maintain the matching.

Thus, constructing an atomistic interface model by simply stacking the two oriented crystal structures of film and substrate on top of each other

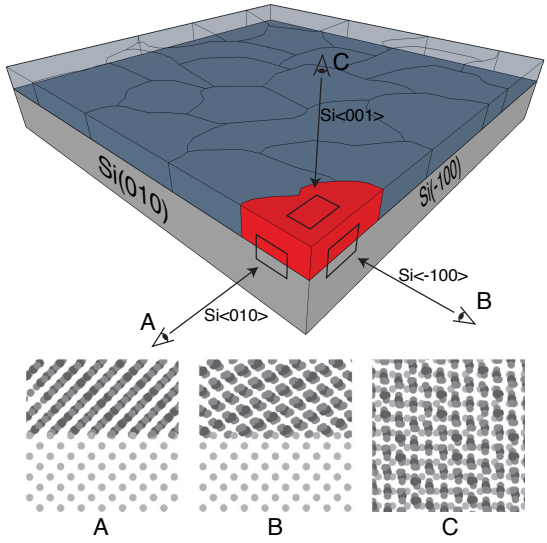

Figure 2.1. *top* Schematic representation of a polycrystalline α-$FeSi_2$ film on a (001) oriented single crystal Si substrate. *bottom* Calculated atomistic interface models viewed along the Si$< 010 >$ (A), $< \bar{1}00 >$ (B) and $< 001 >$ (C, top view) directions for a $FeSi_2$ grain belonging to an epitaxial texture component where a $FeSi_2 110$ plane is parallel to a Si110 plane and $FeSi_2(214)$ is parallel to the interface. The viewing directions are indicated on the top schematic.

results in an oversimplified visualization of the interface. Furthermore, while this technique might seem to result in 'good' visualizations of matching between 'simple' crystal structures (like tetragonal α-$FeSi_2$ on Si(001), see Fig. 2.1), for more complex interfaces (like e.g. orthorhombic NiSi on Si(001) or Si(111), see Fig. 2.2) such visualizations rapidly become cluttered and hard to interpret.

2.2.2 Map of Interfacial Periodicity (MIP)

As an alternative to the real-space atomistic representation of the interface discussed above, we propose a different method to visualize matching at the interface. As was mentioned before, the driving force for an epitaxial alignment is a reduction in interface energy through an optimization of the bonding across the interface. Since both the grain and the substrate have a periodic crystal structure, bonding can only be optimized in a systematic way along the entire length of the interface if the interface structure is

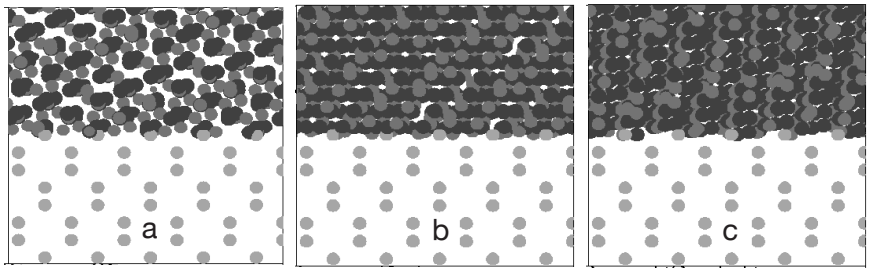

Figure 2.2. Calculated atomistic interface models of the cross section of the interface between a NiSi film and a Si(001) substrate. The figures represent the three epitaxial texture components that are observed for a NiSi film on Si(001), i.e. A_{100} (a), B_{100} (b) and C_{100} (c), which were described in detail by Detavernier *et al.*[18].

periodic. Hence, periodicity in the plane of the interface may be considered as a hallmark of 'matching' interfaces.

To visualize interfacial periodicity, we use the concept of a *map of interfacial periodicity* (MIP). For a certain orientation of a film grain with respect to the single crystal substrate (which can be defined by fixing the direction of two plane poles in both film and substrate), crystal planes from both the film and the substrate intersect the interface at angles ϕ and $90° - \chi$, with χ and ϕ the spherical coordinates (elevation and azimuth) of the pole for each plane (see Fig. 2.3a, $0 \leq \chi \leq 90°$; $0 \leq \phi < 360°$). The different planes in the crystal lattice of film and substrate each have their own d-spacing, which can be naively considered as the wavelength of the periodicity of the crystal lattice in the direction normal to the given plane. In view of evaluating the possibility for interface reconstruction, we are interested in the effective periodicity of film and substrate as seen in the plane of the interface. Therefore, we calculate the d-spacing as projected onto the plane of the interface (see fig. 2.3a)

$$d_p = \frac{d}{\cos(\frac{\pi}{2} - \chi)} = \frac{d}{\sin(\chi)} \tag{2.1}$$

for all low-index planes in both film and substrate (e.g. with h,k,l each ranging between -4 and 4). Two patterns (labeled '$\circ$' for substrate planes and '+' for planes in the film) are created by plotting dots at a distance $1/d_p$ from the origin and at an angle ϕ from the x-axis (see fig. 2.3b). We use the reciprocal $1/d_p$ as the radial distance coordinate, as using the real-space d_p values amounts to a very non-uniformly distributed set of points

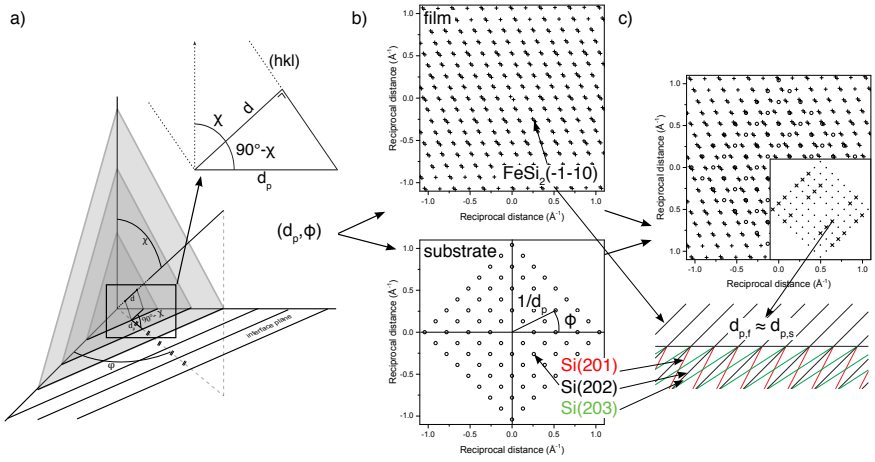

Figure 2.3. Different steps in the construction of a 'Map of Interfacial Periodicity' (MIP). a) Schematic representation of a family of crystal planes (from either the film or the substrate) intersecting the interface plane. The d-spacing of this plane family is depicted as d. Projecting this d-spacing onto the plane of the interface results in d_p. b) An MIP for both the film and substrate is created by plotting '+' or 'o' symbols at the $(\frac{1}{d_p}, \phi)$ coordinates of a collection of low-index planes (usually with (h, k, l) ranging between -4 and +4). c) The combined MIP allows to asses the matching at the interface by looking at the amount of overlap between the two patterns, aided by the overlap MIP visible in the inset. The schematic below sketches the side-on situation at the interface for the indicated planes.

that is hard to inspect. The graph that results from overlaying the patterns for the film and the substrate is what we refer to as a 'Map of Interfacial Periodicity' (MIP) (see Fig. 2.3c, top). In Fig. 2.3, we included the scale and units ($Å^{-1}$) on the x and y axes. Because this scale is not necessary to see the overlap between both patterns and because the reference pattern of the substrate is the same in all MIP graphs given in this paper, we will omit this scale in the graphs shown in the remainder of this work in order to maximize the space for the patterns.

The match of the crystal structures across the interface can then be evaluated by determining the amount of overlap between both patterns in the MIP (i.e. by comparing the effective periodicity of both lattices along each ϕ direction in the plane of the interface). In this way, the MIP provides a straightforward representation of in-plane matching when dealing with hetero-interfaces of low-symmetry (i.e. non-cubic) materials. We define a substrate plane and a film plane as matched at the interface if their difference in ϕ angle is smaller then $1°$ and their difference in pro-

jected d-spacing is less then 1%, i.e. $\Delta\phi = |\phi_{film} - \phi_{subs}| < 1^\circ$ and $\Delta d_p = |\frac{(d_{p,film} - d_{p,subs})}{d_{p,subs}}| < 1\%$. In other words, the projected d-spacings must be nearly identical:

$$d_{p,f} = \frac{d_f}{\sin(\chi_f)} \approx \frac{d_s}{\sin(\chi_s)} = d_{p,s} \tag{2.2}$$

where the subscripts f and s denote the film and substrate respectively. The limits on $\Delta\phi$ and Δd_p are chosen as a rule-of-thumb based on observations made in different silicide materials over the years. The amount of matching at the interface can then be visualized by creating an *overlap MIP* on which we mark the (d_p, ϕ) coordinates for film and substrate planes that match at the interface with a '$\times$' symbol (see the inset of Fig. 2.3c). The substrate MIP grid is included in the background as a reference frame (using '$\cdot$' symbols).

The conditions for matching discussed above are illustrated in more detail in figure 2.4a by the two points f_1 and f_2 representing the film planes $(h_{f,1}, k_{f,1}, l_{f,1})$ and $(h_{f,2}, k_{f,2}, l_{f,2})$ respectively and point s representing the substrate plane (h_s, k_s, l_s). For points f_2 and s, $\Delta\phi$ and Δd_p fall within the aforementioned limits (depicted with the dotted circle around point s), thus these planes match at the interface. This is not the case for f_1 and s, where Δd_p is clearly much larger then 1%. A side-on view of the planes arriving at the interface in the two situations is sketched in figure 2.4b and c.

2.2.3 Plane matching vs. plane alignment

The MIP as constructed above only compares the d_p and ϕ for low-index lattice planes in film and substrate. Comparison of the χ angle at which matching planes approach the interface provides information concerning the nature of the interfacial periodicity. One can distinguish two different mechanisms to create a periodic interface: plane matching or plane alignment. For a film and substrate plane that have a different d-spacing, a matching periodicity within the plane of the interface can only be obtained if both planes have a different χ angle. This is evidenced by eq. 2.2, from which it is clear that a (nearly) identical projected d-spacing for a film and substrate plane with different d-spacings is only possible when the χ angles are different too. This means that the substrate plane is not continued across the interface into the film (or vice versa, see situation in Fig. 2.4c), which is why we call this configuration '*plane matching*'. Alternatively, for

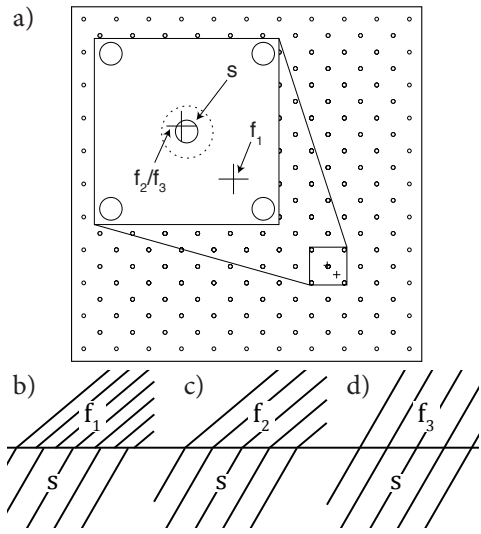

Figure 2.4. a) Illustration of the limits for matching planes at the interface on the MIP, characterized by the dotted circle around the location of the substrate plane 's'. b-d) Side-on views of the situation at the interface for the film planes labeled f_1, f_2 and f_3. The f_2 and f_3 planes end up at the same location on the MIP as they have the same projected d-spacing. To discern between the two situations, an overlap MIP can be constructed with different symbols for matched and aligned planes.

a film and substrate plane that have a (nearly) identical d-spacing, a periodic interface structure ($d_{p,f} \approx d_{p,s}$) is achieved when they share the same χ angle (see eq. 2.2). This means that the substrate and film plane are aligned across the interface and thus that both planes are extended across the interface (see situation in Fig. 2.4d), which is why this configuration is called '*plane alignment*'. In this work, a matching substrate and film plane are considered as 'aligned' across the interface if their difference in χ angle is less then 1°, i.e. $\Delta\chi = |\chi_{film} - \chi_{subs}| < 1^\circ$, meaning that they are (nearly) parallel. It is important to note that in this article, plane alignment inherently implies plane matching, meaning that aligned planes are always matched within the plane of the interface (see fig. 2.4c and d).

As was discussed above, in order to visualize the amount of matching within the plane of the interface for a specific grain orientation, an overlap MIP can be constructed (see inset of Fig. 2.3c). On such an overlap MIP, we can now differentiate between substrate and film planes that are either matched or aligned by using a different symbol in both cases. As such,

matched planes will be marked with a '×' symbol. For aligned planes, a difference is made based on wether the alignment is perfect ($\Delta\chi = 0$) or not ($0 < \Delta\chi < 1°$) using either '■' or '●' symbols respectively. Examples of such overlap MIP plots for certain orientations of α-$FeSi_2$ and NiSi on Si(001) can be found in the insets of figures 2.5d-f and 2.8b-d.

2.2.4 Classification of epitaxial grain orientations

Based on the arguments above about plane alignment and plane matching, the overlap MIP can be used to classify epitaxial grain orientations observed in thin films on single crystal substrates into different categories. For an epitaxial orientation to occur, a match in periodicity at the interface between the film grain and the substrate must be achieved in two different directions within the interface plane, effectively creating a 2-dimensional periodic interface structure. On the overlap MIP, this means that an epitaxial orientation is characterized by either '×', '■' or '●' symbols being visible for at least two different ϕ angles. If plane alignment is only observed in one direction on the overlap MIP (through '■' or '●' symbols), this is indicative of a grain belonging to an axiotaxy component, since axiotaxy is defined as an orientation in which a family of film planes is aligned across the interface with a family of substrate planes [22].

Firstly, if the matching periodicity for an epitaxial orientation in both directions within the interface plane is due to plane alignment, the orientation is classified as a *double-aligned* epitaxy. Practically, this means that either '■' or '●' symbols must be visible on the MIP for at least two independent ϕ angles (independent meaning not exactly 180° apart). Such epitaxial orientations have also been referred to as *double axiotaxy* [16, 29, 31] since an axiotaxy component is characterized by plane alignment in a single direction within the interface plane [22] and they are usually characterized by spots on the pole figures that are located at intersections between axiotaxy lines belonging to two different axiotaxy components. Secondly, when the matching periodicity is caused by plane alignment in only one direction, while mere plane matching is responsible for the match in the second direction, the epitaxy is classified as an *aligned* epitaxy. On the overlap MIP, this results in '■' or '●' symbols being visible at only one ϕ angle, while '×' symbols are visible for another independent ϕ angle. Finally, the epitaxy can result from plane matching in two directions (without alignment), in which case it is classified as a *matched* epitaxy. In this case, only '×' symbols are visible on the overlap MIP for at least two independent

directions.

As this classification might seem quite abstract at this point, we will apply it to two thin film silicides for which the texture has been thoroughly studied in the past, i.e. α-$FeSi_2$ [29] and NiSi [18]. As can already be seen in table 2.1, examples of all the types of epitaxial orientations discussed above will be covered in these case studies.

2.2.5 MIP limitations

It is important to realize that the requirement of periodicity in the plane of the interface is a necessary, though not sufficient condition for optimization of the bonding across the interface. Therefore, some orientations of the grain may result in an apparently good quality match in the overlap MIP, while they are not experimentally observed. It is conceivable that other mechanisms may provide additional selection rules, favoring certain types of alignment. Therefore, sufficient care should be taken when trying to use the MIP to predict which orientations will grow epitaxially for a given combination of film/substrate materials. A second limitation of the MIP consists of its abstraction of the atomistic nature of the interface. For instance, the MIP does not take into account the 'natural' bond angles (e.g. covalent bonding along Si(111) directions in the substrate) for the atoms at the interface, nor the matching of individual atoms along the matching planes.

2.3 Case study: α-$FeSi_2$ on Si(001)

As was mentioned in the introduction, epitaxially matching grains have been reported to occur for several films that are formed by a solid-state reaction [13–17, 19, 28, 29, 32]. In this paragraph, we will show the usefulness of the (overlap) MIP when analysing the texture components found in a tetragonal α-$FeSi_2$ film formed on a cubic Si(001) single crystal substrate.

We published a detailed analysis of the texture of α-$FeSi_2$ formed on Si(001) using synchrotron pole figure measurements in a previous article [29]. In figure 2.5a we included the α-$FeSi_2$ pole figure in which the pattern of lines is created by grains exhibiting an axiotaxial texture for which the α-$FeSi_2$(110) ($d = 1.9049$nm) plane is aligned to a Si{220} ($d = 1.9201$nm) plane in the substrate [29], resulting in an interface that is periodic along a Si[100] direction. The preferred alignment between the $FeSi_2$(110) plane

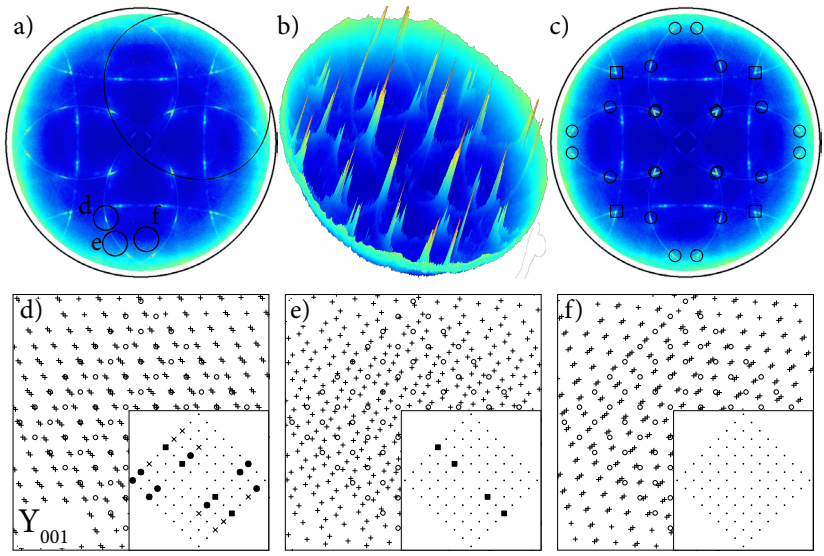

Figure 2.5. a-c) $FeSi_2(101)$ pole figure (reprinted from [29]). The sample is oriented with Si(011) at $(\chi, \phi) = (45°, 45°)$. The highlighted axiotaxy line in a) results from grains exhibiting the $FeSi_2(110)$//Si(110) axiotaxy that have their fiber axis at (χ, ϕ)=$(45°, 45°)$. A 3D-view of the data is provided in b). Fitted (101) pole locations for grains exhibiting epitaxy X_{001} ('□') and Y_{001} ('○') are shown in c). d) MIP for a grain exhibiting epitaxy Y_{001} ($FeSi_2(110)$//Si(110) and $FeSi_2(214)$ parallel to the interface). The points corresponding to lattice planes from the film are indicated by '+', while the substrate planes are shown as '○'. The inset of each MIP shows it's corresponding overlap MIP with '■' for perfectly aligned planes, '●' for aligned planes and '×' for matching planes. e) and f) MIP's for grains that originally satisfied epitaxy Y_{001}, but that are rotated over 5° around the off-normal fiber axis (grain e) or around the pole to a random plane (grain f). Note that the orientation of the three grains is indicated on pole figure a).

and a Si{220} plane manifests itself as an off-normal fiber texture, with the fiber axis along the ($\chi = 45°$; $\phi = 45, 135, 225, 315°$) directions [29]. The intensity variations along the lines of the pole figure are related to periodicity along a second, independent direction in the plane of the interface. The brightest spots on the lines are caused by grains which are epitaxially aligned with the Si substrate. The high intensity of these spots with respect to the background is clearly visible in the 3-dimensional view of the pole figure provided in figure 2.5b. Four different types of epitaxy were found to occur within the same film [29]. For each of these epitaxial components, the $FeSi_2(110)$ plane is aligned to a Si{011} plane and a low-index $FeSi_2$ plane ((001), (100), (111) or (214)) is parallel to the interface.

In the remainder of this case study, we will consider two of these exitaxial components, i.e. the one with $FeSi_2$(001)//Si(001) and the one with $FeSi_2$(214)//Si(001). For easy reference in the remainder of this paper, we will label these epitaxial components as X_{001} and Y_{001} respectively, where the subscripts refer to the orientation of the substrate. The expected pole locations of the $FeSi_2${101} planes for both epitaxies on the $FeSi_2$(101) pole figure are visible in figure 2.5c with epitaxy X_{001} and Y_{001} indicated as '□' and '○' respectively.

As explained in the previous paragraph, the MIP can be used to qualitatively compare the degree of matching in the plane of the interface for a specific grain orientation. As an illustration, Figures 2.5d-f show the MIP for three differently oriented α-$FeSi_2$ grains, marked as d, e and f on the pole figure (fig. 2.5a). Orientation d corresponds to a grain in the Y_{001} epitaxy. The 2D periodicity in the plane of the interface for this grain orientation is clearly visible in the overlap MIP (inset in fig. 2.5d). First, we observe perfectly aligned planes in the $\phi = 135, 315°$ directions (visualised by the '■' symbols), related to the axiotaxial alignment described above. Secondly, we see a rather large collection of other substrate-film plane couples that are either nearly aligned ($\Delta\chi < 1°$, $\Delta\phi < 1°$, $\Delta d_p < 1\%$, marked as '●') or matched at the interface ($\Delta\chi \geq 1°$, $\Delta\phi < 1°$, $\Delta d_p < 1\%$, marked as '×'), thus resulting in a 2D periodic interface structure. Due to the perfect plane alignment in the axiotaxy direction and the near-alignment of other substrate-film plane couples in other directions, the resulting epitaxy is said to be *double-aligned*. For orientation e, which is located on the axiotaxy line but does not coincide with a high intensity spot, only the alignment in the axiotaxy direction is visible in the MIP (see figure 2.5e). Finally, in the case of orientation f, which corresponds to a low intensity region in the pole figure, no matching or aligned planes can be observed in the MIP (see figure 2.5f).

2.3.1 Robustness of the matching interface

The classification of epitaxial components on the basis of plane alignment (for (double-)aligned epitaxy) or plane matching has important consequences for the robustness of the 'matching' nature of the interface. In this paragraph, we will show that achieving periodicity by plane alignment renders the periodic nature of the interface structure more stable with respect to perturbations in grain orientation or interfacial roughness.

2.3.1.1 Perturbations in grain orientation

Firstly, we consider perturbations in grain orientation. In the absence of plane alignment, a rotation of the grain along any axis will transform the 2D periodic interface structure into a random interface without any periodicity. For aligned epitaxy, a small rotation of the epitaxial grain along the off-normal fiber axis (i.e. along the direction perpendicular to the aligned planes) will transform the nature of the interface from 2D into 1D periodic, while a small rotation around any other axis will transform it from 2D periodic into random. This explains the experimentally observed shape of the spots on the pole figures, where the aligned epitaxy is observed in the form of bright, elongated spots along the pattern of lines created by the axiotaxy texture resulting from the alignment. This influence of rotating an aligned epitaxially oriented grain along either the off-normal fiber axis or an arbitrary axis can be readily observed from the three α-$FeSi_2$ orientations discussed above. Indeed, orientation e corresponds to a 25° rotation of the epitaxial orientation Y_{001} around the Si(110) axiotaxy axis and only the 1D periodicity in the axiotaxy direction survives (see figure 2.5e). In the case of orientation f, achieved by a 25° degree rotation around an arbitrary axis (here $FeSi_2$(012)), the periodicity in the interface plane is completely lost (see figure 2.5f).

2.3.1.2 Interfacial roughness

Secondly, we consider perturbations in interface orientation (resulting in interfacial curvature or roughness). As mentioned in the introduction, robustness of texture components against such perturbations is important when considering texture development during the growth of a silicide/germanide phase, since the nucleation of a new silicide/germanide phase during a solid-state reaction usually takes place at a non-flat interface.

For thin films with a reasonably flat interface, the interface will be nominally parallel to the initial surface of the single crystal substrate, which defines the laboratory frame of reference for the pole figure measurements. Interfacial curvature will cause the local interface plane to become rotated with respect to the single crystal substrate and is therefore equivalent to a local rotation of the xy-plane of the reference frame around an arbitrary rotation axis lying within the plane of the non-rotated interface. This rotation results in a tilt of the z-axis of the laboratory frame of reference over a tilt angle α in the direction perpendicular to the rotation axis in the interface plane. This direction, which we call the tilt direction, is defined by

an azimuthal angle β in the laboratory reference frame.

Here, we are interested in the influence of interfacial roughness on the matching and alignment of crystal planes at the interface. Since the relative orientation of the planes does not change when tilting the interface (e.g. parallel planes remain parallel), plane matching will only remain if the projected d-spacing of a film-substrate plane couple remains compatible after interface tilting. Since $d_p = d/\sin(\chi)$, the projected d-spacing along the tilted interface will be given by $d'_p = d/\sin(\chi')$, with χ' the χ angle of the plane in the tilted frame of reference. Thus, the matching periodicity within the plane of the interface is maintained after interface tilting if $\Delta d'_p = |\frac{(d'_{p,film} - d'_{p,subs})}{d'_{p,subs}}| < 1\%$. In other words, the projected d-spacings of the substrate and film planes that were matched before the interface tilt must remain (nearly) identical after the tilt:

$$d'_{p,f} = \frac{d_f}{\sin(\chi'_f)} \approx \frac{d_s}{\sin(\chi'_s)} = d'_{p,s} \tag{2.3}$$

Due to the interface tilt, the χ angle of a lattice plane will change according to:

$$\begin{aligned} \chi' = \quad \arccos \quad & [\cos(\alpha)\cos(\chi) \\ & - \sin(\alpha)\sin(\chi)\cos(\beta - \phi)] \end{aligned} \tag{2.4}$$

Plotting this χ' as a function of the interface tilt α along different tilting directions β for an arbitrary plane (see figure 2.6a) shows that the χ angles will change according to

$$\chi' = \chi + \gamma \quad \text{with} \begin{cases} -|\alpha| \leq \gamma \leq |\alpha| & \text{if} \quad |\alpha| < \chi \\ -\chi \leq \gamma \leq |\alpha| & \text{if} \quad |\alpha| \geq \chi \end{cases} \tag{2.5}$$

for all planes that have the same ϕ direction. This means that the χ angle for film and substrate planes that are matched or aligned changes over the same constant angle γ for a certain interface tilt α. Taking equation (2.5) into account, we can see that for film and substrate planes that were only matched at the untilted interface and thus for which equation (2.2) holds with $d_s \neq d_f$ and $\chi_s \neq \chi_f$, equation (2.3) can never be fulfilled and thus the matching is lost at the tilted interface (see Fig. 2.6b). In contrast, for planes that are aligned at the untilted interface and thus for which equation (2.2) holds with $d_s \approx d_f$ and $\chi_s \approx \chi_f$, equation (2.3) remains valid and the periodic interface match is preserved at the tilted interface (see Fig.

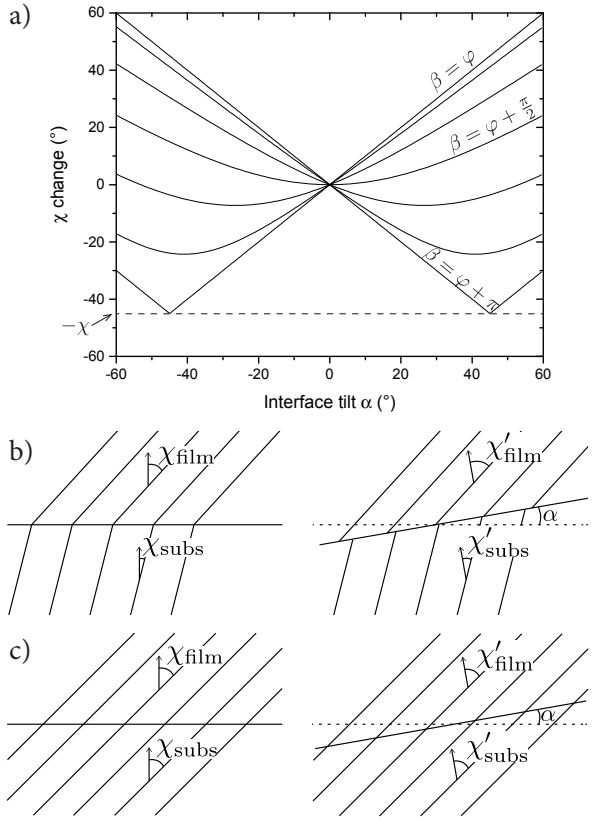

Figure 2.6. a) Resulting χ angle in the reference frame of the tilted interface of a plane pole at $(\chi = 45°, \phi = 45°)$ in the non-tilted reference frame as a function of the amount of interface tilt α for different tilting directions (between parallel to the ϕ direction of the plane pole, i.e. $\beta = \phi$, and opposite to this direction, i.e. $\beta = \phi + \pi$). b) Effect of tilting the interface along a direction parallel to the ϕ direction of matching planes in film and substrate. c) Same as in b) but for aligned planes.

2.6c). Thus, plane alignment is the only way in which a periodic interface may be formed, the periodic nature of which is conserved irrespective of interfacial curvature [22].

As an example of the above arguments, figure 2.7a(1) shows the $FeSi_2$ (101) pole figure along with the overlap MIP for a grain with orientation X_{001} on a Si(001) substrate. The expected epitaxial peak positions for the orientation X_{001} are indicated on the pole figure with '□'. The overlap MIP clearly shows the *double-aligned* nature of this grain orientation, as plane

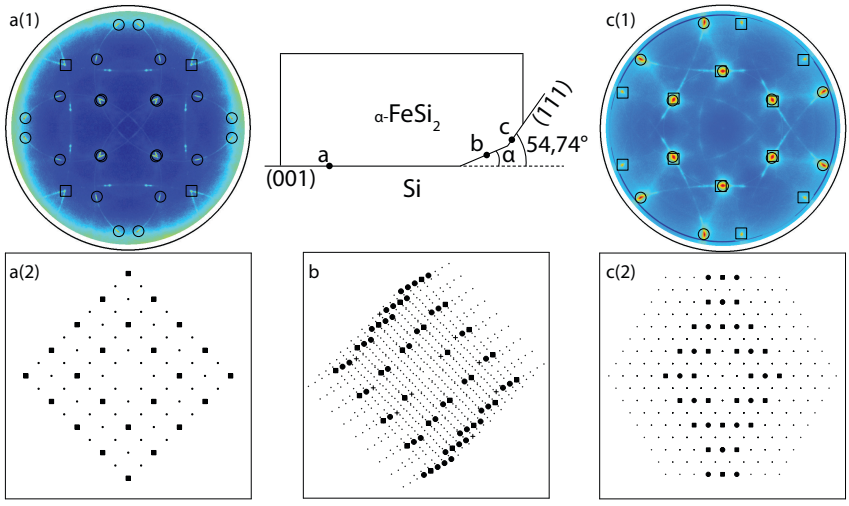

Figure 2.7. (color online) Influence of interface tilt on the overlap MIP of an α-$FeSi_2$ grain in the X_{001} orientation. a) Situation without any interface tilt. b) Arbitrary interface tilt over $\alpha = 27°$ in the $\beta = 30°$ direction. c) Interface tilted from Si(001) to Si(111) ($\alpha = 54,74°$). In a(1) and c(1), experimental pole figures for a α-$FeSi_2$ film formed on Si(001) and Si(111) respectively are included. The calculated locations on the pole figures for the epitaxies X_{001} and Y_{001} are indicated with '□' and '●' respectively.

alignment is achieved in different directions within the interface plane. The influence of tilting the interface over an arbitrary angle α along an arbitrary direction β on the interface structure is shown in figure 2.7b. Since only the matched or aligned plane couples from the non-tilted situation of figure 2.7a are considered here, it is clear that plane alignment is preserved.

In order to experimentally verify the above reasoning, one may consider growing or forming the same film on a different orientation of the same single crystal substrate material as an extreme example of interface roughness: changing from a Si(001) to Si(111) substrate corresponds to tilting the interface plane in the Si<110> direction over an angle $\alpha = 54.74°$. According to the above arguments, only epitaxial components that are the result of plane alignment in at least two directions, i.e. double aligned epitaxies, are expected to be present independent of the orientation of the substrate. In other words, they are 'transferable' from a Si(001) to a Si(111) substrate. This expectation is experimentally confirmed by comparing the pole figure data for α-$FeSi_2$ films formed on a Si(001) and a Si(111) substrate (fig. 2.7, a(1) and c(1)). Figure 2.7c(2) shows the resulting overlap

MIP after an interface tilt towards Si(111) of the grain orientation X_{001}, again showing that plane alignment is clearly preserved. Experimental observation of this epitaxy in a α-$FeSi_2$ film formed on a Si(111) substrate is provided in the $FeSi_2$(101) pole figure in figure 2.7c(1), where the calculated positions for this epitaxial component are again indicated by '□'. It was discussed earlier that also the epitaxial grain orientation Y_{001} has a double-aligned nature. Pole figure analysis has shown that this latter orientation is also present in a α-$FeSi_2$ film on Si(111), fitting the remaining epitaxial spots on the pole figure (see 'o' symbols in the pole figures of figure 2.7).

2.4 Case study: NiSi on Si(001)

As a second example, the MIP analysis was applied to the case of orthorhombic NiSi on cubic Si(001). Although no obvious epitaxial alignment can be derived from a comparison between the unit cells of NiSi and Si, pole figures show a high degree of preferential orientation. In a previous paper, we identified the following texture components for a 60nm NiSi film formed on Si(001) [18] (see fig.2.8a): four different types of axiotaxy (α_{001} with NiSi(202)//Si(220), β_{001} with NiSi(211)//Si(220), δ_{001} with NiSi(103)$\sim$//Si(220) and γ_{001} with NiSi(112)$\sim$//Si(220)), and three different types of epitaxial alignment (A_{100} with NiSi(100)$\sim$//Si(010) and NiSi(0-29)//Si(001), B_{100} with NiSi(211)//Si(011) and NiSi(114)// Si(001), and C_{100} with NiSi(101)//Si(011) and NiSi(1,-2,15)//Si(001)). Types B_{100} and C_{100} are related to the β_{001} and α_{001} axiotaxy components respectively and thus generate bright spots along the axiotaxy related lines on the pole figure. For easy reference, the labels for the axiotaxy and epitaxy components are the same as in ref. [18]. As in the case of α-$FeSi_2$, the subscripts refer to the orientation of the substrate.

Figure 2.8b-d shows the MIP and overlap MIP (insets) for the three epitaxial grain orientations. These MIP plots clearly reveal the match at the interface between the orthorhombic NiSi structure and the cubic Si structure. The difference between the A_{001} epitaxy and the two other aligned epitaxies is clearly visible: the A_{001} orientation results from a fortunate plane matching in two directions, while the two aligned epitaxies display plane alignment in the Si(110) axiotaxy direction.

Similar to the case for α-$FeSi_2$, we can look at the robustness of the matching interface against interfacial roughness. In the case of the A_{001}

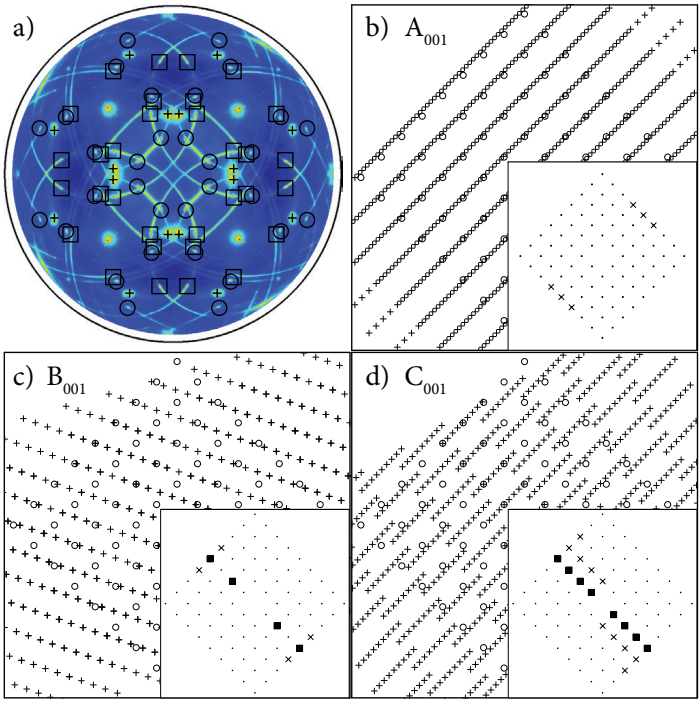

Figure 2.8. (color online) a) NiSi(112) pole figure for a 60nm NiSi layer formed on Si(001). The pattern of lines is indicative of axiotaxy, while the most intense spots on the pole figure are caused by three different epitaxial components : A_{001} indicated by '+', B_{001} by '○' and C_{001} by '□'. MIP's for these three types of epitaxial alignment are shown in b), c) and d), along with their overlap MIP plots as insets.

epitaxy it is clear from the discussions in the $FeSi_2$ case study that due to the absence of plane alignment, any form of interfacial perturbation will destroy the 2D periodicity in the plane of the interface. As a result, we don't expect to observe this type of epitaxial alignment in a NiSi film on a Si(011) or Si(111) substrate, which is experimentally confirmed in [18].

The big difference between the aligned B_{001} and C_{001} epitaxies in NiSi and the double-aligned epitaxies discusssed in the α-$FeSi_2$ case study above, is the nature of the periodicity in the second direction. For the orientations B_{001} and C_{001}, the periodicity in the non-axiotaxy direction is caused by plane matching rather than plane alignment, which should render them less stable with respect to perturbations in interfacial curvature. As an extreme example of interfacial curvature, we again consider a NiSi film

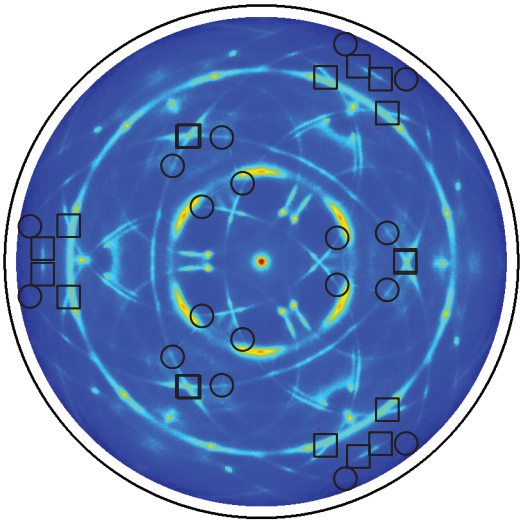

Figure 2.9. NiSi(002)/(011) pole figure for a 60nm NiSi film formed on Si(111). The calculated NiSi(002)/(011) poles for the B_{001} and C_{001} orientations on a Si(111) substrate are indicated by '$\circ$' and '$\square$' respectively and clearly do not correspond to an experimentally observed epitaxial texture component.

formed on Si(111) for which the NiSi(002)/(011) pole figure is shown in figure 2.9 (reprintend from [18]). The expected positions of NiSi(002)/(011) poles for the orientations B_{001} and C_{001} on a Si(111) substrate are overlaid with '$\circ$' and '$\square$' respectively. While it was readily observed for the case of α-$FeSi_2$ that the double-aligned epitaxies generated well-defined, bright spots on the pole figures for both substrate orientations, this is not the case for the present aligned NiSi B_{001} and C_{001} epitaxies (see figure 2.9). This observation reinforces our assumption that good plane alignment (i.e. $\Delta\chi \approx 0^\circ$ and $\Delta d_{p,film} \approx \Delta d_{p,subs}$) in two independent directions is a necessary condition for an epitaxial component to be present irrespective of interfacial curvature (or substrate orientation). This robustness of aligned planes against interfacial curvature can also be observed from the fact that the NiSi(211)//Si(220) and NiSi(202)//Si(220) axiotaxy components (i.e. the direction of aligned planes in the B_{001} and C_{001} epitaxies respectively) are visible in the pole figures on all substrate orientations [18].

2.5 Discussion

The MIP and the corresponding overlap MIP provide a relatively simple way of visualizing and assessing the quality of the match at the interface between two dissimilar phases. In the field of thin film silicide/germanide research, these visualizations provide a viable alternative to the traditional 'ball-and-stick' atomistic interface models, as more information on the quality and nature of the matching is directly accessible. The overlap MIP easily allows to asses the amount of matching within the plane of the interface for a specific orientation of a film grain with respect to the substrate. As such, it can be used to asses:

1. The quality of the matching at the interface for experimentally observed epitaxial texture components as the MIP gives a clear view on (mis)match between the lattice of the film and the substrate at the interface on a percentage level.

2. The geometrical nature of the matching for a specific grain orientation (matching vs. alignment), which allows one to classify and possibly link different texture components that are experimentally observed.

The texture components discussed in this article are summarized in table 2.1. Each component is classified according to the nature of the interfacial periodicity (plane alignment vs. plane matching) in two independent azimuthal directions within the plane of the interface. For each class, references are provided to figures containing an example MIP for that class of grain orientation.

It was argued in the case studies above that the stability of the different grain orientations is determined by the nature of the interfacial periodicity. Only plane alignment *across* the interface results in a periodic interface structure in a direction parallel to the poles of the aligned planes, the periodicity of which is preserved irrespective of interfacial curvature. This stability becomes clear if we look at the transferability of the different orientations to other substrate orientations (e.g. Si(111) or Si(011)): only grain orientations resulting completely from plane alignment should be observed on different substrate orientations. Indeed, in the case studies above, only the double-aligned X_{001} and Y_{001} α-$FeSi_2$ orientations were observed both on Si(001) and Si(111) substrates. Since axiotaxy is defined as the alignment of low-index planes in film and substrate[22] (i.e. plane alignment in one direction), it should also be present on substrates

		direction 2		
		aligned (& matched) '■' '●'	matched '×'	no match
direction 1	aligned (& matched) '■' '●'	'double-aligned' epitaxy $\underline{X_{001} / Y_{001}}$ (figs. 2.5d, 2.7a(2))	'aligned' epitaxy B_{001} / C_{001} (figs. 2.8c, d)	$\underline{\text{axiotaxy}}$ (fig. 2.5e)
	matched '×'	'aligned' epitaxy B_{001} / C_{001} (figs. 2.8c, d)	'matched' epitaxy A_{001} (fig. 2.8b)	-
	no match	$\underline{\text{axiotaxy}}$ (fig. 2.5e)	-	random (fig. 2.5f)

Table 2.1. Classification of texture components discussed in this article based on the nature of the interface (plane alignment vs. plane matching) in two independent azimuthal directions. Transferable components (visible on all substrate orientations) are underlined. The symbol used in the overlap MIP for each class is included in the header as a reference.

with different orientations, which is indeed observed both for NiSi and for α-$FeSi_2$[18, 29]. Furthermore, the stability of plane alignment against interfacial roughness also explains why axiotaxy is observed for a big collection of silicide/germanide films that form through a solid-state reaction between a thin metal film and a Si or Ge substrate, as the interface where new phases nucleate during such a reaction is usually not atomically flat.

2.6 Conclusions

It was shown in this paper that MIP (Map of Interfacial Periodicity) plots can be used to analyse thin film texture, i.e. to evaluate whether interface reconstruction is geometrically feasible (i.e. if a two-dimensional periodic interface can be formed for which the periodicity matches with that of both the film and the substrate lattice), and to identify the nature of the periodicity (plane alignment *across* the interface versus plane matching *at* the interface). Furthermore, it was argued that plane alignment is the only

way to form a periodic interface structure whose periodicity is preserved irrespective of interfacial curvature.

References

[1] Herman, M. A., Richter, W. & Sitter, H. *Epitaxy*. Physical Principles and Technical Implementation (Springer Science & Business Media, 2004).

[2] Herman, M. A. & Sitter, H. *Molecular Beam Epitaxy*, vol. 7 of *Springer Series in Materials Science* (Springer Berlin Heidelberg, Berlin, Heidelberg, 1996).

[3] Tsao, J. Y. *Materials Fundamentals of Molecular Beam Epitaxy* (Academic Press, 1992), 1st edition edn.

[4] Simoen, E. *et al.* Challenges and opportunities in advanced Ge pMOSFETs. *Materials Science in Semiconductor Processing* **15**, 588–600 (2012).

[5] Goley, P. & Hudait, M. Germanium Based Field-Effect Transistors: Challenges and Opportunities. *Materials 2014, Vol. 7, Pages 2301-2339* **7**, 2301–2339 (2014).

[6] Heyns, M. & Tsai, W. Ultimate Scaling of CMOS Logic Devices with Ge and III–V Materials. *MRS Bull.* **34**, 485–492 (2011).

[7] Lourdudoss, S. Heteroepitaxy and selective area heteroepitaxy for silicon photonics. *Current Opinion in Solid State and Materials Science* **16**, 91–99 (2012).

[8] Reiss, P., Protière, M. & Li, L. Core/Shell Semiconductor Nanocrystals. *Small* **5**, 154–168 (2009).

[9] Kocks, U. F., Tomé, C. N. & Wenk, H. R. *Texture and Anisotropy*. Preferred Orientations in Polycrystals and their Effect on Materials Properties (Cambridge University Press, 2000).

[10] Sutton, A. P. & Balluffi, R. W. *Interfaces in Crystalline Materials* (Oxford University Press, 2007).

[11] Fouet, J. *et al.* Silicide formation during reaction between Ni ultrathin films and Si(001) substrates. *Materials Letters* **116**, 139–142 (2014).

[12] Alberti, A. & La Magna, A. Role of the early stages of Ni-Si interaction on the structural properties of the reaction products. *J Appl Phys* **114**, 121301 (2013).

[13] Gaudet, S., Desjardins, P. & Lavoie, C. The thermally-induced reaction of thin Ni films with Si: Effect of the substrate orientation. *J Appl Phys* **110**, 113524 (2011).

[14] De Keyser, K. *et al.* Phase formation and texture of nickel silicides on $Si_{1-x}C_x$ epilayers. *Microelectron Eng* **88**, 536–540 (2011).

[15] De Keyser, K., Van Meirhaeghe, R. L., Detavernier, C., Jordan-Sweet,

J. & Lavoie, C. Texture of Cobalt Germanides on Ge(100) and Ge(111) and Its Influence on the Formation Temperature. *J Electrochem Soc* **157**, H395–H404 (2010).

[16] De Keyser, K., Detavernier, C., Jordan-Sweet, J. & Lavoie, C. Texture of $CoSi_2$ films on Si(111), (110) and (001) substrates. *Thin Solid Films* **519**, 1277–1284 (2010).

[17] Van Bockstael, C. *et al.* Influence of a transient hexagonal phase on the microstructure and morphological stability of NiSi films. *Appl Phys Lett* **94**, 033504 (2009).

[18] Detavernier, C., Jordan-Sweet, J. & Lavoie, C. Texture of NiSi films on Si(001), (111), and (110) substrates. *J Appl Phys* **103**, 113526 (2008).

[19] De Keyser, K. *et al.* Epitaxial Formation of a Metastable Hexagonal Nickel–Silicide. *Electrochem Solid St* **11**, H266 (2008).

[20] Van Bockstael, C. *et al.* Effect of Pt addition on growth stress and thermal stress of NiSi films. *J Appl Phys* **104**, 053510 (2008).

[21] Gaudet, S., Detavernier, C., Lavoie, C. & Desjardins, P. Reaction of thin Ni films with Ge: Phase formation and texture. *J Appl Phys* **100**, 034306 (2006).

[22] Detavernier, C. *et al.* An off-normal fibre-like texture in thin films on single-crystal substrates. *Nature* **426**, 641–645 (2003).

[23] Randle, V. *The Measurement of Grain Boundary Geometry* (CRC Press, 1993).

[24] Bollmann, W. *Crystal Defects and Crystalline Interfaces* (Springer, Berlin, Heidelberg, 1970).

[25] Zhang, M.-X. & Kelly, P. M. Application of edge-to-edge matching model to understand the in-plane texture of $TiSi_2$ (C49) thin films on (001)Si surface. *Scripta Materialia* **55**, 613–616 (2006).

[26] Zhang, M.-X., Qiu, D. & Kelly, P. M. Crystallography of $TiSi_2$ (C54) epitaxy on (111)Si and (001)Si surfaces. *Thin Solid Films* **516**, 5498–5502 (2008).

[27] Kelly, P. M. & Zhang, M.-X. Comments on edge-to-edge matching and the equivalence of the invariant line, Delta g and Moire fringe approaches to the crystallographic features of precipitates. *Scripta Materialia* **52**, 679–682 (2005).

[28] Özcan, A. S. *et al.* Texture of $TiSi_2$ thin films on Si (001). *J Appl Phys* **92**, 5011 (2002).

[29] Detavernier, C., Lavoie, C., Jordan-Sweet, J. & Özcan, A. Texture of tetragonal α-$FeSi_2$ films on Si(001). *Phys. Rev. B* **69**, 174106 (2004).

[30] Bulle-Lieuwma, C. W. T., van Ommen, A. H., Hornstra, J. & Aussems, C. N. A. M. Observation and analysis of epitaxial growth of $CoSi_2$ on (100) Si. *J Appl Phys* **71**, 2211 (1992).
[31] Smeets, D., Vantomme, A., De Keyser, K., Detavernier, C. & Lavoie, C. The role of lattice mismatch and kinetics in texture development: Co(1-x)Ni(x)Si(2) thin films on Si(100). *J Appl Phys* **103** (2008).
[32] Balakrisnan, B. *et al.* Texture of NiGe on Ge(001) and its evolution with formation temperature. *Appl Phys Lett* **87**, 241922 (2005).

3

Phase formation and texture in Ni germanides

3.1 Introduction

As was discussed in the introduction of this thesis, germanium is the top candidate to be used as an alternative channel material to silicon in future MOSFET devices. Thanks to the superior charge carrier mobilities of Ge compared to Si, the use of this material results in better performing transistors, without needing to further reduce their physical dimensions. Of course, as the semiconductor material inside a transistor changes from Si to Ge, the approach for contacting the source and drain regions should be adapted accordingly. The introduction of chapter 1 features a short overview of how different metal silicides have been used over the past decades to contact Si-based devices. As such, it seems only natural that metal germanides should be considered as contacting materials for Ge based transistors. Already in 2006, Gaudet *et al.* published a comprehensive study of different metal germanides by investigating the solid-phase reaction of 30 nm films of 20 different transition metals with a Ge(001) substrate [1]. This study identified NiGe as the most suitable contacting material thanks to its low formation temperature (around 300 °C), low

resistivity (around 22 $\mu\Omega$.cm), limited film roughness, sufficient morphological stability and limited sensitivity to oxidation.

In order to comprehend and eventually engineer the properties of NiGe contacts, a detailed understanding of the formation of these contacts is required. As discussed in chapter 1, such a germanide contact is typically formed through a thermally induced solid-phase reaction between a thin film of the transition metal and a Ge substrate. In this chapter, this kind of reaction between a thin Ni film and a Ge(001) or Ge(111) substrate, resulting in the formation of NiGe, is studied. As an introduction to the subject, an overview is provided of previously published studies of this reaction. Afterwards, the experimental results obtained during the course of this PhD research are presented in two articles. The first article covers a study of the aforementioned solid-phase reaction, but where the initial Ni film is pre-mixed during deposition with a varying amount of Ge. In the case of the solid-phase reaction in the Ni/Si system, such a ratio-controlled study has provided valuable insights on the formation of the first-forming, Ni-rich silicides [2]. In the second paper, a comprehensive study of the solid-phase reaction between a pure Ni film and Ge is presented. The focus of this study was to identify the intermediate Ni-rich phase that forms before NiGe, as the nature of this phase was debated in previous studies. The results of the first paper, together with the use of texture measurements at different temperatures during the reaction allowed for the unambiguous identification of this phase as the hexagonal ϵ-phase.

In the final part of this chapter, it is demonstrated how the technique of interface visualization discussed in chapter 3 was used to identify and understand the different epitaxial texture components of this ϵ-phase that are observed and discussed in the second paper of this chapter.

3.2 Literature overview

In contrast to the vast amount of literature published on the formation of technologically relevant silicide contacts, i.e. C54-$TiSi_2$, $CoSi_2$ and NiSi, reports on the solid-phase reaction between thin Ni films and Ge substrates towards NiGe have been rather rather scarce during the past decades. As a summary, table 3.1 provides an overview of the phase formation sequences that were observed in these studies, together with some experimental details and the reference to the publication.

One of the first studies to report on the reaction between, among some

other metals, a thin Ni film (100-150 nm) and a Ge substrate was published by Wittmer *et al.* in 1977 using RBS and glancing angle X-ray diffraction [3]. Their data suggested the formation of Ni_2Ge (orthorhombic, JCPDS 024-0452) when annealing for 1h at temperatures between 100 and 250 °C. At temperatures above 250 °C, NiGe was observed. The results obtained by Wittmer *et al.* were confirmed in another survey of metal-germanide formation conducted by Marshall *et al.* in 1985 [4].

In 1988, Hsieh *et al.* reported on the reaction between 30 nm Ni films with a Ge(111) substrate using similar heat treatments and measurement techniques as the previous two papers. Again, the formation of Ni_2Ge and NiGe were observed at temperatures of 160 and 250 °C respectively. In addition, Hsieh *et al.* investigated the texture of both phases for the first time, with a focus on the epitaxial quality, which was an important topic at that time (see chapter 1). Using TEM, they observed epitaxial orientations for both phases. Although it is not mentioned in the paper, the observed epitaxial orientation for Ni_2Ge, i.e. $Ni_2Ge(0001)//Ge(111)$ and $Ni_2Ge(10\bar{1}0)//Ge(\bar{2}20)$, suggests that the authors observed a hexagonal Ni_2Ge phase, instead of the orthorhombic one that is put forward in the papers by Wittmer *et al.* and Marshall *et al.* The existence of a hexagonal Ni_2Ge phase (spacegroup $P6_3/mmc$) in the bulk Ni-Ge system was put forward by Lecocq *et al.* in 1963 [10]. However, Nash *et al.* pointed out that, based on the lattice parameters published by Lecocq *et al.* this is probably the same phase as the ϵ-Ni_5Ge_3 phase which is visible in the bulk Ni-Ge phase diagram (see Figure III-1) and which we also identified as the intermediate Ni-rich phase in our experiments (see Paper III in this chapter).

The first investigation of the reaction using a ramp anneal was published in 1994 by Patterson *et al.* [6]. The different phases that occur during a solid-phase reaction between a 30 nm Ni film and an amorphous Ge substrate were identified using $\theta/2\theta$ XRD scans on samples that were quenched at different temperatures during the ramp anneal at 3 °C/min. Again, a single intermediate Ni-rich phase was observed before the formation of NiGe. Based on the XRD scan on a sample quenched at 290 °C (see Figure 3.1), the authors identified the Ni-rich phase as monoclinic Ni_5Ge_3 (JCPDS 024-0449, labeled ϵ'-Ni_5Ge_3 in the Ni-Ge bulk phase diagram). However, the ϵ'-Ni_5Ge_3(312) ($2\theta = 31.9°$), (313) ($2\theta = 44.9°$) and (331) ($2\theta = 46.7°$) peaks identified by the authors could also be attributed to the $(10\bar{1}1)$ ($2\theta = 31.7°$), $(10\bar{1}2)$ ($2\theta = 44.6°$) and $(11\bar{2}0)$ ($2\theta = 46.4°$) planes of the ϵ-phase that we identified as the Ni-rich germanide from our ramp-

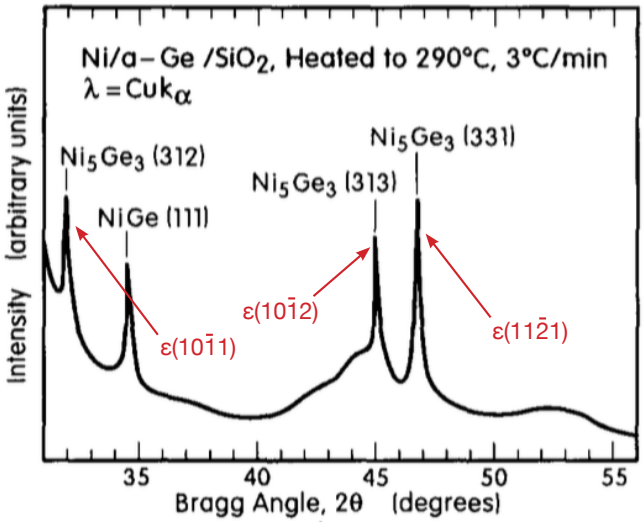

Figure 3.1. $\theta/2\theta$ XRD scan for a Ni/a-Ge sample heated at 3 °C/min and quenched at 290 °C. Figure reprinted from Patterson et al., Thin Solid Films, 253, p. 456-461, 1994.

anneal experiments (see Figure 3.1). Furthermore, since no texture effects are expected on an amorphous substrate, additional diffraction peaks should be visible in the 2θ range covered by the XRD experiment performed by Patterson *et al.* for the ϵ'-Ni_5Ge_3 phase, while for the ϵ-phase, no other peaks than the ones mentioned above are expected. Hence, it is likely that Patterson *et al.* observed the same ϵ-phase as we did in our experiments, but misidentified it as monoclinic ϵ'-Ni_5Ge_3 as they didn't expect the formation of the ϵ-phase at these temperatures.

As the technique of *in situ* XRD had already proven very useful in studying the solid-phase reaction between a thin Ni film and a Si substrate, Nemouchi *et al.* [7, 8] and Gaudet *et al.* [1, 9] applied this technique to study the reaction for a Ge substrate in 2006. In both cases, Ni_5Ge_3 is put forward as the intermediate Ni-rich phase, although it is not specified whether they consider the monoclinic ϵ' or the hexagonal ϵ variant. However, based on the specific planes they attribute to the observed diffraction peaks, they both considered the monoclinic ϵ'-Ni_5Ge_3 line phase.

In the case of Nemouchi *et al.*, the phase formed early during a long-time isothermal anneal at 160 °C between a 50 nm Ni film and either an amorphous or a polycrystalline Ge substrate. The identification of the ϵ'-Ni_5Ge_3 phase was done based on a long-time *ex situ* $\theta/2\theta$ XRD measurement per-

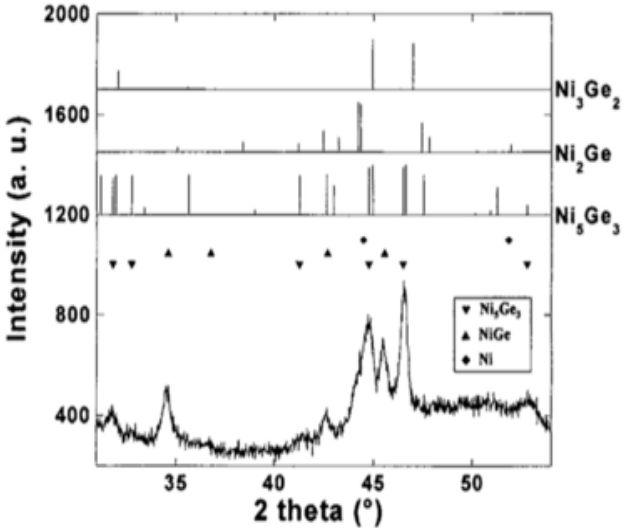

Figure 3.2. $\theta/2\theta$ XRD scan of 50 nm Ni on a-Ge after an isothermal anneal of 8h at 160 °C. The expected peak positions for a random powder of ϵ'-Ni_5Ge_3, Ni_2Ge and Ni_3Ge_2 are indicated above. Figure reprinted from Nemouchi et al., J Appl Phys, 89, p. 131920, 2006.

formed on a sample heated at 160 °C for 8h (see Figure 3.2). However, when taking into account our results discussed in papers III and IV, the peaks that were attributed solely to the ϵ'-Ni_5Ge_3 phase (around 46.5 and 53°) can also be explained by the ϵ-phase $(11\bar{1}0)$ and $(20\bar{2}0)$ planes. Again, due to the fact that texture effects are not expected on these substrates, more peaks should be visible in the measured 2θ if the monoclinic ϵ' phase is present. As a second major observation, Nemouchi *et al.* reported that the Ni-rich phase and NiGe grow simultaneously on both substrate types, which was remarkably different from the typical sequential growth that was always observed in the Ni-Si solid-phase reaction.

In the report by *Gaudet et al.* [1, 9], *in situ* XRD was used to study the solid-phase reaction between a 30nm Ni film and either amorphous-Ge, Ge(001) or Ge(111) during a ramp anneal at 3 °C/s. As a reference to the results that will be discussed in paper IV, the *in situ* XRD results from Gaudet *et al.* on the Ge(001) and Ge(111) substrates are reprinted in Figure 3.3. As mentioned by the author, the identification of the Ni-rich phase is not straightforward based on the limited number of observed diffraction peaks (which was attributed to the texture of this phase, although this was not measured). Again, the identified ϵ'-Ni_5Ge_3 peaks can all be explained

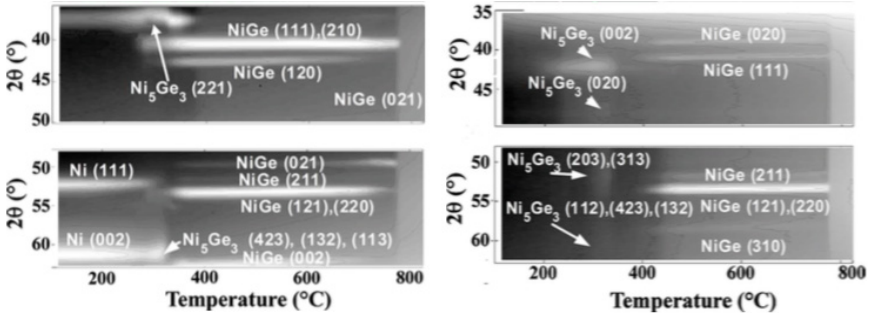

Figure 3.3. *in situ* XRD ($\lambda = 1.797$ nm scan of 30 nm Ni on Ge(001) (left) and Ge(111) (right) during a ramp anneal at 3 °C/s in purified He. Figure reprinted from Gaudet et al., J Appl Phys, 100, p. 034306, 2006.

by the ϵ-phase, as will be discussed in paper IV. Similar to the observations of Nemouchi *et al.*, the results of Gaudet *et al.* revealed a simultaneous growth of the Ni-rich phase and NiGe. However, on Ge(111), their observations suggested a sequential growth of both phases, with a third, heavily textured phase appearing in between Ni_5Ge_3 and NiGe, which they were unable to identify. In paper IV, it will become clear that a highly epitaxial ϵ-phase can explain these observations. In addition, the paper by Gaudet *et al.* discussed in detail the texture of the final NiGe phase. As a confimation, this texture was also measured in the course of this PhD research. However, as the results are the same, this texture will not be discussed in detail here. Hence, for detailed information concerning the texture of the NiGe phase on both substrate types, the reader is referred to ref. [9].

Sequence	Substrate	Anneal type	Experimental	Ref.
$\mathrm{Ni} \xrightarrow{100\,^\circ\mathrm{C}} \mathrm{Ni_2Ge}$ (o) $\xrightarrow{250\,^\circ\mathrm{C}} \mathrm{NiGe}$	Ge(001)	isothermal 1h	grazing-incidence XRD RBS	[3, 4]
$\mathrm{Ni} \xrightarrow{160\,^\circ\mathrm{C}} \mathrm{Ni_2Ge}$ (h) $\xrightarrow{250\,^\circ\mathrm{C}} \mathrm{NiGe}$	Ge(111)	isothermal 1h	TEM	[5]
$\mathrm{Ni} \xrightarrow{270\,^\circ\mathrm{C}} \epsilon\text{'-}\mathrm{Ni_5Ge_3} \xrightarrow{330\,^\circ\mathrm{C}} \mathrm{NiGe}$	a-Ge	ramp 3 °C/min	XRD; TEM	[6]
$\mathrm{Ni} \xrightarrow{160\,^\circ\mathrm{C}} \epsilon\text{'-}\mathrm{Ni_5Ge_3} + \mathrm{NiGe} \rightarrow \mathrm{NiGe}$	a-Ge, poly-Ge	isothermal 8h	(*in situ*) XRD	[7, 8]
$\mathrm{Ni} \xrightarrow{\pm 200\,^\circ\mathrm{C}} \epsilon\text{'-}\mathrm{Ni_5Ge_3} + \mathrm{NiGe} \rightarrow \mathrm{NiGe}$	a-Ge, Ge(001)	ramp 3 °C/s	*in situ* XRD	[1, 9]
$\mathrm{Ni} \xrightarrow{\pm 200\,^\circ\mathrm{C}} \epsilon\text{'-}\mathrm{Ni_5Ge_3} \xrightarrow{380\,^\circ\mathrm{C}} \mathrm{NiGe}$	Ge(111)	ramp 3 °C/s	*in situ* XRD	[9]

Table 3.1. Summary of phase sequences observed for the thermally induced solid-phase reaction between a thin Ni film and a Ge substrate.

References

[1] Gaudet, S., Detavernier, C., Kellock, A. J., Desjardins, P. & Lavoie, C. Thin film reaction of transition metals with germanium. *J Vac Sci Technol A* **24**, 474 (2006).

[2] Van Bockstael, C., Detavernier, C., Van Meirhaeghe, R. L., Jordan-Sweet, J. & Lavoie, C. In situ study of the formation of silicide phases in amorphous Ni-Si mixed layers. *J Appl Phys* **106**, 064515 (2009).

[3] Wittmer, M., Nicolet, M. A. & Mayer, J. W. The first phase to nucleate in planar transition metal-germanium interfaces. *Thin Solid Films* **42**, 51–59 (1977).

[4] Marshall, E. D., Wu, C. S., Pai, C. S., Scott, D. M. & Lau, S. S. Metal-Germanium Contacts and Germanide Formation. *MRS Proceedings* **47**, 161 (1985).

[5] Hsieh, Y. F., Marshall, E. D. & Lau, S. S. Partial Epitaxial Growth of Ni_2Ge and NiGe on Ge(111). *Thin Solid Films* **162**, 287–294 (1988).

[6] Patterson, J. K. *et al.* Kinetics of Ni/a-Ge bilayer reactions. *Thin Solid Films* **253**, 456–461 (1994).

[7] Nemouchi, F. *et al.* Simultaneous growth of Ni[sub 5]Ge[sub 3] and NiGe by reaction of Ni film with Ge. *Appl Phys Lett* **89**, 131920 (2006).

[8] Nemouchi, F. *et al.* A comparative study of nickel silicides and nickel germanides: Phase formation and kinetics. *Microelectron Eng* **83**, 2101–2106 (2006).

[9] Gaudet, S., Detavernier, C., Lavoie, C. & Desjardins, P. Reaction of thin Ni films with Ge: Phase formation and texture. *J Appl Phys* **100**, 034306 (2006).

[10] Lecocq, P. Magnetic and Structural Studies of the Solid Solutions of Ge in Fe, Co and Ni and the Germanides of the Type M_3Ge and M_2Ge. *Ann. Chim.* **8**, 85–116 (1963).

Paper III

Phase Formation in mixed Ni-Ge thin films: influence of Ge content and low-temperature nucleation of hexagonal nickel germanides

B. De Schutter, W. Devulder, A. Schrauwen, K. van Stiphout, T. Perkisas, S. Bals, A. Vantomme and C. Detavernier

Microelectronic Engineering, 120, 168-173, 2013
doi:10.1016/j.mee.2013.09.004

Abstract

In this study, we focus on phase formation in mixed Ni-Ge thin films as they represent a simplified model of the small mixed interface layer that is believed to form upon deposition of Ni on Ge and where initial phase formation happens. A combinatorial sputter deposition technique was used to co-deposit a range of mixed Ni-Ge thin films with Ge concentrations varying between 0 and 50 at.% Ge in a single deposition on both Ge(100) and inert SiO_2 substrates. *In situ* X-ray diffraction and transmission electron microscopy where used to study phase formation. In almost the entire composition range under investigation, crystalline phases where found to be present in the as-deposited films. Between 36 and 48 at.%Ge, high-temperature hexagonal nickel germanides were found to occur below 300° C, both on SiO_2 and Ge(100) substrates. For Ge concentrations in the range between 36 and 42 at.%, this hexagonal germanide phase was even found to be present at room temperature in the as-deposited films. The results obtained in this work could provide more insight in the phase sequence of a pure Ni film on Ge.

III-1 Introduction

The continuous scaling down of microelectronic devices pushes the current Si-based technology to its limits. Alternative materials are being investigated to replace Si in e.g. the gate regions of Metal-Oxide-Semiconducter Field Effect Transistors (MOSFET). According to the industry roadmap, Ge is a top candidate to replace Si in p-channel MOSFET devices due to its higher carrier mobility and relative compatibility with silicon processing [1]. Similar to the current SALICIDE (Self-Aligned Silicide) process, where metal silicides are used to contact the source, gate and drain regions of MOSFETs, metal germanides appear as natural candidates for contacting Ge. A systematic study of germanide formation and properties in 20 transition metal on Ge systems by Gaudet et al. [2], revealed NiGe as the most promising contact material since it exhibits the most suitable properties among all investigated metal germanides, including low formation temperature, low resistivity and a wide stable temperature window during ramp anneals.

If we are to use NiGe as a contact material in future devices, a thorough understanding of the formation mechanisms and properties of the different germanides in the Ni-Ge system is important. For the bulk system, most of the work on this binary Ni-Ge system was done in the 1970's [3, 4] and was summarized in 1987 by Nash et al. [5], which led to the Ni-Ge binary phase diagram as it is known today (see Fig. III-1). For the thin film system, detailed studies on the phase formation upon annealing of a thin Ni film on Ge using *in situ* x-ray diffraction (XRD) were performed by Gaudet et al. [6] and Nemouchi et al. [7]. Both groups reported the simultaneous growth of NiGe and Ni_5Ge_3 on Ge(100), where Ni_5Ge_3 only exists over a small temperature window since it is consumed by the growth of NiGe, which is the stable end phase. However, the existence of other Ni-germanides in this intermediate region could not be ruled out due to overlapping peak positions of different Ni-rich germanides [6]. Interestingly, Jensen et al. [8] reported on the metastable nucleation of the high temperature ϵ-Ni_5Ge_3 when annealing ratio-controlled Ni-Ge multilayers on an inert SiO_2 substrate.

In order to fully understand the phase formation in the Ni-Ge system, more information on this Ni-rich phase region is required. In the Ni-Si system, a similar region of transient Ni-rich phases during a ramp anneal of a thin Ni film on Si can be observed. Recently, a detailed study of a ratio-controlled Ni-Si system was performed in our group to gain more in-

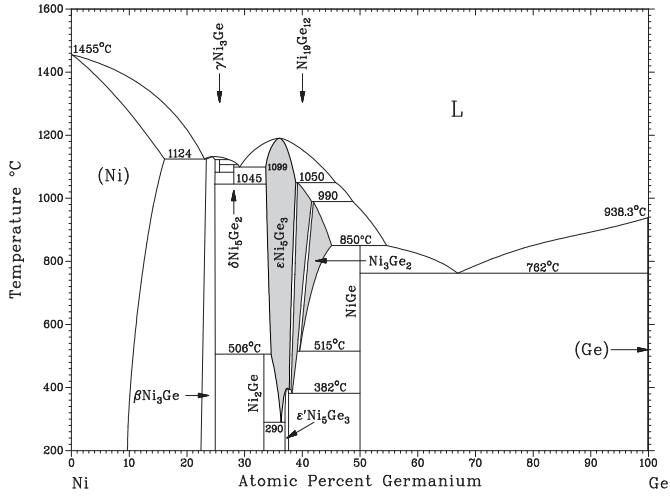

Figure III-1. Equilibrium phase diagram of the Ni-Ge system. This study focuses on the 0-50 at.%Ge composition region. (taken from [5])

sight in the early phase formation in the Ni-Si system, which led to the identification of the metastable hexagonal θ-phase in the Ni on Si phase sequence[9–12]. In this paper, we present a similar study of phase formation in the Ni-Ge system. Ratio-controlled Ni-Ge films were deposited on both SiO_2 and Ge(100) substrates and *in situ* XRD was used to monitor phase formation during linear ramp anneals.

III-2 Experimental

Mixed Ni-Ge films with varying Ge concentrations (from 0 to 50 at.% Ge) were deposited on both 100nm thermal SiO_2 and HF-cleaned p-type Ge(100) substrates using a combinatorial sputter deposition technique. Substrate strips with a length of 15 cm and a width of 1-2 cm were mounted on a rotating carousel in a deposition chamber with a base pressure of 2×10^{-7} mbar. During co-sputtering of Ni and Ge, spatial control of the separate material fluxes resulted in a Ge film with a thickness gradient being mixed with a uniform Ni film. The deposition parameters were tuned in such a way that the Ni content in the resulting film is constant and corresponds to the amount of Ni in a pure 50 nm Ni film (i.e. about 45×10^{16} atoms/cm^2). The outcome of such a single deposition is a 15 cm long strip

with a Ni-Ge film in which the Ge concentration varies from 0 to 50 at.%. This gradient is then cleaved into individual 5 mm long samples for further characterization. This effectively results in 29 samples per deposited strip with a composition difference of ~ 2 at.% between consecutive samples and a ± 1 at.% uniformity within a single sample. The composition of all samples was verified with Rutherford Backscattering Spectrometry (RBS).

Germanide phase formation was studied using a home-built *in situ* XRD setup, consisting of an experimental heating chamber mounted in a Bruker D8 Discover XRD system. All individual samples were subjected to a ramp anneal at 3° C/s from room temperature up to a temperature of 800° C or 650° C for the samples on SiO_2 and Ge(100) respectively. During the anneal, the diffraction pattern was recorded every 3s over a range of 20° in 2θ.

High Resolution Transmission Electron Microscopy (HR-TEM) was performed on a FEI Tecnai G2 electron microscope, operating at 200kV. Sample preparation was done using mechanical polishing followed by ion milling.

III-3 Results

III-3.1 Ni(Ge) on inert SiO_2 substrates

Due to the inert SiO_2 substrate, the Ni-Ge layers have a fixed Ni/Ge composition throughout the anneal. As can be expected from the phase diagram (Fig. III-1), the amount of Ge in the Ni(Ge) mixture will have an influence on the initial crystallization temperature and the first forming phase. Here, *in situ* xrd was used to probe the phase formation sequence while heating the samples to 800° C.

Figure III-2a shows selected *in situ* XRD measurements with 2θ on the vertical axis and temperature on the horizontal axis. The measured XRD intensity is plotted as a logarithmic grayscale map (with black corresponding to the highest intensity). To illustrate the procedure of identifying the phase formation sequence, we will discuss the second *in situ* XRD scan, i.e. the scan of the sample with 33 at.% Ge. From room temperature on, three peaks are clearly visible, indicating the presence of a crystalline phase in the as-deposited film. All these peaks can be attributed to Ni_2Ge: the peak at $2\theta = 41.3°$ can be indexed as $Ni_2Ge(103)$, the intense peak around $2\theta = 44°$ is a superposition of $Ni_2Ge(031)$ and $Ni_2Ge(211)$ and the third peak around $2\theta = 47.5°$ can be indexed as a superposition of $Ni_2Ge(020)$

and Ni_2Ge(113). Around 550° C, a phase transformation occurs as indicated by the disappearance of the three Ni_2Ge peaks and the emergence of three new peaks. The new features at $2\theta = 43.8°$ and 51° can be identified as β-Ni_3Ge(111) and β-Ni_3Ge(200) respectively. The third peak around $2\theta = 45°$ however is not that straightforward to identify, since it can be indexed as either ϵ-Ni_5Ge_3(102), Ni_3Ge_2(102) or $Ni_{19}Ge_{12}$(212). A complementary *in situ* XRD scan (not shown here) in a different 2θ window revealed a second peak around $2\theta = 30.5°$ which can similarly be attributed to the (101) peak of either ϵ-Ni_5Ge_3 or Ni_3Ge_2 or to $Ni_{19}Ge_{12}$(200). Similar identification difficulties of these specific phases, which exist over a broad composition range in the binary Ni-Ge phase diagram (refer to the shaded area in Fig. III-1), were encountered in a vast subset of the measured samples. This identification problem can be related to the very closely related crystal structures of these three phases [3, 13], which makes it nearly impossible to discern between them based solely on powder XRD techniques. Therefore, in our XRD results, we will depict these phases as one single phase which we will refer to as the ϵ-phase.

A similar analysis was performed for all samples, i.e. the phases were identified on the *in situ* XRD scans and the temperature where a particular phase appears/disappears was systematically recorded. In total, we could discern between seven different phase formation sequences for the samples on SiO_2:

O1. Ni(4%-28%Ge) → β-Ni_3Ge / Ni(Ge)

O2. Ni(29%-34%Ge) → Ni_2Ge → ϵ-phase + β-Ni_3Ge

O3. Ni(36%Ge) → ϵ-phase → Ni_2Ge + ϵ-phase → ϵ-phase

O4. Ni(37,5%-41,5%Ge) → ϵ-phase

O5. Ni(42,5%-47,5%Ge) → ϵ-phase → ϵ-phase + NiGe → ϵ-phase

O6. Ni(48,5%Ge) → ϵ-phase + NiGe

O7. Ni(49%-50%Ge) → NiGe → NiGe + ϵ-phase

Representative *in situ* XRD measurements for these cases are shown in figure III-2a (a measurement representing case O6 has been left out since it is the same as for case O7, apart from the as-deposited NiGe phase). For most compositions, the phase sequence can be understood by looking at the relevant region in the Ni-Ge equilibrium phase diagram. However, for samples with a Ge concentration between 36 and 48 at.% (cases O3 through O6), the ϵ-phase which should only be stable above 300° C is

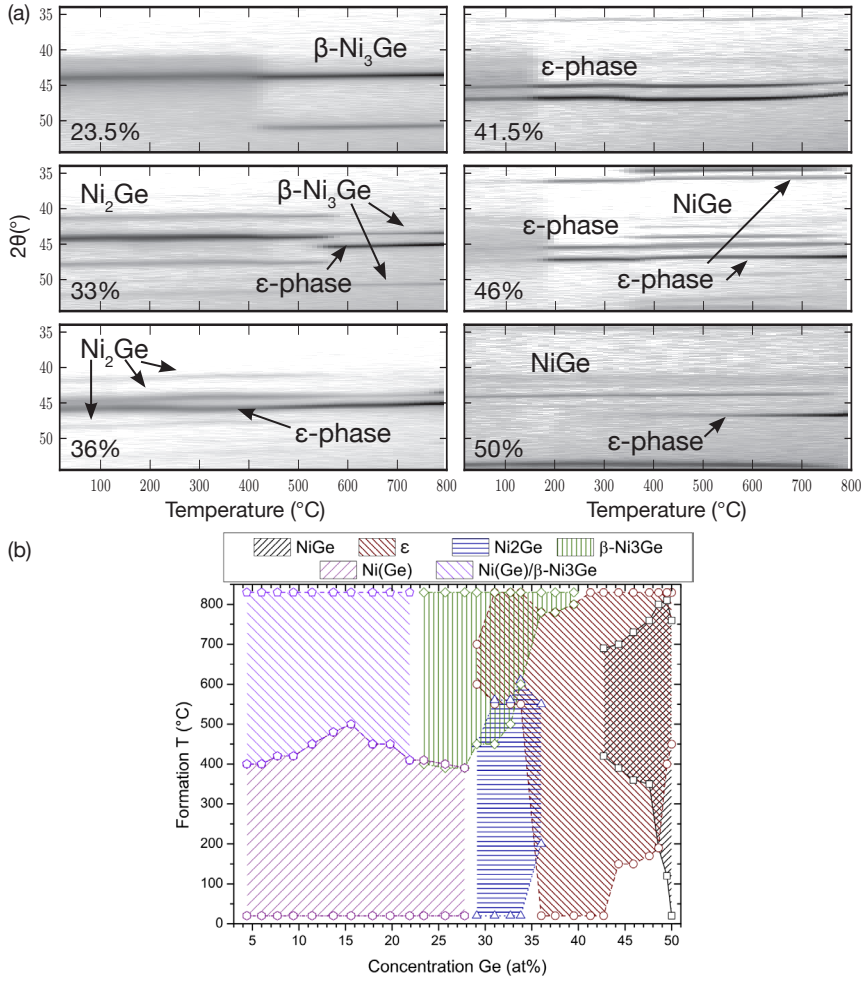

Figure III-2. (a) Selected *in situ* XRD scans representing the different phase formation sequences observed on the oxide samples during an anneal to 800° C at 3° C/s. The XRD intensity is plotted as a function of temperature (x-axis) and 2θ (y-axis) using a grayscale map with black representing the highest intensity. (b) Summary of phase formation for Ni(x%Ge) on SiO_2 samples. The shaded areas mark the regions in Ge concentration and temperature where the respective phase was detected with *in situ* XRD.

surprisingly observed to crystallize below 300° C. For samples with a Ge concentration between 36 at.% and 43 at.%, the ϵ-phase is even present as-deposited (see Fig. III-2), indicating that this phase was formed dur-

ing co-deposition of Ni and Ge at room temperature. Since one could wonder whether the room temperature ϵ-phase formation is related to the deposition technique used to co-deposit the films, we investigated Ni-Ge films with Ge concentrations of 40 and 42 at.% that were co-deposited on SiO_2 using Molecular Beam Epitaxy. Also in this case, XRD results (not shown here) clearly revealed the presence of a crystalline ϵ-phase in the as-deposited state.

In figure III-2b, a complete phase formation summary for the samples on SiO_2 is presented. For each identified phase, the respective shaded areas give the region in both temperature and Ge concentration where this particular phase was visible on the *in situ* XRD scans. Within the white regions on this plot, no diffraction peaks were observed, indicating an amorphous mixture.

III-3.2 Ni(Ge) on Ge(100) substrates

On Ge(100), the phase formation sequence will be influenced by the unlimited supply of Ge from the substrate. We expect the initial crystallization of the film to be similar to the corresponding sample deposited on SiO_2. Subsequently, the reaction proceeds by consuming Ge from the substrate until the whole film has transformed to NiGe, which is expected to be the end phase according to the binary phase diagram.

A similar analysis as for the samples on SiO_2 was performed for the samples on Ge(100). Figure III-3b shows a phase formation summary for these samples. Below 28 at.%Ge, the observed phase sequence is qualitatively the same as what has been observed previously for the reaction of a pure Ni film on Ge(100) [6]. Adding over 28 at.%Ge results in a phase sequence with successive phases increasing in Ge content. As for the samples on SiO_2, the phase sequence systematically changes when more Ge is added to the as-deposited film. In summary, we observed the following phase formation sequences for the samples on Ge(100):

G1. Ni(4%-28%Ge) $\rightarrow$ Ni-rich phase(s) $\rightarrow$ NiGe

G2. Ni(29%-34%Ge) $\rightarrow$ Ni_2Ge $\rightarrow$ ϵ-phase + NiGe $\rightarrow$ NiGe

G3. Ni(36%Ge) $\rightarrow$ Ni_2Ge + ϵ-phase $\rightarrow$ ϵ-phase + NiGe $\rightarrow$ NiGe

G4. Ni(37,5%-47,5%Ge) $\rightarrow$ ϵ-phase $\rightarrow$ NiGe

G5. Ni(48,5%Ge) $\rightarrow$ ϵ-phase + NiGe $\rightarrow$ NiGe

G6. Ni(49%-50%Ge) $\rightarrow$ NiGe

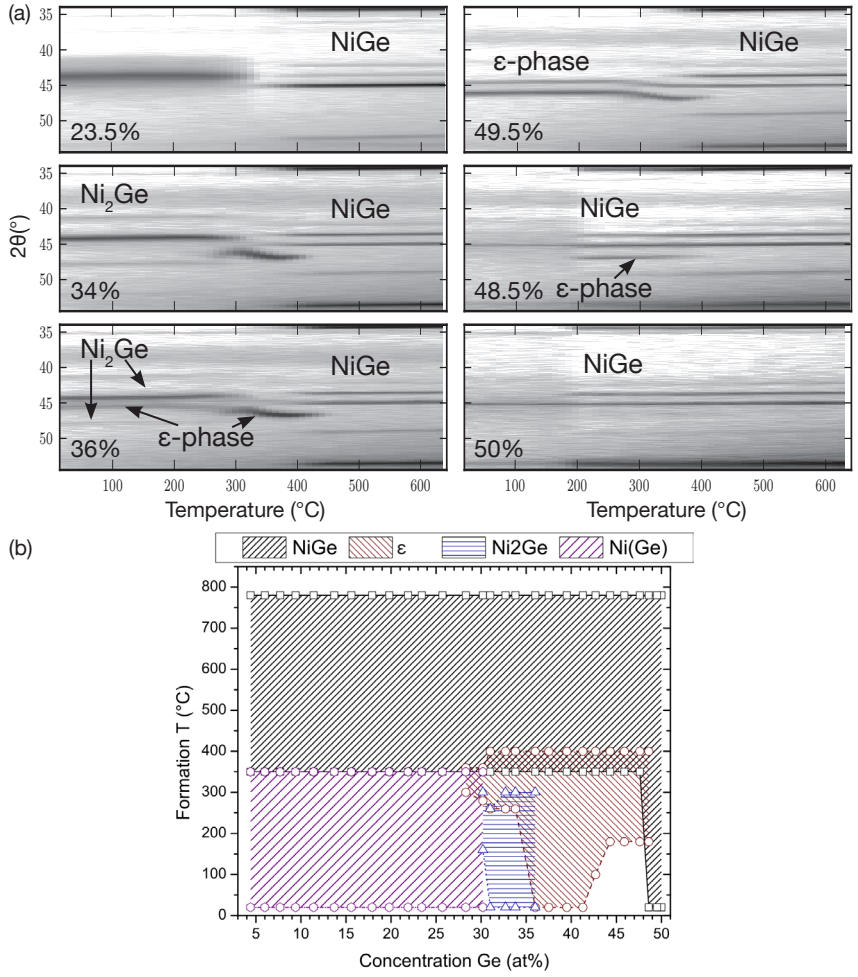

Figure III-3. (a) Selected *in situ* XRD scans representing the different phase formation sequences observed on the Ge(100) samples during an anneal to 650° C at 3° C/s. XRD intensity is plotted as a function of temperature (x-axis) and 2θ (y-axis) using a grayscale map with black representing the highest intensity. (b) Summary of phase formation for Ni(x%Ge) on Ge(100) samples. The shaded areas mark the regions in Ge concentration and temperature where the respective phase was detected with *in situ* XRD.

Again, the selected *in situ* XRD scans visible in figure III-3a are representative for the different cases. Similar to what we have observed for the samples on SiO_2, the ϵ-phase is forming below 300° C for samples on

Ge(100) with a Ge concentation between 36 and 48 at.%. Also in this case, for samples with a Ge concentration between 36 and 42 at.% Ge, the ϵ-phase is present in the as-deposited film (see Fig. III-3)b, again indicating the formation of this phase during the co-sputtering of Ni and Ge at room temperature.

III-4 Discussion

In recent years, detailed phase formation studies in the technologically relevant Ni-silicon system have proven to be an important step in understanding the properties and behavior of Ni-silicide phases. For these planar metal thin film on silicon systems, it is generally accepted that phase formation initiates in a thin mixed amorphous layer which forms at the metal-silicon interface during deposition. Consequently, we can assume that a similar process is true for metal-germanium systems. In this context, the amorphous Ni-Ge layers studied in this work can be considered as simplified models for such an mixed interface layer.

Based on the phase formation summary plots (Fig. III-2b and III-3b), some interesting observations can be made. First, the influence of the unlimited Ge supply from the substrate for the samples on Ge(100) is clearly visible. From figure III-3b it can be seen that NiGe is always the stable end phase for annealing temperatures above $\sim 380°$C, which makes sense because an unlimited supply of Ge is expected to push the system towards the most Ge rich germanide phase. In contrast, for the samples on SiO_2 the NiGe phase only forms when the Ge concentration in the mixed films approaches 50 at.%, which is the Ge content expected in stoichiometric NiGe.

For samples in the ranges O1 and G1, a single (broad) diffraction peak is visible around $2\theta = 44°$ in the *in situ* XRD spectra from the as-deposited state on. This peak could be identified as either Ni(111) ($2\theta = 44, 49°$) or β-$Ni_3Ge(111)$ ($2\theta = 43, 83°$) due to the closely related crystal structures of Ni and β-Ni_3Ge. In fact, β-Ni_3Ge is essentially the Ni structure with site-ordered Ni atoms substituted with Ge, yielding a slightly larger lattice constant [5]. Figure III-4 shows this peak's measured position in the as-deposited layers as a function of Ge concentration and clearly reveals a gradual shift from Ni(111) to β-$Ni_3Ge(111)$ when approaching the stable composition range of the latter phase (according to the Ni-Ge phase diagram in Fig. III-1, depicted by the shaded area in Fig. III-4). The pres-

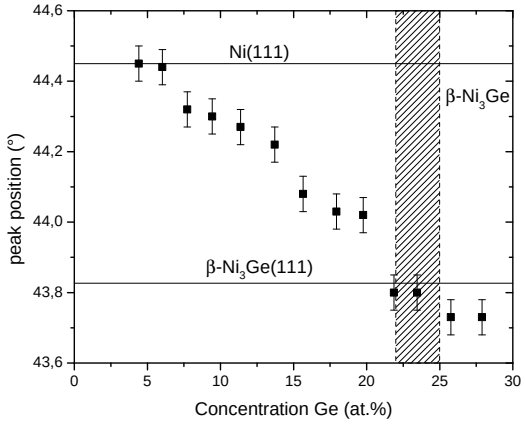

Figure III-4. Evolution of the measured peak position in the as-deposited Ni-Ge layers with Ge concentrations < 28at.% as a function of Germanium concentration. The JCPDS peak positions of Ni(111) and β-Ni_3Ge(111) are indicated by the horizontal lines. The shaded area depicts the stability range of β-Ni_3Ge on the binary phase diagram.

ence of this peak suggests that there is already some local structure in the co-deposited Ni-Ge films that probably resembles the crystal structure of Ni and β-Ni_3Ge. The positional shift of the peak could then be caused by a solid-solution behavior of this mixed phase, meaning that the addition of extra Ge in the co-deposited film drives the local structure from Ni to β-Ni_3Ge as the extra Ge gets systematically incorporated. Around 400° C, for the samples on SiO_2, a sudden improvement of the crystalline quality of this solid-solution phase is clearly evidenced by the intensity increase and narrowing of the peak around 44° and the emergence of a second peak around 51°. For the samples on Ge(100), the mixed phase transforms to NiGe at a similar temperature due to the unlimited supply of Ge from the substrate.

The crystallinity of the as-deposited films is even more pronounced for samples in the ranges O2 and G2. Here, multiple sharp diffraction peaks belonging to Ni_2Ge were found to be present in the co-deposited films, suggesting the presence of fully crystalline Ni_2Ge grains in these films (see figure III-2a and III-3a).

The most interesting composition region comprises the ranges O3 through O6 for the samples on oxide and G3 through G5 for the samples on Ge(100), i.e. the compositional range between 36 and 48 at.%Ge. *In situ* XRD revealed two clear diffraction peaks around 45° and 46.5° for temper-

atures below 300° C. For Ge concentrations in the range $[36, 42]$at.% these peaks are present from the as-deposited state on, again indicating the existence of crystalline grains in these co-deposited films. According to the Ni-Ge phase diagram (figure III-1), four phases are expected to be stable below 300° C and thus could explain the presence of these diffraction peaks: β-Ni_3Ge, Ni_2Ge, NiGe and the low-temperature ϵ'-Ni_5Ge_3 phase. While neither of the two peaks can be attributed to one of the first three phases, they could be explained by superpositions of the ϵ'-Ni_5Ge_3 (203)/(313) and (602)/(331) peaks. Nonetheless, according to the JCPDS data, a lot more diffraction peaks are expected for this ϵ'-Ni_5Ge_3 phase in the measured 2θ window, especially since we do not expect any texture effects on the SiO_2 substrates. Unexpectedly, further investigation of these *in situ* XRD data below 300° C revealed a perfect agreement with the diffraction pattern that is expected for the high-temperature, hexagonal ϵ-Ni_5Ge_3 and Ni_3Ge_2 phases (which we treat together as a single ϵ-phase as mentioned above), i.e. all expected diffraction peaks were present and no extra peaks were found. This was confirmed with *in situ* XRD scans taken in a complementary 2θ window (data not shown here). Since this ϵ-phase is not expected to be stable below 300° C according to the Ni-Ge phase diagram (Fig. III-1), these findings suggest the presence of metastable ϵ-phase grains in these films below 300° C.

To confirm the presence of these metastable ϵ-phase grains, we performed a high-resolution TEM (HR-TEM) measurement combined with electron diffraction on a sample in the range G4 that was quenched at 120° C. The results are shown in figure III-5. The HR-TEM image (Fig. III-5a) shows a crystalline Ni-Ge film on top of the Ge(100) substrate. An electron diffraction pattern collected in the indicated area is shown in figure III-5b, confirming a hexagonal crystal structure. Figure III-5c shows a simulated diffraction pattern of this ϵ-phase using the lattice parameters known from literature (spacegroup $P6_3/mmc$; $a = b \approx 3.9$Å; $c = 5.078$Å; $\alpha = \beta = 90°$; $\gamma = 120°$)[3, 13]. A good agreement between the measured and simulated patterns can be observed, reinforcing the suggested presence of metastable ϵ-phase grains in the co-deposited films. Additional HR-TEM results (not shown here) confirm the presence of this phase throughout virtually the whole Ni-Ge layer. From this observation, it can be assumed that the aforementioned two diffraction peaks around 45° and 46.5° that were visible in *in situ* XRD scans of samples in the range $[36, 48]$at.%Ge are caused by ϵ-phase (102) and (110) diffractions respectively. The *in situ* XRD results thus suggest the metastable occurrence of this ϵ-phase in the wide compo-

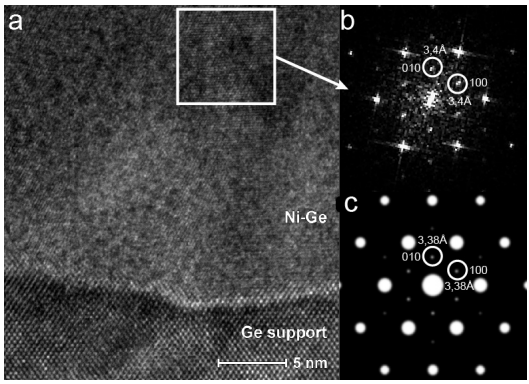

Figure III-5. (a) HR-TEM image of a Ni(38%Ge) film on Ge(100) quenched at 120° C. (b) Electron diffraction pattern recorded within the indicated area. A similar diffraction pattern could be observed virtually everywhere throughout the film. (c) Simulated diffraction pattern for the ϵ-phase crystal structure as known from literature (spacegroup $P6_3/mmc$; $a \approx 3.9$Å; $c \approx 5.078$Å).

sitional range between 36 and 48 at.%Ge. Between 36 and 42 at.%Ge, the crystallization of this phase occurs already during deposition.

Next, we focus on the influence of Ge content on the ϵ-phase crystal structure. In the metastable region discussed above, a systematic shift of the (102) and (110) peaks towards higher diffraction angles over a range of $\sim 2°$ could be observed in the *in situ* XRD measurements, both for the samples on SiO_2 as for those on Ge(100). From the positions of these two diffraction peaks (as determined from the *in situ* XRD scans at 200° C), the lattice parameters a and c of the ϵ-phase can be calculated using Bragg's law and the relation between d-spacing and lattice constants for a hexagonal crystal structure. The influence of the Ge content in the co-deposited Ni-Ge film on the lattice of the metastable ϵ-phase is presented in figure III-6, which shows a systematic contraction of the lattice with increasing Ge content. A similar behavior has been observed previously by Ellner *et al.* in the bulk system [3] and by Jensen *et al.* in multilayer Ni-Ge films [8]. Since the structure of this ϵ-phase can be regarded as intermediate between the two prototype structures of Ni_2In and NiAs, the monotonic decrease of the lattice parameters can be explained by a systematic incorporation of extra vacancies on the Ni sites as more Ge is added to the mixture [8, 13]. The observation of this metastable ϵ-phase and its behavior as a function of Ge content is very similar to what has been observed recently for the

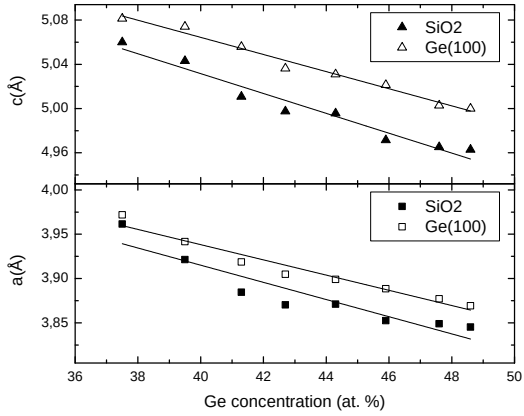

Figure III-6. Influence of the Ge content in the co-deposited film on the lattice parameters a and c of the metastable ϵ-phase crystal structure, both on SiO_2 and Ge(100). The parameters were calculated from the ϵ-phase (102) and (110) peak positions as extracted from the *in situ* XRD scans at 200° C.

θ-phase in the Ni-Si system [11].

Finally, the behavior of this ϵ-phase with increasing Ge content also explains the continuous shift of the ϵ-phase (102) and (110) diffraction peaks between 300 and 400° C that was observed for various samples on Ge(100) (see Fig. III-3a). First, the ϵ-phase nucleates with a certain composition out of the co-deposited film as mentioned above. Then, when the thermal budget supplied to the sample is high enough to allow for a reaction between the substrate and the film (in this case around 300° C), additional Ge from the substrate gets incorporated into the ϵ-phase, inducing a lattice contraction and a corresponding peak shift towards higher 2θ diffraction angles. Additional TEM measurements on a sample with 38 at.%Ge quenched after the peak shift (not shown here) confirmed the presence of ϵ-phase grains with similar electron diffraction patterns than those observed for ϵ-phase grains at 120° C. This confirms our assumption that this peak shift is not due to a phase transformation but to a monotonic compositional change of this ϵ-phase as explained above.

III-5 Conclusions

A detailed study of phase formation in co-deposited Ni-Ge thin films with Ge concentrations ranging from 0 to 50 at.% on both SiO_2 and Ge(100)

substrates was carried out using *in situ* XRD and TEM. A combinatorial sputter deposition technique allowed for the deposition of all investigated samples in a single run. Crystalline phases were found to nucleate already during co-deposition of the films at room temperature for almost the full composition range under investigation. Between 36 and 48 at.%Ge, a metastable high-temperature hexagonal germanide (ϵ-Ni_5Ge_3 or Ni_3Ge_2 in the binary phase diagram, but treated as a single ϵ-phase in this work) was found to be present below its minimum stability temperature of 300° C, adapting its crystal structure to the available amount of Ge. Between 36 and 42 at.%Ge, this ϵ-phase was present already in the as-deposited state.

References

[1] Pillarisetty, R. Academic and industry research progress in germanium nanodevices. *Nature* **479**, 324–328 (2011).

[2] Gaudet, S., Detavernier, C., Kellock, A. J., Desjardins, P. & Lavoie, C. Thin film reaction of transition metals with germanium. *Journal Of Vacuum Science & Technology A* **24**, 474 (2006).

[3] Ellner, M., Gödecke, T. & Schubert, K. Zur struktur der mischung Nickel-Germanium. *Journal of the Less Common Metals* **24**, 23–40 (1971).

[4] Dayer, A. & Feschotte, P. Les systèmes binaires cobalt-germanium et nickel-germanium: Étude comparée. *Journal of the Less Common Metals* **72**, 51–70 (1980).

[5] Nash, A. & Nash, P. The Ge-Ni (Germanium-Nickel) system. *Bulletin of Alloy Phase Diagrams* **8**, 255–264 (1987).

[6] Gaudet, S., Detavernier, C., Lavoie, C. & Desjardins, P. Reaction of thin Ni films with Ge: Phase formation and texture. *Journal Of Applied Physics* **100**, 034306 (2006).

[7] Nemouchi, F. *et al.* Simultaneous growth of Ni_5Ge_3 and NiGe by reaction of Ni film with Ge. *Applied Physics Letters* **89**, 131920 (2006).

[8] Jensen, J., Ly, S. & Johnson, D. Low-temperature preparation of high-temperature nickel germanides using multilayer reactants. *Chemistry Of Materials* **15**, 4200–4204 (2003).

[9] De Keyser, K. *et al.* Epitaxial Formation of a Metastable Hexagonal Nickel–Silicide. *Electrochemical And Solid State Letters* **11**, H266 (2008).

[10] Van Bockstael, C. *et al.* Influence of a transient hexagonal phase on the microstructure and morphological stability of NiSi films. *Applied Physics Letters* **94**, 033504 (2009).

[11] Van Bockstael, C., Detavernier, C., Van Meirhaeghe, R. L., Jordan-Sweet, J. L. & Lavoie, C. In situ study of the formation of silicide phases in amorphous Ni-Si mixed layers. *Journal Of Applied Physics* **106**, 064515 (2009).

[12] Gaudet, S., Desjardins, P. & Lavoie, C. The thermally-induced reaction of thin Ni films with Si: Effect of the substrate orientation. *Journal Of Applied Physics* **110**, 113524 (2011).

[13] Larsson, A.-K. & Withers, R. An electron diffraction study of modulated Ni1+xGe B8 type phases. *Journal of Alloys and Compounds* **264**, 125–132 (1998).

Paper IV

Phase formation and texture of thin Ni germanides on Ge(001) and Ge(111)

B. De Schutter, K. Van Stiphout, N.M. Santos, E. Bladt, J. Jordan-Sweet, S. Bals, C. Lavoie, C.M. Comrie, A. Vantomme and C. Detavernier

Journal of Applied Physics, 119, 135305, 2016
doi:10.1063/1.4945317

Abstract

We studied the solid-state reaction between a thin Ni film and a single crystal Ge(001) or Ge(111) oriented substrate during a ramp anneal. The phase formation sequence was determined using *in situ* X-ray diffraction (XRD) and *in situ* Rutherford Backscattering Spectroscopy (RBS), while the nature and the texture of the phases were studied using X-ray pole figures and Transmission Electron Microscopy (TEM). The phase sequence is characterized by the formation of a single transient phase before NiGe forms as the stable end phase. X-ray pole figures were used to unambiguously identify the transient phase as the ϵ-phase, a non-stoichiometric Ni-rich germanide with a hexagonal crystal structure that can exist for Ge concentrations between 34 and 48% and which forms with a strong epitaxial texture on both substrate orientations. RBS revealed a simultaneous growth of the ϵ-phase and NiGe on a Ge(001) substrate, while on a Ge(111) substrate, the growth of these phases was observed to exhibit a more sequential nature.

IV-1 Introduction

In modern MOSFET (Metal-Oxide-Semiconductor Field Effect Transistor) devices, the limitations of classical dimensional downscaling force scientists and engineers to come up with innovative approaches in order to maintain the continuous improvement of device performance. This has resulted in many material innovations such as the use of strained silicon in the channel region of the MOSFET (e.g. by replacing Si by $Si_{1-x}Ge_x$ in the source and drain regions) and the replacement of the SiO_2/polycrystalline silicon gate by a high-k/metal gate. More recently, alternative channel materials like $Si_{1-x}Ge_x$ are being adopted in industry and research is now focussing on increasing the Ge content in these channels or even adopting pure Ge as a channel material, as both $Si_{1-x}Ge_x$ and pure Ge have much higher carrier mobilities compared to Si [1–5]. In this context, thin film germanides (1-30 nm) appear as a natural candidate to act as contacting material for the germanium-rich source and drain regions [6].

In 2006, Gaudet *et al.* identified NiGe as an ideal contacting material mainly because of its low resistivity ($\sim$ 22 $\mu\Omega$.cm) and low nucleation temperature (around 350 °C at 1 °C/s) [6]. Similar to the the case of widely used silicide contacts, the formation of such a NiGe contact proceeds through a solid-phase reaction between a thin Ni film and a Ge substrate upon annealing. This reaction has been studied by a number of groups on different types of Ge substrates such as amorphous Ge (a-Ge) [7–10], polycrystalline Ge (poly-Ge) [8, 9], Ge(001) [6, 10] and Ge(111) [10–12]. It is generally accepted that the reaction sets off with the formation of a Ni-rich germanide. Afterwards, this Ni-rich phase is consumed by the growth of the NiGe end phase. In literature, disagreement exists concerning the identification of the Ni-rich phase. Earlier studies report it as Ni_2Ge or Ni_3Ge_2[11, 12] while in the more recent reports, orthorhombic ϵ'-Ni_5Ge_3 is suggested [8, 10]. Furthermore, a temperature window was observed in which the Ni-rich and NiGe phase grow simultaneously on a-Ge, poly-Ge and Ge(001) [8, 10], while sequential growth was observed on Ge(111) [10].

In this study, we performed a detailed analysis of the phase formation sequence during a solid-phase reaction between a 30nm Ni film and a single crystal Ge(001) or (111) substrate, with a focus on the nature of the Ni-rich phase, using *in situ* X-ray diffraction (XRD). By performing a detailed study on the texture of this phase at different temperatures, we are able to unambiguously identify it as the 'ϵ-phase', a hexagonal Ni-rich ger-

manide that can exist over a broad composition range and that is known to be stable only above 300 °C in the bulk Ni-Ge system. In addition, we used transmission electron microscopy (TEM) to assess the morphology of the interface during the reaction and Rutherford backscattering spectrometry (RBS) to study the kinetics during the reactions.

IV-2 Experimental

Polycrystalline thin films of 30 nm Ni were deposited on both single crystalline Ge(100) and Ge(111) substrates using magnetron sputtering. The sputter chamber was pumped to a base pressure of 4×10^{-6} mbar prior to deposition and the argon pressure during deposition was fixed at 5×10^{-3} mbar.

To investigate the phase formation sequence, *in situ* XRD was performed at the X20C beamline of the National Synchrotron Lightsource (NSLS) at Brookhaven National Lab (BNL) [6, 10, 13–15]. The samples were subjected to an anneal from 100 to 900 °C at a rate of 1 °C/s in a high purity helium flow. During this anneal, the phase sequence was recorded through XRD using monochromatic X-rays with a wavelength of 1.797 Å. The diffraction pattern was recorded every second using a linear detector with a 2θ window of 14°, which is fixed at a certain 2θ angle. For both types of substrate, samples were measured twice with the detector first centered at 42° and then at 55° to fully cover 2θ values reaching from 35 to 62°, effectively targeting lattice planes with a d-spacing ranging from 1.745 to 2.988 Å.

As our *in situ* experiment is performed with a fixed geometry, it accesses only a very small fraction of possible diffracting grains. Indeed, because the position of sample and detector remains fixed during the measurement, only those grains having the diffracting plane (nearly) parallel to the substrate surface will be visible in the resulting XRD pattern. As a result, strongly textured phases consisting of grains that have a specific lattice plane parallel to the substrate surface are possibly characterized by only a single peak or might not be visible at all in the XRD data (i.e. if the diffraction conditions for that plane are not fulfilled in the given fixed geometry).

In order to unambiguously identify the phases present at different stages of the solid-phase reaction and to study their texture, complete pole figures were measured on samples quenched at different stages of the reac-

tion, both on Ge(001) and Ge(111) substrates. These pole figures were recorded at the X20A beamline of the NSLS synchrotron using a high-range linear Si-strip detector which effectively collects 640 pole figures in a single measurement for a 2θ range from 20 to 60° ($\lambda = 1.54\,\text{Å}$). The pole figures were measured using a 1° stepsize in χ (sample tilting) and an adaptive stepsize in ϕ (sample rotation) in order to obtain a uniform pole figure coverage. Accounting for the substrate symmetry, ϕ was measured between 0 and 90° for the Ge(001) and between 0 and 120° for the Ge(111) substrate, χ was measured between 0 and 90° in both cases.

Next to the X-ray diffraction techniques used to identify the crystal structure of the different phases in the sequence, *in situ* RBS was used to complement these results with elemental depth information. In thin film research, RBS is a powerful and well-established technique as it provides quantitative information on elemental composition and depth. Applying this technique *in situ* during an anneal allows one to accurately probe the atomic diffusion process and the thickness evolution of the growing and shrinking phases during the phase formation sequence that results from the heat treatment [16–18]. The *in situ* RBS measurements were performed in a vacuum chamber with a pressure below 10^{-7} mbar using a two-stage ramp anneal. First, a fast ramp rate of 20 °C/min to about 110 °C was used to reduce the measuring time prior to the onset of the solid-phase reaction. Next, the reaction itself was monitored at a slower ramp rate of 2 °C/min from 110 °C until the film had completely transformed in NiGe, i.e. 350 °C on Ge(001) and 437 °C on Ge(111). During the annealing, RBS spectra were collected using a 2 MeV $^4He^+$ beam with a beam current of 38 nA. Backscattered ions were detected using two detectors placed at scattering angles of 150° and 165° (to optimize depth and mass resolution) and the sample normal was tilted 40° with respect to the incoming ion beam to enhance the depth resolution. RBS spectra were acquired every 30 seconds during the anneal. To obtain sufficient statistics, the spectra are summed in groups of 4 for analysis, resulting in one spectrum every 2 minutes and a temperature resolution of 4 °C. In order to optimize the depth resolution and the statistics in the *in situ* RBS measurements, samples were used with a Ni thickness of 60 nm.

Finally, Transmission electron microscopy (TEM) imaging was performed on cross-sections of the interface between the Ge substrate and the Ni film for selected quenches in order to assess the interface morphology. Furthermore, Fourier transforms of high resolution TEM images acquired on the same quenches enable us to complement the phase identification results

from X-ray diffraction analysis on a microscopic level. The TEM results were all acquired using a FEI Tecnai G2 electron microscope, operating at 200 kV on samples that were prepared by ion milling.

IV-3 Results & discussion

IV-3.1 Phase formation & texture

To study the phase formation sequence for a 30 nm Ni film deposited on either a Ge(001) or Ge(111) oriented substrate, *in situ* XRD was performed. Figures 1a and b show *in situ* XRD spectra for both substrate orientations obtained using the standard diffraction geometry, but with the sample tilted in such a way that its normal is placed at an angle of 4° with respect to the scattering plane to spare the detector from intense substrate diffraction peaks, a standard procedure on the X20C beamline. Our results are very similar to those obtained by Gaudet *et al.* in 2006 [10] using the same experimental setup. According to these measurements the reaction commences with the formation of a transient Ni-rich germanide around 200 °C characterized by a single diffraction peak around 37° on Ge(001) or around 42° on Ge(111). For both substrate orientations, NiGe forms as the final phase and is visible until it melts around 765 °C.

As no Ge diffraction peaks are expected within the 2θ window used for the *in situ* XRD measurements displayed in Figure 1, we also performed the same *in situ* XRD experiments without the 4° tilt in χ. The results are shown in Figures 1c and d and reveal a very different picture of the phase formation sequence, especially on the Ge(111) substrate. In both cases, the diffraction peak resulting from the Ni-rich phase is much more pronounced. On the Ge(111) substrate, this phase does not disappear before the formation of NiGe, as suggested by the results from the tilted sample. Furthermore, it is present over a much wider temperature window than what could be concluded from the previous results. These observations indicate that the Ni-rich phase is highly textured, possibly with an epitaxial alignment.

IV-3.1.1 Ni-rich phase identification

As mentioned in the introduction, no clear consensus exists in literature concerning the nature of the Ni-rich germanide. In the most recent study performed by Gaudet *et al.* on single crystal Ge substrates, the transient

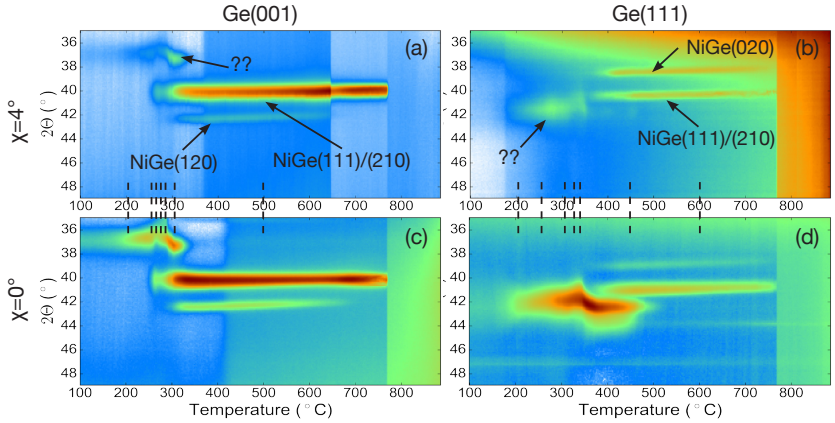

Figure 1. *In situ* XRD spectra recorded during annealing of a 30nm Ni film at 1 °C/s on Ge(001) (left column, (a) and (c)) and Ge(111) (right column, (b) and (d)). The spectra in the top row were collected with the sample tilted over 4° in χ. The bottom row spectra were collected on samples having 0° tilt. The dashed lines indicate the temperatures where quenches were made for more detailed pole figure and TEM measurements.

phase was cautiously identified as *monoclinic* ϵ'-Ni_5Ge_3 (*JCPDS* 00-024-0449) based on the weak diffraction peaks observed in the *in situ* XRD measurements visible in the top row of Figure 1 (marked with '??'). Indeed, the peak around 37° on the Ge(001) substrate might be caused by either ϵ'-Ni_5Ge_3 (221), (312) or (021) and the peak around 42° on the Ge(111) substrate by ϵ'-Ni_5Ge_3 (002). However, we recently observed that annealing mixed layers of Ni with 36-48% Ge deposited on a Ge(001) substrate results in the formation of a metastable, hexagonal germanide [19]. According to the bulk Ni-Ge binary phase diagram [20], three non-stoichiometric *hexagonal* nickel germanides exist above 300 °C in the Ge concentration range between 35 and 44%, i.e. ϵ-Ni_5Ge_3, $Ni_{19}Ge_{12}$ and Ni_3Ge_2. Due to the similar crystal structure and non-stoichiometric nature of these phases, they can be regarded as a single phase [19–21] which we will refer to as the 'ϵ-phase'. As this phase is not expected to exist below its minimum stability temperature of $\pm$ 300 °C, it was not considered as a possible candidate for the transient phase in previous studies. However the diffraction peaks around 37° and 42° in the *in situ* XRD measurements can perfectly be ascribed to the (101) and the (002) diffraction peaks of the ϵ-phase.

In order to unambiguously identify this Ni-rich phase, we performed X-ray pole figure measurements on samples quenched at different temper-

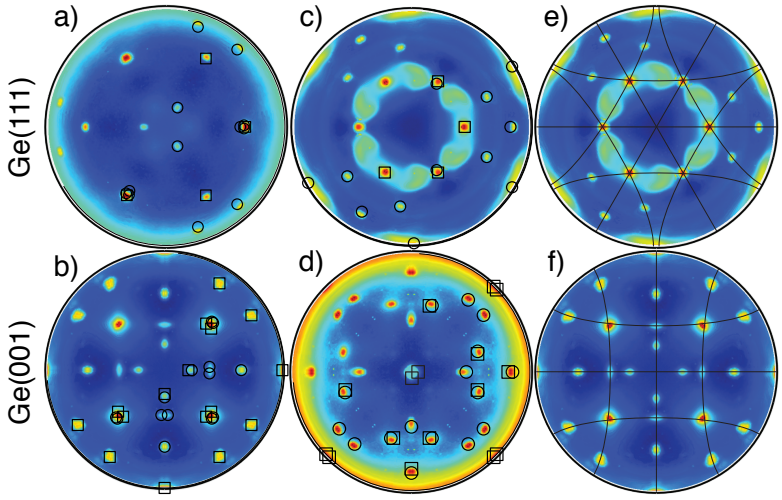

Figure 2. Pole figures recorded at $2\theta = 31.73°$ ($d = 2.82$ Å) (a, b) and $2\theta = 44.62°$ ($d = 2.03$ Å) (c, d, e, f) on both substrate types. The first diffraction angle corresponds to the $\epsilon(10\bar{1}1)$ plane, the second to $\epsilon(10\bar{1}2)$. On figures a, b, c and d, the calculated locations of diffraction spots for the epitaxial components listed in table 3.2 are overlaid on the pole figures. The symbol used for each component can be found in table 3.2. Calculated axiotaxy lines for the hypothetical $\epsilon(2\bar{1}\bar{1}0)$//Ge{110} axiotaxy are overlaid on pole figures e and f.

atures (indicated by the vertical dashed lines in Figure 1) during the phase formation sequence. Figure 2 shows pole figures recorded on samples quenched at 240 °C on Ge(001) (Figure 2b, d, f) and at 260 °C on Ge(111) (Figure 2a, c, e), i.e. at temperatures where only the peak of the Ni-rich phase is visible in the *in situ* XRD measurements. The pole figures in the first column (a and b) are obtained at $2\theta = 31.73°$ ($d = 2.82$ Å), those in the second and third column (c, d, e and f) at $2\theta = 44.62°$ ($d = 2.03$ Å). These angles correspond to the Bragg diffraction condition for the ϵ-phase (101) and (102) planes respectively. Clear diffraction spots can be observed at both angles and on both substrates, suggesting an epitaxially textured phase being present. We also observed diffraction spots on pole figures corresponding to the other diffracting planes of the ϵ-phase within the 2θ window covered by the linear detector, while no diffraction features were observed on pole figures for other 2θ values. As the diffraction spots observed on the pole figures can indeed be fitted with an epitaxially textured ϵ-phase (see the next section for more details on this epitaxy) and not with any of the other known nickel germanides, we are confident in identifying the observed Ni-rich phase as the hexagonal ϵ-phase. Furthermore,

high-resolution TEM diffraction experiments (See supplemental material figures S1 and S2) have confirmed the presence of ϵ-phase grains in samples quenched at 240 and 280 °C on Ge(001) and at 260, 330 and 345 °C on Ge(111).

The formation of the hexagonal ϵ-phase at a temperature below its thermodynamically stable temperature window (as defined in the bulk Ni-Ge phase diagram) is similar to what has been observed for a thin Ni film on single crystal silicon substrates. First, the formation of epitaxially textured θ-nickel-silicide was observed when annealing mixed Ni(x%Si) films with $37 \leq x \leq 42$ % deposited on Si(001) and Si(111) [22, 23]. Later, Gaudet *et al.* observed the formation of this phase during the reaction of pure Ni films on Si(001), where it forms as a transient phase with a fiber texture before NiSi formation [24, 25]. On Si(111), it was only observed in the as-deposited film with an epitaxial texture [25]. It is interesting to note that the θ-phase in the Ni-Si system and the ϵ-phase in the Ni-Ge system have a similar hexagonal crystal structure (spacegroup $P6_3/mmc$) and can both exist within a certain concentration window [19, 22, 26].

IV-3.1.2 ϵ-phase texture

Next to the identification of the ϵ-phase, the pole figure measurements also allow for an investigation of its texture. On both substrate types, the analysis of the pole figures revealed the presence of two epitaxial texture components. A summary of the geometrical relations defining these components along with the symbol used in Figure 2 to mark the expected peak locations for these grain orientations is provided in table 3.2.

ϵ-phase on Ge(111) On Ge(111), the texture of the ϵ-phase is characterized by two epitaxial components. The highest intensity spots on the pole figures correspond to orientation A_{111} ('□' symbols on Figure 2a and c), for which the hexagonal basal plane of the ϵ-phase is parallel to the substrate, while the $\epsilon(2\bar{1}\bar{1}0)$ plane is parallel to a Ge$\{1\bar{1}0\}$ plane. This preferential alignment of the film's basal plane with the substrate (111) plane can be understood if we compare the positions of the Ge atoms in the Ge(111) and the ϵ(0001) planes. Figure 3a shows the topmost layer of atoms in the Ge(111) substrate. Half of the atoms are located slightly below the surface and are bonded to the Ge atoms below (white atoms in Figure 3a), while the other half lay at the surface (black atoms in Figure 3a) and have a dangling bond perpendicular to the Ge(111) interface. These

Ge(111) substrate		
label	relations	symbol
A_{111}	$\epsilon(0001)//\text{Ge}(111)$, $\epsilon(2\bar{1}\bar{1}0)//\text{Ge}(01\bar{1})$	□
B_{111}	$\epsilon(02\bar{2}1)//\text{Ge}(111)$, $\epsilon(2\bar{1}\bar{1}0)//\text{Ge}(01\bar{1})$	◯

Ge(001) substrate		
label	relations	symbol
A_{001}	$\epsilon(0001)//\text{Ge}(\bar{1}11)$, $\epsilon(2\bar{1}\bar{1}0)//\text{Ge}(01\bar{1})$, $\epsilon(01\bar{1}1)\sim//\text{Ge}(001)$	□
B_{001}	$\epsilon(01\bar{1}\bar{2})//\text{Ge}(\bar{1}11)$, $\epsilon(2\bar{1}\bar{1}0)//\text{Ge}(\bar{1}10)$, $\epsilon(01\bar{1}4)\sim//\text{Ge}(001)$	◯

Table 3.2. Overview of the different ϵ-phase epitaxial texture components that have been identified in 30nm Ni films on Ge(001) or Ge(111), quenched at 240 and 260 °C respectively. For each component, a label and the symbol used to mark the locations of diffraction spots for that component in figure 2 are given.

topmost (black) Ge atoms are characterized by an interatomic distance of 4.00 Å and display a hexagonal symmetry. In the $\epsilon(0001)$ plane (Figure 3b), the Ge atoms are located at the vertices of triangles, effectively creating the same hexagonal symmetry as the topmost Ge atoms in the Ge(111) plane. The Ge atoms in the $\epsilon(0001)$ plane have a dangling bond perpendicular to the plane of the triangles. Due to the large concentration window over which the ϵ-phase can exist, the inter-atomic distance between the Ge atoms in the $\epsilon(0001)$ plane varies between 3.963 and 3.834 Å for a Ge concentration of 35 and 44 % respectively [20]. As will be discussed in detail later, RBS measurements suggest that at the early stages of the reaction, the Ge concentration in the ϵ-phase is around 35-37 %. At these Ge concentrations, the interatomic distance between the Ge atoms in the $\epsilon(0001)$ plane is about 3.963 Å [20]. This $\epsilon(0001)$ plane thus has a nearly perfect fit on the Ge(111) substrate (mismatch $\sim$ 0.9 %) which saturates the dangling bonds and leads to a low energy interface.

Next to the A_{111} orientation which explains the highest intensity spots, there are some less intense spots visible on the pole figures for the ϵ-phase formed on Ge(111) (see figure 2a, c) that cannot be explained by this orientation. These features can be explained by a second epitaxial texture component, labeled B_{111}, for which the $\epsilon(02\bar{2}1)$ plane is parallel to the

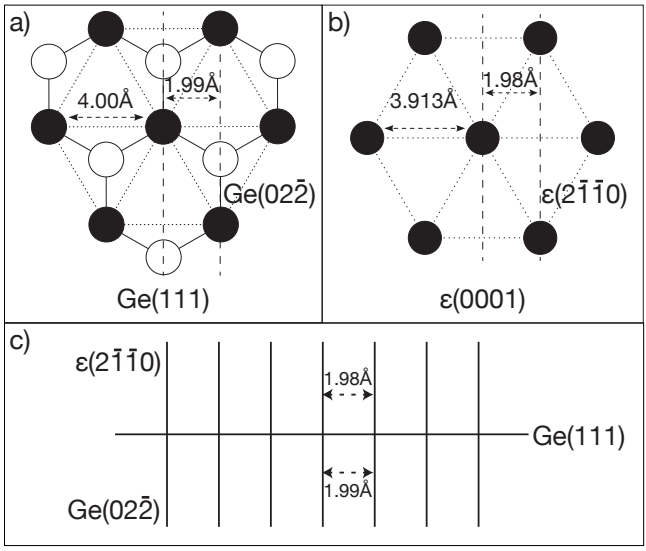

Figure 3. a) Ge atoms in the Ge(111) interface plane. Black ones are located at the interface and have a dangling bond. White ones are located slightly below the interface. b) Ge atoms in the ϵ(0001) basal plane. c) Alignment across the interface of the Ge(01$\bar{1}$) and the ϵ(2$\bar{1}\bar{1}$0) planes, which is observed both in the A_{111} and B_{111} epitaxial components.

Ge(111) interface and an $\epsilon\{2\bar{1}\bar{1}0\}$ is parallel to a Ge$\{1\bar{1}0\}$ plane. When comparing the B_{111} to the A_{111} orientation discussed above, it is observed that both orientations have in common that an $\epsilon\{2\bar{1}\bar{1}0\}$ plane is parallel to a Ge$\{1\bar{1}0\}$ plane. As the difference in d-spacing between an $\epsilon(2\bar{1}\bar{1}0)$ and a Ge{220} plane is only 0.33% (ϵ-phase at its lowest Ge concentration), this results in a (near) alignment of these planes across the interface. Such an alignment of lattice planes from film and substrate across the interface is also observed in the case of an axiotaxy texture [27]. The geometry of this alignment is the same for both components and is sketched in Figure 3c, from which it can be observed that both planes are aligned perpendicular to the interface. For the A_{111} orientation, the alignment assures the nice overlap between the hexagonal arrangements of the Ge atoms in the Ge(111) and the ϵ(0001) planes at the interface. This can be seen in Figure 3a and b, where the intersection of the interface plane with the Ge(01$\bar{1}$) (Figure 3a) and the $\epsilon(2\bar{1}\bar{1}0)$ planes (Figure 3b) are indicated by the vertical dashed lines. For the B_{111} orientation, the alignment of an $\epsilon\{2\bar{1}\bar{1}0\}$ with a Ge$\{1\bar{1}0\}$ plane also results in a reasonable overlap between the Ge atoms of the Ge(111) plane and the $\epsilon(02\bar{2}1)$ at the interface. Figure 4 shows a

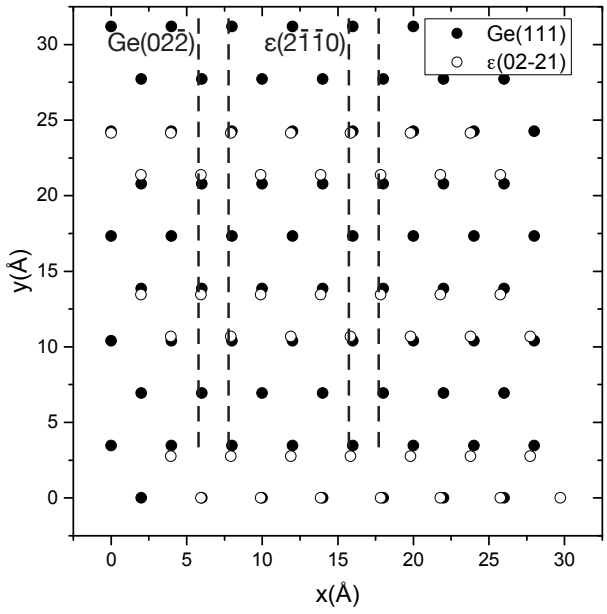

Figure 4. Top-view of the interface structure for the B_{111} orientation. The Ge atoms in the $\epsilon(02\bar{2}1)$ and the Ge(111) planes at the interface are indicated with open and filled circles respectively. The intersections of the aligned Ge$(01\bar{1})$ and $\epsilon(2\bar{1}\bar{1}0)$ planes with the interface plane are indicated by the dashed lines.

top view of this interface structure where the Ge atoms from the $\epsilon(02\bar{2}1)$ plane and the Ge(111) plane near the interface are indicated with open and filled circles respectively.

The fact that the two observed epitaxial texture components A_{111} and B_{111} share the alignment of the aforementioned planes is visually clear if we plot the axiotaxy lines that would result from a hypothetical $\epsilon(2\bar{1}\bar{1}0)$// Ge{110} axiotaxy on the pole figure (see Figure 2e). All the observed diffraction spots resulting from the ϵ-phase are situated along these lines. In fact, the A_{111} orientation can be transformed into the B_{111} orientation through a rotation over 71.5° around the normal to a Ge{110} plane. However, an axiotaxy texture component resulting from the observed alignment does not seem to be present here, as it is not visible in the pole figures in Figure 2. This suggests that the interfaces created by the two observed epitaxial grain orientations are very stable, as all grains are oriented according to either the A_{111} or the B_{111} epitaxial component.

ϵ-phase on Ge(001) Similar to the case on Ge(111), the texture of the ϵ-phase formed from a 30 nm Ni film on Ge(001) is characterized by two epitaxial components (see Table 3.2). The A_{001} orientation is identical to the A_{111} orientation observed on the Ge(111) substrate. In this case however, the ϵ(0001) basal plane and a Ge{111} plane are not parallel to the substrate-film interface, but they form an angle of 54.74° with the interface. Based on the alignment of the ϵ(0001) and Ge{111} planes, one could also expect faceting to occur, a phenomenon where pyramidal structures are observed at the interface. The formation of such pyramidal structures would be driven by the formation of a matching interface between ϵ(0001) and Ge{111} as discussed in Figure 3 at the sides of the pyramids. As will be discussed in more detail in section IV-3.2, such a pronounced faceting was not observed here. A side-on view of the Ge atoms in the vicinity of the interface for the A_{001} orientation is plotted in Figure 5. The Ge{111} and ϵ-phase {0001} planes are shown, intersecting the interface. Because the Ge atoms in these planes have nearly identical interatomic spacing, dangling bonds at the interface will be saturated wherever these planes meet. From Figure 5, it is clear that about one in three of the Ge{111} planes meet an ϵ{0001} plane at the interface. This alignment is very similar to what has been observed previously for the θ-nickel-silicide phase formed from a Ni(40 %Si) film deposited on Si(001) [22].

Similar to what was observed on Ge(111), both observed epitaxies on Ge(001) are characterized by the alignment of an $\epsilon\{2\bar{1}\bar{1}0\}$ with a Ge{110} plane, both perpendicular to the interface in both orientations. In Figure 2f, this shared alignment is visualized by overlaying the axiotaxy lines for a hypothetical $\epsilon(2\bar{1}\bar{1}0)$//Ge{110} axiotaxy on the pole figure. An actual axiotaxy texture component resulting from the alignment was not observed.

IV-3.1.3 Phase formation sequence

As the information regarding the phase formation sequence gained from the *in situ* XRD results is influenced by the texture of the different phases, a more detailed investigation was done by performing pole figure measurements on samples quenched at different temperatures during the heat treatment on both substrate types. The temperatures of the different quenches are indicated on the *in situ* XRD spectra in Figure 1. In Figure 6, we show pole figures collected on the different quenched samples at $2\theta = 44.5°$ ($d = 2.03$ Å), as one can expect to see diffraction features of planes from the three phases that occur during the phase formation sequence

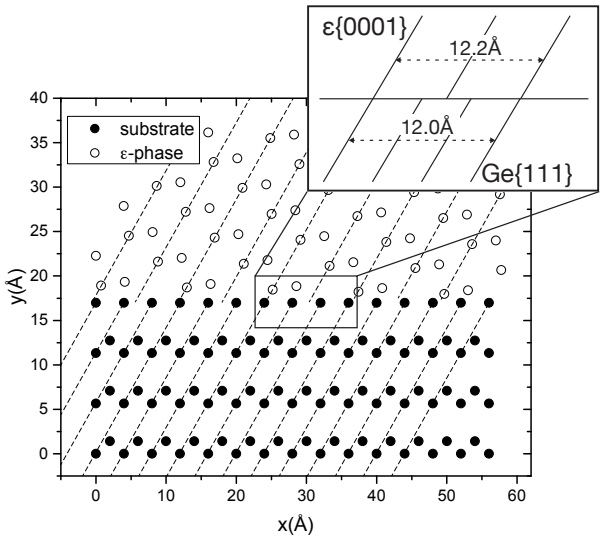

Figure 5. Cross-sectional view of the alignment across the interface of the $\epsilon(0001)$ and Ge(111) planes for the A_{001} orientation. The view direction is perpendicular to the Ge$(0\bar{1}1)$ plane. Ge atoms in the ϵ-phase and the Ge substrate are plotted using open and filled circles respectively.

- Ni(111) ($d = 2.034\,$Å), $\epsilon(10\bar{1}2)$ ($d = 2.028\,$Å) and NiGe(211) ($d = 2.049\,$Å) - at this diffraction angle. It must be noted that a contribution from the Ge{220} ($d = 2.00\,$Å) substrate planes is also expected, resulting in intense diffraction peaks on the displayed pole figures at χ =45°, ϕ =45, 135, 225, 315° and at χ =90°, ϕ =0,90,180,270° for the Ge(001) substrate. For the Ge(111) substrate, Ge{220} contributions are visible at χ =35.26°, ϕ =0,120,240°. In Figure 6, one of each set of these peaks is indicated on the as deposited pole figure for both substrate types.

Both on Ge(001) and Ge(111), the phase formation sequence was determined by combining the *in situ* XRD results with the pole figure data collected at the different quenching temperatures. At each temperature, we identified the phases present in the system through the characteristic set of diffraction features on the pole figure for each phase. For the ϵ-phase, these characteristic features resulting from diffraction of the $\epsilon(10\bar{1}2)$ plane were discussed in the previous section (see Figure 2). For NiGe, the characteristic diffraction features can be observed in the pole figures quenched at the highest temperature on both substrate types, i.e. 500 °C on Ge(001) and 600 °C on Ge(111), as only NiGe is present at those temperatures. As

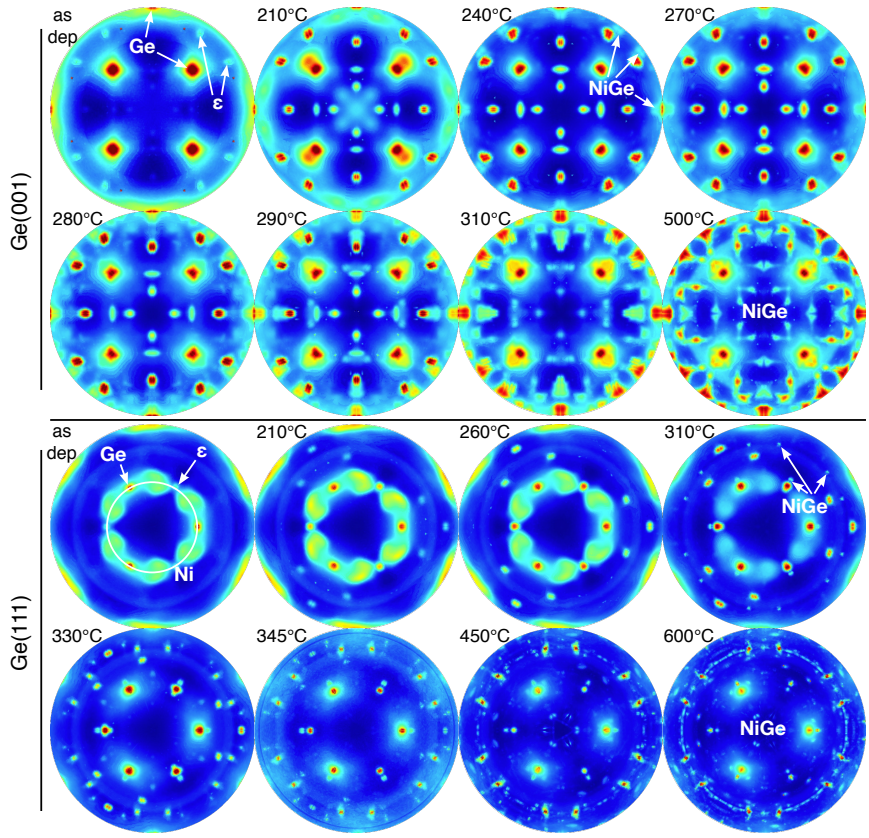

Figure 6. Selection of pole figures (2θ =44.5°; d = 2.03 Å) recorded on samples quenched at different temperatures on both substrate orientations.

our pole figure measurements reveal the same texture for the NiGe phase as observed and discussed by Gaudet *et al.*, the reader is referred to ref. [10] for more details.

Summaries of the phases that are present according to the pole figure and *in situ* XRD data at the different quenching temperatures during a ramp anneal at 3 °C/s are provided in tables 3.3 and 3.4 for the reaction on Ge(001) and Ge(111) respectively. A more detailed discussion on the formation sequence observed on both substrate orientations is given below.

temperature (°C)	identified phases
as deposited	Ni, ϵ-phase
210	Ni, ϵ-phase
240	Ni, ϵ-phase, NiGe
270	Ni, ϵ-phase, NiGe
280	Ni, ϵ-phase, NiGe
290	ϵ-phase, NiGe
310	ϵ-phase, NiGe
500	NiGe

Table 3.3. Identified phases in the pole figures recorded on samples quenched at the temperatures indicated in the first column on Ge(001).

30nm Ni on Ge(001) On Ge(001), no diffraction features resulting from the deposited Ni layer were observed on the pole figure acquired on the as deposited sample, while the Ni(111) and (002) peaks were observed in an *in situ* XRD measurement at a higher 2θ window (See supplemental material Figure S3a). This indicates a polycrystalline Ni film with a random texture being present after deposition. The Ni peaks remain visible in the *in situ* XRD data up until a temperature of 280 °C.

The most important observation from the pole figure acquired on the as deposited sample is the presence of (weak) diffraction spots characteristic for the ϵ-phase at χ =78.4° (see top left pole figure of Figure 6), indicating that this phase already forms during deposition of the Ni film. This is similar to what has been observed by Gaudet *et al.* in as-deposited Ni films on Si(111), where a very thin epitaxially aligned θ-nickel-silicide layer is present at the interface [25]. In contrast to the θ phase observed for as-deposited Ni films on Si(111), which transforms immediately into δ-Ni_2Si upon heating, the ϵ-phase here remains present as the sole phase until it is consumed by NiGe. In our recent study on phase formation in co-deposited Ni(x%Ge) films on SiO_2 and Ge(001) substrates [19], we also observed the metastable formation of this ϵ-phase in films with a Ge concentration between 36 and 48%. Furthermore, in the Ge concentration window between 36 and 44%, the ϵ-phase was observed to have formed during deposition of the mixed Ni(x%Ge) layer on both SiO_2 and Ge(001) substrates. As it is generally accepted that a very thin mixed Ni-Ge (or

temperature (°C)	identified phases
as deposited	Ni, ϵ-phase
210	Ni, ϵ-phase
260	Ni, ϵ-phase
310	Ni, ϵ-phase, NiGe
330	ϵ-phase, NiGe
345	ϵ-phase, NiGe
450	ϵ-phase, NiGe
600	NiGe

Table 3.4. Identified phases in the pole figures recorded on samples quenched at the temperatures indicated in the first column on Ge(111).

Ni-Si) layer forms during deposition of Ni on a Ge (or Si) substrate, the as-deposited ϵ-phase nucleation observed in this study can be intuitively understood from the previous results if we assume that the thin intermixed Ni-Ge film is characterized by a Ge concentration between 36 and 44%. However, the exact physical reasons as to why the ϵ-phase nucleates that easily under these conditions are still an open question.

On the pole figure for the sample quenched at 240 °C, NiGe{211} diffraction spots become weakly visible near the edge (see Figure 6). The formation of this phase is also visible in the *in situ* XRD measurements through the emergence of the NiGe(111)/(210) diffraction peak around the same temperature. The ϵ-phase and NiGe both remain present up to a temperature of 335 °C, when the ϵ-phase is completely consumed by the growing NiGe phase which then remains the stable end phase until it melts around 780 °C. According to the pole figure recorded on the sample quenched at 500 °C (where NiGe is the only phase present), the NiGe phase is characterized by a complex texture. As was mentioned before, the texture of this phase on Ge(001) was studied in detail by Gaudet *et al.* [10] and was found to be a combination of five different epitaxial components and three very weak axiotaxy components for which either the NiGe(121), (220) or (211) plane is aligned with a Ge{110} plane.

30nm Ni on Ge(111) On Ge(111), no diffraction peaks from the as-deposited Ni film were observed at the expected diffraction angles for the Ni(111) and (002) peaks (at $2\theta = 52.4°$ and $61.3°$, see supplemental material Figure S3b), which is indicative of a textured Ni film after deposition. Indeed, the pole figure collected on the as-deposited sample suggests that the Ni film is deposited with a broad Ni(110) fiber texture (i.e. the Ni(110) plane is parallel to the interface), which is characterized by the broad ring visible around $\chi = 35°$ (see Figure 6, pole figure on as-deposited Ge(111) sample), resulting from the Ni{111} planes that have a $35.26°$ angle with respect to the Ni(110) plane. Furthermore, it can be observed that the diffracted intensity is not uniformly distributed around the fiber ring, but is concentrated in broad lobe-like features. Deeper analysis suggests that the rotation of the different Ni grains around the substrate normal is not uniformly distributed, but that there is a tendency for the Ni grains to align their $(1\bar{1}1)$ or $(1\bar{1}\bar{1})$ plane with the Ge$(1\bar{1}0)$. As these planes are all perpendicular to the Ge(111) interface plane and the difference in d-spacing between these Ni planes and the Ge$(2\bar{2}0)$ plane is only 0.19 % ($d_{\mathrm{Ni}\{1\bar{1}1\}} = 1.992\,\text{Å}; d_{\mathrm{Ge}\{2\bar{2}0\}} = 1.988\,\text{Å}$), this should indeed result in a better match at the interface.

Next to the textured Ni film, the pole figure collected on the as-deposited sample (see Figure 6) again shows the presence of the ϵ-phase, similar to what was observed on Ge(001). The presence of this phase is evidenced by the faint diffraction spots around $\chi = 35°$, characteristic for the A_{111} epitaxy (see Figure 2c). Thus, the initial ϵ-phase nuclei that form during the deposition of the Ni film have their (0001) basal plane parallel to the Ge(111) interface plane, resulting in the excellent match at the interface as discussed above (see Figure 3). The ϵ-phase then grows at the expense of Ni as the temperature is ramped. On the 210 °C pole figure, one can observe diffraction features of the B_{111} epitaxy as well. However, because the absence of an $\epsilon(02\bar{2}1)$ diffraction peak in the *in situ* XRD measurements and the limited number of temperatures where pole figures were collected, it is hard to pinpoint the exact temperature at which grains with this orientation start to form.

Weak diffraction spots characteristic for the NiGe phase are first observed in the pole figure recorded on the sample quenched at 310 °C. In the *in situ* XRD measurements, the formation of this phase is characterized by the NiGe(111)/(210) and NiGe(020) peak at $2\theta = 41°$ and $2\theta = 39°$ respectively. Up until a temperature of ~ 500 °C, both NiGe and the ϵ-phase are visible both in the *in situ* XRD and in the pole figure measurements. At that

point, the ϵ-phase has been completely consumed by the growing NiGe, which remains present until it melts around 780 °C. Gaudet *et al.* discussed in detail the texture of this NiGe phase formed on Ge(111), which is a combination of two strong fiber components (either a NiGe{010} or {101} plane parallel to the interface), no less than eight epitaxial components and the same, weak axiotaxy components that were also observed on Ge(001) [10].

Compared to the results on the Ge(001) substrate discussed above, the temperature window over which the ϵ-phase is present is extended by more than 150 °C. As the interface with the lowest lattice mismatch between the ϵ-phase and the Ge substrate is obtained for the A_{111} orientation on Ge(111), this will likely result in the lowest interface energy. The extended stability window of the ϵ-phase on the Ge(111) substrate thus suggests that the interface energy plays an important role in the stabilization of this phase. The low energy interface makes the nucleation of the NiGe phase more difficult, which leads to the elevated NiGe formation temperature on the Ge(111) substrate. This is similar to what has been observed for $CoGe_2$ formation on Ge(111), on which the epitaxial orientation of the preceding Co_5Ge_7 phase results in an elevated $CoGe_2$ formation temperature compared to a Ge(001) substrate, where the epitaxial Co_5Ge_7 orientation is less pronounced[15].

IV-3.2 Film structure

Figure 7 shows three TEM cross-section of the interface on samples that were used for the pole figure measurements quenched at 280 °C on Ge(001) (Figure 7a) and 330 °C on Ge(111) (Figure 7b), as well as on the as-deposited Ge(111) sample (Figure 7c). On both substrates, the layered growth typical for solid-phase silicidation/germanidation reactions [9, 28, 29] is visible. Taking into account the phases identified based on the X-ray pole figure measurements, a corroborative identification was performed using a HR-TEM Fourier transform study. For all quenches, the same phases were identified using these two techniques.

For the sample on Ge(001) quenched at 280 °C, two distinct layers are clearly visible (Figure 7a). The two phases were identified as the ϵ-phase and NiGe, which corresponds to what is expected from the XRD results. Indeed, when looking at the *in situ* XRD spectra on Ge(001) (Figure 1c), both the $\epsilon(10\bar{1}1)$ and NiGe(111)/(210) peaks are visible at that temperature. At this stage of the reaction, the NiGe phase is growing beneath the

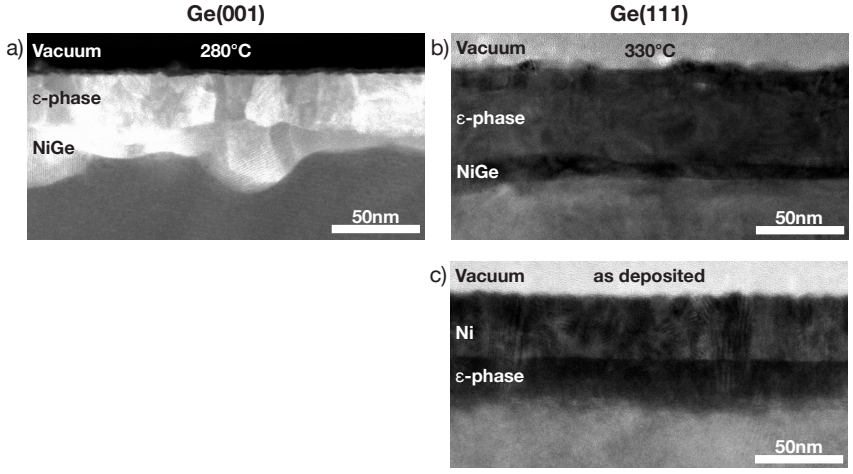

Figure 7. Cross-section HAADF-STEM (a) and BF-TEM (b and c) images for Ni films deposited on both Ge(001) (a) and (111) (b, c) substrates and quenched at different temperatures (indicated on the figures).

preceding ϵ-phase by consuming it. The HAADF-STEM cross-section also reveals a quite rough interface between the NiGe layer and the Ge(001) substrate. A similarly rough interface was observed by Nemouchi *et al.* [9] for a NiGe layer formed by an isothermal anneal at 180 °C during 110 min on an amorphous Ge substrate, but an explanation for this interface roughening was not provided. In our case, we believe that the texture of the preceding ϵ-phase can at least partly explain this rough interface. The alignment and the high quality match between the ϵ(0001) and Ge(111) planes, which form an angle of 54.74° with the interface, can result in some degree of faceting through the formation of pyramid-like structures at the interface, much like what is observed for epitaxial $NiSi_2$ on Si(001) [30]. We also observed a similar faceting with the θ-nickel-silicide formed from a Ni(40%Si) film on Si(001), which displays a similar texture as the ϵ-phase [22, 31]. However, cross-section images on a sample quenched at lower temperatures on Ge(001) are needed to support this hypothesis.

The sample quenched at 330 °C on the Ge(111) substrate shows a much flatter interface. Again, both a thin, growing NiGe can be observed that consumes the ϵ-phase layer above. Since on this substrate orientation the ϵ-phase (0001) has a nearly perfect match with the Ge(111) plane which is now parallel to the interface, no faceting is expected to occur. This results in a flat ϵ-phase/Ge interface, which we have observed in BF-TEM cross-

sections on samples quenched at lower temperatures (See supplemental material Figure S4). The NiGe phase can then nucleate at a flat interface, resulting in the observed, flat NiGe/Ge(111) interface.

In Figure 7c, we included a BF-TEM cross-section of an as-deposited sample on Ge(111). The pure Ni layer is clearly visible, together with a $\sim$ 20 nm thick layer containing both Ni and Ge in contact with the Ge(111) substrate. The formation of an intermixed layer with such a thickness is quite surprising, as for metals deposited on Si, the intermixed interface layer is typically only a few nanometers thick [32]. In this layer, several ϵ-phase grains were detected using high resolution TEM imaging, all at the interface with the Ge substrate. The fact that we only observed very weak ϵ-phase diffraction features in the pole figure collected on this sample (see Figure 6) suggests that a large fraction of this layer is still amorphous.

IV-3.3 Kinetics

Details on the kinetics during the phase formation sequence were investigated using *in situ* RBS, a technique that yields quantitative elemental depth maps as a function of temperature. These maps are displayed as a contour plot by merging the successive RBS spectra collected during the ramp anneal in Figure 8a and b for the reaction between a 60 nm Ni film and a Ge(001) or (111) substrate respectively. To allow for a good comparison between both substrates, the temperature axes are drawn with the same scale, although no RBS spectra were collected on the (001) substrate above 340 °C because the reaction had already finished. The scattering energies for Ni and Ge atoms located at the sample surface are marked along with an indication of the expected backscattering energy for a Ni or Ge atom located at 60 nm below the surface (i.e. the thickness of the deposited Ni film). Before these results are discussed, two important points have to be considered. First, due to the smaller mass of Ni compared to Ge, the signals of Ni and Ge overlap. As the Ni surface energy is only slightly smaller than that of Ge, the Ni peak is superimposed on the plateau resulting from the 'infinitely' thick Ge substrate. Therefore, phase transformations are harder to distinguish from these raw data compared to a case where the signals are separated (e.g. for Ni on Si [16, 18, 33]) and the individual spectra are much more difficult to analyse. Second, the ramp rate used in these experiments (2 °C/min) is much slower than the one used for the *in situ* XRD measurements (1 °C/s). Therefore, formation temperatures obtained with *in situ* RBS are not directly comparable to those obtained

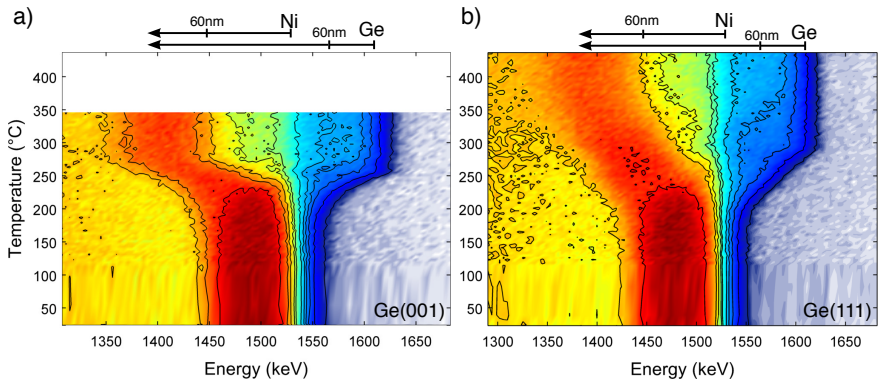

Figure 8. *In situ* RBS measurements of a 60 nm Ni film deposited on (a) Ge(001) and (b) Ge(111), performed during an anneal at 2 °C/min. An indicative depth scale is provided for both Ni and Ge.

from *in situ* XRD due to the different thermal budget applied at a specific temperature.

From the RBS maps in Figure 8, it is clear that the reaction on the Ge(001) substrate proceeds much faster than on the Ge(111) substrate. In both cases, the reaction sets off around 200 °C, indicated by the concentration drop in the Ni peak and the bending of the contour lines of both the Ni peak and the Ge shoulder. On Ge(001), the reaction seems to be completed around 280 °C, while on the Ge(111) substrate, the bending of the contour lines only stops around 350-400 °C. This confirms the XRD-based observations discussed above, where a difference of more than 150 °C was observed between both substrate orientations for the temperature at which NiGe has completely consumed the ϵ-phase.

In order to study the kinetics of the solid-phase reaction from the *in situ* RBS results, a 3-layer model was fitted to all individual RBS spectra using an *artificial neural network* (ANN), a technique which allows for the quasi-instantaneous analysis of a huge set of RBS spectra without deteriorating the quantitative accuracy [34]. The output of the ANN analysis was subsequently refined using the NDF code [35]. Based on the phases that were identified by XRD, as discussed above, the spectra were fitted using a pure Ni layer, a Ni-rich Ni_xGe_y layer with a variable Ni:Ge concentration (as a model for the ϵ-phase) and a NiGe layer with a fixed Ni:Ge ratio of 1:1. The fits were validated by comparing simulated RBS spectra generated by using the results of the ANN with the raw RBS spectra at each temperature.

Figure 9 shows the thickness evolution of the various fitted phases as a

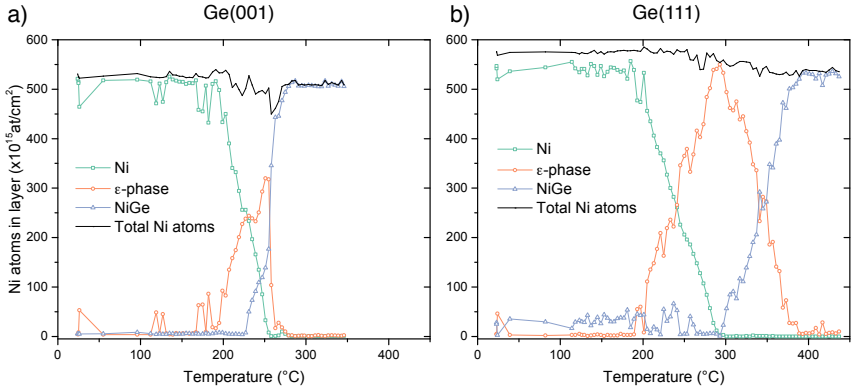

Figure 9. Thickness evolution of the different phases during the ramp anneal of a 60 nm Ni film at 2 °C/min on (a) Ge(001) and (b) Ge(111). The thicknesses are fitted from the *in situ* RBS data using an artificial neural network (ANN) approach and are expressed in Ni atoms/cm^2 for normalization purposes.

function of temperature (using the same temperature scale on the x-axis) on both the Ge(001) substrate (a) and Ge(111) substrate (b). This thickness is expressed in the number of Ni atoms in each phase (at/cm^2) as this allows us to normalize the layer thicknesses in such a way that the sum of the individual layer thicknesses (i.e. the total Ni content in the entire system) is constant. In this way, the proportion of the formed layers becomes clear and the consistency of the values is validated, as the total sum of Ni atoms across all layers should remain constant. As can be observed in both figures, there is quite some noise on the fitted thicknesses, in particular for low values ($<$ 100 at/cm^2). This is due to the overlapping Ni and Ge signals in the RBS spectra, which impedes the fitting procedure when the layers are very thin (i.e. at the initial formation stage). Therefore, absolute values of the fitted thickness below 150 at/cm^2 should not be given too much attention. Nevertheless, these fitted thickness evolutions give us some valuable qualitative insights on the phase formation sequence.

On both substrate orientations, the growth of the ϵ-phase sets off around 200 °C. However, from the *in situ* XRD results, we observed the presence of the ϵ-phase in the as-deposited films. This suggests that at lower temperatures there is only limited growth of this phase. As the ϵ-phase layer is thin at these temperatures compared to the total thickness of the deposited film (60 nm for the RBS samples), it is hard to reliably fit its thickness in the RBS spectra. A possible explanation for this limited

growth below 200 °C can be the as-deposited formation of only a very thin crystalline ϵ-phase layer in contact with the interface within the intermixed layer. The vertical growth of this crystalline layer could then be slow as it depends on diffusion through this intermixed layer. The extended temperature window over which the presence of the ϵ-phase was detected in the XRD measurements is also visible in the RBS results. While the ϵ-phase is completely consumed around 260 °C on Ge(001), it remains present up until almost 400 °C on Ge(111).

According to the RBS results on the Ge(001) substrate (Figure 9a), the NiGe phase starts growing around 230 °C. At that time, the Ni is not yet fully consumed by the ϵ-phase, which is still growing, indicating that both phases grow simultaneously until the Ni is completely consumed by the ϵ-phase around 260 °C. This simultaneous growth of the ϵ-phase and NiGe has also been observed by Gaudet *et al.* for a 30 nm Ni film on Ge(001) and amorphous Ge during a 3 °C/s ramp anneal [10] and by Nemouchi *et al.* on amorphous and polycrystalline Ge substrates during an isothermal anneal at 160 °C [8, 9]. On the Ge(111) substrate, the RBS results show that NiGe only starts growing when the ϵ-phase reaches its maximum thickness, i.e. when all Ni has been transformed into the ϵ-phase (Figure 9b). This implies sequential growth of both phases on this substrate orientation, which was also put forward by Gaudet *et al.* [10]. However, on the pole figure quenched at 310 °C on the Ge(111) substrate (see Figure 6) faint diffraction spots from the NiGe are already visible while the fiber ring from the pure Ni layer can also still be weakly observed. This suggests that simultaneous growth of both phases also takes place on a Ge(111) substrate, although a simultaneous thickness increase of the NiGe phase is not observed in the RBS results on this substrate orientation. This is possibly due to the fact that the ϵ-phase grows at the NiGe/ϵ-phase interface by consuming NiGe as long as pure Ni is still available. As such, the NiGe phase is growing at the Ge/NiGe interface and is being consumed at the NiGe/ϵ-phase interface at the same time, resulting in its thickness staying more or less constant (and below the detection limit of the RBS setup). Once the Ni supply is exhausted, the NiGe continues to grow by consuming the ϵ-phase and its thickness starts to increase. This same phase competition is possibly happening on the Ge(001) substrate too, but different growth rates for both phases on that substrate orientation might allow the NiGe to grow thicker on Ge(001) while pure Ni is still present (thus, above the RBS detection limit). These different growth rates might result from the different orientation of both phases on either Ge(001) or Ge(111), which

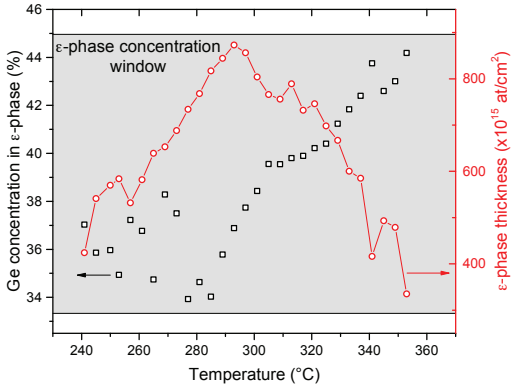

Figure 10. Evolution of the Ge concentration within the ϵ-phase as a function of temperature as fitted from the RBS data. The thickness of the ϵ-phase is overlaid on the right y-axis. The grey area depicts the allowed concentration range for the ϵ-phase according to the Ni-Ge binary phase diagram [20]

results in different interface energies and different diffusion coefficients for Ni in both phases on Ge(001) vs. Ge(111).

Lastly, the large temperature interval for ϵ-phase growth and the high relative thickness that is reached by this phase on the Ge(111) substrate allows us to look at the variation of the Ni:Ge ratio in this phase as a function of the annealing temperature. This is plotted in Figure 10 for the temperature window between 240 and 360 °C, i.e. centered around the temperature where the pure Ni layer is completely consumed (around 290 °C). In this figure, the variation in Ge concentration in the ϵ-phase is overlaid with its corresponding thickness (right y-axis, expressed in at/cm^2). These data suggest that the Ge concentration is somewhere between 34-38% during the growth, which is around the concentration at the lowest temperatures where the ϵ-phase can exist according to the bulk Ni-Ge phase diagram [20]. This was confirmed in an additional *ex situ* RBS measurement with a higher resolution performed on an as-deposited sample, where it was observed that the Ge concentration in the initial intermixed Ni-Ge layer is around 37% (data not shown). Once the maximum thickness is reached, the Ge concentration steadily rises as the ϵ-phase is consumed by the growth of NiGe. This change in Ge concentration of the ϵ-phase during its consumption by the growing NiGe phase explains at least partly the observed change in 2θ angle of the ϵ-phase diffraction peak in the *in situ* XRD measurements once NiGe forms (see Figure 1). Indeed, according to

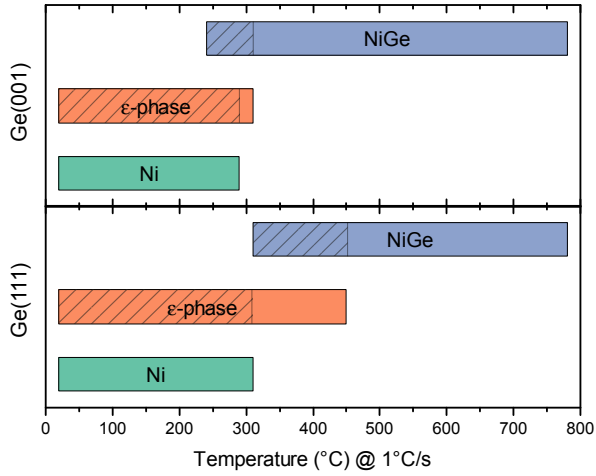

Figure 11. Summary of the phase formation sequence for a 30 nm Ni film deposited on Ge(001) and Ge(111) during a ramp anneal at 1 °C/s. The horizontal bars indicate the temperature ranges over which the different phases are present. The shaded areas represent the temperatures at which the specific phase is growing.

Ellner *et al.* [26], the lattice constants of the ϵ-phase decrease when the Ni:Ge ratio becomes more Ge rich, which translates in a decrease of the $\epsilon(0002)$ and $(10\bar{1}1)$ lattice spacings and thus a shift towards higher 2θ angles for the corresponding diffraction peaks. Besides this effect, also stress and thermal expansion should be taken into account. Hence, a quantitative interpretation of this peak shift was not attempted based on the data collected in this work.

IV-4 Summary & conclusions

We studied the phase formation sequence and texture evolution of nickel germanides forming during a ramp anneal of a thin Ni film on Ge(001) and Ge(111) oriented substrates. The phase formation sequence was determined using *in situ* XRD and *in situ* RBS and is summarized in Figure 11. The temperature windows over which the different phases are present are marked by the horizontal bars. The temperature scale in the figure is based on the 1 °C/s ramp rate used for the *in situ* XRD results. The shaded areas of these bars indicate the temperature ranges over which the specific phase is growing (as deduced from the RBS measurements). It was found that

the general phase sequence on both substrate orientations is as follows:

$$\text{Ni} \rightarrow \epsilon\text{−phase} \rightarrow \text{NiGe}$$

The unambiguous identification of the transient Ni-rich germanide as the hexagonal, metastable ϵ-phase was done using XRD pole figure measurements. On both substrate orientations, the texture of this phase is characterized by two epitaxial components. Furthermore, weak ϵ-phase diffraction features were observed in pole figures collected on as-deposited samples, suggesting that small nuclei of this phase already form within the intermixed Ni-Ge region that forms at the interface during deposition of the Ni film.

In situ RBS was used to study the kinetics during the phase formation sequence. Our results indicate the simultaneous growth of the ϵ-phase and NiGe on a Ge(001) substrate (also observed in previous studies), whereas on Ge(111), simultaneous growth of these phases could not be observed by RBS. However, pole figures collected on a sample quenched at the very onset of NiGe growth do reveal the simultaneous presence of very thin layers of Ni and NiGe, suggesting that the growing NiGe is consumed by the ϵ-phase as long as pure Ni is present.

Finally, the results obtained in this work indicate that the incorrect identification of the transient phase on single crystal Ge substrates from past studies can be attributed to the limited information that is gained from the standard $\theta/2\theta$ geometry used for *in situ* XRD measurements in case of textured phases, because only planes (almost) parallel to the substrate holder are measured. Hence, texture measurements combined with compositional depth profiles (providing stoichiometry information) can provide valuable added insight when studying phase formation on single crystal substrates.

IV-5 Supporting Information

In this section, the supplemental figures S1-S4 are provided that are referred to in the paper.

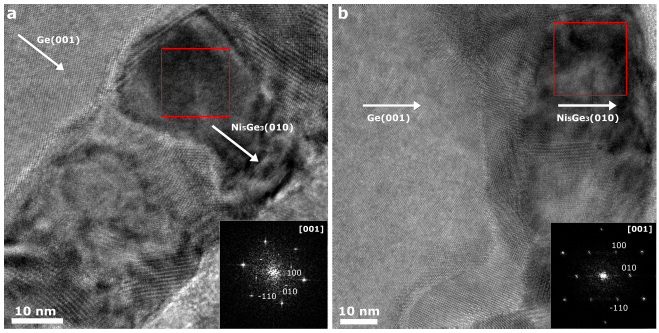

Figure S1. High-resolution TEM images of samples on Ge(001) quenched at 240°C (a) and 280°C (b). In both images, an ϵ-phase grain is indicated by the red square and the corresponding diffractogram is shown in the inset. For the quench at 280°C (b), a separate NiGe layer is visible between the ϵ-phase and the substrate.

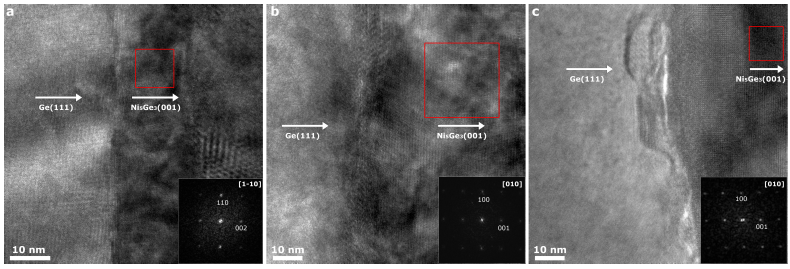

Figure S2. High resolution TEM images of samples on Ge(111) quenched at 260°C (a), 330°C (b) and 345°C (c). In all images, an ϵ-phase grain is indicated by the red square and the corresponding diffractogram is shown in the inset. For the quenches at 330°C and 345°C, a NiGe layer is visible between the ϵ-phase and the substrate.

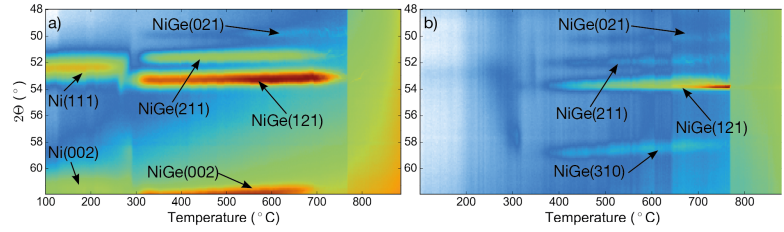

Figure S3. In situ XRD spectra recorded during annealing of a 30nm Ni film at 1°C/s on Ge(001) (a) and Ge(111) (b) for a 2 window containing the Ni(111) and Ni(002) peaks.

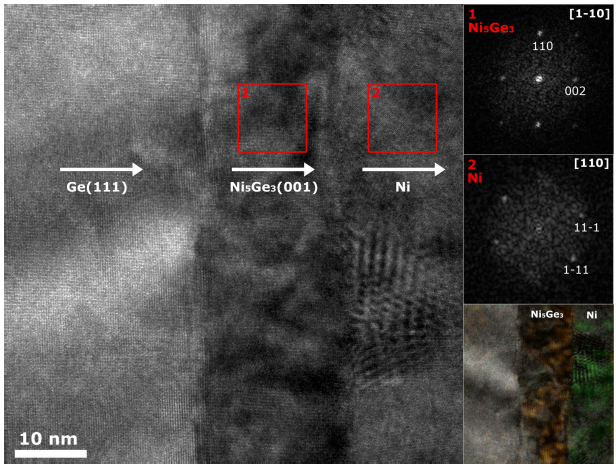

Figure S4. High-resolution TEM image of a sample on Ge(111) quenched at 260°C. The ϵ-phase layer is visible in contact with the substrate (evidenced by the diffractogram labeled '1'). The flat interface between the ϵ-phase and the substrate is clearly visible. The remaining Ni layer is still present above (evidenced by the diffractogram labeled '2'). The EDX map in the lower right corner shows the presence of both layers.

References

[1] Goley, P. & Hudait, M. Germanium Based Field-Effect Transistors: Challenges and Opportunities. *Materials 2014, Vol. 7, Pages 2301-2339* **7**, 2301–2339 (2014).

[2] Kamata, Y. High-k/Ge MOSFETs for future nanoelectronics. *Materials Today* **11**, 30–38 (2008).

[3] Brunco, D. P. *et al.* Germanium MOSFET Devices: Advances in Materials Understanding, Process Development, and Electrical Performance. *J Electrochem Soc* **155**, H552 (2008).

[4] Pillarisetty, R. Academic and industry research progress in germanium nanodevices. *Nature* **479**, 324–328 (2011).

[5] Xie, Q. *et al.* Germanium surface passivation and atomic layer deposition of high-k dielectrics—a tutorial review on Ge-based MOS capacitors. *Semicond Sci Tech* **27**, 074012 (2012).

[6] Gaudet, S., Detavernier, C., Kellock, A. J., Desjardins, P. & Lavoie, C. Thin film reaction of transition metals with germanium. *J Vac Sci Technol A* **24**, 474 (2006).

[7] Patterson, J. K. *et al.* Kinetics of Ni/a-Ge bilayer reactions. *Thin Solid Films* **253**, 456–461 (1994).

[8] Nemouchi, F. *et al.* Simultaneous growth of Ni[sub 5]Ge[sub 3] and NiGe by reaction of Ni film with Ge. *Appl Phys Lett* **89**, 131920 (2006).

[9] Nemouchi, F. *et al.* A comparative study of nickel silicides and nickel germanides: Phase formation and kinetics. *Microelectron Eng* **83**, 2101–2106 (2006).

[10] Gaudet, S., Detavernier, C., Lavoie, C. & Desjardins, P. Reaction of thin Ni films with Ge: Phase formation and texture. *J Appl Phys* **100**, 034306 (2006).

[11] Hsieh, Y. F., Marshall, E. D. & Lau, S. S. Partial Epitaxial Growth of Ni_2Ge and NiGe on Ge(111). *Thin Solid Films* **162**, 287–294 (1988).

[12] Jin, L. J. *et al.* The interfacial reaction of Ni with (111)Ge, (100)Si0.75Ge0.25 and (100)Si at 400°C. *Thin Solid Films* **462-463**, 151–155 (2004).

[13] Geenen, F. *et al.* Formation and texture of palladium germanides studied by in situ X-ray diffraction and pole figure measurements. *Thin Solid Films* **551**, 86–91 (2014).

[14] Geenen, F. *et al.* On the formation and structural properties of hexagonal rare earth (Y, Gd, Dy, Er and Yb) disilicide thin films. *J Alloys Compd* **611**, 149–156 (2014).

[15] De Keyser, K., Van Meirhaeghe, R. L., Detavernier, C., Jordan-Sweet, J. & Lavoie, C. Texture of Cobalt Germanides on Ge(100) and Ge(111) and Its Influence on the Formation Temperature. *J Electrochem Soc* **157**, H395–H404 (2010).

[16] Demeulemeester, J. *et al.* Pt redistribution during Ni(Pt) silicide formation. *Appl Phys Lett* **93**, 261912 (2008).

[17] Demeulemeester, J. *et al.* On the growth kinetics of Ni(Pt) silicide thin films. *J Appl Phys* **113**, 163504 (2013).

[18] Schrauwen, A. *et al.* On the nucleation of PdSi and NiSi2 during the ternary Ni(Pd)/Si(100) reaction. *J Appl Phys* **114**, 063518 (2013).

[19] De Schutter, B. *et al.* Phase formation in intermixed Ni–Ge thin films: Influence of Ge content and low-temperature nucleation of hexagonal nickel germanides. *Microelectron Eng* **120**, 168–173 (2014).

[20] Nash, A. & Nash, P. The Ge-Ni (Germanium-Nickel) system. *Bulletin of Alloy Phase Diagrams* **8**, 255–264 (1987).

[21] Larsson, A.-K. & Withers, R. An electron diffraction study of modulated Ni1+xGe B8 type phases. *J Alloys Compd* **264**, 125–132 (1998).

[22] De Keyser, K. *et al.* Epitaxial Formation of a Metastable Hexagonal Nickel–Silicide. *Electrochem Solid St* **11**, H266 (2008).

[23] Van Bockstael, C., Detavernier, C., Van Meirhaeghe, R. L., Jordan-Sweet, J. & Lavoie, C. In situ study of the formation of silicide phases in amorphous Ni-Si mixed layers. *J Appl Phys* **106**, – (2009).

[24] Gaudet, S., Coia, C., Desjardins, P. & Lavoie, C. Metastable phase formation during the reaction of Ni films with Si(001): The role of texture inheritance. *J Appl Phys* **107**, 093515 (2010).

[25] Gaudet, S., Desjardins, P. & Lavoie, C. The thermally-induced reaction of thin Ni films with Si: Effect of the substrate orientation. *J Appl Phys* **110**, 113524 (2011).

[26] Ellner, M., Gödecke, T. & Schubert, K. Zur struktur der mischung Nickel-Germanium. *Journal of the Less Common Metals* **24**, 23–40 (1971).

[27] Detavernier, C. *et al.* An off-normal fibre-like texture in thin films on single-crystal substrates. *Nature* **426**, 641–645 (2003).

[28] d'Heurle, F. M. Nucleation of a New Phase from the Interaction of Two Adjacent Phases. *Journal of Materials Research* 100 (1987).

[29] d'Heurle, F. M. & Gas, P. Kinetics of formation of silicides: A review. *Journal of Materials Research* **1**, 205–221 (1986).

[30] Tung, R. T., Poate, J. M., Bean, J. C., Gibson, J. M. & Jacobson, D. C. Epitaxial silicides. *Thin Solid Films* **93**, 77–90 (1982).

[31] De Keyser, K. *Texture of thin silicide and germanide films*. Ph.D. thesis, Ghent University (2011).

[32] Chen, L. J. Solid state amorphization in metal/Si systems. *Mat Sci Eng R* **29**, 115–152 (2000).

[33] Demeulemeester, J. *et al.* The influence of Pt redistribution on $Ni_{1-x}Pt_xSi$ growth properties. *J Appl Phys* **108**, 043505 (2010).

[34] Demeulemeester, J. *et al.* Artificial neural networks for instantaneous analysis of real-time Rutherford backscattering spectra. *Nucl Instrum Methods Phys Res B* **268**, 1676–1681 (2010).

[35] Barradas, N. P., Jeynes, C. & Webb, R. P. Simulated annealing analysis of Rutherford backscattering data. *Appl Phys Lett* **71**, 291–293 (1997).

3.3 Interface visualization of ϵ-phase texture

During the analysis of the texture measurements on the ϵ-phase discussed in paper IV, the interface visualization technique introduced in chapter 2 was extensively used to identify and analyze the observed texture components. However, as the article on interface visualization (paper II) was not yet accepted at the time that paper IV was written and submitted, MIP plots for the orientations discussed in that paper could not be included. Therefore, this section will show how this interface visualization technique was used in practice and how it helped to understand the details of the ϵ-phase texture components.

Typically, pole figure analysis in our research group is performed using an in-house developed software package called *GUSTAV*. As described in the PhD dissertation by Koen De Keyser [1], this program allows to analyze collections of pole figures either obtained using a point detector or extracted from a set of pole figures collected using a linear detector. The different texture components can then be identified by interactively specifying the location of visible poles in different pole figures and allowing the software to search for epitaxial or axiotaxial orientations that can explain the specified poles. For each possible component, GUSTAV is able to overlay a simulation of expected diffraction features (points for epitaxy, arcs for axiotaxy) on the pole figures. By visually comparing these simulations with the underlying experimental pole figures, one can determine which of the orientations are likely present in the film.

Once a set of texture components is obtained that accurately describes the observed diffraction features in the pole figures, a deeper analysis of the orientations can be performed using the interface visualization technique described in chapter 2. This allows to answer questions such as which low-index planes of substrate and film are parallel, matched or aligned (see chapter 2 for a definition of these concepts)? Which film plane is parallel to the interface? Is an epitaxial component axiotaxy or double-axiotaxy related (aligned or double-aligned)? During the course of this PhD, two ways have been developed in order to generate and analyse these interface visualization plots. First, a python package was developed that generates MIP (map of interfacial periodicity, see chapter 2) plots in a publication-friendly way. Second, the source code of GUSTAV was updated and extended to include the capability to interactively generate and analyze such visualizations. Both options will be briefly discussed in the remainder of this section using the A_{111} epitaxial component of the ϵ-phase on Ge(111)

as a working example.

3.3.1 Python: generating MIP plots

As a means to construct publication friendly MIP plots, a dedicated python package called *ccncryst* was developed during the course of this PhD. In essence, it provides a similar functionality to GUSTAV, but without the user interaction that the GUSTAV user interface provides. As such, the package also allows to simulate diffraction features and generate publication-friendly pole figure overlays for epitaxial or axiotaxial texture components. Below, a typical workflow for the generation of an MIP for the A_{111} epitaxial orientation is discussed.

The package is imported in a python session or script as follows:

```
import ccncryst as cc
import logging
rootLogger = logging.getLogger()
rootLogger.setLevel(logging.INFO)
```

In this way, the functions provided by the ccncryst package can be accessed by using the *cc* prefix. By creating a logger object and setting the log level to *INFO* in an interactive python session, valuable information is printed by the package when different functions are executed.

First, the substrate and film material must be created, either by specifying the crystallographic properties (spacegroup, lattice constants) explicitly or by reading them from a *.cif* (*crystallographic information file*, `http://www.iucr.org/resources/cif`) or *.cry* (file format used by GUSTAV and the *hkl* EBSD software package) file. In addition, the orientation of the unit cell of the material with respect to the laboratory frame must be provided. To this end, constants are provided for the orientations that are typically used in pole figure measurements. For the A_{111} orientation, a (111) oriented Ge substrate and an ϵ-phase film must be defined:

```
Ge = cc.Material('Ge', 'Fd-3m',
    a=5.623, b=5.623, c=5.623,
    alpha=90*cc.degree, beta=90*cc.degree,
    gamma=90*cc.degree,
    reference_orientation=cc.ORI_SUBS_111)
e_phase = cc.Material.load_from_cry('e_phase.cif',
    reference_orientation=cc.ORI_FILM)
```

The previous code block creates two materials and stores them in the variable *Ge* and *e_phase*. Next, epitaxial components can be generated by specifying the substrate and film material and by providing two constraints for the orientation of the film material:

```
components = cc.Epitaxy.generate_epitaxy_components(
    e_phase, Ge,
    '(001)//(111)', '(2-10)//(01-1)',
    substrate_symmetry=False
)
A_111 = components[0] # First array element
```

Alternatively, the orientational constraints can be provided by specifying the (χ, ϕ) angles for the film pole, e.g. *'(2-10) at (90, 150)'* for the second constraint in this case. The *substrate_symmetry* argument determines whether symmetrically equivalent substrate planes are taken into account. If one or multiple epitaxial components are found that comply to the given constraints, they are returned in an array. In the present case, an array with a single component, i.e. the A_{111} component, is returned.

Finally, the MIP plot can be generated by constructing an *IntefaceVisualiser* object with the component under investigation as an argument. One can then determine which sets of planes from film and substrate must be included in the plot (by specifying the maximum absolute value that h, k and l may acquire) and plot both the MIP and the overlap MIP:

```
A_111_MIP = cc.InterfaceVisualiser(A_111)
A_111_MIP.add_planes_for_substrate(max_indices=4)
A_111_MIP.add_planes_for_film(max_indices=4)

# Plot the standard MIP
A_111_MIP.show()

# Plot the overlap MIP
A_111_MIP.plot_matching_planes(delta_dp_max_perc=1.0,
    delta_chi=1*cc.degree,
    delta_phi=1*cc.degree)
```

As can be seen from the code block above, the limits for matching and aligned planes discussed in paper II can be changed through the arguments provided when plotting the overlap MIP (the defaults are $\Delta d_{p,\max} = 1.0\%$, $\Delta\chi_{\max} = 1^\circ$ and $\Delta\phi_{\max} = 1^\circ$). The resulting MIP and overlap MIP are displayed in Figure 3.5. Furthermore, the python package allows to export the

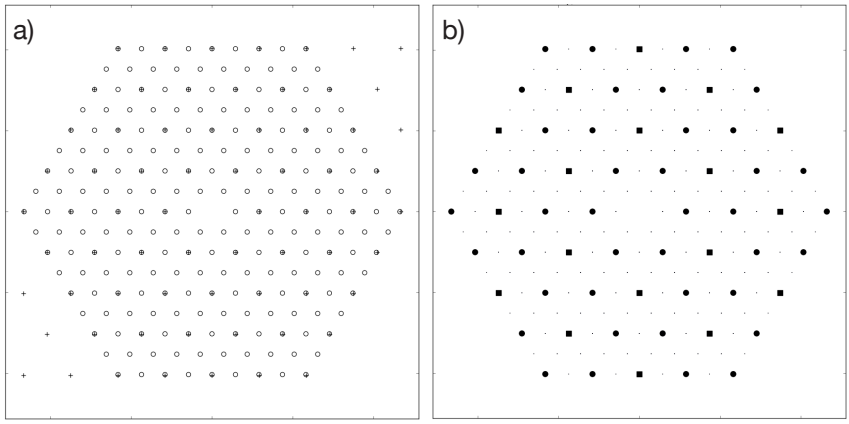

Figure 3.5. a) MIP for the ϵ-phase A_{111} epitaxial orientation discussed in paper IV and b) overlap MIP for the same orientation.

$(1/d_p, \phi)$ coordinates of the film and substrate planes and of the (perfectly) aligned and matched plane pairs to a text file that can then be imported into a different plotting program like OriginPro to create publication-ready figures.

From these figures, it is already clear that the A_{111} orientation shows plane alignment in multiple directions, allowing us to classify the component as a *double-aligned* epitaxy. Hence, the excellent match at the interface for the A_{111} orientation between the atoms in the $\epsilon(0001)$ and $Ge(111)$ planes (see paper IV) also amounts to plane alignment across the interface for different sets of lattice planes (as was discussed for the $\epsilon(2\bar{1}\bar{1}0)$ and $Ge(02\bar{2})$ planes in paper IV). According to the discussion of chapter 2, this *double-aligned* nature provides an explanation for the stability of the A_{111} component and thus for the large temperature window over which the ϵ-phase is observed.

However, to answer such questions as 'Which planes are (perfectly) aligned?' or 'At what angle do the aligned planes intersect the interface?', one needs to know which substrate and/or film planes are represented by which spots on the (overlap) MIP. Here, the interactivity of GUSTAV comes into play.

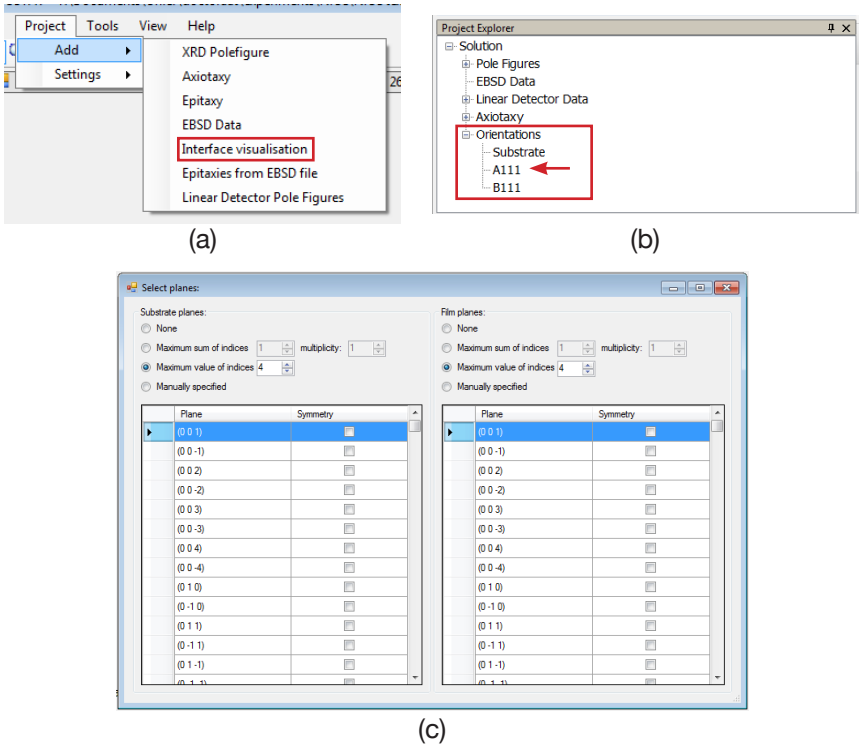

Figure 3.6. (a) Location of the menu command to add an interface visualization to the project. (b) GUSTAV project explorer. Double-clicking an orientation in this list activates it and immediately generates its MIP plot. (c)

3.3.2 GUSTAV: interactive MIP analysis

The main functionalities of the in-house developed GUSTAV software have been briefly discussed in the opening paragraph of this section and in the PhD thesis by Koen De Keyser [1]. Here, we will use the example of the A_{111} orientation to demonstrate the interface visualization capability of GUSTAV, which has been updated and extended during the course of this PhD.

When working on a project in GUSTAV, one can add an interface visualization through the menu command *'Project > Add > Interface Visualization'* (see Figure 3.6a), which will create an empty interface visualization plot within GUSTAV. Before the patterns can be generated, the epitaxial orientation being investigated must be activated by double-clicking it in the

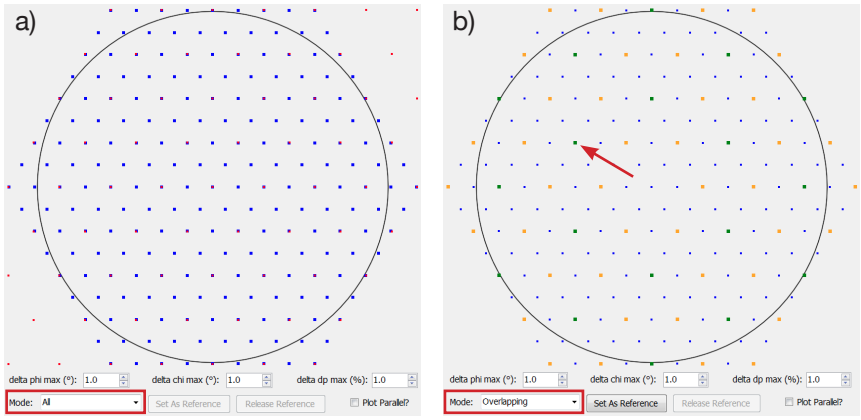

Figure 3.7. GUSTAV generated MIP (a) and overlap MIP (b). On the MIP, substrate planes are depicted with blue squares and film planes with red squares. On the overlap MIP, blue squares represent the reference grid of substrate planes, green squares represent perfectly aligned planes, yellow squares represent aligned planes and black squares depict matched planes.

project explorer (see Figure 3.6b). One can specify the collection of planes to show in the visualization by right clicking on the plot area and selecting *'Edit planes'*, which will bring up the window shown in Figure 3.6c. Here, one can choose for both the film and the substrate to either generate a list of planes based on a maximum value for the sum $|h| + |k| + |l|$ or on a maximum value for each of the individual indices or to specify a limited list of planes manually.

Once a set of planes is defined, the MIP can be generated by right clicking on the plot area and choosing *'Visualisation mode > Phi vs. 1/d'*. The MIP for the A_{111} orientation generated by GUSTAV is displayed in Figure 3.7a. Here, the substrate planes are depicted with blue squares and the film planes with red squares. One can switch to the overlap MIP by changing the *mode* to *'Overlapping'* (see Figure 3.7b). In that case, perfectly aligned planes are depicted in green, aligned planes in yellow and matched planes in black.

The biggest added value for the interface visualization capability of GUSTAV is the interactivity. By clicking on a point within a MIP or overlap MIP, an information window is shown containing the χ, ϕ, d and d_p values of all planes from film and substrate that have (d_p, ϕ) coordinates that coincide with the clicked location. Furthermore, a summary is shown

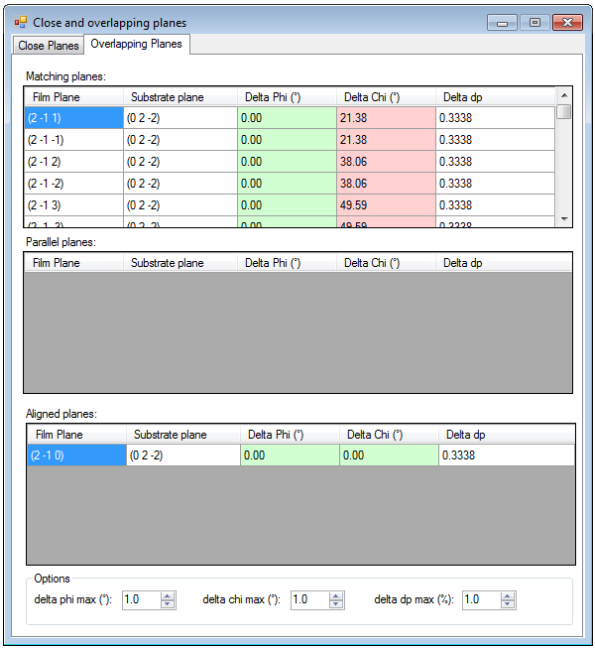

Figure 3.8. Screenshot of the summary dialog that shows when a point on the (overlap) MIP in GUSTAV is clicked. The summary shows matched, parallel and aligned planes. perfect alignment in χ or ϕ is indicated by a green cell. A red cell indicates a nonzero $\Delta\chi$ or $\Delta\phi$ value.

of matched, parallel and aligned planes from film and substrate for the active epitaxial component. For example, Figure 3.8 shows a screenshot of this summary for the A_{111} component when clicked on the green point (for 'aligned planes') indicated by the arrow in Figure 3.7b. In this case, the green point at that position results from the alignment across the interface of the $\epsilon(2\bar{1}\bar{1}0)$ and $Ge(02\bar{2})$ planes, which was discussed in detail in paper IV. Furthermore, GUSTAV displays the difference in χ, ϕ and projected d-spacing between the two planes. By changing the values at the bottom of the dialog, the allowed mismatches in χ, ϕ and d_p that are used as boundary conditions to define plane matching and alignment can be altered. More general information like the d-spacing of the planes and the angle at which they intersect the interface plane can be found under the *'Close Planes'* tab. The combination of all this geometric information that is readily available for every point in the (overlap) MIP allows a systematic analysis of the geometry of different epitaxial components in a straightforward way.

3.3.3 Conclusion

In this section, a practical overview was given on how the technique of interface visualization developed in chapter 2 was and can be used to investigate observed epitaxial texture components. During the course of this PhD, two main efforts were made to render this technique more practical. First, a python package was developed that allows plotting of publication-ready (overlap) MIP plots and second, the existing GUSTAV software package was extended with interactive MIP analysis capabilities. Hopefully, the combination of these complementary software packages will support the use of the interface visualization technique in future research and publications on texture in thin silicide or germanide films.

References

[1] De Keyser, K. *Texture of thin silicide and germanide films*. Ph.D. thesis, Ghent University (2011).

4

Conclusions and Suggestions for Future Work

4.1 Summary and Conclusions

Thin films of silicides and germanides are an important part of modern semiconductor devices, as they are actively used as contacting materials for individual MOSFETs -the basic building blocks of any digital microelectronics circuit- in CMOS technology. In this thesis, we focussed on the texture of these films. This concept of texture describes the orientation of the different grains in a polycrystalline thin film with respect to the single crystal Si or Ge substrate. More specifically, we investigated how this texture influences certain properties of the resulting film and how a better understanding of the silicide/germanide formation reaction can be achieved by studying the texture evolution during this reaction. Experimentally, the work presented in this thesis focussed on the solid-phase reaction between a thin Ni film and a single crystal Ge substrate, which ultimately results in the formation of NiGe, the top candidate for contacting future Ge-rich MOSFET devices. Below, the conclusions of the different chapters are briefly summarized.

The first chapter reviewed literature that has been published on the

topic of texture in thin film silicide or germanide materials since the second half of the previous century. Different measurement techniques that have been and are still being used to study texture over the years were discussed, with a focus on the technique of high-resolution, synchrotron based X-ray pole figure measurements. This technique was pioneered at IBM in the early 2000s and enabled detailed investigations of the multitude of texture components that are typically found in polycrystalline silicide/germanide films. These investigations revealed a significant influence of the texture on different thin film properties such as phase stability, morphological stability and electrical properties. Furthermore, different studies have pointed out that texture measurements are often crucial to unambiguously identify the correct phase formation sequence during silicide/germanide formation, as highly textured phases are easily overlooked. This latter phenomenon also proved important during the investigation of the solid-phase reaction in the Ni-Ge system discussed in chapter 3. In the last part of the first chapter, studies were discussed that investigated how texture is influenced by different factors such as substrate doping and alloying of the initial metal film with ternary elements. Such knowledge could eventually enable texture engineering as a means to tune the properties of the silicide/germanide films.

When analyzing thin film texture, it is often difficult to get a thorough understanding of how the match between the film and the substrate is achieved at the interface. In the past, people tried to visualize the crystal structure of film and substrate near the interface through atomistic ball-and-stick models, which led to cluttered and complex visualizations that were not able to visualize shared periodicity between film and substrate over distances greater then a few lattice constants. In chapter two, we introduced the MIP (map of interfacial periodicity) which visualizes lattice planes of film and substrate that match at the interface, leading to shared periodicity within the interface plane. As such, the quality of an epitaxial texture component can be evaluated by the amount of matching plane families in different directions and the nature of the match (plane alignment *across* the interface vs. plane matching at the interface). It was discussed in detail that plane alignment is the only way to form a periodic interface structure whose periodicity is preserved irrespective of interfacial curvature. As such, epitaxial orientations that are caused by plane alignment in one (called *aligned* or *axiotaxy related* epitaxies) or two (called *double-aligned* or *double axiotaxy related* epitaxies) directions are often observed to be very stable, as the low energy interface can be preserved even for the some-

times rough interfaces that form during a silicide or germanide forming solid-phase reaction.

Experimentally, this thesis focussed on the solid-phase reaction between thin Ni films and a single crystal Ge substrate. This reaction results in the formation of NiGe, a top candidate contacting material for Ge-rich MOSFET devices. As past experience with the widely adopted NiSi contacting material has shown, a thorough understanding of the basic formation reaction of the thin film material is of utmost importance to be able to adapt the material to the stringent requirements for the contacting material in the small dimensions of modern MOSFET devices. The experimental results obtained in this context were discussed in chapter 4 through two papers.

First, the reaction between thin Ni films that are premixed during deposition with a variable amount of Ge (between 0 and 50 %) and either an inert SiO_2 or a single crystal Ge(001) substrate was studied. Studying such a ratio-controlled system can provide valuable insights on the formation of the first-forming phase, as has been demonstrated in the past for solid-phase reactions in the Ni/Si system. The depositions in this study were performed using a newly developed combinatorial sputter deposition technique, which allows to deposit thickness gradients of a certain element, in this case Ge. Co-depositing such a Ge thickness gradient with a Ni film of uniform thickness results in a thin Ni film with a Ge concentration gradient varying from 0 to 50 %. The main conclusions of this study are listed below:

- For almost the complete composition range under investigation, crystalline phases were found to nucleate during co-deposition of the films at room temperature.
- Below 36 %Ge, the nucleating germanides correspond to those that can be expected from the Ni-Ge binary phase diagram for an equilibrium mixture of Ni and Ge with a similar Ge concentration.
- Between 36 and 48 %Ge, a metastable hexagonal germanide (called the ϵ-phase) was found to form at temperatures lower than the minimum stability temperature (300 °C) of this phase in an equilibrium Ni-Ge mixture with similar composition.
- Between 36 and 42 %Ge, this ϵ-phase was observed to have nucleated during deposition of the mixed Ni-Ge film.

The second study in this chapter focussed on the solid-phase reaction between a pure Ni film and a Ge(001) or Ge(111) substrate. In particular, the experiments aimed to identify the intermediate Ni-rich germanide that forms from the pure Ni, prior to NiGe, as the nature of this phase was debated in previous studies. To this end, the texture of this phase was investigated in detail to aid in the identification. Experimentally, *in situ* XRD and RBS were used to follow the phase sequence during the reaction and high-resolution synchrotron-based pole figure measurements allowed to study the texture of the different phases in detail. Below, the main conclusions of these experiments are listed:

- The Ni-rich phase was identified to be the same, metastable ϵ-phase that was observed in the previous study on intermixed Ni(Ge) films. As such, the general phase sequence for a 30 nm Ni film on Ge(001) or Ge(111) is:
$$\text{Ni} \rightarrow \epsilon\text{-phase} \rightarrow \text{NiGe}$$
- On both substrate orientations, the ϵ-phase is highly epitaxial (two epitaxial components were observed on both substrate types), which is why this phase was wrongly identified in previous studies.
- On both substrate orientations, weak ϵ-phase diffraction features were observed in pole figures collected on as-deposited samples, suggesting that small nuclei of this phase already form during deposition of the Ni film.
- *In situ* RBS clearly revealed simultaneous growth of the ϵ-phase and NiGe on a Ge(001) substrate. On Ge(111), *in situ* RBS was not able to reveal this simultaneous growth. However, texture measurements did reveal the presence of both pure Ni and the ϵ-phase at the onset of NiGe formation, suggesting that simultaneous growth of the ϵ-phase and NiGe also occurs on this substrate orientation.

4.2 Suggestions for Future Work

In the second chapter, a visualization method was introduced to evaluate epitaxial texture components in thin silicide/germanide film systems. However, the texture prediction capabilities of this method are very limited. Ideally, one would like to calculate, using first-principles methods like *density functional theory*, the texture components that will form during

a solid-phase reaction. However, as is clear from the experimental results on texture in thin silicide or germanide films, a huge number of grains will have to be incorporated in the calculation to gather enough statistics to make a quantitative prediction on the resulting texture. At this moment, the computational power for such huge calculations is far from sufficient. However, one can only guess what the future will bring. Alternatively, one can try to predict texture using a more qualitative geometric approach, in which possible matching between planes or lattice volumes between adjacent phases are taken into account. In this context, the *coincidence site lattice* and *O-lattice* theories have been successful in homogeneous bulk systems, but they fail at predicting texture for the heterogeneous thin films/substrate systems discussed here[1]. More recently, the *edge-to-edge* matching theory has had moderate success in predicting the texture of $TiSi_2$ on Si[2]. Perhaps, the concepts of plane alignment vs. plane matching that were used in chapter 2 can help to improve these models.

In chapter three, a peak shift was observed for the diffraction peaks of the ϵ-phase, both for the mixed layers on Ge(001) as for the pure Ni layers on Ge(001) and Ge(111). This peak shift seemed to kick in at the moment when the pure Ni is completely consumed. However, as the shift could not be explained solely by compositional changes in the ϵ-phase, a detailed investigation of this shift was beyond the scope of this thesis. Therefore, future work could be aimed towards explaining this shift by taking into account stress and thermal expansion. Perhaps, the presence of only a single intermediate, Ni-rich phase could make this Ni-Ge system an ideal model system for the development of a stress evolution model for thin film silicidation/germanidation reactions, a topic that has received quite some debate in past literature.

Without doubt, NiSi has been the most important contacting material over the past decade, as it allowed the development of sub 65 nm technology nodes. As a result, a huge amount of literature is available on this material. In particular, a lot of effort has been devoted to studying the influence of introducing ternary elements into the initial Ni film (either through alloying or through the introduction of inter- or capping layers) and of the NiSi thickness (in particular ultra-thin thicknesses) on the thermal and morphological stability and the texture of the NiSi contacts (see

[1] De Keyser, K. Texture of thin silicide and germanide films. PhD thesis, Ghent University (2011)

[2] Zhang, M.-X., Kelly, P. M. Application of edge-to-edge matching model to understand the in-plane texture of TiSi2 (C49) thin films on (001)Si surface. Scripta Materialia 55, 613–616 (2006)

e.g. part of the discussion in chapter 2). For future technology nodes, NiGe is considered as an important contact candidate. However, literature reports on such topics as NiGe alloying and ultra-thin NiGe contacts are very limited compared to the vast amount of literature available for NiSi. Therefore, future investigations of this material should definitely address these topics.

Finally, next to NiGe, the 2006 overview study by Gaudet *et al.* identified a couple of other potentially interesting germanide materials like $CoGe_2$ or Co_5Ge_7, PdGe and some of the Pt-germanides. Detailed investigations of the texture of the Co and Pd germanide materials have been performed recently by De Keyser *et al.*[3] and Geenen *et al.*[4] respectively. However, a detailed investigation of the phase formation sequence and the texture evolution during a solid-phase reaction between a thin Pt film and Ge(001) and Ge(111) substrates is still lacking. During the course of this PhD, a comprehensive set of texture measurements have been performed on this material system, however a detailed analysis of this data could not be completed within the timeframe of this work. Hence, this dataset should definitely be picked up and analyzed in a future PhD thesis.

[3] De Keyser, K. et al, Texture of Cobalt Germanides on Ge(100) and Ge(111) and Its Influence on the Formation Temperature. J Electrochem Soc 157, H395–H404 (2010)

[4] Geenen, F. et al. Formation and texture of palladium germanides studied by in situ X-ray diffraction and pole figure measurements. Thin Solid Films 551, 86–91 (2014)

List of Publications

A1 papers (first author)

- **Texture in thin film silicides and germanides: a review**
  B. De Schutter, K. De Keyser, C. Lavoie and C. Detavernier
  Submitted to *Applied Physics Reviews*, November 2015

- **Visualization and classification of epitaxial alignment at hetero-phase boundaries**
  B. De Schutter, K. De Keyser and C. Detavernier
  Thin Solid Films, vol. 599, pp. 104-112, January 2016

- **Phase Formation in intermixed Ni-Ge thin films: influence of Ge content and low- temperature nucleation of hexagonal nickel germanides**
  B. De Schutter, W. Devulder, A. Schrauwen, K. Van Stiphout, T. Perkisas, S. Bals, A. Vantomme and C. Detavernier
  Microelectronic Engineering, vol. 120, pp. 168-173, May 2014

- **Phase formation and texture of thin Ni films on Ge: Formation of a transient hexagonal germanide and influence of substrate orientation**
  B. De Schutter, K. Van Stiphout, N. M. Santos, E. Bladt, J. Jordan-Sweet, S. Bals, C. Lavoie, A. Vantomme and C. Detavernier
  Submitted to *Journal of Applied Physics*, January 2015

A1 papers (contributing author)

- **Phase formation and texture of nickel silicides on $Si_{1-x}C_x$ epilayers**
  K. De Keyser, B. De Schutter, C. Detavernier, V. Machkaoutsan, M. Bauer, S. G. Thomas, J. Jordan-Sweet and C. Lavoie
  Microelectronic Engineering, vol. 88, no. 5, pp. 536–540, 2011

- **The role of composition and microstructure in Ni-W silicide formation and low temperature epitaxial $NiSi_2$ growth by premixing Si**
  A. Schrauwen, K. Van Stiphout, J. Demeulemeester, B. De Schutter, W. Devulder, C. M. Comrie, C. Detavernier, K. Temst and A. Vantomme
  submitted to *Journal of Applied Physics*

- **Ternary silicide formation from Ni-Pt, Ni-Pd and Pt-Pd alloys on Si(100): nucleation and solid solubility of the monosilicides**
  A. Schrauwen, J. Demeulemeester, B. De Schutter, W. Devulder, C. M. Comrie, C. Detavernier, K. Temst and A. Vantomme
  submitted to *Acta Materialia*

- **Semiconductor-metal transition in thin VO_2 films grown by ozone based atomic layer deposition**
  G. Rampelberg, M. Schaekers, K. Martens, Q. Xie, D. Deduytsche, B. De Schutter, N. Blasco, J. Kittl, and C. Detavernier
  Applied Physics Letters, vol. 98, no. 16, 2011

- **Crystallization and semiconductor-metal switching behavior of thin VO_2 layers grown by atomic layer deposition**
  G. Rampelberg, D. Deduytsche, B. De Schutter, P.A. Premkumar, T. Michael, M. Schaekers, K. Martens, I. Radu and C. Detavernier
  Thin Solid Films, vol. 550, pp. 59-64, Jan. 2014

- **In situ X-ray diffraction study of the controlled oxidation and reduction in the V–O system for the synthesis of VO_2 and V_2O_3 thin films**
  G. Rampelberg, B. De Schutter, W. Devulder, K. Martens, I. Radu and C. Detavernier
  Journal of Materials Chemistry C, vol. 3, pp. 11357-11365, 2015

- **VO_2 thin films and nanoparticles prepared by atomic layer deposition and controlled post-deposition annealing**
  G. Rampelberg, B. De Schutter, W. Devulder, M. Schaeckers, K. Martens, C. Dussarrat and C. Detavernier
  submitted to *Journal of Materials Chemistry C*

- **Influence of Carbon Alloying on the Thermal Stability and Resistive Switching Behavior of Copper-Telluride Based CBRAM Cells**
  W. Devulder, K. Opsomer, F. Seidel, A. Belmonte, R. Muller, B. De Schutter, H. Bender, W. Vandervorst, S. Van Elshocht, M. Jurczak, L. Goux, and C. Detavernier
  ACS Applied Materials & Interfaces, vol. 5, no. 15, pp. 6984–6989, Aug. 2013

- **Influence of carbon content on the copper-telluride phase formation and on the resistive switching behavior of carbon alloyed Cu-Te conductive bridge random access memory cells**
  W. Devulder, K. Opsomer, A. Franquet, J. Meersschaut, A. Belmonte, R. Muller, B. De Schutter, S. Van Elshocht, M. Jurczak, L. Goux and C. Detavernier
  Journal of Applied Physics, vol. 115, no. 5, Feb. 2014

- **Improved thermal stability and retention properties of Cu–Te based CBRAM by Ge alloying**
  W. Devulder, K. Opsomer, G. Rampelberg, B. De Schutter, K. Devloo-Casier, M. Jurczak, L. Goux and C. Detavernier
  Journal of Materials Chemistry C, vol. 3, pp. 12469-12476, Nov. 2015

- **Structural and Kinetic Study of the Reduction of CuO-CeO_2/Al_2O_3 by Time-Resolved X-ray Diffraction**
  V. V. Galvita, H. Poelman, G. Rampelberg, B. De Schutter, C. Detavernier, and G. B. Marin
  Catalysis Letters, vol. 142, no. 8, pp. 959–968, Aug. 2012

International Conference Contributions

- **In-situ study of the formation of germanide phases in amorphous Ni-Ge mixed layers**
  B. De Schutter, C. Van Bockstael, K. De Keyser, D. Deduytsche, J.

Jordan- Sweet, C. Lavoie and C. Detavernier
Poster presentation at *the 2012 Metals for Advanced Metallization (MAM) conference*, Grenoble, France, March 11-14, 2012

- **Phase Formation in Intermixed Ni-Ge Thin Films: Influence of Ge Content and Low- Temperature Nucleation of Hexagonal Nickel Germanides**
  B. De Schutter, C. Van Bockstael, W. Devulder, A. Schrauwen, J. Jordan-Sweet, C. Lavoie, A. Vantomme and C. Detavernier
  Oral presentation at *the 2013 Metals for Advanced Metallization (MAM) conference*, Leuven, Belgium, March 10-13, 2013

- **Phase formation and texture of 30nm Ni films on Ge(100): identification of a transient hexagonal germanide**
  B. De Schutter, J. Jordan-Sweet, C. Lavoie and C. Detavernier
  Oral presentation at *the 2014 Metals for Advanced Metallization (MAM) conference*, Chemnitz, Germany, March 2-5, 2014

- **Texture in thin film Germanium-based contacting materials for future microelectronic devices**
  B. De Schutter, K. De Keyser, J. Jordan-Sweet, C. Lavoie and C. Detavernier
  Oral presentation at *the 2014 International Conference On Texture Of Materials (ICOTOM)*, Dresden, Germany, August 24-29, 201

- **Semiconductor-metal transition in thin VO_2 films deposited by ozone based atomic layer deposition**
  G. Rampelberg, M. Schaekers, K. Martens, Q. Xie, D. Deduytsche, B. De Schutter, N. Blasco, J. Kittl, C. Detavernier
  Oral presentation at *the 2012 Metals for Advanced Metallization (MAM) conference*, Grenoble, France, March 11-14, 2012

- **Elemental redistribution of Pt and Pd in nickel silicides: a comparative study**
  A. Schrauwen, J. Demeulemeester, A. Kumar, B. De Schutter, W. Vandervorst, C. Detavernier, C.M. Comrie, K. Temst and A. Vantomme
  Oral presentation at *the 2012 Metals for Advanced Metallization (MAM) conference*, Grenoble, France, March 11-14, 2012

- **Influence of carbon doping on the thermal stability of copper tellurium CBRAM source layers**
  W. Devulder, K. Opsomer, L. Goux, K. Devloo-Casier, B. De Schutter, S. Van Elshocht, M. Jurczak, C. Detavernier
  Oral presentation at *the 2013 Metals for Advanced Metallization (MAM) conference*, Leuven, Belgium, March 10-13, 2013

Acknowledgements

Het is gelukt! Na vijf jaar zijn er de resultaten, de artikels en uiteindelijk ook deze thesis. De voorbije jaren op de vakgroep vastestofwetenschappen (waar ik reeds begon tijdens mijn masterthesis, ondertussen al bijna 7 jaar geleden) zullen mij nog lang bijblijven. Natuurlijk zou het onmogelijk geweest zijn om dit resultaat te bereiken zonder de steun en hulp van verschillende mensen. Vandaar dat ik hier toch even een dankwoord wil richten aan hen.

In de eerste plaats is er natuurlijk mijn promotor Christophe. Als ik zie hoe zijn groep gegroeid is in de kleine 7 jaar dat ik hier heb vertoefd, dan kan ik alleen maar concluderen dat ik geluk heb gehad om bij zo een goede promoter mijn doctoraatsonderzoek te mogen gedaan hebben. Bedankt Christophe, voor de steun die je me steeds ben blijven geven, ook toen na twee jaar bleek dat ons originele onderzoeksonderwerp een onhaalbare kaart bleek en we dan maar overschakelden op silicides en germanides, een onderwerp waarvan je wist dat er op kortere tijd heel wat uit te halen viel. Bedankt ook om me de vrijheid te geven om me buiten het echte onderzoek mijn interesse in programmeren te laten gebruiken en ontwikkelen om zo enkele interessante applicaties voor de groep te maken. Dit komt mij in mijn huidige job heel goed van pas en ik hoop dat jullie er ook nog lang gebruik van kunnen maken.

Dan zijn er natuurlijk de S1 collega's, waarvan ik er toch een groot aantal ondertussen bij mijn vrienden mag rekenen. In het bijzonder wil ik Koen De Keyser bedanken die mij begeleide bij mijn masterthesis en mij daarna introduceerde in de wereld van textuur in dunne films. Dan is er natuurlijk Davy bij wie iedereen altijd terecht kan bij technische defecten aan de (ondertussen talrijke) onderzoeksopstellingen in de labo's. Met Geert had ik een zeer leuke tijd tijdens het bouwen van de gerobotiseerde *in situ* XRD opstelling. Liesje wil ik bedanken voor de goede vriendschap die we ondertussen hebben opgebouwd en de leuke lunches 's middags, dikwijls in het toffe gezelschap van Kilian, Delphine en Jolien. Bedankt Filip

voor het aangename gezelschap op de bureau en de leuke meetcampagnes in Brookhaven. Thomas, Boris, Arne, Jonathan, Bartel, Mathias VH en Mathias M wil ik bedanken voor het aangename gezelschap tijdens de vele middagmalen die ik in die 7 jaar verorberd heb in de cafetaria van het UZ. Felix en Phillipe bedank ik voor de hulp bij het organiseren van de jaarlijkse barbecue (samen met alle andere collega's die een handje hielpen). Karl, Wouter, Kevin, Jan, Ranjith, Jacob, Shaoren en alle andere collega's die ik hier vergeet, bedankt voor de vele interessante discussies en informele gesprekken, zowel tijdens de werkuren als daarbuiten.

Een speciaal woord van dank wil ik richten tot de technische staf van de S1. Zij zorgen ervoor dat de vele doctoraatsstudenten op technisch vlak alles voorhanden hebben om hun onderzoek op een professionele manier te kunnen uitvoeren. Bedankt Lode, voor de toffe gesprekken en de hulp bij het ontwerpen van mijn nanowire reactor in het begin van mijn doctoraat. Bedankt Stefaan, voor de hulp bij het organiseren van en vlees bakken tijdens onze jaarlijkse barbecue, voor de ontspannende babbels en de doe-het-zelf tips. Olivier wil ik graag bedanken voor de vele hulp en tips tijdens de SEM metingen en Nico voor het steeds paraat staan bij computerproblemen.

The huge amount of pole figure measurements that were collected during this research were made possible through a very productive collaboration with the people of the IBM X20C beamline in brookhaven. Thank you Jean and Christian for the support, interesting discussions and many tips during the long hours of conducting measurements. I sincerely hope that we can meet again in the future (and we'll have a good belgian beer then).

The (real-time) RBS and TEM measurements in this work have been made possible through collaborations with the IKS group at KU Leuven and the EMAT group at Antwerp University respectively. Here, I want to especially thank Koen for conducting and analyzing the RBS experiments and for some very interesting discussions. Within EMAT, a special thanks to Eva for performing and analyzing the TEM measurements.

En dan zijn er natuurlijk nog de familie en vrienden, mensen waarbij ik altijd terecht kon, hetzij voor een beetje steun, hetzij voor de nodige afleiding. In het bijzonder wil ik eerst mijn ouders bedanken voor de steun (zowel mentaal als financieel), maar vooral ook voor de vrijheid die ik altijd gekregen heb tijdens mijn studies. Zonder hen had ik dit nooit voor elkaar gekregen. Tenslotte is er natuurlijk mijn fantastisch gezinnetje. Niets is leuker dan tijdens een vermoeiend proces zoals het schrijven van een doctoraat 's avonds te kunnen thuiskomen in een warm nest en te geni-

eten van elkaar, van de kindjes, van een leuke babbel, van lekker eten, van gezellig samen in de zetel zitten,… Dank je!

Bob
Ghent, June 2016